




EX LIBRIS
UNIVERSITATIS
ALBERTENSIS

The Bruce Peel
Special Collections
Library



Digitized by the Internet Archive
in 2025 with funding from
University of Alberta Library

<https://archive.org/details/0162014920613>

UNIVERSITY OF ALBERTA

Library Release Form

Name of the Author: **Jennifer Jane Adams**

Title of Thesis: **Numerical modelling of regional gravity-driven flow systems in the Alberta basin**

Degree: **Master of Science**

Year this Degree Granted: **2001**

Permission is hereby granted to the University of Alberta Library to reproduce single copies of this thesis and to lend or sell such copies for private, scholarly, or scientific research purposes only.

The author reserves all other publication and other rights in association with the copyright in the thesis and except as herein before provided, neither the thesis nor any substantial portion thereof may be printed or otherwise reproduced in any material form whatever without the author's prior written permission.

UNIVERSITY OF ALBERTA

Numerical modelling of regional gravity-driven flow systems in
the Alberta basin

BY

Jennifer Jane Adams



A thesis submitted to the Faculty of Graduate Studies and Research in partial fulfilment of
the requirements for the degree of Master of Science.

Department of Earth and Atmospheric Sciences

Edmonton, Alberta

Fall 2001

UNIVERSITY OF ALBERTA

Faculty of Graduate Studies and Research

The undersigned certify that they have read, and recommend to the Faculty of Graduate Studies and Research for acceptance, a thesis entitled Numerical modelling of regional gravity-driven flow systems in the Alberta basin by Jennifer Jane Adams in partial fulfillment of the requirements for the degree of Master of Science.

This thesis is dedicated in memory of Dr. Bruce Nesbitt,
who revolutionized economic geology
by exploring the relationship between fluids and tectonics,
as the key to deciphering mineralization mechanisms
and
to Dr. John G. Fyles, my grandfather,
who first sparked my interest in geology and later
took me into the field, starting me on my career in earth sciences.

ABSTRACT

Regional topography-driven flow systems related to Laramide tectonic rebound were simulated using two-dimensional, coupled fluid-flow, heat-flow and solute-transport, numerical models to account for present day salinity and the accumulation of the Athabasca oil sands and Pine Point Pb-Zn ore deposits. Measured permeabilities and other observed basin features were incorporated into basin models along two sections. These adjustments prolong the duration of ore-forming conditions at Pine Point, but do not predict observed ore tonnage and mineralization temperatures. Along the Peace River Arch section, extension of the Mannville aquifer and inclusion of published permeabilities replicate present day salinity distributions, assuming uplift occurred around 60 Ma. The dissolved-phase hydrocarbon transport cannot explain the formation of the Athabasca oil sands, due to low fluxes. Simulations of erosion of the Peace River model predict the gradual decay of regional topography-driven flow by decreasing flow rates, underpressuring near the disturbed belt, and late, local topography-driven flow.

ACKNOWLEDGEMENTS

The impetus for this thesis grew out of stable isotope research done by B. Nesbitt and K. Muehlenbachs, which indicated that Pine Point may have formed during the late Devonian or Mississippian. Development of a numerical model to test this hypothesis proved to be a bigger task than previously thought. This thesis represents a portion of my research and learning relating to fluid flow, formation water evolution and collisional tectonics in sedimentary basins. My thanks go to my supervisors, B. Rostron and C. Mendoza, for their patience and permission to pursue several projects and attend many conferences. I have appreciated the discussions with Dr. D. Sangster about MVT deposits. I would also like to acknowledge the encouragement and support I have received from K. Muehlenbachs, H. Machel, E. Mountjoy, J. Richards and D. Sangster. I extend my thanks to P. Hsieh, who kindly held my hand while I learned to use RIFT2D. C. Neuzil and E. Bekele were quick to respond to my questions regarding modelling problems and M. Person generously reviewed input files and evaluated model solutions for me. Despite my contradictory results, G. Garven graciously reviewed some preliminary work and opened my mind to the transience of basin tectonics.

This work has only been possible through the support and love of George, Elizabeth, Nathan and Brian. A special thanks to Brian for agreeing to move thousands of miles from home and for having faith and hope in the face of so many challenges. Many discussions, revisions and sharing with Heather, Kristine, and Tannis have been appreciated.

This research was supported by NSERC funding to B. Rostron and C. Mendoza, as well as a PGA NSERC scholarship to myself. I have also received teaching assistantships in the Department of Earth and Atmospheric Sciences and other funding, including the Eugene Brody Graduate Scholarship, Vega Graduate Scholarship, Jean Isabel Soper Memorial Graduate Scholarship and Mary Louise Imrie Graduate Student Award.

Table of Contents

CHAPTER 1: INTRODUCTION	1
CHAPTER 2: BASIN MECHANICS	4
2.1 Basin tectonics	4
2.2 Driving forces of regional fluid flow	5
2.2.1 Topography-driven flow	6
2.2.2 Thermo-haline convection.....	7
2.2.3 Tectonically-driven flow.....	7
2.2.4 Compaction-driven flow	8
2.2.5 Erosional rebound.....	8
2.3 Heat transfer	9
2.4 Brine origin and evolution	10
2.5 Zn/Pb transport.....	11
2.6 Summary	11
CHAPTER 3: ALBERTA BASIN	15
3.1 Basin evolution	15
3.2 Hydrostratigraphy.....	17
3.3 Present day fluid flow	18
3.4 Paleohydrogeology	20
3.4.1 Basin tectonics	20
3.4.2 Geochemistry of formation waters.....	21
3.4.3 Thermal evolution	22
3.5 Summary	23
CHAPTER 4: PINE POINT, NWT.....	29
4.1 Pine Point ore district.....	29
4.2 Numerical modelling	32
4.3 Base case Pine Point model	34
4.4 Variations on the base case.....	36
4.4.1 Permeability variations.....	37
4.4.2 Temperature variations.....	42
4.4.3 Salinity variations	44
4.5 Discussion	47
CHAPTER 5: ATHABASCA OIL SANDS.....	85
5.1 Athabasca oil sands	85
5.2 Numerical modelling	87
5.3 Revised Model	88
5.3.1 Best case solutions.....	90
5.3.2 Salinity model.....	91
5.3.3 Western Mannville permeability.....	92
5.3.4 Fixed grid conclusions	92

5.4 Effect of erosion	93
5.4.1 Model design	94
5.4.2 Erosion case	95
5.5 Discussion	99
CHAPTER 6: CONCLUSIONS	128
REFERENCES	134
APPENDIX A: DESCRIPTION OF THE RIFT2D NUMERICAL MODEL	143
APPENDIX B: RIFT2D INPUT FILES.....	146
APPENDIX C: PECLET NUMBERS.....	147
APPENDIX D: PINCHOUT MODEL	152
APPENDIX E: COMPUTER SIMULATION REQUIREMENTS FOR ALL MODELS	156
APPENDIX F: EROSION MODEL PARAMETERS.....	157

List of Tables

Table 4.1:	Hydrostratigraphic parameters for the Pine Point original model.....	33
Table 4.2:	Hydrostratigraphic parameters for the base case model.....	35
Table 4.3:	Scenarios in the sensitivity analysis of the base case model.....	37
Table 4.4:	Hydrostratigraphic parameters for the measured permeability model.....	39
Table 4.5:	Summary table of ore-forming parameters for variations of the base case.....	48
Table 5.1:	Hydrostratigraphic parameters for the replicated and revised models.....	88
Table 5.2:	Scenarios run along the Peace River Arch section.....	89
Table 5.3:	Modelling parameters used in the Athabasca erosion models.....	96
Table C.1:	Finite element mesh parameters and Peclet numbers.....	148
Table E.1:	Summary of computer simulation time for all models.....	156

List of Figures

Figure 2.1:	Flexural response of lithosphere to loading and unloading.....	13
Figure 2.2:	Basinal flow regimes.....	14
Figure 3.1:	Map of western Canada.....	24
Figure 3.2a:	Stratigraphy and hydrostratigraphy of the Alberta basin.....	25
Figure 3.2b:	Hydrostratigraphic cross-section in central Alberta.....	26
Figure 3.3:	Present day fluid flow zones in the Alberta basin.....	27
Figure 3.4:	Present day formation water salinity in the Alberta basin.....	27
Figure 3.5:	Maximum burial temperature profile along the Peace River arch.....	28
Figure 4.1:	Middle Devonian paleo-geography of western Canada.....	50
Figure 4.2:	Stratigraphy along the Presqu'île barrier.....	51
Figure 4.3a-c:	Replicated model flow and temperature solutions at steady-state.....	52
Figure 4.3d-f:	Garven's original model solution at steady-state.....	53
Figure 4.4:	Initial conditions applied to Pine Point models.....	54
Figure 4.5:	Transient salinity profiles of the replicated model.....	55
Figure 4.6:	Transient temperature profiles of the replicated model	56
Figure 4.7:	Base case flow and temperature solutions at steady-state.....	57
Figure 4.8:	Transient salinity profiles of the base case.....	58
Figure 4.9:	Comparison of transient darcy velocity values for base cases.....	59
Figure 4.10:	Comparison of transient temperature values for base cases.....	60
Figure 4.11:	Comparison of transient salinity values for base cases.....	61
Figure 4.12:	Low permeability model solutions.....	62
Figure 4.13:	Measured permeability model solutions.....	63
Figure 4.14a-b:	Funnel model permeability distributions (plan view and cross-section),...	64
Figure 4.14c-e:	Funnel model solutions	65
Figure 4.15:	Comparison of transient darcy velocity values for permeability cases.....	66
Figure 4.16:	Comparison of transient temperature values for permeability cases.....	67
Figure 4.16e:	Relationship between fluid velocity and temperature.....	68
Figure 4.17:	Comparison of transient salinity values for permeability cases.....	69
Figure 4.18:	Low thermal conductivity model solutions	70
Figure 4.19:	Transient temperatures of the low thermal conductivity model	71
Figure 4.20:	Basal heat flux of 100 mW/m ² model solutions	72
Figure 4.21:	Comparison of transient darcy velocity values for temperature cases.....	73
Figure 4.22:	Comparison of transient temperature values for temperature cases.....	74
Figure 4.23:	Comparison of transient salinity values for temperature cases.....	75

Figure 4.24:	Salinity model solutions.....	76
Figure 4.25:	Model domains for two variations of the salinity model.....	77
Figure 4.26:	Deep basin model solutions.....	78
Figure 4.27:	Basement model solutions	79
Figure 4.27d:	Transient concentration of solute at Pine Point for basement case.....	80
Figure 4.28:	Comparison of transient darcy velocity values for salinity cases.....	81
Figure 4.29:	Comparison of transient temperature values for salinity cases.....	82
Figure 4.30:	Comparison of transient salinity values for salinity cases.....	83
Figure 4.31:	Transient solutions at Pine Point for low permeability models.....	84
Figure 5.1:	Location map of Canadian oil sands deposits.....	103
Figure 5.2:	Stratigraphy along the Peace River Arch section.....	104
Figure 5.3a-c:	Replicated model flow and temperature solutions at steady-state.....	105
Figure 5.3d-f:	Garven's original Athabasca model solution at steady-state.....	106
Figure 5.4:	Initial conditions applied to Athabasca models.....	107
Figure 5.5:	Transient salinity profiles of the replicated model.....	108
Figure 5.6:	Transient solutions at 5 observation points of the replicated model	109
Figure 5.7:	Transient salinity profiles at present day for calibration models.....	110
Figure 5.8:	Best case steady-state solutions.....	111
Figure 5.9:	Best case transient salinity profiles.....	112
Figure 5.10:	Comparison of best case and salinity models.....	113
Figure 5.11:	Hydrostratigraphy for Mannville scenarios.....	114
Figure 5.12:	Transient flow solutions for the Mannville scenarios.....	115
Figure 5.13:	Transient concentration solutions for the Mannville scenarios.....	116
Figure 5.14:	Comparison of transient darcy velocity values for Athabasca models...	117
Figure 5.15:	Comparison of transient salinity values for Athabasca models.....	118
Figure 5.16:	Transient evolution of model domain in the erosion model.....	119
Figure 5.17:	Transient evolution of freshwater heads in the erosion model.....	120
Figure 5.18:	Transient evolution of temperature in the erosion model.....	121
Figure 5.19a-c:	Transient evolution of salinity in the erosion model up to 48 Ma.....	122
Figure 5.19d-f:	Transient evolution of salinity in the erosion model up to 6 Ma.....	123
Figure 5.20:	Present day erosion solution.....	124
Figure 5.21:	Comparison of transient darcy velocity values for erosion cases	125
Figure 5.22:	Comparison of transient temperature for erosion cases.....	126
Figure 5.23:	Comparison of transient salinity for erosion cases.....	127

Figure C.1:	Comparison of base case solutions for testing of Peclet numbers.....	150
Figure C.2:	Comparison of best case solutions for testing of Peclet numbers.....	151
Figure D.1:	Pinch out model fluid flow and heat flow solutions.....	154
Figure D.2:	Pinch out model transient salinity distributions.....	155
Figure F.1:	Estimated topography curves at instantaneous uplift and at 2 Ma.....	157

CHAPTER 1

INTRODUCTION

In sedimentary basins, extensive epigenetic alteration, such as dolomitization, base-metal deposits and hydrocarbon reservoirs, has been interpreted as the product of large-scale flow systems (Bethke and Marshak, 1990; Deming and Nunn, 1991; and others referenced therein). For instance, paleomagnetic, fission track and radiometric dating have recently confirmed the genetic connection between Mississippi Valley-type (MVT) ore formation and orogenic activity adjacent to the parent basin (Brannon et al., 1992; Nakai et al., 1993; Christensen et al., 1995). This correlation reflects the development of regional topography-driven flow systems in response to tectonic rebound along the orogenic belt (Leach, 1999). However, compression, rapid sedimentation, uplift and erosion of basin strata all generate significant driving forces for fluids, heat and solute within a basin.

In general, flow regimes are dependent on i) *parent basin configuration* or spatial distribution of physical properties, e.g., aquifer connection, permeabilities and compressibilities, and ii) *driving forces* active in the basin, e.g., tectonics, fluid salinity and heat flow. Different driving forces of fluids become active and rock characteristics change as a basin evolves through time. Poor understanding of the timing of fluid flow and origin of alteration products has resulted in the proposal of many conceptual models to explain the formation of epigenetic deposits. Over the past two decades, numerical models have been developed to quantitatively evaluate the viability of these conceptual models (Garven and Freeze, 1984a,b; Bethke, 1985; Bethke, 1986; Garven et al., 1993; Arnold et al., 1996; Garven et al., 1999; and others). The modelled driving forces include compaction, tectonic collision, topographic uplift and thermo-haline gradients. For MVT Pb-Zn ore districts, only gravity-driven flow provides sufficient fluid fluxes to account for ore tonnage and formation temperatures of

districts at the margins of sedimentary basins (Garven, 1985; Bethke, 1986; Garven et al., 1993).

Topography-driven flow systems provide large driving forces over immense distances for long periods of time, thus accounting for the accumulation of giant MVT ore districts and hydrocarbon reservoirs (Garven, 1985; 1989). High permeabilities implicit in numerical models of topography-driven flow systems predict high flow rates, which account for ore tonnage and mineralization temperatures in MVT districts (Fowler, 1986). Steady-state solutions rapidly flush all of the solute out of the basin and distort temperature distributions, in contrast to observed temperatures and formation water salinity (Cathles and Smith, 1983; Deming and Nunn, 1991; Morrow, 1998; Adams et al., 2000a). These results suggest that a different flow mechanism is responsible for mineralization or the system is transient and short-lived. The majority of modelling has ignored the transient nature of driving forces and fluid salinity during tectonic uplift and subsequent erosion of the uplifted terrain (Corbett and Bethke, 1992). Appold and Garven (1999) considered the exhumation of a foreland basin, however due to high hydraulic conductivities in their model, the basin was flushed of brine within 2 million years. The discrepancy between measurements and simulations of these systems suggests that the dynamics of gravity-driven flow systems are poorly understood.

Further investigation of these discrepancies in terms of the structural and temporal controls on regional fluid migration can best be accomplished in the Alberta basin. The Alberta basin is a typical foreland basin, which hosts the Pine Point Pb-Zn ore district and the Athabasca oil sands, one of the largest petroleum deposits in the world. These resources are thought to have accumulated following the Laramide orogeny in the Early Tertiary. There is evidence of relict topography-driven flow in the basal aquifers of the basin (Hitchon, 1969; Bachu, 1995) and some studies have documented erosion-induced underpressures in Cretaceous shales (Tóth and Millar, 1983; Tóth and Corbett, 1986; Corbett and Bethke, 1992; Parks and Tóth, 1995). Extensive petroleum exploration has enabled detailed mapping of stratigraphy, fluid pressures, water salinity and temperatures across the basin. Permeability measurements of all hydrostratigraphic intervals have been used to estimate regional permeability (Bachu and Underschultz, 1992; Bachu et al., 1993). Eroded thicknesses have been proposed using a variety of techniques. These data can facilitate the development of transient regional fluid flow models for investigation of topography-driven flow in the Alberta basin. Furthermore,

previous modelling of both Pine Point and the Athabasca oil sands within steady-state flow regimes can be used as a basis for further work (Garven, 1985, 1989).

In this thesis, the regional flow systems responsible for the formation of Pine Point and the Athabasca oil sands have been remodeled using a transient, coupled fluid-flow, heat-flow and solute-transport numerical model. The objective of the modelling is to simulate systems that predict both the present day temperature and salinity distributions in the basin and the formation of economic deposits at the eastern margin of the basin. Garven's models (1985 and 1989) are used as a starting point from which to test the impact of general basin structure, permeability and thermal properties of basin strata on the salinity and temperature distributions. The Pine Point model is used to evaluate the importance of various basin characteristics, whereas measured regional permeabilities are incorporated into the Athabasca oil sands model and calibrated to observed water salinity. Lastly, the transience of the topography-driven flow and implications of erosional rebound were simulated by eroding the uplifted strata in the Athabasca model. The effects of these changes were evaluated based on the reproducibility of measured temperatures and salinities along each section.

CHAPTER 2

BASIN MECHANICS

A corollary of plate tectonic theory holds that the distribution and movement of mass and energy in the earth's crust are dynamically coupled to the evolution of terrestrial tectonics (Bredehoft and Norton, 1990; Garven, 1995). The relationship between tectonics and the rock cycle has been clearly established; however, recent studies show that all geological processes are mediated to varying degrees by crustal fluids (Ingebritson and Sanford, 1998). The worldwide extent of hydrothermal ore deposits, petroleum reservoirs, evaporites and epigenetic alteration attests to the wide-spread movement of fluids (Bethke and Marshak, 1990). Present day remnants of paleo-regional fluid migrations suggest that rock permeability is sufficient to conduct fluids regionally in the upper crust (Deming, 1994).

In sedimentary basins, regional-scale fluid migration occurs in response to sediment compaction, tectonic compression and/or loading, thermo-haline gradients, topographic relief, petroleum generation and erosion (Garven, 1995 and others). The duration and scale of this fluid flow is dependent on both the magnitude of the driving force and the hydrostratigraphic framework of the basin. The following discussion addresses the mechanics of basin tectonics, fluid flow, heat transport, and brine development.

2.1 Basin tectonics

Plate tectonics control the localization and development of most sedimentary basins. Initially, rifting causes subsidence and sedimentation into a new intracratonic basin. Further sedimentation may persist or compressional tectonics may trigger the evolution of a foreland basin. Convergent tectonics causes thrusting onto adjacent lithospheric plates. The elastic properties of the lithosphere accommodate the load by flexural downwarping in the foredeep and uplift in the forebulge (Figure 2.1a; Beaumont et al., 1993). Over time, the viscoelasticity of the lithosphere allows bending stresses to relax, causing further subsidence

in the foredeep and migration of the forebulge towards the load (Figure 2.1a). Abatement of compression results in orogenic unloading by erosion and/or extension of the fold and thrust belt (Beaumont et al., 1993). During unloading, isostatic rebound uplifts the foredeep with a flexural response similar to that of loading (Figure 2.1b). Concomitantly, dynamic subsidence, which is large-scale lithospheric deflection due to sublithospheric loading, moves the whole plate vertically either up or down (Catuneanu et al., 1997).

Over the course of an orogeny, high frequency cycles of flexural tectonics in tandem with dynamic subsidence ordain sedimentation, erosion and flow patterns in the foreland basin (Catuneanu et al., 1999). This cyclicity results in subaerial exposure of the uplifted foredeep or forebulge at distinct intervals. Meteoric recharge at these uplifts may infiltrate into the sediments, although there is little evidence for significant fluid flow within a basin during an orogeny. Maximum burial marks the end of overthrusting and compression in an orogeny. At the end of the orogeny, an extended period of unloading begins, which may initiate regional topography-driven fluid flow systems (Rayer et al., 1998). Although small-scale loading and unloading cycles occur throughout the orogeny, the final stage of unloading generates significant uplift, on the order of kilometres in the foredeep. The unloading process stops when erosion renders the topography flat.

2.2 Driving forces of regional fluid flow

Regional-scale migration of water, gas and oil characteristically occurs at various stages in the evolution of a sedimentary basin. In theory, hydraulic, capillary and buoyancy forces propel fluids through porous media. Hydraulic head gradients develop in response to elevation differences, affected by uplift and erosion in basins, and pressure differences, generated by vertical or horizontal loads and changes in pore fluid volume. Fluid flow is most significantly affected by hydraulic conductivity, which is proportional to fluid density and inversely proportional to fluid viscosity, which is a measure of internal friction within a fluid. In a sedimentary basin environment, the range of water temperature and salinity can significantly affect the hydraulic conductivity of a hydrostratigraphic unit.

Buoyancy is a function of fluid density, which is affected by salinity, temperature and pressure in a basin setting. Buoyancy forces often dampen the hydraulic gradient since basinal water salinity can increase with depth (Hanor, 1994). Buoyancy-driven fluid flow

commonly dominates where high heat flow or disequilibrium salinity conditions exist. In basins, buoyancy forces can alter the flowpaths of oil, gas and brine.

Capillary forces are active in pores containing at least two immiscible fluids, i.e., vadose zone or oil-water-gas environments. Capillary pressure is defined as the average pressure difference across a fluid-fluid interface, which develops due to molecular attraction of the liquid and solid phases (Dullien, 1992; Ringrose and Corbett, 1994). In other words, capillary pressure is the minimum pressure difference needed for the non-wetting fluid to displace the wetting fluid phase. As pores decrease in diameter, capillary pressure increases. In the subsurface, capillary forces assist in moving petroleum out of fine-grained, water-wet rocks and into more coarse-grained strata, as occurs during primary migration (England et al., 1991). Proposed mechanisms of basinal fluid flow are summarized in Figure 2.2.

2.2.1 Topography-driven flow

The shape of the water table is a subdued replica of the land surface topography in humid climates (Tóth, 1962; 1963). Elevation differences, between the water table in highlands and low-lying regions, create hydraulic head gradients. In foreland basins, regional-scale, topography-driven flow systems develop in response to tectonic rebound. At the foothills of the associated mountain ranges, meteoric water infiltrates into the basin and moves along permeable conduits to discharge at the margins of the basin (Garven and Freeze, 1984a,b). These flow systems can transport water, gases, petroleum, heat and solutes over hundreds of kilometres (Tóth, 1978; Bethke, 1986). Significant distortion of a conductive temperature profile can develop in fast flowing topography-driven flow systems (Hitchon, 1984; Garven and Freeze, 1984b; Garven, 1985).

Garven (1985) developed a numerical model to simulate gravity-driven flow and predicted sufficient flux (1-10 m/yr) to account for MVT ore districts. He and others (e.g., Majorowicz et al., 1988) argued that thermal anomalies in the Alberta basin reflect the advection of heat by fluid migration. Others argue that a steady-state topography-driven flow system poorly reproduces the salinity distributions of basins (Deming and Nunn, 1991; Morrow, 1998). However, no quantitative solution is able to account for both the formation of giant epigenetic deposits at the margins of foreland basins and the salinity and temperature distributions observed today in sedimentary basins.

2.2.2 Thermo-haline convection

Free convection of groundwater operates where salinity or temperature gradients lead to unstable density conditions (e.g., Evans and Nunn, 1993). The density dependent form of Darcy's law shows that any lateral fluid-density gradient induces convection (Bethke, 1989); however, the gradient must be great enough to overcome the inertia and viscosity of the fluid (Deming, 1994). Small-scale convective flow patterns over long periods of time may account for large-scale diagenesis (e.g., Morrow, 1998).

Thermo-density convection often develops due to the high heat fluxes and increased salinity in extensional settings (Person and Garven, 1994). Density-driven convection cells (0.1-1 m/yr) dominate as the gravity-driven flow system decays, which marks the beginning of the flexural stage of rift basin genesis (Person and Garven, 1994). Recently, numerical modelling of reflux dolomitization has shown that significant convection cells can develop in pinnacle reefs (Gareth Jones, pers. comm., 1999). These types of systems operate at local or intermediate scales and may explain the formation of unconformity-type uranium deposits (Raffensperger and Garven, 1995).

2.2.3 Tectonically-driven flow

Oliver (1986) proposed that fluid migration could be induced by thrust sheets 'overriding' sedimentary packages in foreland basins. Vertical and/or horizontal compression is thought to force fluids out of fold and thrust belts into the adjoining foreland basin. Numerical modelling demonstrated that a compressional pulse produces flowrates of 0.1-1 m/yr; however, overpressures last for little more than 10 000 years and move fluids no more than 100 km into the adjacent basin (Ge and Garven, 1994). More extensive transport distances may be attained by focusing fluids into aquifers.

The abundance of base-metal deposits within or close to the disturbed belt of the Alberta basin may be the product of localized and repeated tectonically-driven fluid flow. $^{87}\text{Sr}/^{86}\text{Sr}$ signatures of carbonate cements in Devonian carbonates are in excess of basin-derived radiogenic Sr in adjacent shales (Machel and Cavell, 1999). This enrichment is restricted to within 200 km of the fold and thrust belt, suggesting that tectonically-driven flow forced fluids out of Cambrian clastics or basement metasedimentary rock into the foreland basin.

This driving force does not persist for adequate periods of time to explain deposits removed from the fold and thrust belt, at the margins of a basin (Ge and Garven, 1994).

During orogenies, flexure of the lithosphere can cause reactivation of deep-seated basement faults. Deep brines can be discharged upwards along the faults (Garven, 1995). This driving force is locally associated with major structural faults and generally only influences areas along these trends. Some evidence of this type of flow has been identified along the Great Slave Lake shear zone at Pine Point and near the Peace River Arch in the Alberta basin (Campbell, 1967; Hitchon, 1993).

2.2.4 Compaction-driven flow

Measured porosity profiles in sedimentary basins document a systematic reduction in porosity with depth (Deming, 1994). Subsidence, sedimentation and burial result in the compaction of sediments and expulsion of water at rates of 0.1 to 1 cm/yr, proportional to sedimentation rate (Bethke and Corbett, 1989). Intracratonic basins have low sedimentation rates of approximately 0.01 to 0.1 mm/yr, whereas foreland basins accumulate over 0.1 to 1 mm/yr of sediment. An end member of compaction-driven flow is episodic basin dewatering from overpressurized zones in a rapidly subsiding basin (Cathles and Smith, 1983). This mechanism is dependent on sedimentation of shaley material deposited at a minimum rate of 1 mm/yr and the rapid expulsion of water through confined aquifers.

In these environments, e.g. Gulf Coast basin, flow rates can reach up to 1 cm/yr. Bethke (1985) demonstrated that steady-state compaction-driven flow rates (0.1-1 cm/yr) are insufficient to alter the temperature distribution in a basin and to form MVT deposits. Compaction-driven flow has been documented by diagenetic sulphides in the Upper Mississippi Valley region of the Illinois basin (Kutz and Spry, 1989). The Canning basin in Australia underwent regional compaction-driven flow responsible for the formation of the Mt. Isa MVT deposits (Leach, 1999).

2.2.5 Erosional rebound

In response to mechanical unloading by erosion or glacial ice melt, the rock framework dilates and pore water expands due to compressibility. Rock dilation generates subhydrostatic pressures or underpressures, which re-equilibrate by fluid flow (Neuzil and Pollock, 1983). The degree and duration of underpressuring is dependent on the rate of

unloading, specific storage, permeability, and the amount of vertical rock dilation (Neuzil and Pollack, 1983). Thus, underpressuring in low permeability, high compressibility rocks can persist for periods of geological time after significant unloading has stopped (Tóth and Millar, 1983). The propensity for erosion-induced flow is towards the fold and thrust belt, because greater erosion and therefore dilation occurs in the foothills region.

In the Alberta basin, subhydrostatic fluid pressure in the Colorado aquitard system developed in response to erosion of overlying strata (Tóth and Corbet, 1986). Corbet and Bethke (1992) simulated the flow system described in Tóth and Corbet (1986) using a numerical model. The model predicted the pressure distribution along the section, but only if the vertical permeability of the shale aquitards was less than $3 \times 10^{-20} \text{ m}^2$. Mapping of fluid pressures in the overlying foreland sandstones and siltstones revealed convergent flow into the Lower Edmonton Group and Bearpaw Formation due to erosion (Parks and Tóth, 1995). Erosional-rebound fluid flow is constrained to permeability zones within regional aquitards and dominates when erosion rates are high.

2.3 Heat Transfer

Heat transfer occurs in sedimentary basins by conduction and convection. Heat is conducted by the exchange of kinetic energy during molecular collision in solid and fluid phases. Conductive heat transfer rates are dependent on the temperature gradient and thermal conductivity of the intervening material. In sedimentary basins, the temperature gradient is constrained by surface temperatures and by primordial and radioactive heat transferred into the bottom of the sedimentary package. Constant, conductive heat transport, in homogeneous isotropic strata, generates basin temperature profiles that are a linear function of depth. Over time, however, the conductive temperature distribution changes as a direct result of variations in basal heat fluxes associated with tectonics, i.e., either local tectonic features such as a shear zone or arch, or regional-scale tectonics, such as the development of a subduction zone or rifting. In addition, the conductive temperature distribution is affected by climatic variations and, more importantly, regional-scale fluid flow.

In contrast, the movement of a heated substance is referred to as convective heat transfer. The low thermal conductivity and high heat capacity of water allows heat to be transported by fluid flow. At a regional scale, slow vertical and high lateral flow rates may distort a

conductive temperature distribution significantly. For instance, vertical recharge of meteoric water at 1 cm/yr to a depth of 1 km would decrease the surface conductive heat flow by 41% (Deming, 1994). Domenico and Palciauskas (1979) showed that for typical thermal conductivities and hydraulic gradients, fluids transported heat effectively for an average permeability greater than 10^{-17} m^2 . However, extremely high flow rates (e.g., tens of m/yr) generally decrease convective heat transfer because the water does not have time to be heated by conduction (Garven, 1985).

2.4 Brine origin and evolution

Sedimentary basins contain thousands of cubic kilometres of water. The salinity of this water varies over five orders of magnitude from meteoric water to hypersaline brines, far exceeding seawater salinity. In general, formation water salinity increases with depth; however, the spatial distribution of water compositions can be used to decipher paleo-fluid flow and rock-water interactions (Hitchon and Friedman, 1969; Carpenter, 1978; Connolly et al., 1990a,b; Stueber and Walter, 1994).

The chemical character of any water is the product of the original water composition, rock-water interactions and fluid flow, i.e., dispersion or mixing. During deposition of basin strata, water is buried in pore spaces of the sediments. This water may be fluvial or marine in origin. In restricted embayments, significant evaporation of seawater concentrates dissolved solutes, sometimes past halite saturation. The chemical composition of water buried with sediments can range from meteoric to highly saline brine. Once buried, water compositions evolve towards equilibrium with its host rock. With depth, formation water temperatures increase, thereby increasing the rate of rock-water interaction and the solubility of silicate minerals. Precipitation, exchange and redox reactions, such as albitization, dolomitization, silicate hydrolysis, thermochemical sulphate reduction and other processes, affect the relative concentrations of cations in basinal waters (Tóth, 1984). Generally, chloride accounts for over 95% by mass of anions in basinal waters, with the exception of meteoric waters, which are dominated by HCO_3^- or SO_4^{2-} (Hanor, 1994). As brine salinity increases, Na and Cl become the dominant ions. Ca, Mg and K may also become significant species past halite saturation. High TDS brines can have a pH below 4, which increases complexation of metals by Cl and bisulphides (Hanor, 1994).

Fluid flow redistributes solute within a basin through precipitation/dissolution reactions, leaching of cations and/or metals, and mixing of two miscible fluids. In gravity-driven flow systems, meteoric water recharges at uplifts and infiltrates into the deep basin, thereby diluting formation waters (Connolly et al., 1990a). In the Williston basin, a similar flow system is thought to be responsible for extensive dissolution of the halite-rich Prairie Formation (Downey, 1986). Many MVT deposits are understood to be the product of regional brine migration, which mobilizes Pb and Zn.

2.5 Zn/Pb transport

High ore grades found in MVT deposits and current metal concentrations in Gulf Coast brines (>1 mg/L) are difficult to reconcile with the low solubility of Pb and Zn. At sedimentary temperatures, only complexation of metals with a soluble ligand can explain metal transport (Hanor, 1996). A variety of ligands complex with base metals, such as chloride, bisulphide, organic acids and thiosulphate (Barrett and Anderson, 1982; Spirakis and Heyl, 1992; Giordano, 1994). Laboratory and field measurements of formation waters reveal a direct correlation between water salinity and concentrations of dissolved Zn and Pb, As salinity increases, measured in-situ pH decreases and higher order metal chloride complexes ($\text{Me}^{2+} \rightarrow \text{MeCl}_2^0 \rightarrow \text{MeCl}_4^{2-}$) progressively dominate. Thermodynamics predict that total dissolved metal (Zn or Pb) content increases as temperature and pressure increase, pH decreases, Cl concentration increases and H_2S concentration decreases (Hanor, 1996). Calculations show that more than 150 g/L Cl are required at 100°C to dissolve 1 ppm of Zn or Pb in a typical basinal brine. In Gulf Coast brines, the Zn concentration increases by three orders of magnitude at 100 g/L Cl, to values above the minimum requirement of 1 ppm Pb and Zn in MVT ore-forming fluids. Thermodynamic analysis and empirical relationships have demonstrated that highly saline (>100 g/L Cl) brines are required to mobilize metals from a source rock for transport to an MVT host rock (Hanor, 1996).

2.6 Summary

The development of a foreland basin leads to regional-scale fluid flow, hydrocarbon generation, mountain building and erosion. Initially, loading at the margin of the basin causes subsidence and accumulation of marine clays, rich in organics. As loading persists, continued sedimentation and burial of these high porosity sediments drives compaction-driven fluids out of the deep basin. Episodic thrusting leads to crustal shortening and

tectonically-driven fluid flow a short distance into the foreland basin. Deep burial and heating initiates petroleum generation following by migration and trapping around the time of maximum burial. As loading dissipates, erosion of the disturbed belt results in uplift of the foreland basin and initiation of regional topography-driven flow. Topography-driven flow systems can enhance rock-water interaction and transport heat, solute and metals for long distances. The formation of MVT ore districts is linked to orogenic activity in the parent basin and the flux of highly saline metal-bearing fluids through carbonate rock. Erosion gradually leads to the decay of regional topography-driven flow systems and can cause hydraulic underpressuring in areas with high rates of erosion and high diffusivity strata. As relief becomes minimal and tectonics pacify, local-scale fluid flow dominates.

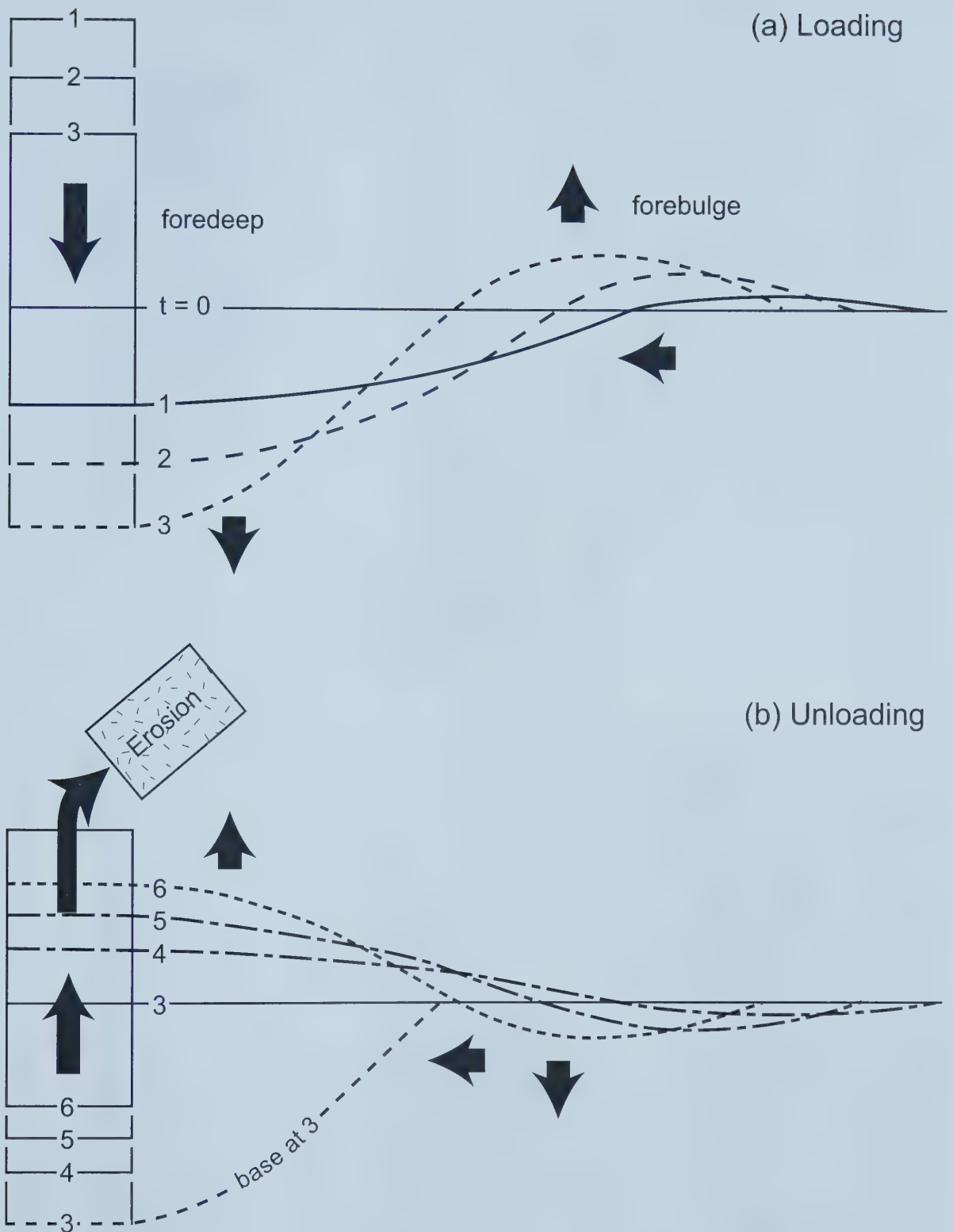


Figure 2.1: Schematic showing the flexural response of a lithospheric plate during (a) loading and (b) unloading (Modified from Beaumont et al., 1993). The numbers represent sequential time slices during loading and then unloading. The lines represent the shape of the plate. To determine the outline of surface topography during unloading or loading, dynamic subsidence and erosion must be taken into account. Generally during loading, the topography is thought to be more or less flat.

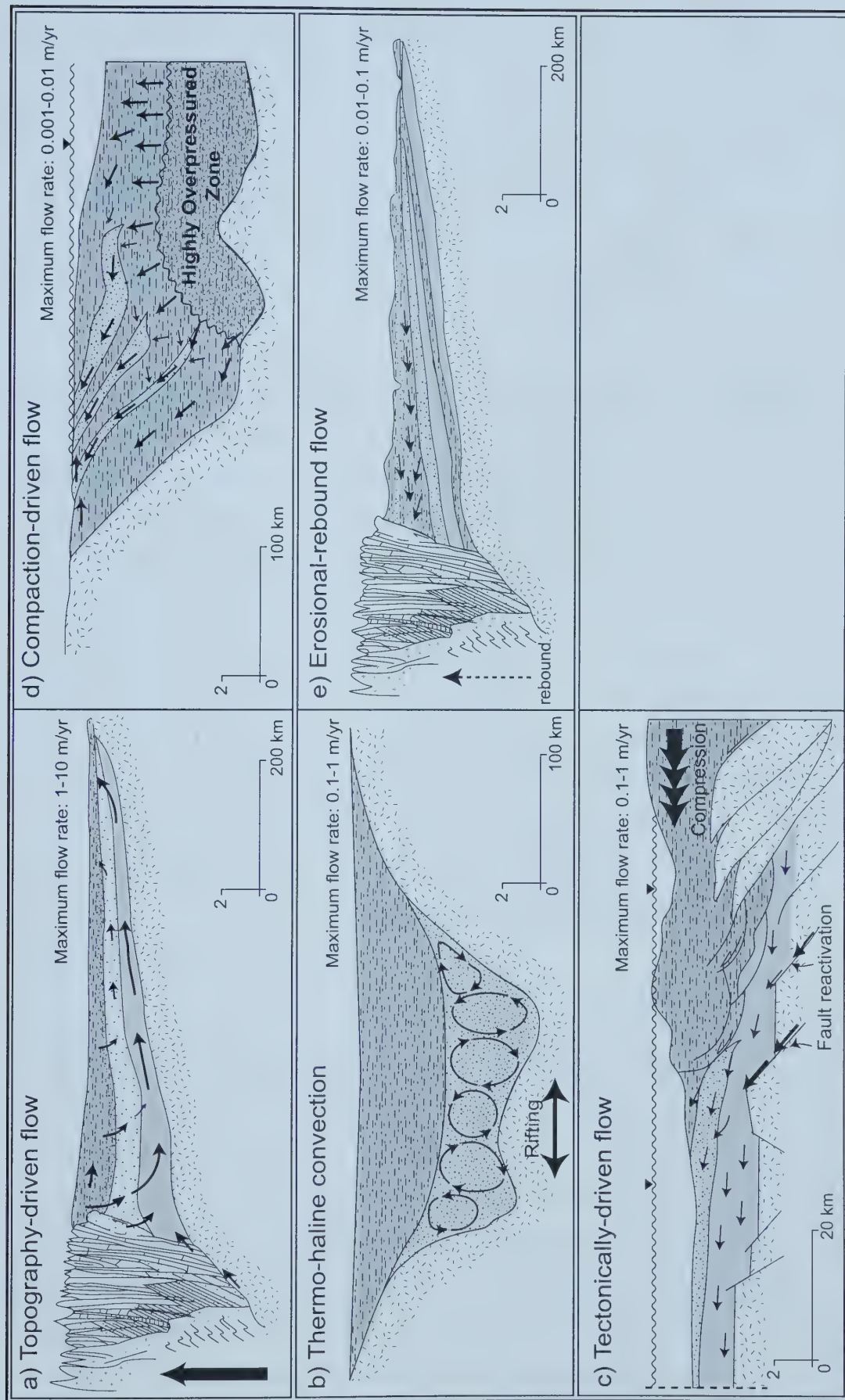


Figure 2.2: Basinal flow regimes: a) Topography-driven flow due to tectonic rebound; b) Thermo-haline convection during rifting; c) Tectonically-driven flow during orogenic activity; d) Compaction-driven flow; e) Erosional-rebound flow; and f) Tectonic rebound flow. Small arrows indicate direction of groundwater flow. Large arrows indicate basal forces or stresses. Note scale changes for each case. (Modified from Garven, 1995).

CHAPTER 3

ALBERTA BASIN

The Alberta basin hosts rich hydrocarbon reservoirs and many economic base-metal ore districts. Genetic models and direct dating of these deposits suggest that their accumulation is closely linked to Laramide tectonics and associated fluid flow. Extensive exploration for hydrocarbons has allowed for detailed characterization of present day basin hydraulics, resources and configuration (e.g., Bachu and Underschultz, 1992; Bachu, 1995; Bachu, 1999). In central Alberta, geochemical analyses of brines have constrained the timing of the decay of the Laramide topography-driven flow system (Connolly et al., 1990a,b). Furthermore, paleotemperature measurements throughout central Alberta have been used to estimate thicknesses of eroded material and maximum burial (Willett et al., 1997). The extent of massive dolomitization and homogeneity of epigenetic minerals across the basin has sparked much study of regional paleohydrogeology (Mountjoy et al., 1997; and others referenced). This previous work allows for numerical modelling of the evolution of foreland basin fluid flow related to compressional tectonics and the impact of flow on the development of economic resources.

3.1 Basin evolution

The Alberta basin is a wedge-shaped foreland basin, which is bounded to the west by the disturbed belt and thins onto the Canadian Shield to the east (Figure 3.1). In the southeast, the Bow Island Arch separates the Alberta basin from the Williston basin and the northern limit of the basin is defined by the Tathlina uplift. The Phanerozoic cover consists of a thick sequence of carbonates and intervening shales, characteristic of a passive margin, which are overlain by a foreland sequence of synorogenic shales and siltstones, interbedded with thin sandstone units (Figures 3.1 and 3.2a). The following description was compiled based on Porter et al. (1982), Ricketts (1989) and Mossop and Shetsen (1994).

During the Proterozoic era, rifting initiated subsidence and deposition in the Alberta basin. Erosion of the adjacent craton deposited clastics on the irregular topography of the Precambrian basement during Cambrian time. Local tectonic highs controlled the spatial distribution of passive margin strata consisting of shelf carbonates and evaporitic deposits until the Middle Devonian. In particular, the Peace River Arch, trending southwest-northeast and orthogonal to the disturbed belt, was a dominant structural feature that affected reefal development and acted as a source of clastics until the Late Devonian. In the central section of the basin, platformal carbonates of the Cooking Lake Formation and local reefs or reef trends, such as found in the Leduc Formation, were deposited early in the Upper Devonian. Transgression from the north induced deep marine conditions, depositing the Ireton shale and its equivalents. At the end of the Upper Devonian, thick packages of reefal carbonates of the Winterburn and Wabamun groups were laid down across the basin. Deep marine conditions in the early Carboniferous deposited the tight, organic-rich Exshaw shale that grades into the carbonates of the Banff Formation. The passive margin sequence culminated with the deposition of interbedded carbonates, and siltstones of the Stoddart and Rundle groups.

Accretion of allocthonous terranes commenced during the Mesozoic, and caused deposition of shales and evaporites in the Triassic. During the Jurassic, tilting of the basin in response to compressional tectonics eroded most Triassic and Permian strata across the basin. Further tectonic activity ensued in the Middle to Late Jurassic with the development of a subduction zone during the Columbian orogeny. Repeated thrusting deposited a sequence of sandstones and shales throughout the Cretaceous. Fluvial and estuarine valley-fill sediments along with sheet sands and shales of the Mannville group were laid down across the basin. A thick package of Colorado Group clastics straddles the Lower-Upper Cretaceous boundary and acts as a significant barrier to fluid flow. These thick shales are interbedded with thin, discrete sandstone units, whose distribution varies across the basin. The Laramide orogeny commenced in the Late Cretaceous and is recognized as the final episode of tectonic convergence in the formation of the Cordillera. A series of compressional pulses placed large thrust sheets onto the foreland basin (Aitken et al., 1993). In the southern and central portions of the basin, non-marine clastics interfinger with

argillaceous sediments of the Edmonton Group (Bachu, 1999). However, in the northern portion of the basin over 1 km of low permeability sediments were deposited (Stott, 1982).

The Alberta basin experienced maximum burial during the Paleocene (~60 Ma), at which time hydrocarbon generation and possible migration occurred (Mossop and Shetsen, 1994; Issler et al., 1999). Dissipation of compressional stress resulted in tectonic rebound of the basin and the erosion of over 3 km of rock at the western margin of the basin (Beaumont et al., 1993; Mountjoy et al., 1997). This rebound initiated the development of a large gravity-driven flow system, which may have been instrumental in the migration of hydrocarbons and the formation of base-metal deposits (Garven, 1985; 1989). Subsequent glaciation sculpted the landscape during the Holocene, leaving thick blankets of glacial drift on the bedrock.

3.2 Hydrostratigraphy

For regional-scale interpretation of wellhead measurements or numerical modelling, the previously described package of rock can be subdivided into general hydrostratigraphic units (Figure 3.2a,b). Many diachronous facies changes have been identified along a trend parallel to the disturbed belt, primarily due to the size of the basin. Because of these lateral lithological discontinuities, hydrostratigraphic designations may be laterally heterogeneous. The following discussion applies to the southern and central sections of the Alberta basin as defined by Bachu (1995). Equivalent units for the most northern part of the basin are outlined in Figure 3.2a and the following discussion is based on work presented in Bachu (1995 and 1997).

The Precambrian basement has been defined as an aquiclude; however, the upper 3 to 5 m is highly fractured and permeable due to long periods of sub-aerial weathering. A thin veneer of Cambrian sandstone acts as an aquifer capped by the Cambrian aquitard adjacent to the Cordillera (Bachu et al., 1986). Due to a paucity of data and the limited extent and thickness of the basal aquifer, the lower impermeable boundary in numerical models is often defined as the top of the regional Elk Point aquiclude. The first significant aquifer consists of platform carbonates of the Winnipegosis or Keg River aquifer. The overlying Prairie aquiclude is locally considered an aquitard due to areas of dissolution and radial facies changes associated with a salt pan environment.

In this study, the sequence of aquifers and aquitards, on top of the Middle Devonian succession, is designated as a low permeability aquifer system, because the Ireton shale and the Leduc Formation pinnacle reefs are locally discontinuous. In contrast, the equivalent northern hydrostratigraphic unit consists of several hundred metres of low permeability Fort Simpson shale. The overlying Upper Devonian carbonates represent a laterally extensive and extremely permeable aquifer. The Exshaw Formation shale and lower section of the Banff Formation are grouped into an aquitard. The Carboniferous to Jurassic strata are considered to be a poor aquifer system in the central part of the basin. Farther north, the upper Banff, Rundle and Stoddart formations can be treated as an aquifer and the Triassic strata as an aquitard.

In the foreland succession, the regionally continuous Mannville sandstone is highly permeable; however, the deep basin section of this unit became gas saturated around 35 Ma (Welte et al., 1984). Spatial and temporal variations in hydraulic conductivity of the Mannville aquifer must be taken into account when interpreting or modelling flow in the basin. The Colorado aquitard system restricts vertical fluid flow (Bachu, 1995). Similarly, the post-Colorado succession is a mixture of aquifers and aquitards that are in sum a poor aquifer system. Minor thicknesses of unlithified sediments at the surface are negligible within the regional-scale flow system.

3.3 Present day fluid flow

The Alberta basin has experienced rapid sedimentation, tectonic compression, mechanical unloading, hydrocarbon generation, topographic uplift, and glaciation over the past 80 million years. In addition, dense brines, oil, gas and meteoric water fill the porosity of the heterogeneous Phanerozoic strata. The combination of these driving forces, fluid types and the permeability distribution has produced complex fluid flow patterns observed in the basin today. Hydraulic potentials from over 200 000 wells in the Alberta basin have been mapped for each major hydrostratigraphic unit. The well head measurements have been corrected by industry (Rahkit Consultants, Ltd.) for brine density, to accurately estimate gradients and flow directions.

General fluid flow directions have been established for the central portion of the basin (Figure 3.3a). Variations in topography and diachronous facies changes across the basin

account for local deviations from the general case. Furthermore, the Peace River Arch has acted as a major hydraulic and thermal divide, separating northern from central and southern regions of the basin (Mountjoy et al., 1997). The Colorado group aquitard separates flow in the post-Colorado clastic wedge from the flow system in the passive margin succession (Figure 3.3; Tóth, 1978; Tóth and Corbet, 1986; Bachu, 1995; Rostron et al., 1997). Local topography-driven flow systems dominate the post-Colorado zone, whereas flow, in the underlying Colorado group, is controlled by erosional rebound. In the underlying, passive-margin strata, fluids move updip along permeable carbonate aquifers, as in a classic gravity-driven flow system (Bachu, 1995).

Flow in the post-Colorado sequence is characterized by local topographic highs, i.e., meteoric water recharges at topographic highs and local river valleys act as discharge zones. Post-Colorado formation water salinity increases with depth, but is generally low. These formation waters are Na-HCO_3^- rich, suggesting that meteoric water has recently recharged near-surface aquifers (Figure 3.4; Connolly et al., 1990a). Thus, buoyancy forces due to salinity or temperature variations are insignificant. The flow system has reached pseudo-steady state or has reached equilibrium with topography (Parks and Tóth, 1995).

Within the western portion of the Colorado group aquitard, measured hydraulic pressures are less than the lowest surface elevation in the basin. Thus water moves down dip to the west-southwest or towards the disturbed belt. This severe underpressuring is interpreted as delayed adjustment to Cenozoic erosion due to extremely low permeability of Colorado shales (Tóth and Millar, 1983; Parks and Tóth, 1995). At the eastern margin of the basin, salinity and flow in all strata are controlled by local topographic relief (Barson et al., in preparation). Brines in the Paleozoic aquifers mix with meteoric water at the contact with the Cretaceous succession. Similarly, a mixing zone exists between the passive margin succession and foreland basin strata, approximately in the Mannville aquifer (Bachu, 1995).

Fluid pressures in the passive margin succession are subhydrostatic in the deep basin; however, the hydraulic gradient drives fluids updip to discharge at the erosional margin. This flow system resembles gravity-driven flow documented in the Denver and Palo Duro basins (Bachu, 1995), but the pattern is difficult to understand because stiff, low permeability, Colorado shales restrict recharge into the underlying aquifers (Bachu, 1995).

Tóth (1978) and (Tóth and Millar, 1983) proposed that this flow pattern was a relic from an earlier period dominated by topography-driven flow most likely prevalent shortly after maximum burial. Numerical models of the Red Earth region could not be calibrated to predict such a state of hydraulic disequilibrium (Corbet and Bethke, 1992). High salinity formation waters occupy pore space in the carbonate aquifers; buoyancy forces dampen the updip driving force. Although low permeability aquitards are part of this zone, multiple periods of compaction have fully compressed Paleozoic shales, such that no disequilibrium underpressuring due to erosion has been observed.

3.4 Paleohydrogeology

For exploration purposes, an understanding of paleohydrogeology assists in deciphering processes involved in hydrocarbon migration and ore formation. The evolution of fluid flow in the basin is dependent on the secular variations of driving forces and hydrostratigraphy. For these reasons, a series of cross-basin studies have investigated stable and radiogenic isotopes, as well as solute chemistry of formation waters and fluid inclusions to delineate the timing, direction and magnitude of paleoflow. The following discussion presents the evolution of physical, thermal and chemical components during and after the Laramide orogeny in the Alberta basin.

3.4.1 Basin tectonics

Basin tectonics not only control driving forces of regional-scale fluid migration, but also alter the physical framework through which fluids flow. In the Alberta basin, accretion of exotic terranes along the western margin marked the beginning of the Columbian orogeny at the end of the Jurassic. This loading of the lithosphere initiated subsidence and sedimentation of foreland clastics into the basin. Throughout the Columbian and Laramide orogenies, compressional pulses caused cycles of deep marine conditions that gradually shallowed upwards, culminating in a period of erosion. Two driving forces are a product of these cycles. First, tectonically-driven flow may be active during compressional pulses or loading; however, this type of flow only affects the vicinity of the disturbed belt due to the limited duration of the driving force (Oliver, 1986; Ge and Garven, 1994). Second, after a period of relaxation, small-scale tectonic rebound may cause short-lived periods of gravity-driven flow. Finally, the rapid accumulation of low permeability sediments (~ 1 mm/yr) can result in significant overpressures at depth, which drive compaction-driven flow (Bethke, 1985).

The last compressional pulse of the Laramide orogeny occurred during the Late Paleocene to Early Eocene (Fermor and Moffat, 1992). In the central portion of the Alberta basin, maximum burial was reached at approximately 58 Ma (Fermor and Moffat, 1992; Willet et al., 1997). Oil and gas generation, close to the time of maximum burial, may also have caused overpressuring, especially in the deep basin (Bekele, 1999). This overpressuring would have fuelled secondary migration of petroleum along permeable conduits capped by low permeability shales (Creaney and Allan, 1990).

Extensional faulting and erosion of the fold and thrust belt caused tectonic rebound of the foreland basin. This topographic uplift is understood to have initiated regional topography-driven flow through the foreland basin (Garven, 1985). As erosion decreased the topographic gradient, this flow system decayed back to local-scale flow near surface (Garven, 1989). By the late Miocene, erosional rebound generated underpressures in low permeability shales, which reversed flow directions in the Colorado group (Tóth and Millar, 1983).

3.4.2 Geochemistry of formation waters

Chemical and isotopic signatures can be used to decipher the origin and evolution of formation or fluid inclusion waters. Generally, the salinity and isotopic compositions of waters increase with depth in the Alberta basin. Mapping of the major and minor ion chemistry of formation waters revealed three distinct water types along a section through central Alberta (Figure 3.4b; Connolly et al., 1990a,b). These three groups correlate to the three fluid flow zones delineated in the basin. Group I waters are Na-Ca-Cl brines found in the Paleozoic carbonates and Jurassic aquifers. Chemistry of Group I brines was controlled by silicate hydrolysis, ankeritization and clay-carbonate rock-water interaction. Group II waters are Na-Cl brines found in the foreland basin clastics below the Second White Speckled shale. Connolly et al. (1990a,b) interpreted the chemical signatures of the group as the product of cation leaching from clays and feldspars during Laramide gravity-driven flow. Group I and II waters developed through mixing of two end member waters: i) Devonian evaporated seawater brine; and, ii) post-Laramide, but pre-Quaternary, meteoric water. Na-HCO₃⁻ waters are unrelated to the Group I and II waters, in the uppermost clastic succession. Connate water buried with the Group III sediments has been completely flushed by Holocene meteoric water.

Isotopic analysis of these waters confirms the chemical classification and allows for approximate dating of fluid migrations (Connolly et al., 1990a,b). Group I and II waters form a mixing line that intersects the meteoric water line at $\delta^{18}\text{O} = -13.3\text{‰}$ and $\delta\text{D} = -96\text{‰}$ SMOW. These values are equivalent to average Neogene meteoric water, corrected for temperature. Connolly et al. (1990b) proposed that Group I and II formation waters became isolated from meteoric recharge in the Miocene. The chemistry and isotopic character of Alberta formation waters suggest that brines in the passive margin succession mixed with meteoric water in a topography-driven flow system initiated by post-Laramide tectonic rebound. During the flow system, cations were leached from Colorado group rocks and seawater was displaced by meteoric water in the post-Colorado strata. Isolation of the Group I and II waters from meteoric recharge occurred during the Miocene as the flow system decayed. Manipulation of measured isotopic signatures revealed that most waters are not in isotopic equilibrium with their present day host. No systematic deviation from equilibrium could be identified in either clastic- or carbonate-hosted waters, suggesting that fluids have recently moved or still are moving through the subsurface (Connolly et al., 1990b).

3.4.3 *Thermal evolution*

Thermal evolution of sedimentary strata documents the burial history and variations in geothermal gradients. Apatite fission track dating and track length modelling have provided the most comprehensive analysis of secular variations in the gas thermal regime of the Alberta basin (Ravenhurst et al., 1994; Willett et al., 1997). Measurements in basement to the Upper Cretaceous rocks record significant thermal overprinting from Laramide burial and cooling. Most samples appear to have experienced maximum burial simultaneously around 58 Ma, which correlates with the timing of extensional faulting in the southern Cordillera (Parrish, 1995). Maximum burial temperatures were calculated along the Peace River Arch section (Figure 3.5; Willett et al., 1997). Today, geothermal gradients generally increase from the south-southwestern limit to the north-northeastern end of the basin. Paleogeothermal gradients at maximum burial seem to vary spatially and temporally across the Peace River Arch section (Willett et al., 1997). Gradients of $\sim 30^\circ\text{C}/\text{km}$, in the central part of the section, have remained relatively constant since the end of the Laramide orogeny; however, geothermal gradients seem to have been much greater in the eastern and western

margins of the basin. These discrepancies may be explained by advective heat transport during regional fluid migration (Bachu, 1993) and/or perturbations in the basal heat flux related to compressional tectonics (Willet et al., 1997).

The thickness of Cretaceous strata removed by erosion can be estimated empirically using a relationship between maximum burial depth and moisture content of near surface coals. This method yields profiles that are consistent with flexural tectonic models and stratigraphic thickness projections (Beaumont et al., 1993; Issler et al., 1999). Eroded thickness profiles can be used to reconstruct the topographic gradients driving fluids since the Laramide (Figure 3.5; Willet et al., 1997).

3.5 Summary

The Alberta basin is a westward thickening wedge of sedimentary strata. A thick basal sequence of passive margin carbonates and intervening shales is overlain by a foreland sequence of tight shales and siltstones interbedded with thin sandstone units. Present day fluid flow patterns document relict topography-driven flow through the basal Upper Devonian and Middle Devonian aquifers while erosion-induced, westward flow dominates in the Colorado group near the disturbed belt. Near surface, local topography-driven flow has replaced connate waters with Tertiary meteoric water (Group III). Geochemistry of existing formation waters in the Paleozoic and Jurassic carbonates are evolved Na-Ca-Cl brines (Group I), whereas Group II waters found in Cretaceous strata are Na-Cl brines. Burial history and petroleum maturation studies estimate maximum burial at 58 Ma followed by rapid uplift and regional topography-driven flow. Subsequent erosion has removed over 3 km of Cretaceous strata in the west, causing underpressures to develop in high diffusivity rocks.

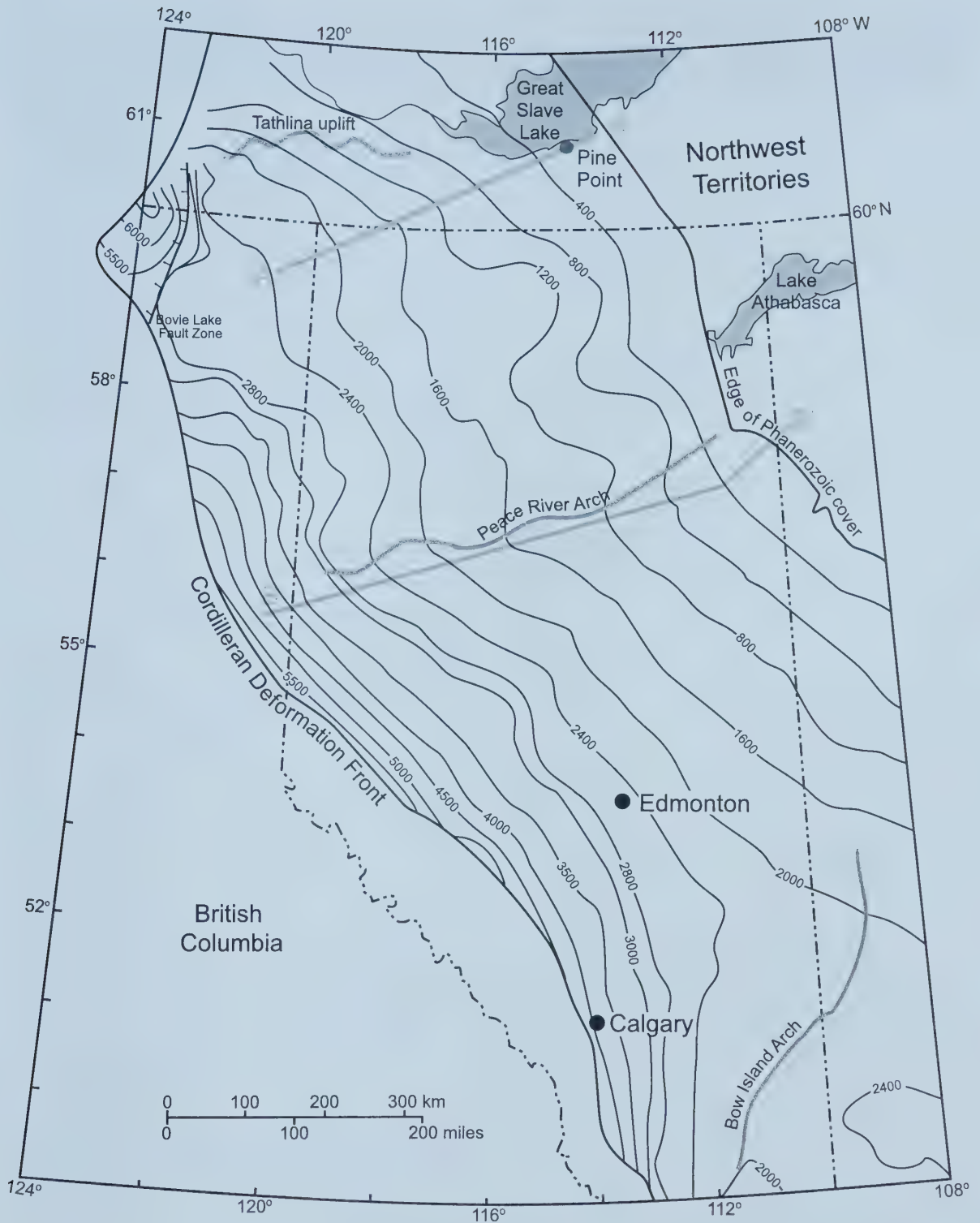


Figure 3.1: Map of Western Canada showing the thickness of Phanerozoic cover (m). The structural northern and southern limits of the Alberta basin are defined by basement highs (Adapted from Mossop and Shetson, 1994). Note the shift in contour interval from 400 m to 200 m to 500 m near the disturbed belt. A-A' represents the section used in the Pine Point models and B-B' is the Peace River section along which the Athabasca oil sands system was modelled.

			Stratigraphic Nomenclature		Hydrostratigraphy					
Period			Group Formation		Central Alberta	Northern Alberta				
Quaternary			Pre and Glacial Drift							
Tertiary			Paskapoo		Scollard-Paskapoo aquifer					
Cretaceous	Upper	Edmonton	Scollard		post-Colorado aquifer-aquitard system					
			Battle							
			Whitemud							
			Horseshoe Canyon			Dunvegan aquifer				
			Bear Paw							
			Belly River							
	Lower	Colorado	Lea Park Milk River		Colorado aquitard system					
			Cadium							
			Second White Speckled Sandstone							
			Viking							
		Mannville Clearwater	Upper Mannville aquifer	Fort St. John aquitard						
			Clearwater aquitard							
		Lower Mannville aquifer								
		Jurassic aquitard								
Jurassic					Mississippian-Jurassic aquifer system					
Triassic										
Permian										
Pennsylvanian										
Mississippian			Stoddart		Carboniferous-Permian aquifer system					
			Rundle							
			Banff							
			Exshaw							
Devonian			Wabamun		Upper Devonian aquifer system					
			Winterburn							
			Upper	Woodbend	Ireton	Grosmont		Fort Simpson aquitard		
						Leduc				
				Middle	Elk Point	Upper	Beaverhill Lake Cooking Lake		Slave Point aquifer	
							Prairie/Muskeg			
Lower	Elk Point	Lower	Keg River/Winnipegosis		Muskeg aquitard system Presqu'ile aquifer					
					Keg River aquifer					
Silurian			Not Deposited		Elk Point aquiclude system					
Ordovician					Elk Point aquitard system					
Cambrian	U			Cambrian aquitard system			Cambrian aquitard			
	M	Basal sandstone							Basal aquifer	
	L									
Precambrian					aquiclude			aquiclude		

Figure 3.2: a) Stratigraphy with equivalent hydrostratigraphic units for the central and northern Alberta basin (Adapted from Bachu, 1995 and 1997).

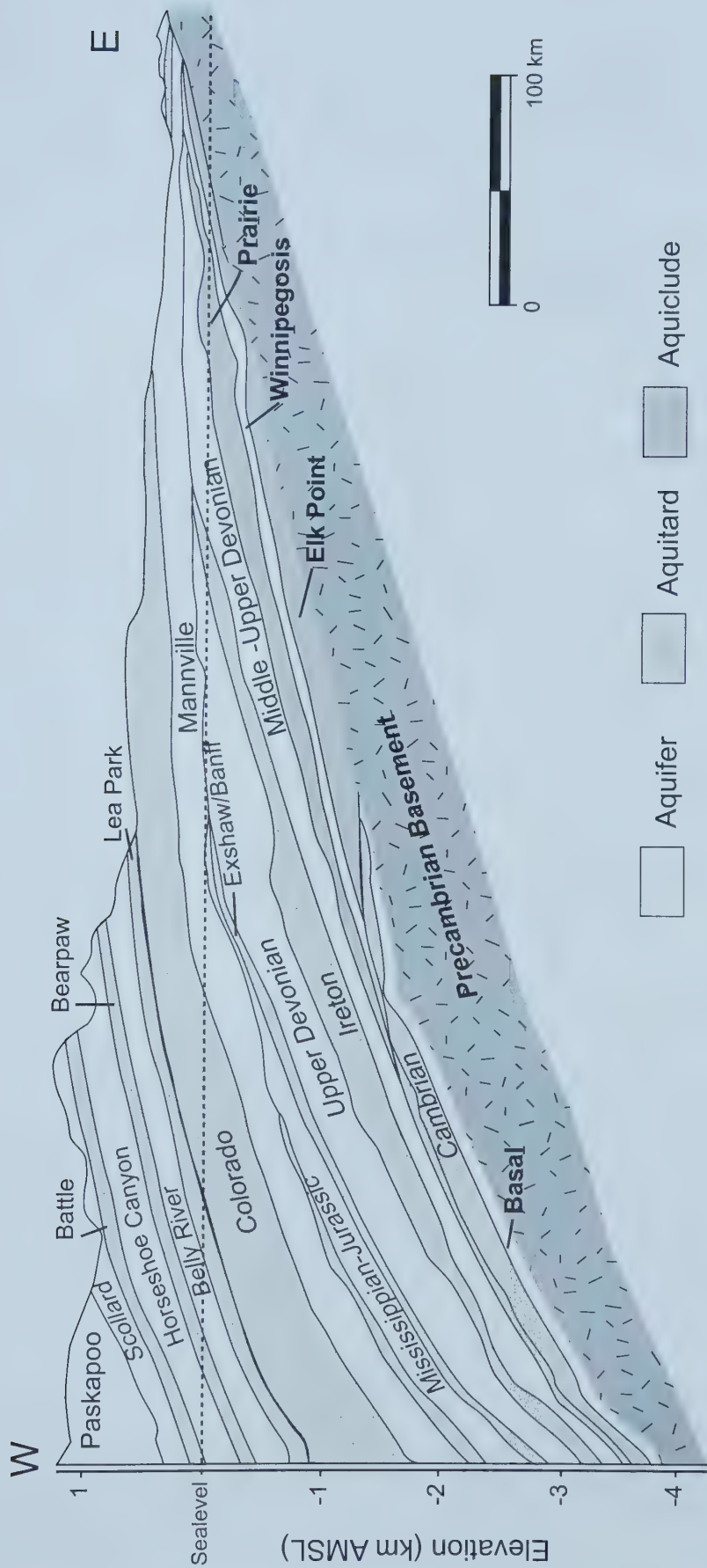


Figure 3.2: b) Generalized hydrostratigraphy for the central Alberta basin region (Modified from Bachu, 1995).

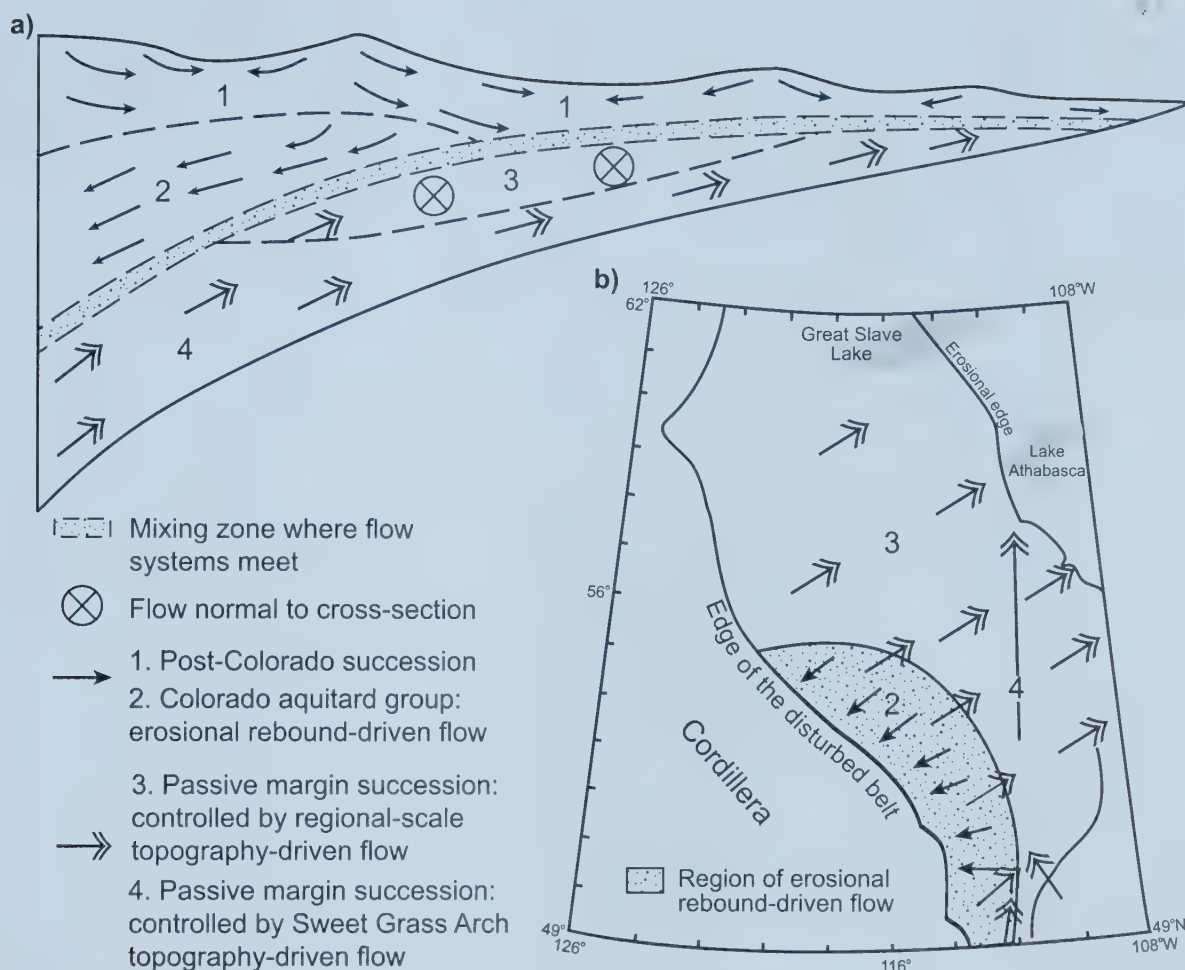


Figure 3.3: Present day fluid flow zones in the Alberta basin, a) along a cross-section through central Alberta; and b) in plan view (Modified from Bachu, 1995).

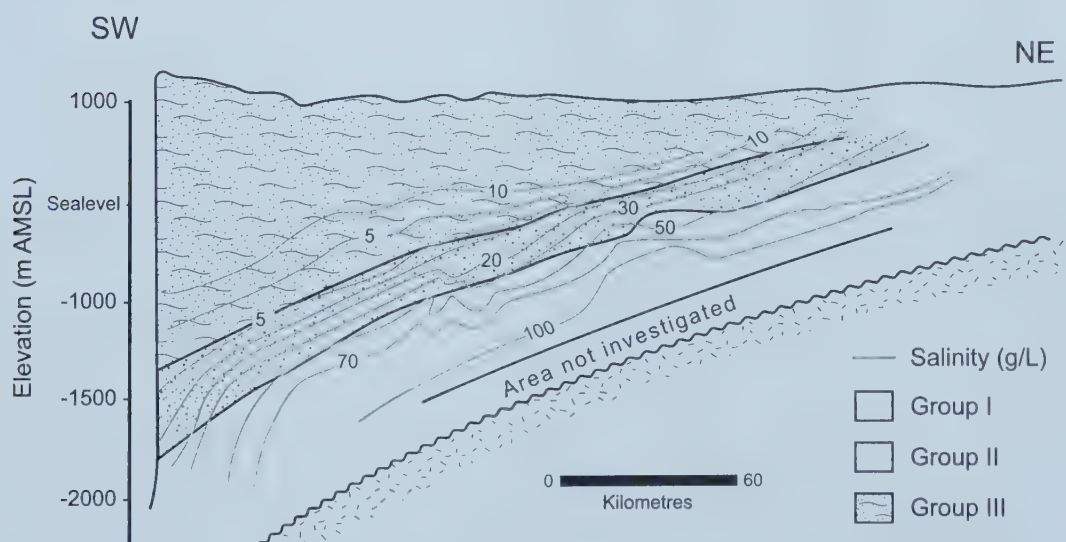


Figure 3.4: Cross-section through central Alberta basin, showing present day formation water salinity (Adapted from Connolly et al., 1990a). Shaded areas denote formation water Groups I to III as defined by Connolly et al. (1990a).

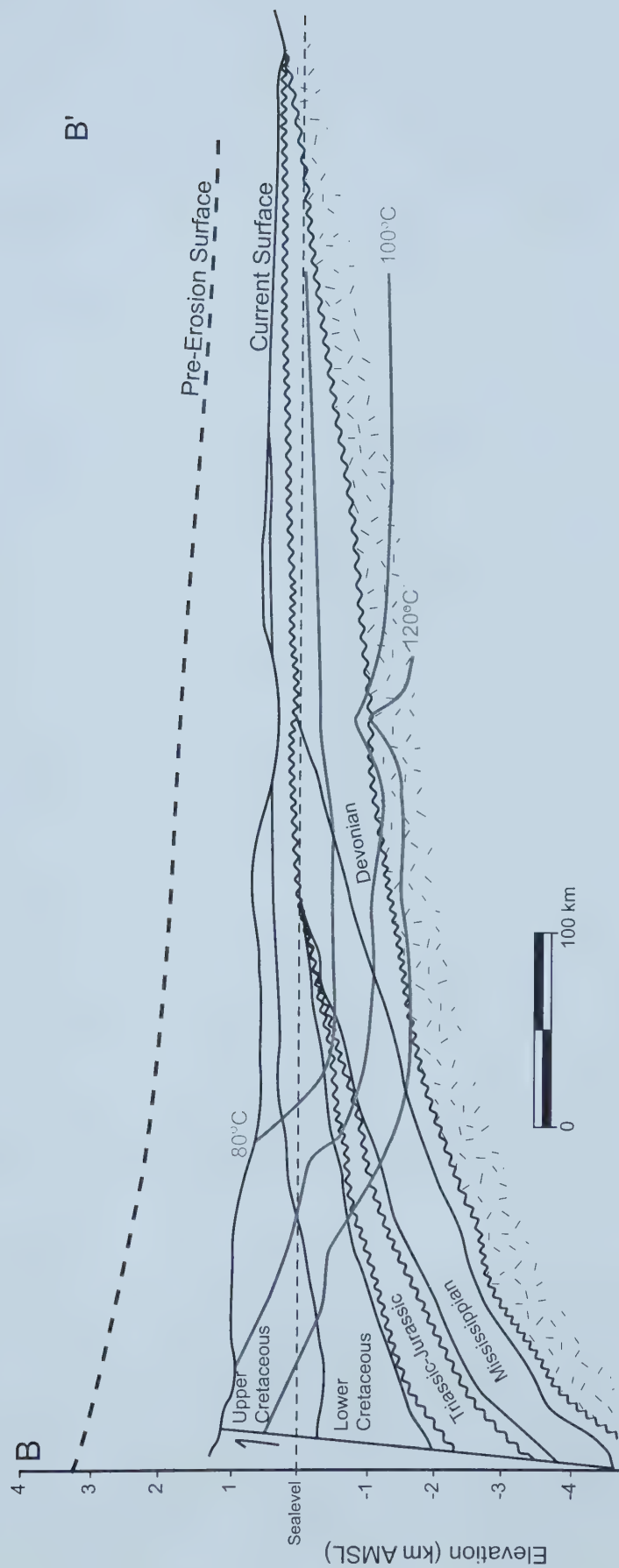


Figure 3.5: Apatite fission track data for the Peace River Arch section of the Alberta basin (Willet et al., 1997). The pre-erosion surface shown by a dashed line and is based on paleotemperatures at maximum Laramide burial temperatures at 80°C, 100°C, and 120°C. Jagged lines represent stratigraphic unconformities (Adapted from Willet et al., 1997.)

CHAPTER 4

PINE POINT, NWT

The successful development of a MVT ore district relies on the co-existence of large volumes of high salinity ore-forming fluids, warm temperatures and a robust, fluid driving force for the duration of mineralization in permeable, carbonate host rock. The high grades (5 to 10 wt%) and large tonnage in MVT deposits combined with low solubility of Pb and Zn in basinal brines suggest that a large volume of water is required for the formation of observed ore deposits (Anderson and Macqueen, 1982). Furthermore, metal-bearing fluids, usually Na-Ca-Cl brines, must contain at least 100 g/L Cl to complex metals at mineralization temperatures (75-200°C) (Hanor, 1996). The rate at which the metal-charged waters are delivered to the deposit site depends on the *driving force* and permeability of the *flowpath*. Estimation of this rate can be done from thermal anomalies recorded in some ore districts, which document advection of heat into the area by ore-forming fluids (Sangster et al., 1994). The ore formation process is accelerated or retarded by the overall efficiency of precipitation at the deposit site, which depends on the availability of chemical constituents and their ability to react. The localization of an ore district can be as much a function of geological structure and permeability, e.g., breccias, karst or local basement highs, as chemical traps, e.g., mixing zones, redox barriers or temperature and pressure changes.

4.1 Pine Point ore district

The Pine Point ore district is hosted by the Middle Devonian Presqu'île barrier complex, which separates the Mackenzie shale basin to the northwest and the Elk Point evaporite basin to the south. The reef complex outcrops just south of Great Slave Lake and extends into the subsurface of northern British Columbia (B.C.) (Figure 4.1; Qing, 1998a and others referenced). The barrier developed during the Middle Givetian in response to differential subsidence along the McDonald Fault zone that marks the boundary between the Slave and

Churchill Provinces (Hanmer, 1988). Over 80 Pb-Zn stratabound orebodies are found at the eastern end of the Presqu'île barrier reef, which consists of typical reef complex facies including diagenetic and epigenetic dolomites. In descending order, these are underlain by platformal carbonates of the Keg River Formation, Chinchaga anhydrite/dolomite sequence and basal clastics (Figure 3.2a; Skall, 1975).

Detailed descriptions of the ore and host rocks at Pine Point have been provided by many authors (Campbell, 1966; Jackson and Beales, 1967; Roedder, 1968; Beales and Jackson, 1968; Fritz and Jackson, 1972; Skall, 1975; Kyle, 1981; Rhodes et al., 1984; Sangster, 1988; Qing and Mountjoy, 1992; 1994a-c; Qing 1998a,b). The ore bodies are restricted to interconnected paleokarst networks found in the lower sections of the epigenetic Presqu'île dolomite that developed through preferential alteration of upper barrier limestones. This coarse (Presqu'île) dolomite occurs principally along the North and Main Hinges, which are subparallel to the McDonald Fault zone. Pre-mineralization karstification facilitated transmission of hydrothermal or ore-forming fluids responsible for extensive karstification and brecciation coincident with the hinge lines (Rhodes et al., 1984). Ore grade mineralization is restricted to the largest cavities of karst (Rhodes et al., 1984).

During the main ore stage, galena, sphalerite, marcasite and pyrite were emplaced pervasively into karst zones by open-space filling and replacement. This is supported by the fluid inclusions in sphalerite, which have homogenization temperatures of 50 to 100°C and salinities of 15-35 eq. wt% NaCl (Roedder, 1968; Kyle, 1981). Dissolution, fracturing and collapse of carbonates and sulphides accompanied the precipitation of saddle dolomite during mineralization (Krebs and Macqueen, 1984; Haynes and Kesler, 1987). Texturally and mineralogically identical saddle dolomite has been traced across the WSCB and can be considered a proxy for mineralization fluids (Aulstead et al., 1987; Nesbitt and Muehlenbachs, 1994b; Mountjoy et al., 1997). Sampling of saddle dolomite fluid inclusions along the Presqu'île barrier has revealed trends of decreasing homogenization temperatures (178°C to 92°C), associated with increasing $\delta^{18}\text{O}$ values (14‰ to 23‰ SMOW; Qing and Mountjoy, 1992). These data record the cooling of hot fluids flowing laterally, from northern B.C. to Pine Point, along the Presqu'île barrier.

The age of mineralization of Pine Point is controversial due to the variety of measured age dates using paleomagnetism, Rb-Sr analyses, Pb-isotopes, apatite fission track analysis, and stable isotopes (Kyle, 1981; Beales and Jackson, 1982; Cumming et al., 1990; Arne, 1991; Nakai et al., 1993; Symons et al., 1993; Nesbitt and Muehlenbachs, 1994a). If MVT formation is linked to orogenic activity adjacent to the parent basin, Pine Point could be related to either the Antler (Late Devonian-Early Carboniferous), or Laramide (Early Cretaceous-Late Tertiary) orogenies (Leach, 1999). The well-accepted genetic model for Pine Point mineralization holds that uplift of the western margin of the Alberta basin, during the Tertiary, caused a large gravity-driven flow system to propel warm metal-rich brines along the Middle Devonian carbonates to the Pine Point ore district (Garven, 1985; Qing and Mountjoy, 1992). This scenario is supported by formation water salinity patterns in the Middle Devonian aquifer today, which exhibit a low salinity tongue in the western portion of the barrier (Bachu, 1997). A numerical model of this scenario showed that ore at Pine Point could have accumulated over 0.5 to 5 million years, assuming 1 ppm of dissolved Pb and Zn in brines travelling updip along the barrier at rates of 1 to 10 m/yr (Garven, 1985).

Previous numerical modelling poorly honoured the geological, geochemical and hydrogeological character of the Pine Point section. Garven (1985) used hydraulic conductivity values two or three orders of magnitude larger than any other estimates for similar units in the basin, to maintain the temperature of the ore-forming fluid (Fowler, 1986). These flow rates completely flush the basin of saline water over the duration of mineralization, which is inconsistent with the presence of brines in the basin today (Connolly et al., 1990a). Formation temperatures of saddle dolomites along the barrier record a cooling trend towards Pine Point (Qing and Mountjoy, 1992), which is opposite to the temperature distribution predicted by Garven's model. In addition, Garven's model did not calculate coupled solute transport, which considers buoyancy forces generated by dense brines. Finally, only steady-state flow solutions have been considered for the Pine Point flow system. The short duration of mineralization of MVT deposits (30 000 to 5 million years) compared to the lifespan of a gravity-driven flow system, suggests that transient solutions best elucidate the dynamics of MVT mineralization (Appold and Garven, 1999).

To address these problems, Garven's Pine Point model was modified, using RIFT2D, a transient two-dimensional numerical model that couples fluid flow, heat flow and solute

transport (Person et al., 2000; see Appendix A for description of RIFT2D). Furthermore, an extensive sensitivity analysis was performed to quantify the influence of different basin components on a topography-driven flow system and to match temperature and salinity profiles recorded by saddle dolomite fluid inclusions. The resulting simulations are discussed in terms of aquifer flow rates, basin flushing patterns, duration of high salinity conditions and the maximum temperature reached in the ore district.

4.2 Numerical modelling

Garven (1985) developed a two-dimensional, finite-element model, which extends 500 km from Fort Nelson along the Presqu'île barrier to 50 km east of Pine Point (Figure 4.2). In the present study, Garven's *original* solution was reproduced (*replicated model*), using the transient RIFT2D model (Person et al., 2000). Based on estimated Laramide stratigraphy, the model domain is 3 km thick at the western boundary and thins to 1 km at the eastern boundary. The finite element mesh contains 10 rows and 41 variably-spaced columns (Figure 4.3a). Western, lower and eastern limits of the model domain were defined as no-flow boundaries. The upper limit of the model domain was assigned as a water table boundary, with a linear gradient of 0.002 m/m and the addition of approximately 500 to 1000 m of eroded material to the present day topography. A heat flux of 70 mW/m² was assigned along the lower boundary and a surface temperature of 20°C was imposed on the upper boundary (Figure 4.4b).

The stratigraphic sequence, in ascending order along the cross-section, includes a basal clastic unit, overlain by evaporitic dolomites, and the principal aquifer of Middle Devonian carbonates. These are capped by a thick succession of low permeability shales of the Ft. Simpson Formation, and interbedded Mississippian carbonates and shales. A thick package of Cretaceous, foreland, interbedded shales and sandstones lies on top of the Phanerozoic strata. Garven simplified this sequence into four hydrostratigraphic units: Middle Devonian aquifer, Upper Devonian aquitard, Mississippian shale and limestone moderate aquitard and Lower Cretaceous shale and sandstone aquitard (Figure 4.3a). Permeability anisotropy ($k_x:k_v$) was defined as 100:1 and other fluid flow and heat transport parameters are shown in Table 4.1. Garven's steady-state simulations calculated coupled fluid flow and heat flow, assuming a constant salinity gradient of approximately 0.01 eqv. wt% NaCl/m (Figure 4.4c). *Replicated*

model simulations of the Pine Point flow system used time steps of 200 years and Garven's salinity gradient only as an initial condition. (Input files for RIFT2D are in Appendix B.)

Replicated model simulations reach steady state 500 000 years after instantaneous uplift (Figures 4.3b & c). At the western end of the model, topographic elevation drives water downward across the Cretaceous aquitard and updip along the Middle Devonian aquifer, to discharge at the surface 400 km along the section. Calculated darcy velocities in the Middle Devonian aquifer reach 1 to 6 m/yr, in agreement with Garven's findings (1985). Water, heat and solute are preferentially conducted along the Middle Devonian aquifer, but a minor proportion of fluids move to the east in the Mississippian carbonates and shales. The temperature distribution is depressed by cool meteoric water in the foothills and elevated at shallow depths at the margins of the basin due to movement of warm basinal brines updip. Simulated temperatures at Pine Point range from 65 to 85°C at steady state, with a maximum transient temperature of 100°C. This agrees with fluid inclusion data from sphalerites (Roedder, 1968). The *replicated* model solution closely matches that shown in Garven (1985; Figures 4.3b-f). Any discrepancies between the two solutions can be attributed to differences in water density at steady state. The salinity of fluids was held constant depending on depth in the *original* model, whereas the *replicated* model contains only freshwater at steady state.

Table 4.1: Hydrostratigraphic parameters for Garven's (1985) original Pine Point model.

Hydrostratigraphic Unit	Porosity (%)	Horz. Hydraulic Conductivity* (m/yr)	Log Hydraulic Permeability (m ²)	Thermal Conductivity** (W/m·°C)	Longitudinal Dispersivity# (m)
Cretaceous shale & sandstone	15	25	-13.1	2.0	1
Mississippian shale & carbonates	10	50	-12.8	2.5	1
Upper Devonian shale	10	20	-13.2	1.9	1
Middle Devonian carbonates	25	1000	-11.5	3.0	1

* Anisotropy (k_x/k_z) was assigned as 100 for all units. Reference fluid density and viscosity are 998.2 kg/m³ and 1.0x10⁻³ Pa·s, respectively.

** Thermal conductivity of the fluid was defined as 0.63 W/m·°C for all units.

Transverse mass and heat transport dispersivities were defined as 0.1 for all units. The apparent diffusion coefficient was assigned as 3x10⁻³ m²/yr for all units.

Evolution of flow rates, flow paths, temperatures and salinity, following instantaneous uplift provides insight into the timing of ore-forming conditions at Pine Point. The flow system quickly adjusts from hydrostatic conditions to vertical flow in the recharge and discharge

zones, with the majority of flow along the principal deep aquifer. Initially in the deep basin, high temperatures drive heavy brines upward (Figure 4.5b,c), while meteoric water pushes brine out of the recharge zone and along the main aquifer (Figure 4.5b). Early in this flow system a slug of brine is advected along the Middle Devonian aquifer. This transport occurs slowly due to the high water density. The brine slug is followed by a slug of hot brackish water, which discharges from the basin after 180 000 years. The *replicated* model simulations show that maximum temperatures and maximum salinity values at Pine Point are not contemporaneous, suggesting no or little mineralization could take place (Figures 4.5 and 4.6). High temperature gradients around the heat slug locally increase darcy velocities, causing vertical flow which moves saline water towards the surface (Figure 4.5b). Transient simulations predict complete flushing of the Middle Devonian aquifer of brine, 160 000 years after instantaneous uplift and flushing of the basin with meteoric water after 475 000 years (Figures 4.5 and 4.11d). Generally, lateral flow rates increase as the brines are flushed out of the basin (Figure 4.5). Small oscillations in flow rate, temperature and salinity occur primarily at the Pine Point observation point and can be attributed to high Peclet numbers or poor refinement of the finite element mesh (Appendix C).

Garven concluded that this steady-state flow system could account for the formation of Pine Point assuming one million years of fluid flow. However, simulations of the transient *replicated* model show that ore-forming temperature and salinities exist together at Pine Point for a maximum of 50 000 years. To extend the duration of ore-forming conditions, either an additional heat source or a large solute source is needed to match measured conditions at Pine Point. No geological or geochemical evidence has been found to support significant halite dissolution near Pine Point (Telser, 1999). Similarly, no district-wide thermal anomalies have been reported at Pine Point (Sangster et al., 1994). Therefore, the Pine Point model must consider solute transport and the relationship between flow rates, temperatures and water salinity in the basin to determine a plausible ore-forming system.

4.3 Base case Pine Point model

Garven's application of a gravity-driven flow system to the formation of MVT deposits agrees with the understanding of tectonics in sedimentary basins world-wide. Garven's models predicted Pine Point ore temperatures by using unrealistic permeability values (Fowler, 1986); however, the models cannot match measured temperatures from saddle

dolomites along the barrier (Qing and Mountjoy, 1992). This study evaluates the ability of modifications to Garven's model to predict the formation of Pine Point, based on the probable duration of ore-forming conditions at Pine Point. Accordingly, a modified model must deliver at least 12 eqv. wt% NaCl brine at temperatures close to 100°C through Pine Point for an adequate period of time to account for observed ore tonnage (Chapter 2). The transient nature of an MVT flow system is investigated using simulations of coupled fluid flow, heat flow and solute transport. The simplified hydrostratigraphy and basin shape makes this model unsuitable to calibrate with detailed geochemical data from Pine Point; however, agreement with generalized observations is a requirement.

To consider solute transport, the finite element mesh and dispersivities in the *replicated* model were revised to minimize numerical error in solute transport solutions (*base case* model). The finite element mesh was refined to $\Delta x = 2500$ m, and $\Delta y = 50$ to 160 m (see Appendix C for Peclet numbers). Aquifer longitudinal and transverse dispersivities were increased to 100 and 10 m, respectively, except in the Middle Devonian aquifer, in which the longitudinal dispersivity was defined as 240 m (Table 4.2). Aquitard dispersivities were assigned uniformly as 10 m, which better approximate the scale of heterogeneities in a regional-scale flow system than Garven's values. The model domain was left unaltered, because Garven's topography is approximately the average between estimated maximum Laramide uplift and present day topography (Issler et al., 1999). The hydrostratigraphy was not adjusted to fit published sections (Bachu, 1997), which are too complex for this study and do not assume that the Presqu'ile barrier is the principal conduit of paleoflow.

Table 4.2: Hydrostratigraphic parameters for the *base case* Pine Point model.

Hydrostratigraphic Unit	Porosity (%)	Horz. Hydraulic Conductivity* (m/yr)	Log Hydraulic Permeability (m ²)	Thermal Conductivity** (W/m·°C)	Longitudinal Dispersivity# (m)
Cretaceous shale & sandstone	15	25	-13.1	2.0	100
Mississippian shale & carbonates	10	50	-12.8	2.5	100
Upper Devonian shale	10	20	-13.2	1.9	100
Middle Devonian carbonates	25	1000	-11.5	3.0	240

* Anisotropy (k_x/k_z) was assigned as 100 for all units. Reference fluid density and viscosity are 998.2 kg/m³ and 1.0x10⁻³ Pa·s, respectively.

** Thermal conductivity of the fluid was defined as 0.63 W/m·°C for all units.

Transverse mass and heat transport dispersivities were defined as 10 for all units. Apparent diffusion coefficient was assigned as 3x10⁻³ m²/yr for all units.

The *base case*, with a refined mesh and realistic dispersivities, provides a more accurate solution than the *replicated* model, e.g., flow in the Mississippian aquitard is better delineated (Figure 4.7b and c). Generally, the *base case* flow rates are higher in the western part of the aquifer than in the *replicated* model because meteoric water replaces heavy, deep-basin brines (Figure 4.9). Temperatures are slightly lower across the Middle Devonian aquifer reflecting higher darcy velocities (Figure 4.10). Higher dispersivities eliminate flow-rate oscillations seen at Pine Point in the *replicated* model and elongate the heat slug, thereby reducing local vertical flow (Figure 4.9d). Two temperature and solute maxima, representing the slugs of brine and temperature being flushed from the basin, are still evident in transient plots at barrier observation points (Figures 4.10 and 4.11). The *base case* simulations are similar to those of the *replicated* model (comparison of Figures 4.9 to 4.11); however, small variations between the two solutions may be due to placement of observation points in each model. Larger differences in flow rate can be attributed to refinement of the grid in the *base case* model. Because of relatively close agreement, the *base case* model is considered to be a proxy for the *original* model, in simulations of transient solute transport.

Transient *base case* solutions again show that Garven's model cannot match measured temperatures and salinity values for the duration of mineralization at Pine Point. In the *replicated* model, ore-forming fluids passed through Pine Point, 20 to 60 thousand years following instantaneous uplift (Figure 4.8). During this period, the lowest flow rates and temperatures are predicted at Pine Point (Figures 4.9 and 4.10). To account for the ore grade and tonnage at Pine Point using this model, the ore-forming brine would have to have been carrying a minimum of 100 ppm of Zn, which is 10 to 100 times the maximum estimated metal concentrations in ore-forming fluids.

4.4 Variations on the base case

MVT ore districts document co-existence of large volumes of warm, high-salinity ore-forming fluids, propelled through the host rock by a robust driving force for the duration of mineralization. The transient simulations of the *replicated* model do not predict any overlap between high temperature and salinity within the Pine Point ore district. Recent modelling of the Missouri ore district showed that the coincidence of high temperatures and salinity in a topography-driven flow system was short-lived and rare (Appold and Garven, 1999).

Variations of permeability, basin shape, solute distribution and other parameters may allow for the prediction of ore-forming conditions at Pine Point. Some sample simulations were run to ensure that the *base case* solution did not reflect boundary condition influence (*pinchout* model: Appendix D). Although better defined boundary conditions and extension of the model domain to the east might produce a better solution, the computer time required for these models was prohibitive (Appendix E) and the Cretaceous configuration of strata to the east is unknown. Therefore, the following sensitivity analysis of the *base case* model investigates the effects of varying permeability, heat and solute transport parameters to establish other significant controls on the flow rate, temperature and salinity distributions at the ore district (Table 4.3). Each scenario is evaluated in terms of its ability to predict both Pine Point mineralization and present day salinity patterns.

Table 4.3: Sensitivity analysis for the *base case* Pine Point model. The $\log(k_{\text{tard}}):\log(k_{\text{fer}})$ ratio is calculated by averaging the aquitard permeabilities and dividing by the Middle Devonian aquifer permeability. 'NA' means 'not applicable'.

Model Name	Parameter Varied	$\log(k_{\text{tard}}):\log(k_{\text{fer}})$
Permeability variations:		
<i>High permeability</i>	Middle Devonian aquifer permeability increased to $10^{-10.5}\text{m}^2$	1.24
<i>Low permeability</i>	Middle Devonian aquifer permeability decreased to $10^{-12.5}\text{m}^2$	1.04
<i>All low permeability</i>	All permeabilities decreased by one order of magnitude	1.13
<i>Measured permeability</i>	All permeabilities defined as maximum measured permeability	1.23
<i>Funnel</i>	Middle Devonian permeability gradually increased west to east	NA
Temperature variations:		
<i>High thermal conductivity</i>	Thermal conductivity of each unit increased by $0.5 \text{ W/m}\cdot^\circ\text{C}$	1.13
<i>Low thermal conductivity</i>	Thermal conductivity of each unit decreased by $0.5 \text{ W/m}\cdot^\circ\text{C}$	1.13
<i>Medium heat flux: 85 mW/m²</i>	Basal heat flux was increased to 85 mW/m^2	1.13
<i>High heat flux: 100 mW/m²</i>	Basal heat flux was increased to 100 mW/m^2	1.13
Salinity variations:		
<i>Salinity</i>	Middle Devonian has constant initial salinity of $0.25 \text{ g NaCl/g H}_2\text{O}$	1.13
<i>Deep basin</i>	Western lower boundary deepened by 250 m	1.13
<i>Basement</i>	1 km thick package of basement rock added to lower boundary	1.13

4.4.1 Permeability variations

Permeability of the Middle Devonian aquifer most significantly affects the volume of fluid that passes through the Pine Point ore district during mineralization or the darcy velocity of a system. The *original* model required high permeabilities to advect heat into the Pine Point ore district; however, measured regional permeabilities within the Alberta basin are orders of magnitude lower than Garven's original values (Table 4.1; Bachu and Underschultz, 1992). Estimated permeabilities for the Middle Devonian aquifer, based on core plug

measurements, vary from $10^{-11.5}$ to 10^{-16} m², making Garven's value of $10^{-11.5}$ a maximum. Similarly, maximum measured permeabilities of overlying aquitards are $10^{-14.9}$, $10^{-13.5}$ and 10^{-14} m² for the Fort Simpson, Mississippian and Cretaceous aquitards, respectively. For these reasons, a variety of low permeability scenarios are discussed in terms of the ratio of average aquitard permeability to barrier permeability ($\log(k_{\text{tard}}):\log(k_{\text{fer}})$), which is unity for a homogeneous model.

To delay flushing of the basin, the permeability of the Middle Devonian aquifer was reduced by an order of magnitude to $10^{-12.5}$ m² (*low permeability case*). At steady state, the *low permeability* flow system resembles that of the *base case*; however, lateral flow across the basin is divided almost evenly between the Mississippian and Middle Devonian units. This behaviour can be attributed to the almost equivalent permeability of the Middle Devonian and Mississippian units and a $\log(k_{\text{tard}}):\log(k_{\text{fer}})$ ratio of 1.04. Steady-state flow rates decrease accordingly by one order of magnitude across the aquifer, keeping the temperature at Pine Point just above 60°C (Figures 4.15 and 4.16). Temperatures are lower at Pine Point than the *base case*, but in the rest of the model they are consistently higher, suggesting that little heat is being transferred by advection. Transient solutions show that solute is swept from the basin like a squeegee, i.e., the Middle Devonian aquifer is not flushed more quickly than the rest of the basin (Figure 4.12c). Complete flushing of the Middle Devonian aquifer occurs after 800 000 years and flushing of the basin with meteoric water after 900 000 years (Figure 4.17). Despite lower flow rates, the total solute mass flux through Pine Point increases 45% over the *base case* flux, because barrier brines are less diluted by meteoric water. High salinity, ore-forming conditions persist for approximately 700 000 years; however, Pine Point temperatures are cool, and ultimately the basin is flushed of brine.

Maintaining a high $\log(k_{\text{tard}}):\log(k_{\text{fer}})$ ratio promotes advection of heat and solute along the barrier; however, permeability values of all model units are much higher than regional values calculated from measured cores (Bachu and Underschultz, 1992; Bachu, 1997). In the *all low permeability* case, permeabilities for each hydrostratigraphic unit were decreased by one order of magnitude, thereby keeping the permeability ratio constant (1.13). Transient simulations exhibit identical flow and flushing patterns to the *base case*, but flow rates are 10 times slower (Figure 4.15). The steady-state temperature distribution is dominantly conductive, causing slightly higher temperatures at Pine Point. The aquifer is preferentially flushed 2 million

years after instantaneous uplift and the basin is flushed with fresh water after 2.7 million years. Flow rates are always less than 0.3 m/yr, yet the total solute mass flux through Pine Point increases 75% in relation to the *base case*. High salinity conditions are maintained for only 850 000 years, although low salinity fluids pass through Pine Point for an additional one million years. The decrease in flow rates results in a 20% increase in total solute mass through Pine Point, compared to the *low permeability case*.

Comparison of the *low permeability* and *all low permeability* cases shows that the contrast between the Middle Devonian aquifer permeability and the permeabilities of the overlying aquitards significantly affects flushing patterns in the basin. Assigning maximum measured permeabilities to each unit (Table 4.4) produces a larger permeability contrast than in the *base case*. The $\log(k_{\text{tar}}):\log(k_{\text{fer}})$ for this scenario (*measured permeability case*) is 1.23, approximately the same ratio as found in the *high permeability case* (Table 4.3). In both cases, the increased permeability ratio promotes vertical flow into the barrier, which funnels heat and solute from the deep basin along the barrier (Figure 4.13). Lower permeabilities in overlying aquitards limit the flow rates, e.g., in the *high permeability case*, flow rates range from 10 to 12 m/yr, which are only 2 times, rather than 10 times, faster than the *base case* rates (Figure 4.15). Similarly, the *measured permeability* rates are 2 times slower than the *base case* rates, despite their common barrier aquifer permeability.

Table 4.4: Hydrostratigraphic parameters for the *measured permeability case* Pine Point model.

Hydrostratigraphic Unit	Porosity (%)	Horz. Hydraulic Conductivity* (m/yr)	Log Hydraulic Permeability (m ²)	Thermal Conductivity** (W/m·K)	Longitudinal Dispersivity# (m)
Cretaceous shale & sandstone	15	3	-14	2.0	100
Mississippian shale & carbonates	10	10	-13.5	2.5	100
Upper Devonian shale	10	1	-14.5	1.9	100
Middle Devonian carbonates	25	1000	-11.5	3.0	240

* Anisotropy (k_x/k_z) was assigned as 100 for all units. Reference fluid density and viscosity are 998.2 kg/m³ and 1.0x10⁻³ Pa·s, respectively.

** Thermal conductivity of the fluid was defined as 0.63 W/m·K for all units.

Transverse mass and heat transport dispersivities were defined as 10 for all units. Apparent diffusion coefficient was assigned as 3x10⁻³ m²/yr for all units.

Despite similar permeability ratios, temperatures in the *measured permeability case* remain high due to low flow rates, whereas the *high permeability case* predicts temperatures below 60°C at Pine Point (Figure 4.16d). Garven (1985) demonstrated that temperature at Pine Point is a

function of flow rate (Figure 4.16e), such that a maximum temperature can be attained with a Middle Devonian permeability of $10^{-11.7} \text{ m}^2$. Garven's function is asymmetric, predicting more significant decreases in temperature at hydraulic conductivities greater than the optimal value. This relationship holds true for both *low* and *high permeability* cases, whereas the *measured permeability* case predicts lower flow rates for an identical aquifer permeability, but slightly higher temperatures. This discrepancy can be attributed to having altered the overlying aquitard permeability and ostensibly changing the curves. The permeability in the *high permeability* case generates flow rates that do not allow water to be heated by basal heat flow. Flushing of solute in the *high permeability* case occurs within 50 000 years, which is ridiculously fast (Figure 4.17). The *measured permeability* flushing pattern shows preferential flow along the barrier; however, the extremely low permeability of the overlying Ft. Simpson shale inhibits infiltration of meteoric water into the barrier (Figure 4.13c). The shale also limits movement of saline fluids into the barrier, resulting in a 17% decrease in total solute mass flux through Pine Point compared to the *base case*.

The Pine Point model assumes that the Presqu'île barrier acted as a tubular conduit for ore-forming fluids to Pine Point. In fact, the barrier narrows from a width of 250 km near Fort Nelson to 10 km at Pine Point, which effectively increases the volume of saline fluids. A *funnel* model was developed to test the effect of the barrier as a gradually narrowing conduit towards Pine Point, similar to modelling done in the Illinois basin (Bethke, 1986). Funnelling can be simulated in a 2D model by increasing the barrier permeability to reflect the increased volume of water being funnelled through the barrier. In the *funnel* model, the barrier aquifer is divided into five zones of permeability ranging from $10^{-12.8}$ to $10^{-11.5} \text{ m}^2$ (Figure 4.14a). The westernmost 200 km of the barrier is assigned the same permeability as the Mississippian aquitard, whereas the permeability at Pine Point is identical to the *base case* (Figure 4.14b).

At steady state, the *funnel* flow pattern follows the Mississippian aquifer then moves down into the Middle Devonian aquifer, reaching flow rates greater than 3 m/yr at Pine Point (Figure 4.14c). The temperature distribution reflects cooling of the deep basin by meteoric water; however, a large slug of hot brine gets trapped between 50 and 200 km along the section (Figure 4.14d). A large component of meteoric water entering the Devonian, just past 200 km, cools subsurface temperatures significantly. Interpretation of the flushing

pattern and duration of ore-forming conditions is difficult: no correction was made for the additional volume of saline water housed in the funnel-shaped barrier prior to uplift. Flushing at Pine Point occurs by 400 000 years, but a slug of brine trapped in the deep basin, slowly feeds the aquifer with low salinity fluids for a long period of time (Figures 4.14e and 4.17c-d). The implications of the trapping include a long period of low salinity at Pine Point and much lower maximum salinity values at Pine Point, attributed to dilution of deep basinal brines downdip of Pine Point.

Permeability Conclusions

Permeability variations of the *base case* show that permeability dramatically affects not only flow patterns and rates, but also temperature and salinity distributions. To address the criticism of Garven's effectively high permeabilities, either the barrier permeability was decreased or all permeability values were adjusted to measured values. In all cases, the duration of the ore-forming conditions at Pine Point lengthened and the total mass flux of solute through the ore district increased. Simulations with barrier permeabilities less than $10^{-12.4} \text{ m}^2$ predict primarily conductive heat flow, which eliminates any temporal offset between the temperature and brine slugs; however, predicted Pine Point temperatures are low ($\sim 60^\circ\text{C}$). The *measured permeability* model generates higher temperatures than the *base case* at Pine Point due to the low permeability of overlying units, but maximum temperatures and salinity values are not concomitant at Pine Point. In the low permeability models, conductive heat flow is transported by conduction.

Comparison of the permeability simulations reveals that increasing $\log(k_{\text{tard}}):\log(k_{\text{fer}})$ promotes vertical flow at recharge and discharge zones, causing preferential flushing of the aquifer, whereas low $\log(k_{\text{tard}}):\log(k_{\text{fer}})$ values decrease vertical flow, resulting in flushing of the basin like a squeegee. High permeability contrasts due to low aquitard permeability cause lower aquifer flow rates and preferentially flush the overlying units. The *funnel* scenario predicts a disconnected flushing pattern, which develops due to a low permeability contrast in the deep basin and high contrast at Pine Point. Poor approximation of solute volumes in the *funnel* model makes the solution inconclusive in terms of Pine Point mineralization.

Generally, lowering the permeability of the barrier aquifer and/or overlying aquitards slows flow rates and moderates temperatures. These simulations also predict the presence of high

salinity fluids at Pine Point for approximately 1 million years; however, flushing of the basin occurs within 2 million years, which does not explain the current observed salinity profile. An additional drawback of the slow flow rates is lower mineralization temperatures, but applying higher heat flow conditions could increase these temperatures.

4.4.2 *Temperature variations*

In previous modelling (Garven, 1985), temperature anomalies measured in MVT ore have been simulated by increasing advective heat transfer, i.e., adjusting aquifer permeabilities. Alternative methods of increasing temperatures in the ore district include varying the thermal conductivity, surface temperature and basal heat flux. The following section explores the influence of thermal conductivity and higher heat fluxes on this system. Surface temperature variations will not be considered in this analysis, because any uniform adjustment of surface temperature across the top of the model causes the subsurface temperature at all times and depths to uniformly increase or decrease by the same increment made in the surface temperature.

Thermal conductivity and heat capacity mediate heat flow through any substance. Values for sedimentary rock vary from 0.8 to 6.3 W/m·K (Blackwell and Steele, 1989), and in the Alberta basin average thermal conductivity varies from 1.4 in the west to 2.0 W/m·K in the east (Bachu, 1993). Based on lithology, the Middle Devonian aquifer and Mississippian aquitard should have higher thermal conductivity values and the other aquitards lower values. For Garven's model, average thermal conductivity for the section is 2.3 W/m·K. For this sensitivity analysis, the thermal conductivity of each unit was increased by 0.5 in the *high thermal conductivity* model and decreased by 0.5 in the *low thermal conductivity* model.

Both thermal conductivity cases predict the same steady-state hydraulic heads as the *base case*. At steady state, temperatures and flow rates in the three thermal conductivity cases only differ significantly at Pine Point (Figures 4.21 to 4.23). To start, the *high thermal conductivity* temperatures are slightly cooler than the *base case* (Figure 4.22), whereas *low thermal conductivity* case temperatures are warmer. The *high thermal conductivity* case easily allows meteoric water into the deep basin, but flow rates along the barrier remain low due to a negligible lateral temperature gradient. In the *low thermal conductivity* case, high temperatures in the deep basin initially inhibit penetration of meteoric water into the barrier (Figure 4.18). Thus over time,

a long, flat heat slug develops in the barrier, generating a high lateral temperature gradient, which provides a greater lateral driving force for fluid movement than in the *base case* (Figure 4.19). In both cases, the heat and brine slugs move along the barrier more slowly than the *base case*. The effect of thermal conductivity compounds towards Pine Point, e.g., at steady state, the *low thermal conductivity* temperature at Pine Point is 20°C higher than the *high thermal conductivity* model, but deep basin temperatures match the *base case* (Figure 4.22d). The *high thermal conductivity* case temperatures at Pine Point reach 60°C at steady state, whereas the *low thermal conductivity* case temperatures reach 90°C. In both the *high* and *low thermal conductivity* cases, the basin is flushed more slowly, but in the same pattern, as the *base case*. Slower flow rates and minimal vertical temperature gradients in the heat slug, in the *high thermal conductivity* case, keep saline fluid in the barrier for longer. In the *low thermal conductivity* case, early high vertical temperature gradients in the deep basin slow flow initially and the long, flat heat slug then diminishes vertical flow into overlying aquitards. Total solute mass flux of the *low thermal conductivity* case is 94% greater than the *base case* and the *high thermal conductivity* case is 54% greater. *Low thermal conductivity* case retains heat, slows flushing and increases flow rates, all of which enhance ore-forming processes at Pine Point.

Alternatively, high flow rates to transport heat to Pine Point are not required with higher basal heat fluxes. Basal heat fluxes vary across a basin depending on the thermal connectivity of basement structures to the mantle (Bachu, 1993). Intracratonic basins typically experience basal heat fluxes of 40 to 70 mW/m² (Garven et al., 1993); however, downhole measurements of heat fluxes around the Great Slave Lake shear zone are as high as 120 mW/m² (Lewis and Hyndman, 1999). Modelled fluxes greater than 120 mW/m² predicted temperatures at Pine Point greater than measured ore mineralization temperatures, thus two cases are presented: 85 and 100 mW/m².

Both high heat flux simulations generate solutions with higher temperatures than the *base case*. At Pine Point, the *high heat flux* case reaches over 100°C and maintains a temperature of ~90°C at steady state, whereas the *medium heat flux* case reaches a maximum of 90°C and settles at 80°C (Figure 4.22). Again, as in the *low thermal conductivity* case, high temperatures in the deep basin retard flushing, but increase barrier flow rates. The long, flat heat slug dampens local upwards flow along the barrier, which results in higher salinities and total solute mass flux 89% greater than the *base case* (Figure 4.20). The *medium heat flux* case

(Figures 4.21 to 4.23) predicts almost identical flow rate, temperature and salinity solutions as the *low thermal conductivity* case. The *high heat flux* case (Figure 4.20) produces higher flow rates than the *medium heat flux* case, which flush brines out of the basin more quickly, but has no effect on total solute mass flux. Thus, a basal heat flux no greater than 85 mW/m² is necessary to maximize the mass flux and predict ore-forming temperatures at Pine Point.

Temperature Conclusions

Either lowering thermal conductivities or increasing basal heat fluxes increases transient and steady-state temperatures in the barrier compared to the *base case*. Higher temperatures delay infiltration of meteoric water into the deep basin, resulting in slower flushing of saline waters. The development of a long, flat heat slug diminishes local vertical flow observed in the *base case*, which both contains salinity within the barrier and increases lateral flow rates. Adjustment of the temperature parameters does not change the flushing pattern appreciably from that of the *base case*. Higher flow rates and greater solute mass flux in these models suggest that integration of high heat fluxes or lower conductivity values could be combined with a low barrier permeability to better simulate the Pine Point flow system.

4.4.3 Salinity variations

Garven's conceptual model maintains that brines moving along the Presqu'île barrier transport Pb and Zn to Pine Point. At temperatures near 100°C, minimum chloride concentrations in these brines would need to be 100 g/L to complex at least 1 ppm Zn or Pb (Hanor, 1996). Assuming that the metal-bearing brine is dominantly NaCl, a mass fraction of 0.12 g NaCl/g H₂O would be the minimum concentration for chloride complexation of metals. In the *base case*, these high salinity conditions exist at Pine Point for only 50 000 years. Various temperature and permeability scenarios can extend the duration of high salinity conditions at Pine Point; however, basin shape and initial salinity conditions may also be able to prolong ore-forming salinity conditions.

A wide range of salinities and brine types exists in the Alberta basin today. Generally, salinities gradually increase with depth; however, 100 to 150 g/L brines reside in the Middle Devonian strata near surface today. Thus, the basic salinity gradient applied to the Pine Point models underestimates the total salinity in the basin. In the *salinity* model, the barrier aquifer is assigned an initial salinity of 0.25 g NaCl/g H₂O (Figure 4.24a). The steady-state

solution for the *salinity* model is identical to the *base case* solution due to complete flushing of the brine. However, transient simulations predict slower flow rates soon after uplift due to high-density barrier brines. These lower flow rates limit advective heat transport, causing high temperatures in the deep basin and lower temperatures at Pine Point. Again, the *base case* flushing pattern is observed and the two western observation points document the same fluid evolution as the *base case*. The duration of mineralization at Pine Point is prolonged by defining a uniform initial salinity of 0.25 g NaCl/g H₂O along the barrier and delaying flushing with lower flow rates in the barrier. These two factors increase the total solute mass flux by 15% compared to the *base case*, extending the high salinity conditions until 65 000 years; however, no comparison can be made with the present day salinity distribution because the barrier is flushed after 300 000 years.

In the Alberta basin, the slope of the basement increases sharply near the disturbed belt. Garven's section does not extend far enough to the west to include the thicker basin, in which a 2 km-thick package of early Devonian shelf carbonates have been preserved and may have acted as a source of warm, hypersaline brines. In the *deep basin* model (Figure 4.25b), the lower boundary was deepened by 250 m at the western, margin of the model domain and curved up to meet the original boundary at 40 km. This 8% depth increase produces much hotter temperatures through time and at steady state. High temperatures and brine densities in the deep basin delay movement of the heat and brine slugs along the barrier (Figures 4.29d and 4.30d). At Pine Point, 10°C variations in temperature occur from 100 000 to 200 000 years after uplift. At steady state, the highest temperatures in the barrier (~90°C) are located between 250 and 400 km (Figure 4.26). The flushing pattern mimics that of the *base case*; however, the *deep basin* model results in 19% more solute moving through Pine Point than in the *base case*. Thus, this relatively small change in model domain shape has a significant effect on temperatures and salinity at Pine Point. Deepening of the basin only occurs in the Alberta basin adjacent to the disturbed belt, and therefore this scenario is only truly applicable to a longer model, extending to the west, which would increase the topographic gradient.

The involvement of basement rocks in sedimentary basin flow systems is poorly understood. Studies of the Upper Mississippi Valley ore district have found evidence for large-scale fluid flow through the basement rock adjacent to the Mt. Simon aquifer, feeding the ore district

(Fishman, 1997). Recent numerical modelling of the Missouri Pb-Zn deposits included approximately 6 km of basement rock in the flow system (Appold and Garven, 1999). Along the modelled Pine Point section, an evaporite-redbed sequence and the Precambrian basement underlie the Middle Devonian aquifer. Despite the predominately low permeability of these units, diffusion or leakage into the overlying strata may considerably affect the salinity profile in the basin over long periods of time. In the *basement* model (Figure 4.25a), 1 km of low permeability strata ($k = 10^{-20} \text{ m}^2$) was added arbitrarily to the lower limit of the model. The salinity gradient was left as in the *base case*, assigning high salinities in the basement.

For early time, the *basement* model solution is relatively similar to the *base case*, especially in the western part of the basin (Figure 4.27). After 50 000 years, high-density fluids continue to retard travel of the heat slug up the barrier and keep flow rates low (Figure 4.28c-d). These slightly lower flow rates reduce advective heat transport. The influence of temperature and brine slugs on the flow system is significantly dampened in the *basement* case (Figures 4.29 and 4.30). The flushing pattern is close to the *base case* pattern for 60 000 years and then leakage of the basement fluids into the barrier aquifer provides additional solute and delays flushing of the basin (Figure 4.27d). The slow influx of saline fluids from the basement prolongs the saline conditions at Pine Point for over 10 million years and increases total solute mass flux by 26% over the *base case*. The rate of discharge from the basement to the aquifer is dependent on basement permeability. The duration of the discharge is also a function of thickness of basement active in the flow system or volume and salinity of basement brines. Increasing basement permeability would affect the *base case* flushing pattern earlier and may prolong ore forming conditions at Pine Point.

Salinity Conclusions

Additional sources of salinity, in the deep basin, basement and along the barrier, prolong the period of ore formation in this model; however, the flushing patterns remain unaffected during mineralization. In all cases, flow rates are dampened by high-density brines, resulting in equal or higher temperatures at Pine Point. The *salinity* model increases the volume of solute passing through Pine Point by 15%, which is not significant. Deepening the model domain a small amount moderately increases temperatures and salinities along the section and moves the highest heat zone down dip. Adding a basement unit on the model increases

the mass flux by 26% and prolongs the flushing for many millions of years. Further analysis of this scenario would require constraints on permeability, thickness and salinity values for the basement.

4.5 Discussion

Based on simulations, Garven (1985) concluded that a topography-driven flow system could have transported the observed tonnage of ore at Pine Point. Garven's solution predicts measured mineralization temperatures at Pine Point, but ignores formation water salinity. The goal of remodelling Garven's Pine Point flow model was to ascertain the feasibility of topography as a driving force to account for ore mineralization temperatures, 80 million tonnes of ore and ore-forming fluid composition at Pine Point. For this study, we have assumed that the minimum conditions for ore formation are a water salinity of 0.12 g NaCl/g H₂O, and temperature of 60°C; however, a maximum temperature of at least 80°C would be better. In addition, based on recent studies (Bachu and Underschultz, 1992; Bachu, 1997), permeability values used by Garven are considered to be too high for the aquitard succession; therefore, simulations with lower permeabilities are preferred. In the *base case*, mineralizing conditions existed for only 50 000 years. Therefore, 100 ppm Zn-Pb brines are required to account for Pine Point ore tonnage. Reasonable mobile metal concentrations range from 1 to 10 ppm Zn-Pb, dictating that the total solute mass flux through Pine Point actually be at least 10 times that of the *base case*.

Sensitivity analysis of the Pine Point model has shown that incorporation of observed basin features or measured values into the *base case* model lengthen the duration of ore formation by increasing salinity, maintaining temperatures and/or decreasing flow rates at Pine Point. Lowering the permeability of each hydrostratigraphic unit or the barrier decreased flow rates, increased solute mass flux and increased temperatures at Pine Point, predicting ore-forming conditions for 0.5 to 1 million years (Table 4.5). Increasing the basal heat flux or lowering thermal conductivity had the most beneficial effect on the ore-forming flow system. These modifications increased temperatures and flow rates and doubled the total solute mass flux. However, these permeability values are probably too high. Moderate increases in solute mass flux were obtained by deepening the basin, adding a basement unit, increasing the salinity in the barrier and funnelling fluids into the barrier.

Table 4.5: Variations on the *base case* Pine Point model. Total solute mass fluxes, maximum temperatures and average flow rates were calculated only during ore-forming conditions defined as salinity of at least 0.12 g NaCl/g H₂O. All values are measured at observation point 4 at Pine Point.

Model Name	Normalized total solute mass flux	Maximum temperature (°C)	Average flow rate (m/yr)	log(k_{tard}):log(k_{fer})
<i>Base case</i>	1.00	68	2.10	1.13
Permeability variations:				
<i>High permeability</i>	0.88	71	4.48	1.24
<i>Low permeability</i>	1.45	62	0.25	1.04
<i>All low permeability</i>	1.75	64	0.22	1.13
<i>Measured permeability</i>	0.78	69	0.78	1.23
<i>Funnel</i>	0.36	60	0.62	NA
Temperature variations:				
<i>High thermal conductivity</i>	1.54	60	2.01	1.13
<i>Low thermal conductivity</i>	1.94	84	2.57	1.13
<i>Medium heat flux (85 mW/m²)</i>	1.90	81	2.52	1.13
<i>High heat flux (100 mW/m²)</i>	1.89	92	2.82	1.13
Salinity variations:				
<i>Salinity</i>	1.15	69	1.68	1.13
<i>Deep basin</i>	1.19	69	1.58	1.13
<i>Basement</i>	1.26	64	2.33	1.13
Best simulations:				
<i>All low permeability best</i>	0.92	86	0.24	1.13
<i>Funnel best</i>	0.83	87	0.43	NA

Combining these favourable attributes into one model may predict high temperatures, large total solute mass flux and slow flow rates in a low permeability model. Many scenarios combining various components of the sensitivity analysis were simulated; however, none of the simulations generated total solute mass fluxes greater than the *base case* solution. Two of the best cases are shown in Figure 4.31: *all low permeability best* and *funnel best* cases. For these models, the basin was not deepened and no basement was added due to computer time restrictions (Appendix E). In both cases, the thermal conductivity of the Middle Devonian and Mississippian units were increased by 0.5 W/m·K and the thermal conductivity of the Cretaceous and Upper Devonian units were decreased by 0.5 W/m·K. The basal heat flux was assigned as 85 mW/m² and the initial salinity of the Middle Devonian aquifer was defined as 0.25 g NaCl/g H₂O. In the *all low permeability best* model, the permeability of each unit was decreased by an order of magnitude from *base case* values. The *funnel best* model is based on the *funnel* model, but the permeability values in the aquitards and the eastern permeability blocks of the barrier were reduced by 10^{-0.7} m². To promote downward flow the western permeability blocks in the barrier were assigned permeability values 10^{-0.4} to 10^{-0.5} m² lower than in the *funnel* model.

Transient simulations of these two models showed that the *funnel best* model produced the highest flow rates (~ 1 m/yr). The *all low permeability best* solution predicted flow rates of 0.4 m/yr, which are higher than the *all low permeability* model values. The higher basal heat fluxes increased temperatures at Pine Point to $\sim 92^{\circ}\text{C}$ and $\sim 86^{\circ}\text{C}$ for the *funnel best* and *all low permeability best* cases, respectively. These temperatures are substantially greater than the *funnel* or *all low permeability* temperatures (Table 4.5). Flushing of solute from the basin occurs more quickly than anticipated due to higher flow rates. Total solute mass fluxes are 17% and 8% less than the *base case* value for the *funnel best* and *all low permeability best* cases, respectively.

Of the many models considered, only these two models and the heat flux cases meet the criteria for mineralization at Pine Point, i.e., reach temperatures greater than average ore-forming temperatures. Regardless, none of these models predict total solute mass fluxes 10 times those of the *base case*. Even in the best simulations, the basin is flushed with freshwater within 2 million years, which cannot explain brines in the barrier today.

In conclusion, because of a lack of salinity none of the variations on the *base case* model can adequately predict the development of the Pine Point ore district. This suggests that either barrier ore-forming fluid dissolved a large volume of halite or another source of saline fluid existed. Solute chemistry analyses of ore fluid inclusion waters show no evidence of halite dissolution (Telser, 1999); however, there is evidence of highly saline water mixing with barrier fluids at Pine Point (Adams et al., 2000b). Alternatively, the flow model and/or conceptual model may need revision. Extension of the modelled section to the disturbed belt and the incorporation of a realistic basement unit might provide higher temperatures and a greater volume of brine at Pine Point. Further refinement of the hydrostratigraphy and conceptual model might also generate a more plausible ore-forming system. Lastly, consideration of basin tectonics related to the Laramide orogeny may elucidate the processes and timing of mineralization at Pine Point.

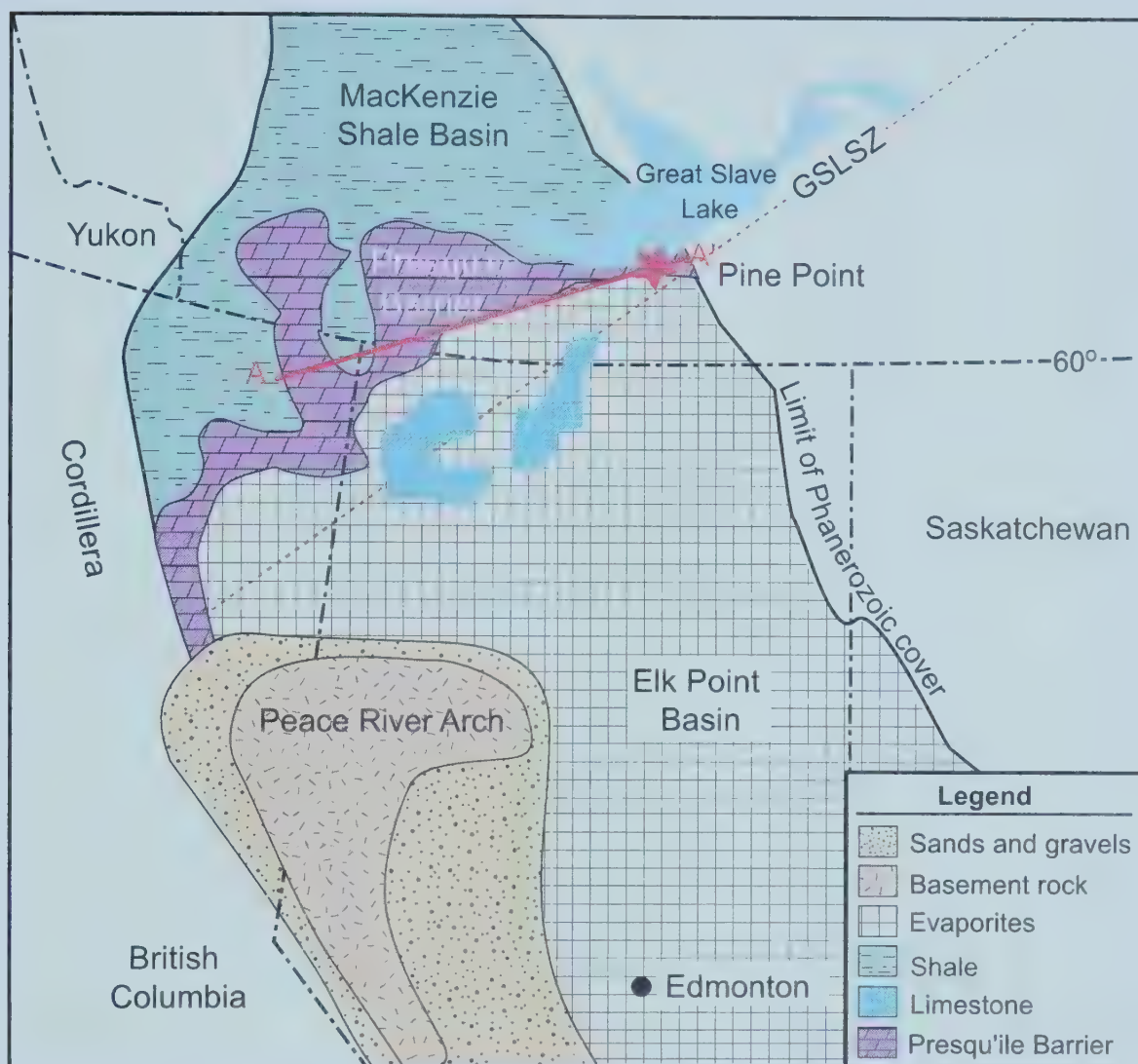


Figure 4.1: Paleogeography during the Middle Devonian, showing location of Pine Point (adapted from Qing, 1998a). Cross-section used in Garven (1985) is delineated by a red line, extending from A to A'. GSLSZ stands for Great Slave Lake shear zone.

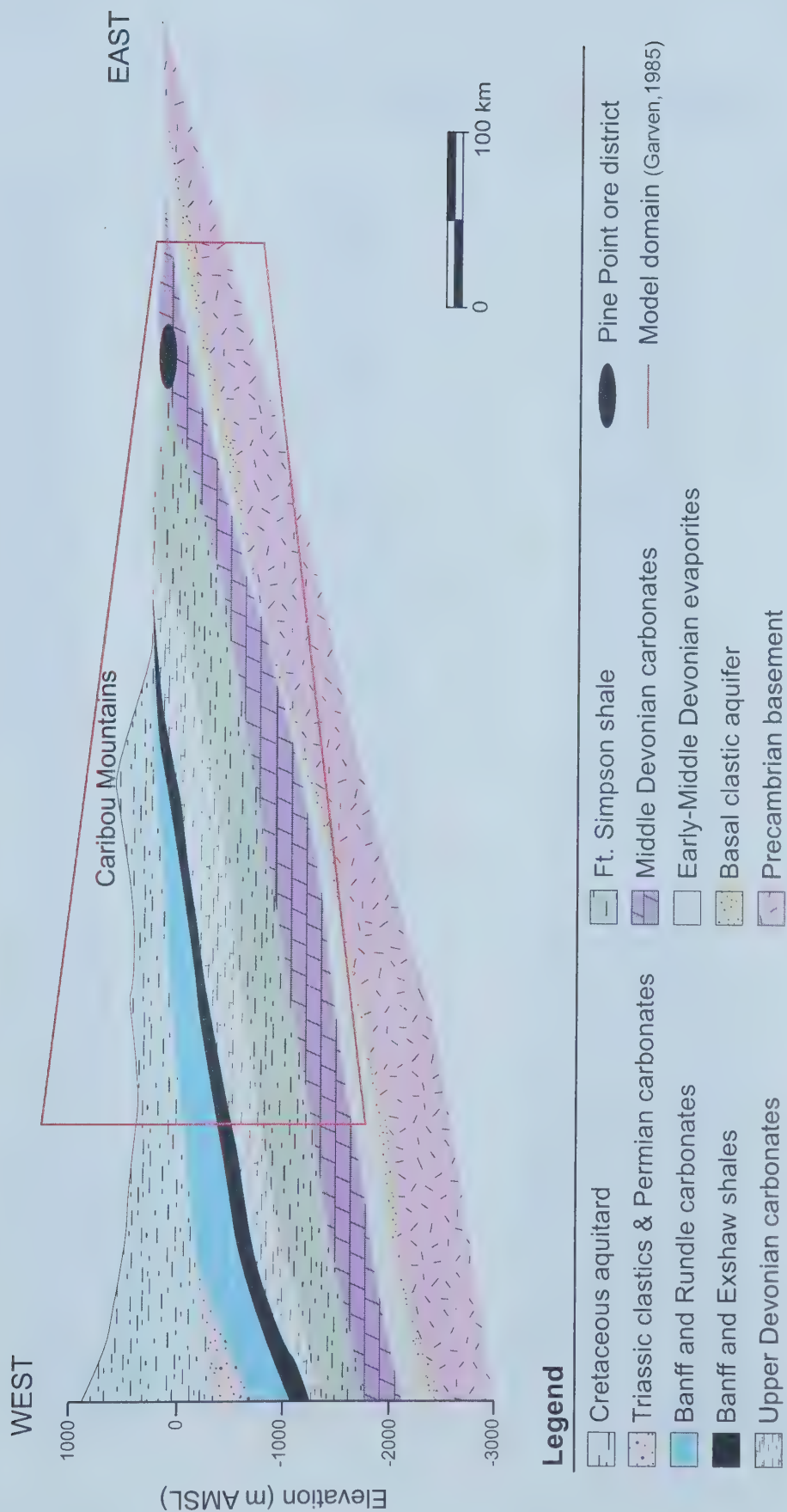


Figure 4.2: Stratigraphy along the Presqu'île barrier from the disturbed belt to the erosion edge of the WCSB. Garven's (1985) model domain is shown in red.

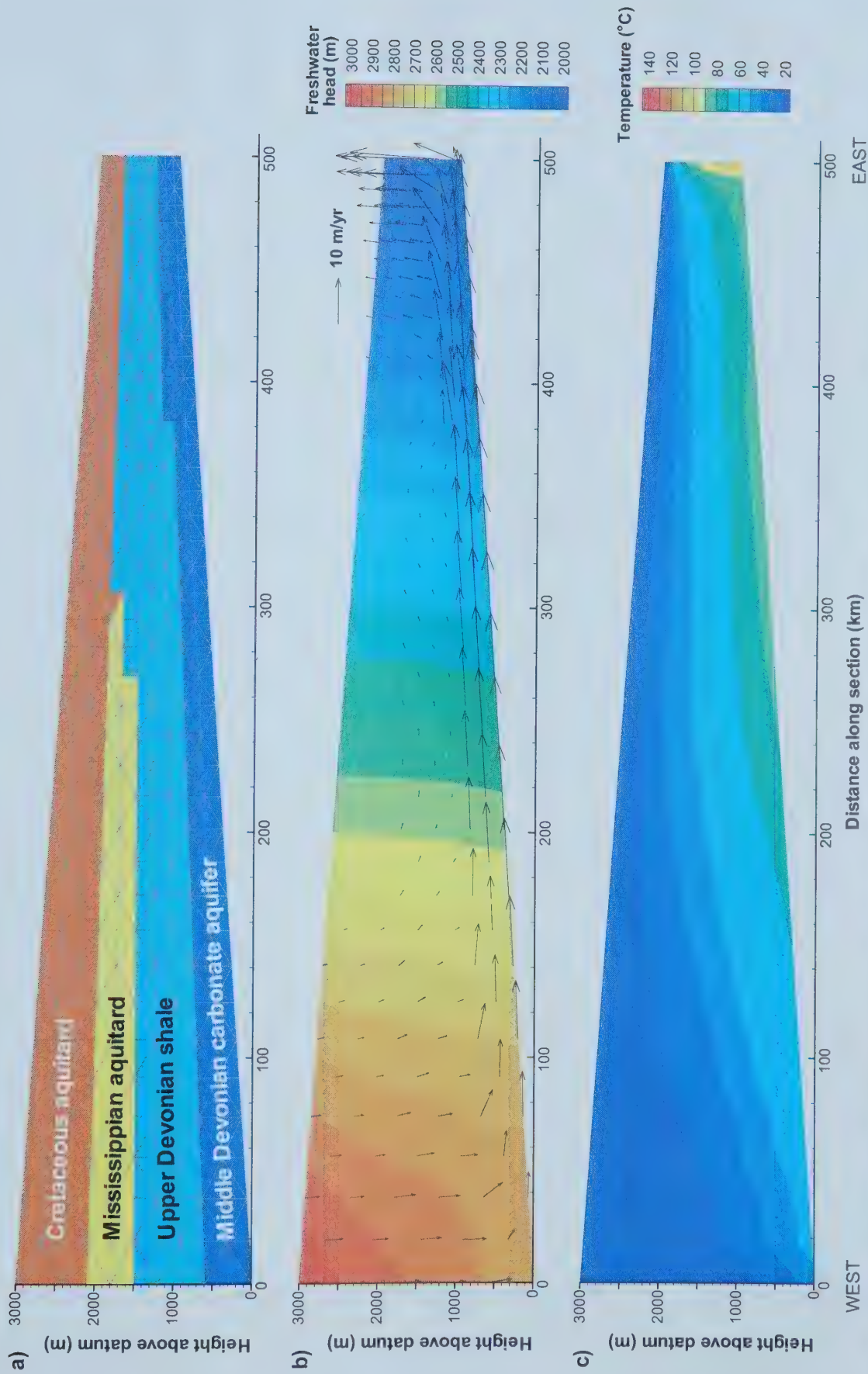


Figure 4.3: Replicated model of Pine Point flow system (Garven, 1985), a) finite element mesh and hydrostratigraphy in RIFT2D model; b) fresh-water hydraulic heads and velocity vectors at steady state (500 ka following instantaneous uplift); and c) temperature profile at steady state.

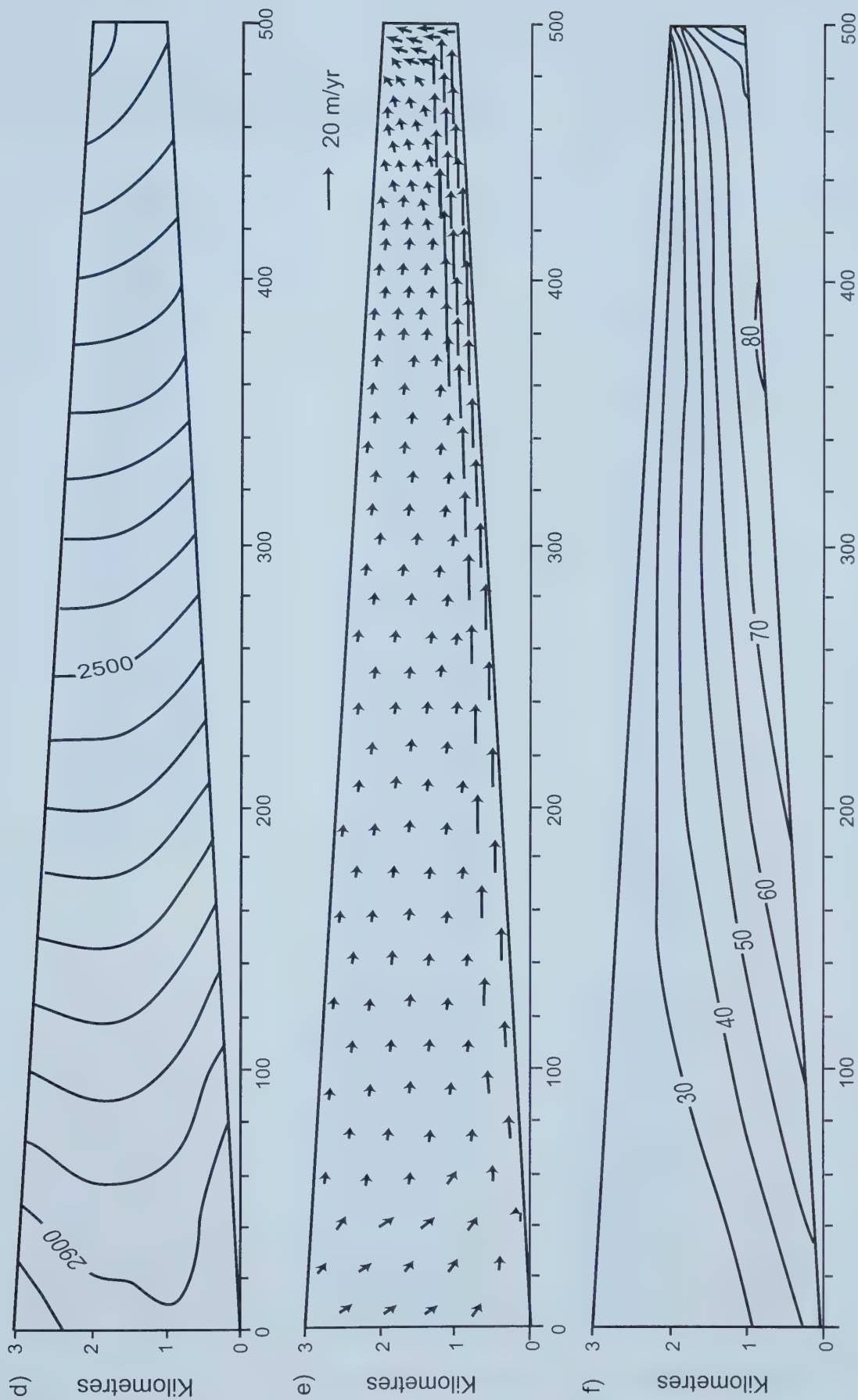


Figure 4.3 (cont'd): Pine Point model steady-state solution as published by Garven (1985), d) freshwater hydraulic heads displayed with a 50 m contour interval; e) velocity distribution displayed with a 10°C contour interval.

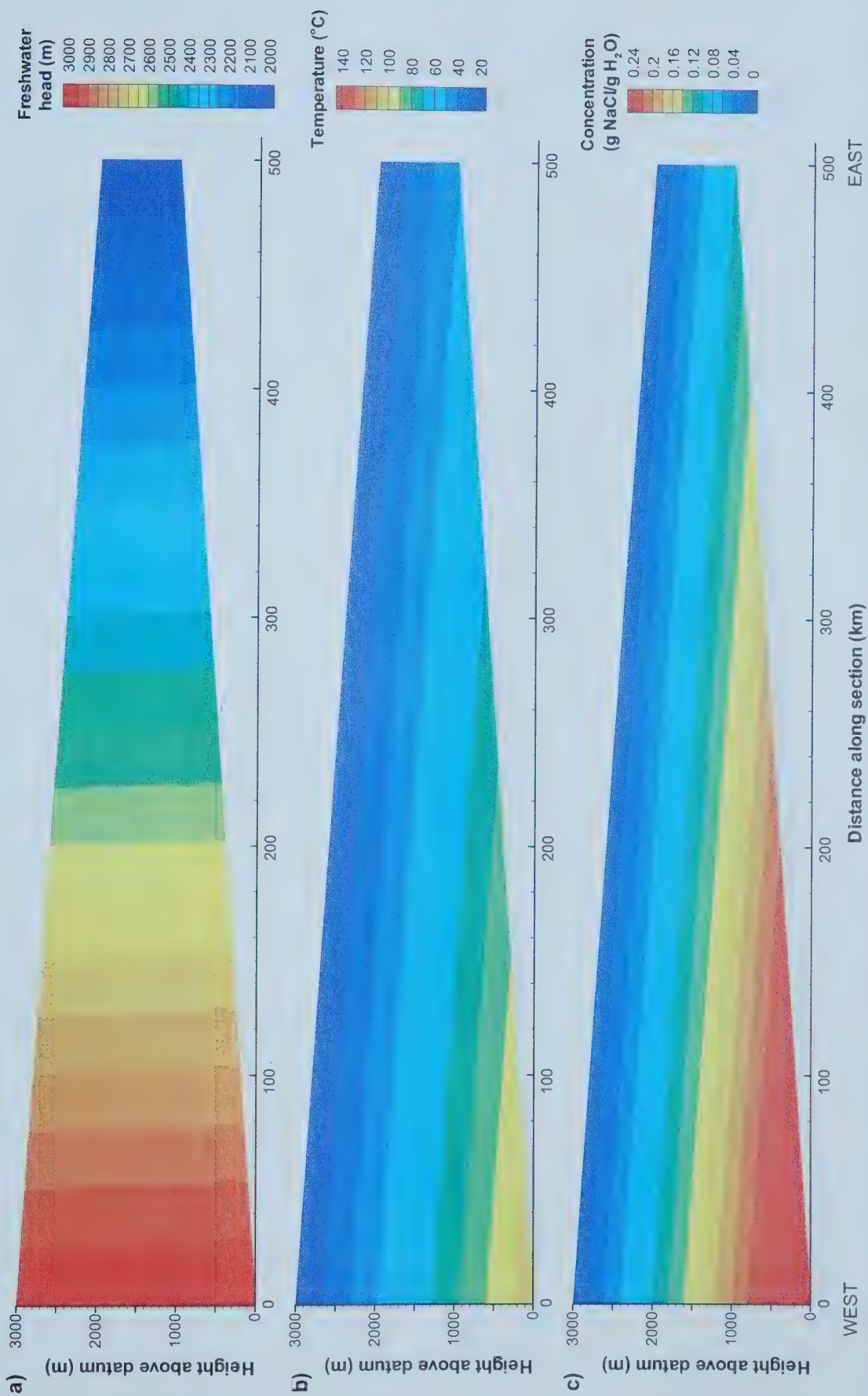


Figure 4.4: Initial conditions applied to Pine Point models a) hydrostatic freshwater hydraulic head distribution defined by the water table condition; b) conductive temperature distribution controlled by a surface temperature of 20°C and basal heat flux of 70 mW/m²; and c) salinity gradient of 1.0E-4 g NaCl/g H₂O per metre depth from surface.

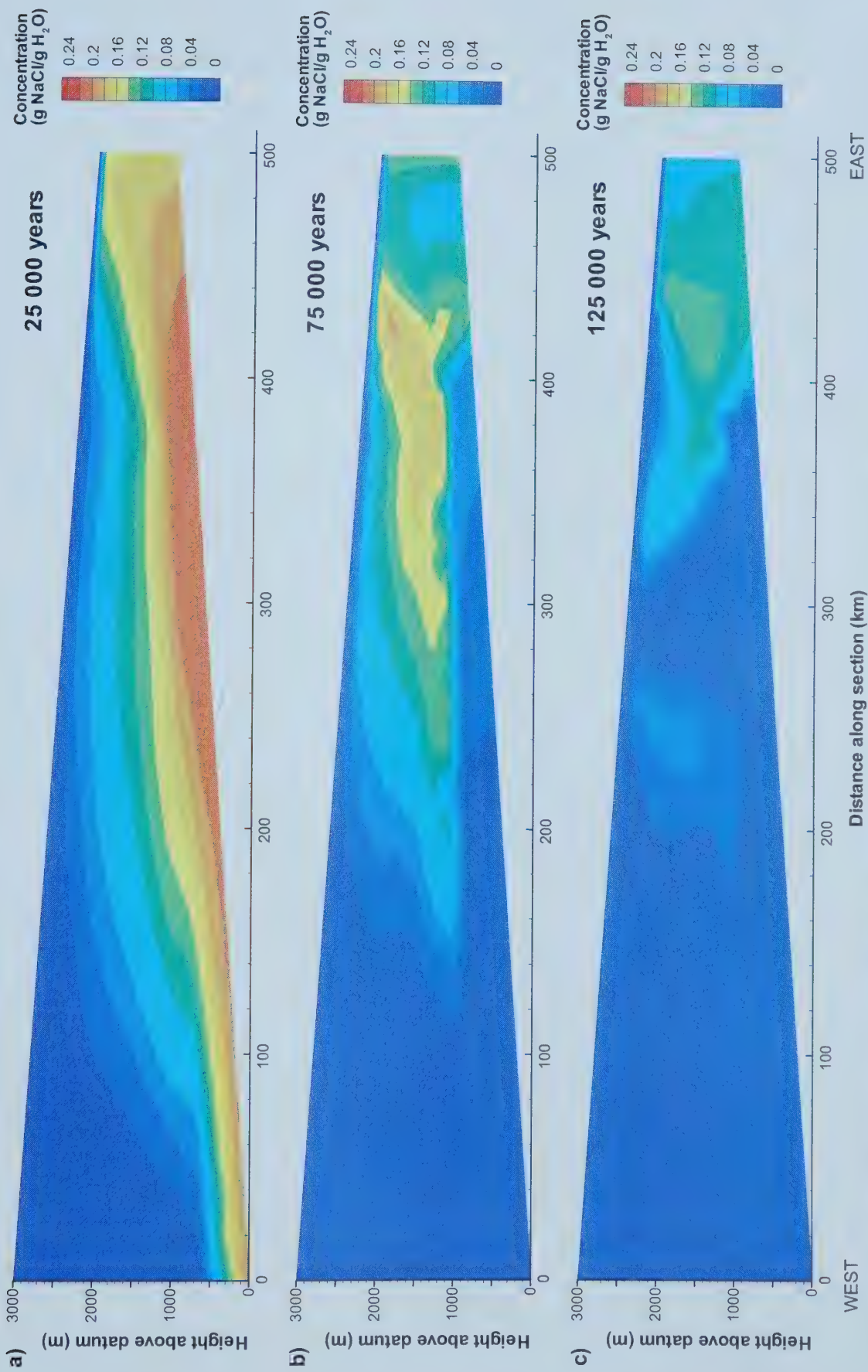


Figure 4.5: Transient simulations of salinity distributions for replicated model a) 25 000 years; b) 75 000 years; and c) 125 000 years following instantaneous uplift. Note: Peclet numbers for this mesh are approximately 10000, suggesting that some numerical error exists in these solutions.

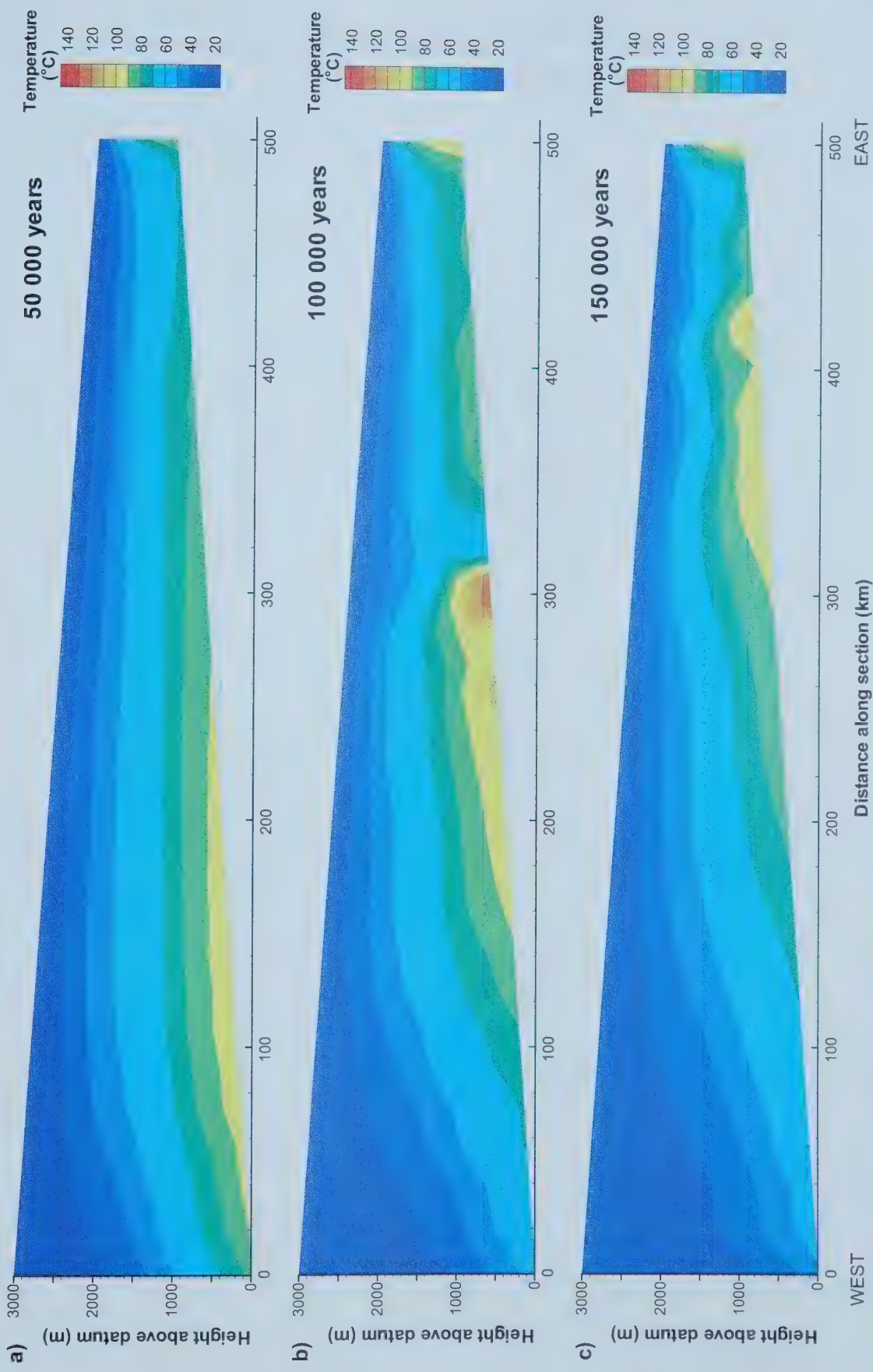


Figure 4.6: Transient simulations of temperature distributions for the replicated model at a) 50 000 years; b) 100 000 years; and c) 150 000 years following instantaneous uplift.

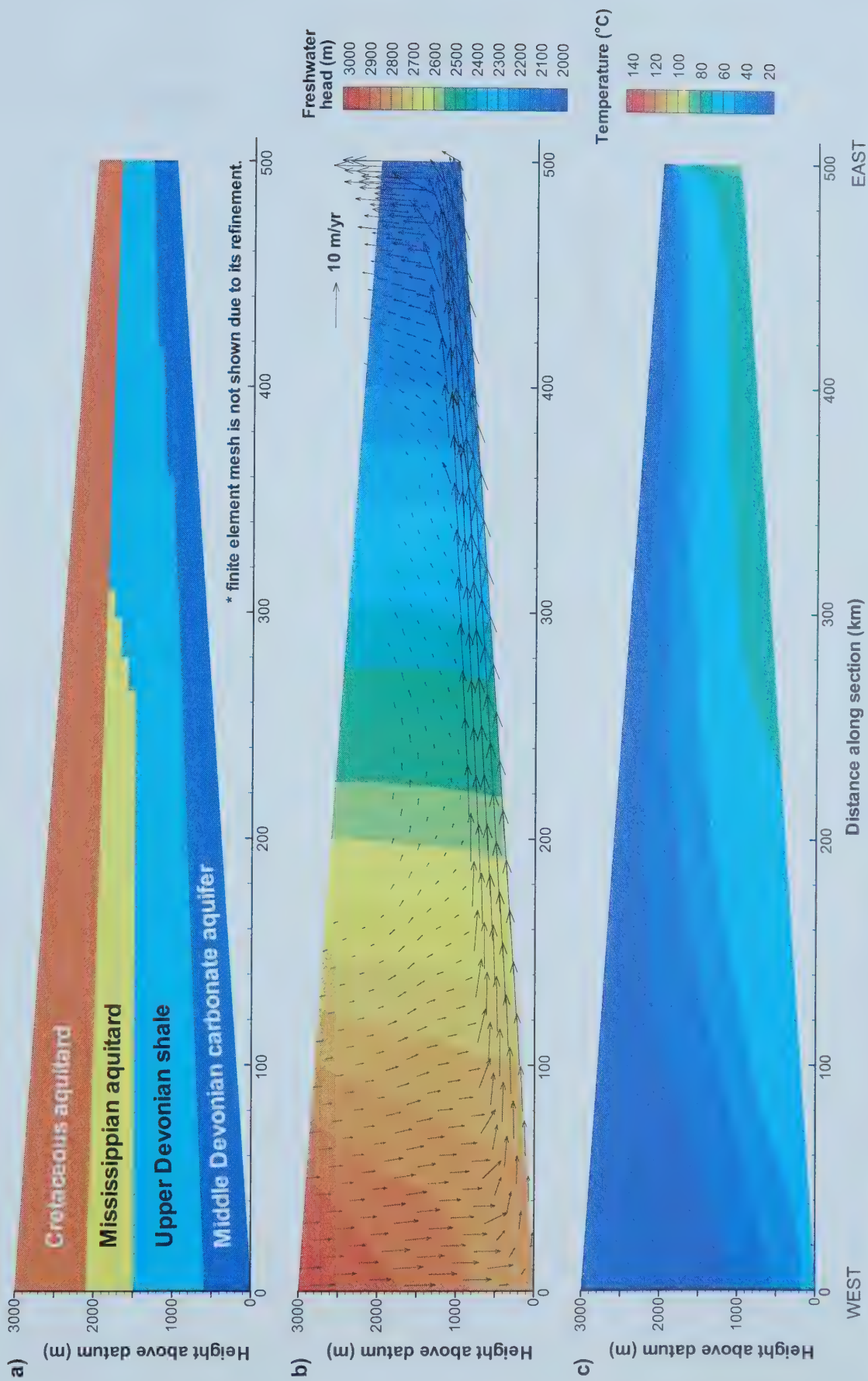


Figure 4.7: Base case model of Pine Point flow system, a) model domain and hydrostratigraphy used in RIFT2D model; b) freshwater hydraulic heads and velocity vectors at steady state (500 000 years following instantaneous uplift); and c) temperature profile at steady state.

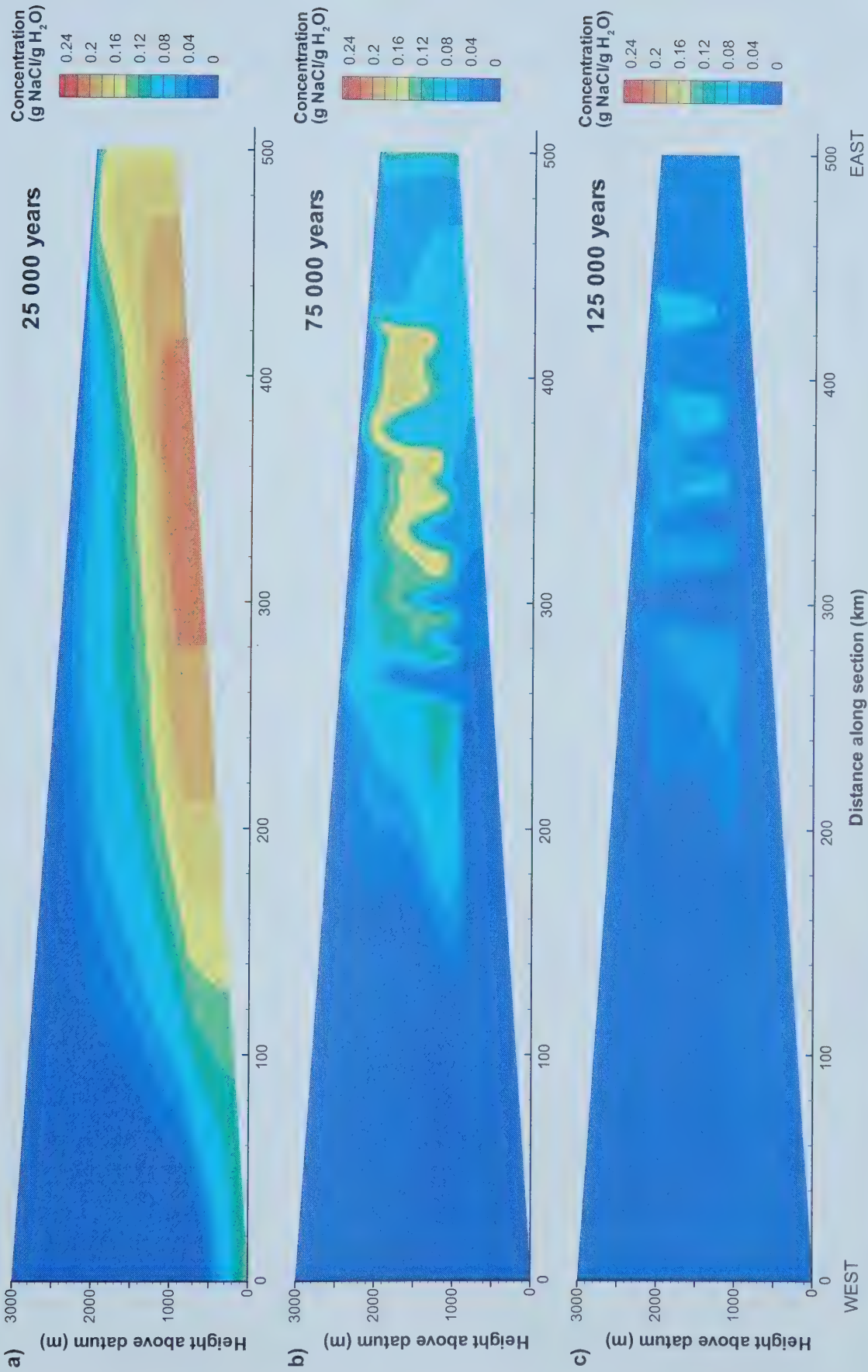


Figure 4.8: Transient simulations of salinity distributions for the base case model a) 25 000 years; b) 75 000 years; and c) 125 000 years following instantaneous uplift.

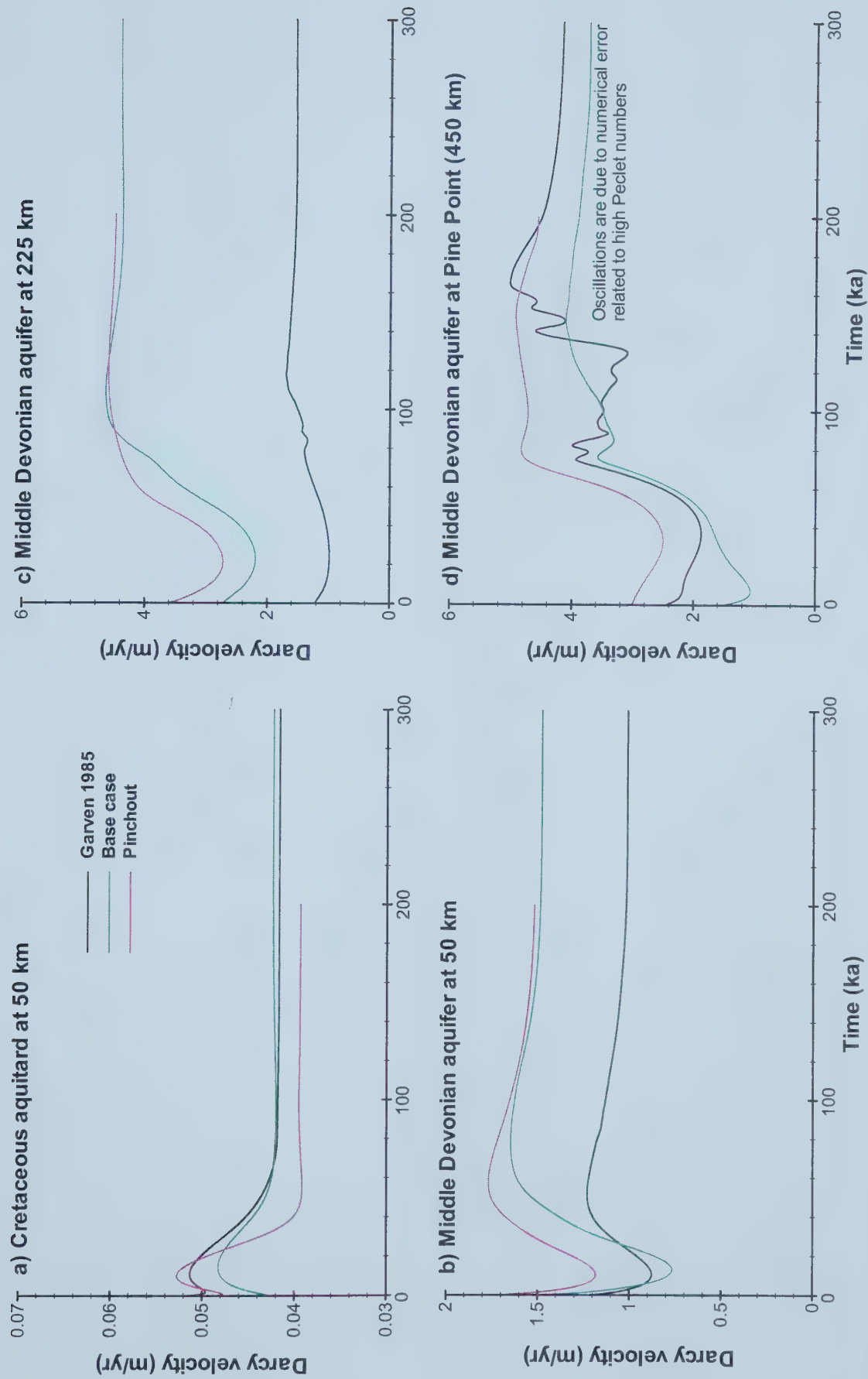


Figure 4.9: Comparison of darcy velocities in the replicated, base case and pinchout models (Appendix C) at observation points, a) in Cretaceous aquitard 50 km along the section at z=2500 m; in the Middle Devonian aquifer, b) 50 km; c) 225 km; and d) 450 km (Pine Point) along the section.

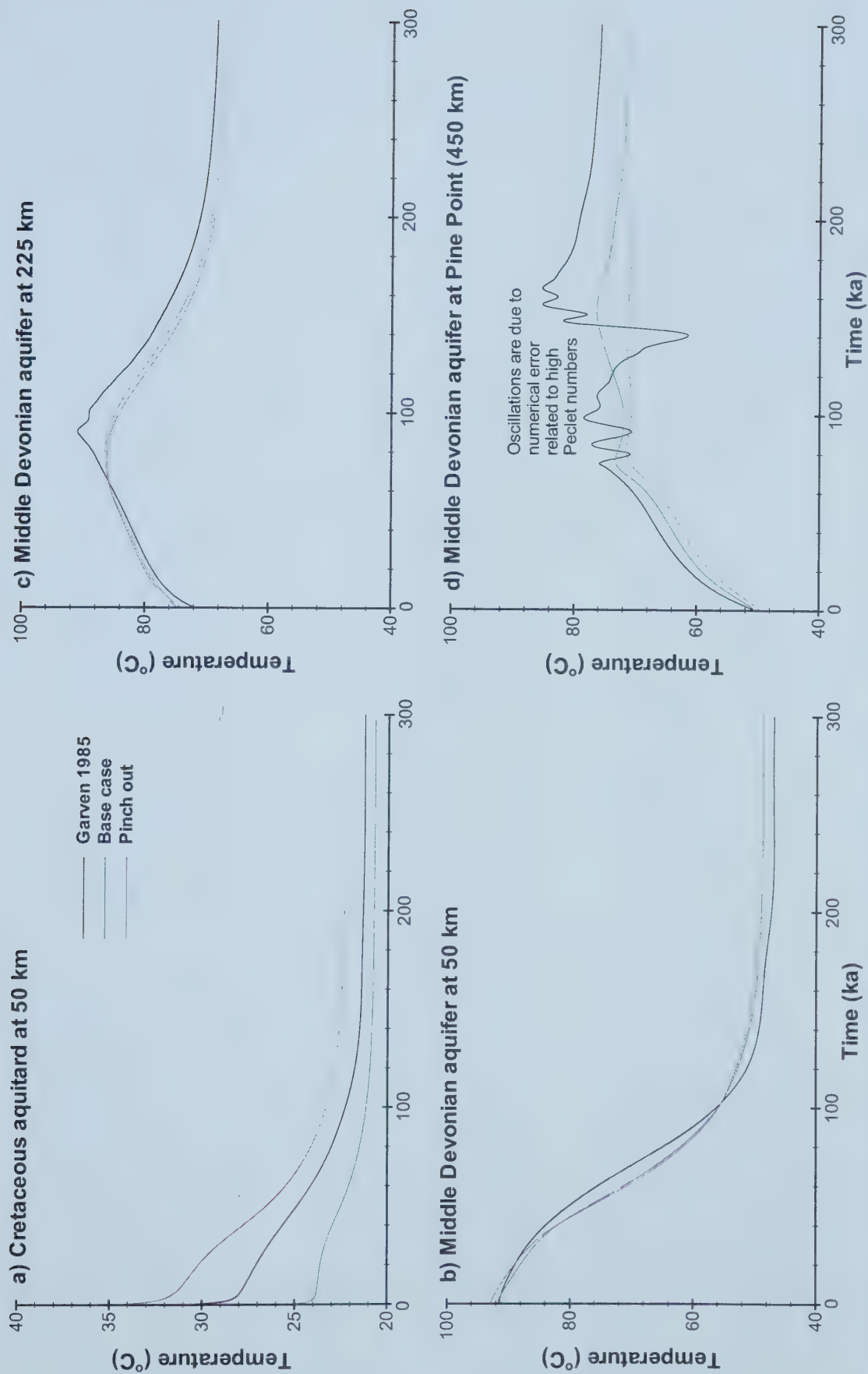


Figure 4.10: Comparison of temperatures in the Pine Point replicated, base case and pinchout models at observation points, a) in the Cretaceous aquitard 50 km along the section at $z=2500$ m; in the Middle Devonian aquifer, b) 50 km; c) 225 km; and d) 450 km (Pine Point) along the section.

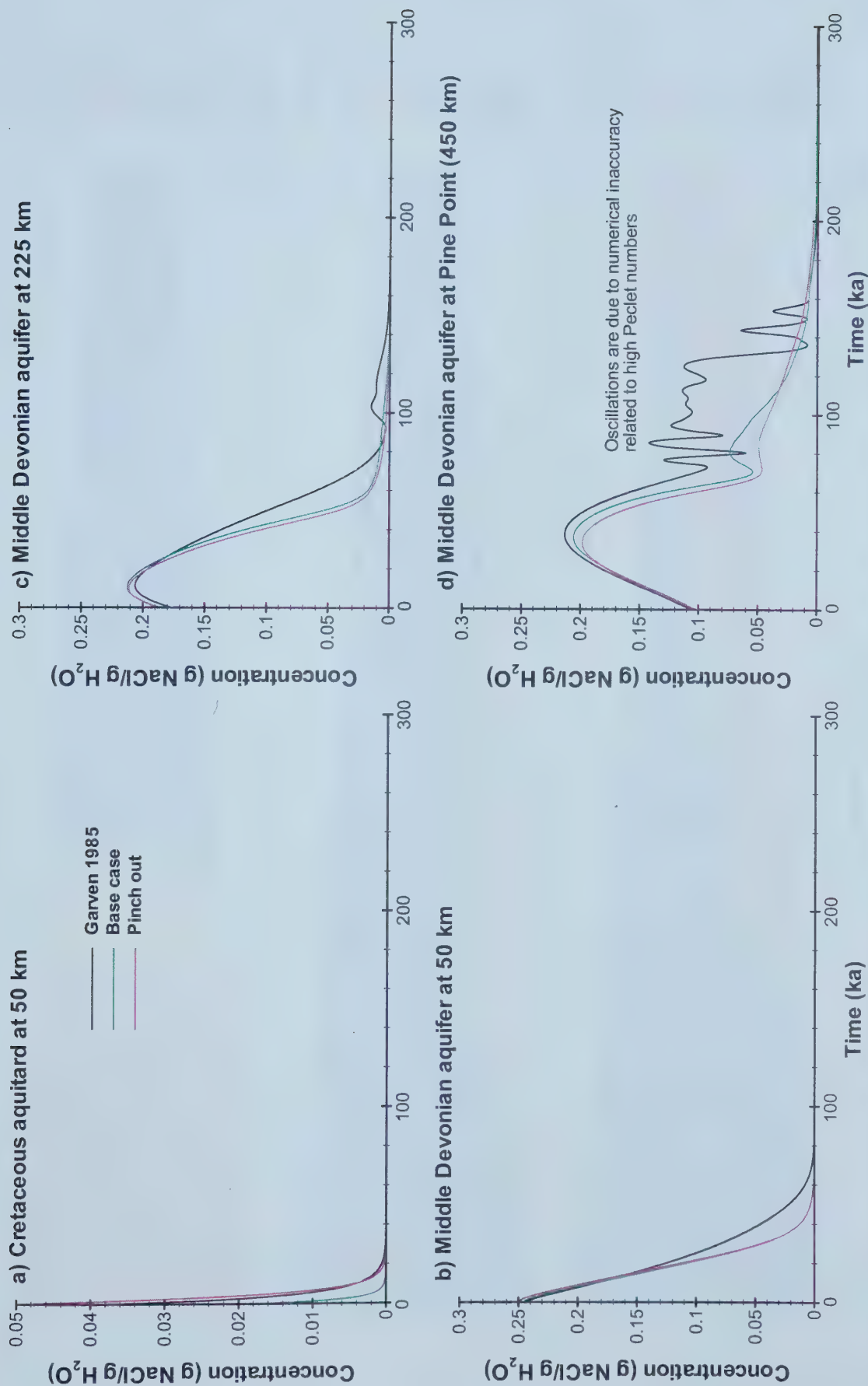


Figure 4.11: Comparison of the Pine Point replicated, base case and pinch out model results at 4 observation points, a) in the Cretaceous aquitard 50 km along the section at a height of 2500 m; in the Middle Devonian aquifer, b) 50 km; c) 225 km; and d) 450 km (Pine Point) along the section.

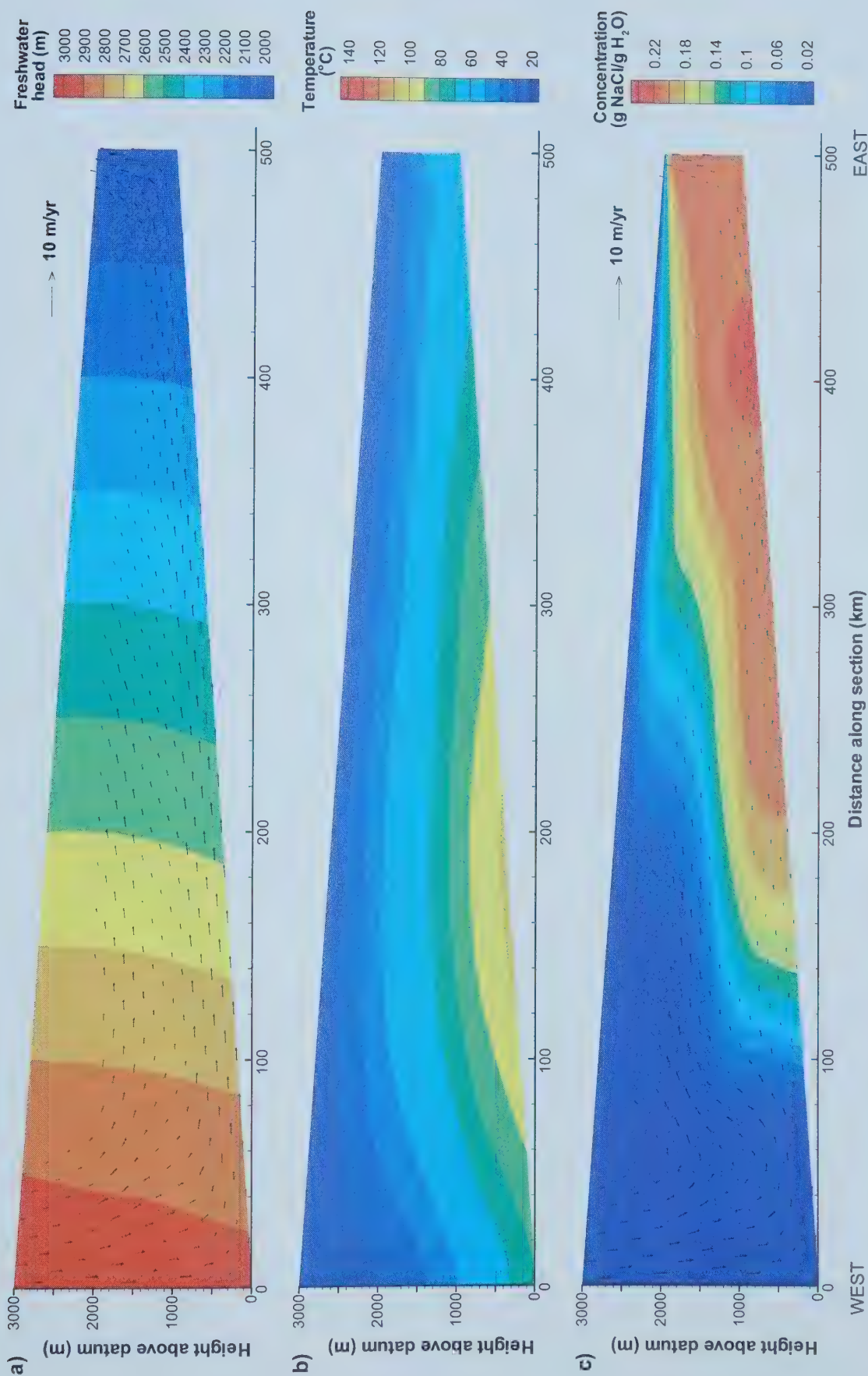


Figure 4.12: Low permeability model of the Pine Point flow system, a) freshwater hydraulic heads and velocity vectors at steady state (2 Ma following instantaneous uplift); b) temperature profile at steady state; and c) salinity distribution 300 ka after instantaneous uplift.

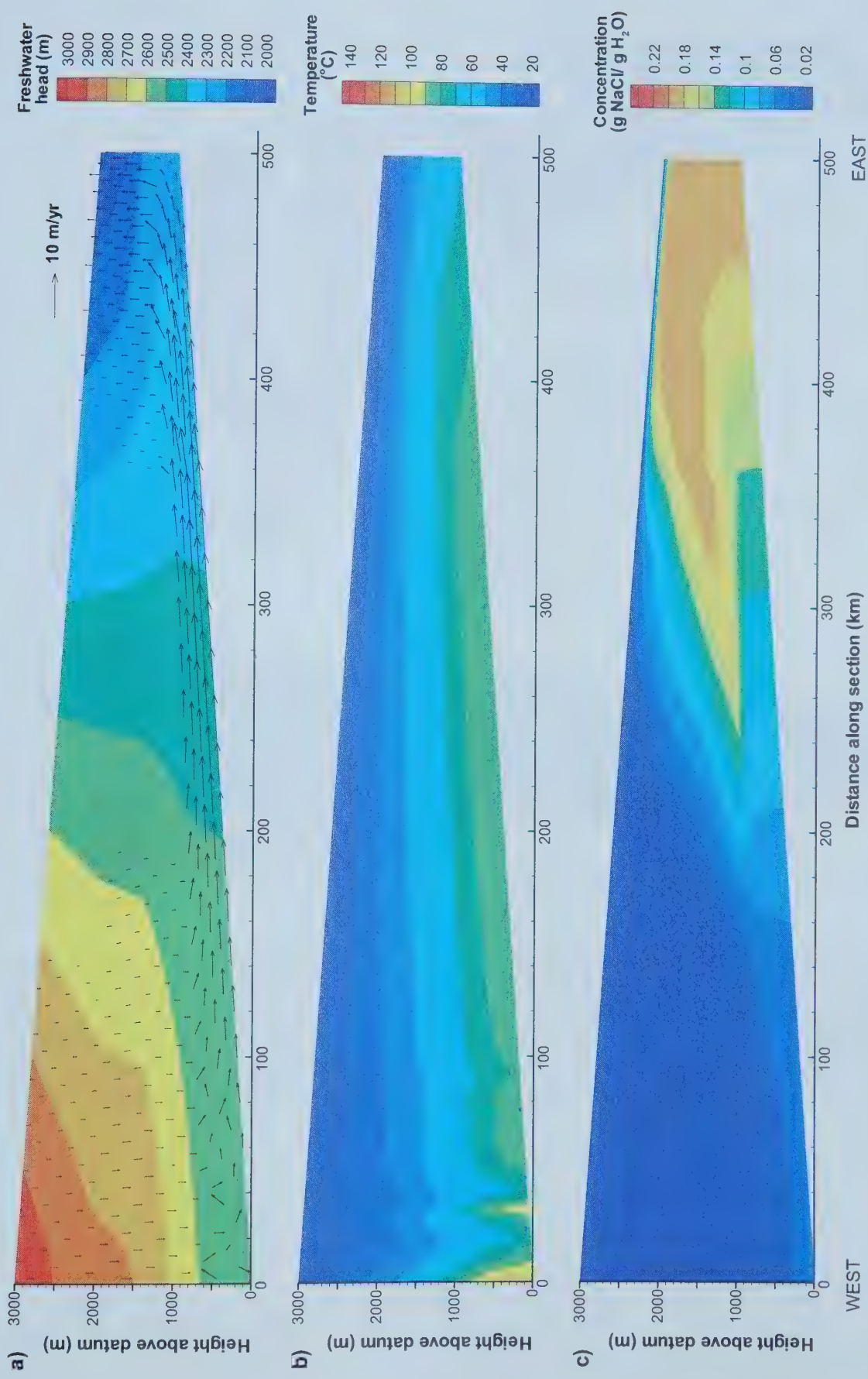


Figure 4.13: Measured permeability model of the Pine Point flow system, a) freshwater hydraulic heads and velocity vectors at steady state (2 Ma following instantaneous uplift); b) temperature profile at steady state; and c) salinity distribution 100 000 years after instantaneous uplift.

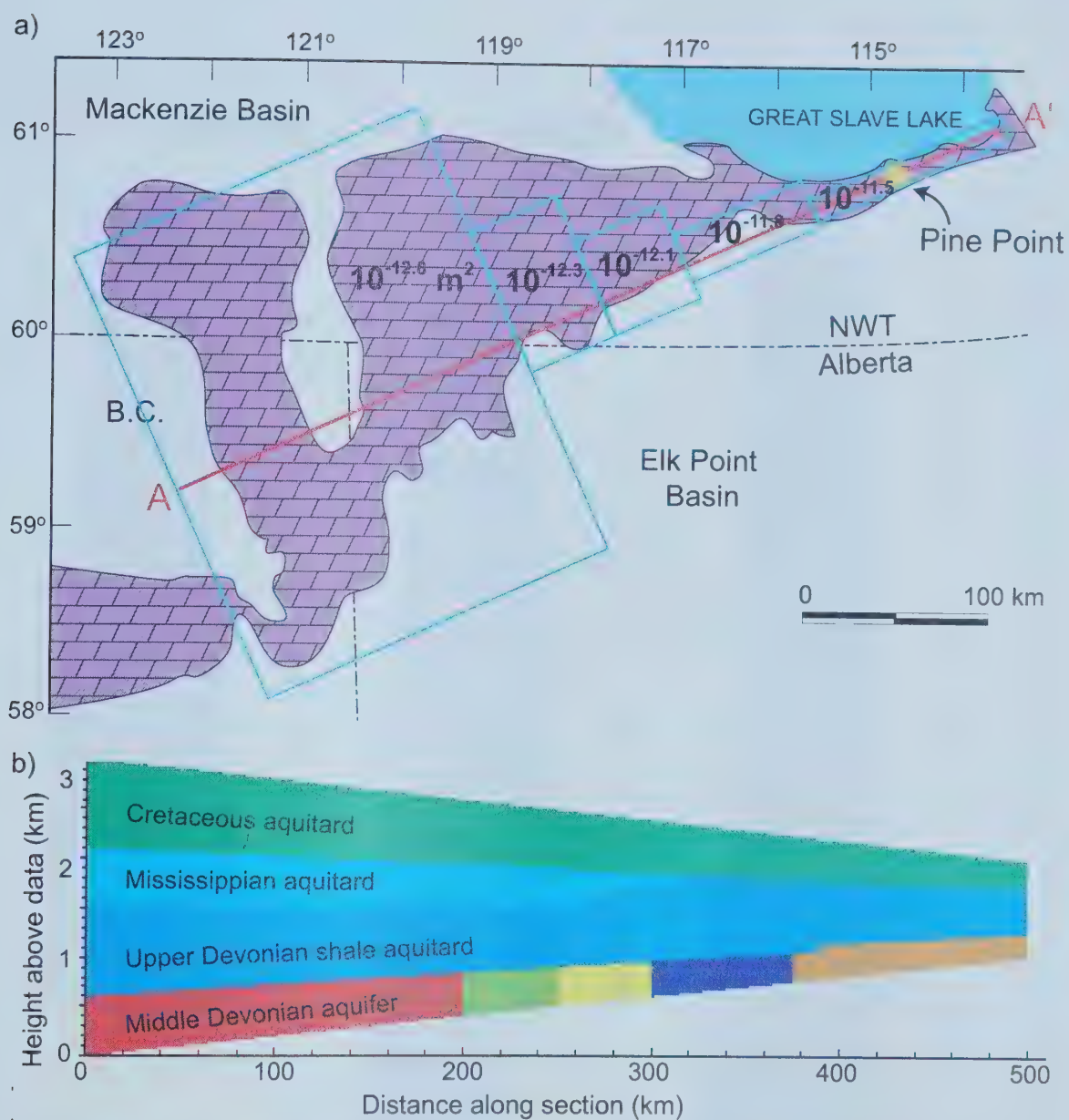


Figure 4.14 : a) Diagram of Presqu'île barrier reef, showing the modelled section from A to A' in red. The barrier thins from 250 km width to 10 km at Pine Point. In the *funnel* model, the permeability decreases by a factor of 20 across the section as shown by the yellow numbers, which are the assigned permeability in each zone. The blue boxes show the lateral extent of each permeability zone. b) Cross-sectional hydrostratigraphy used in RIFT2D model. The Middle Devonian aquifer is divided into 5 sections as outlined in a).

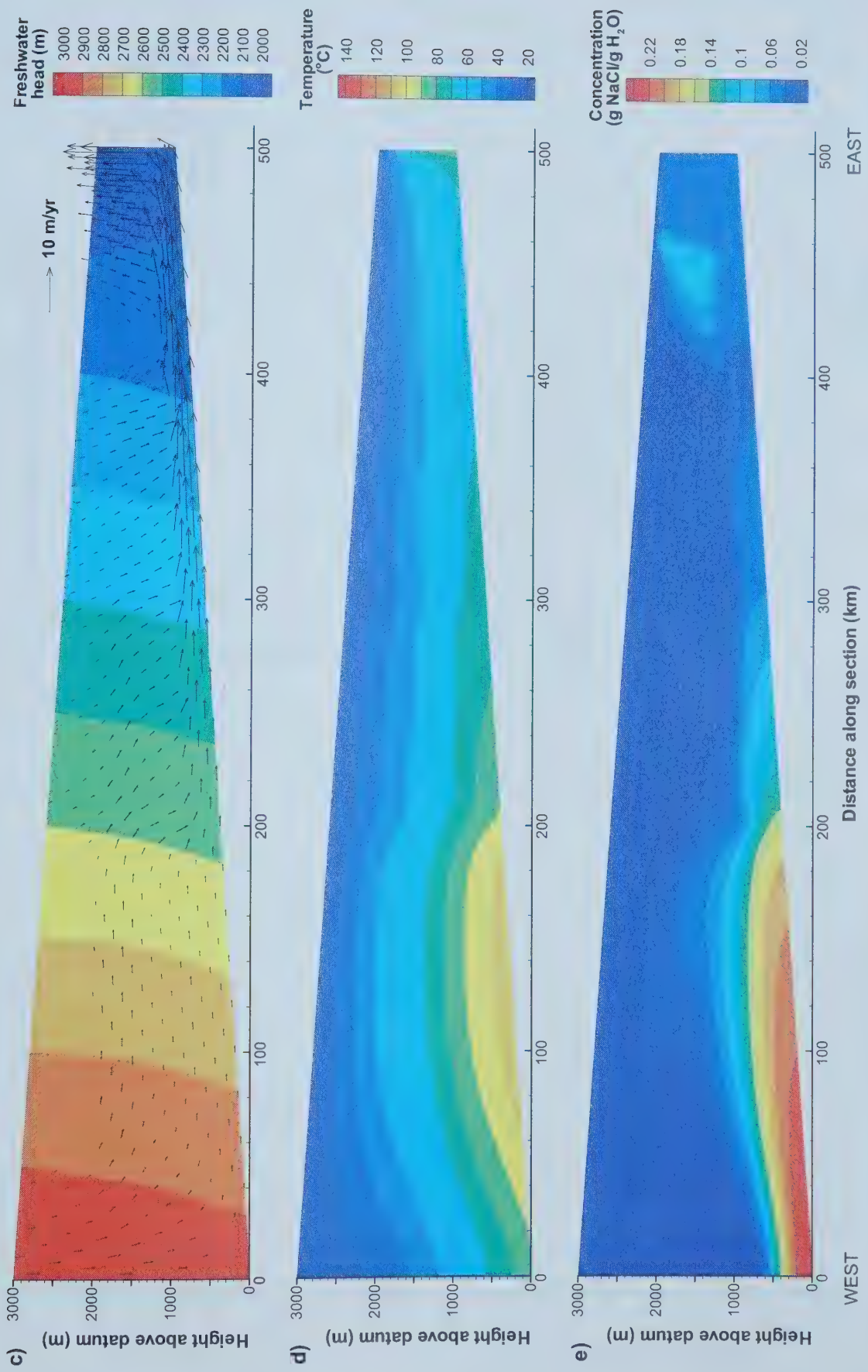


Figure 4.14: Funnel model of Pine Point flow system, c) freshwater hydraulic heads and velocity vectors at steady state (500 000 years following instantaneous uplift); d) temperature profile at steady state; and e) salinity distribution 100 000 years after instantaneous uplift.

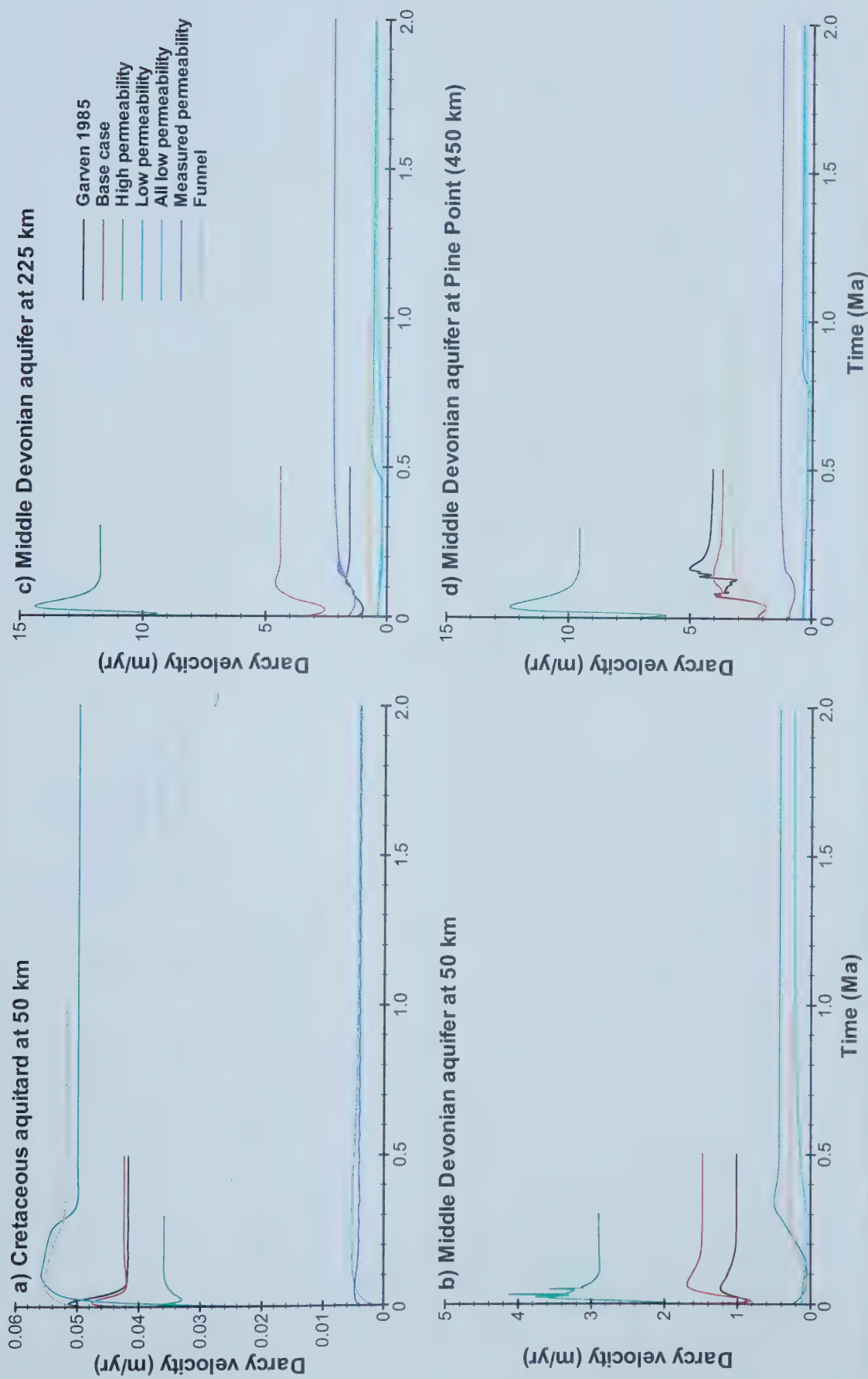


Figure 4.15: Transient variations in darcy velocity for the base case Pine Point flow model and variations related to permeability at 4 observation points along the section. The points are a) situated 2500 m above the datum; and b), c), d) centred vertically in the Middle Devonian aquifer.

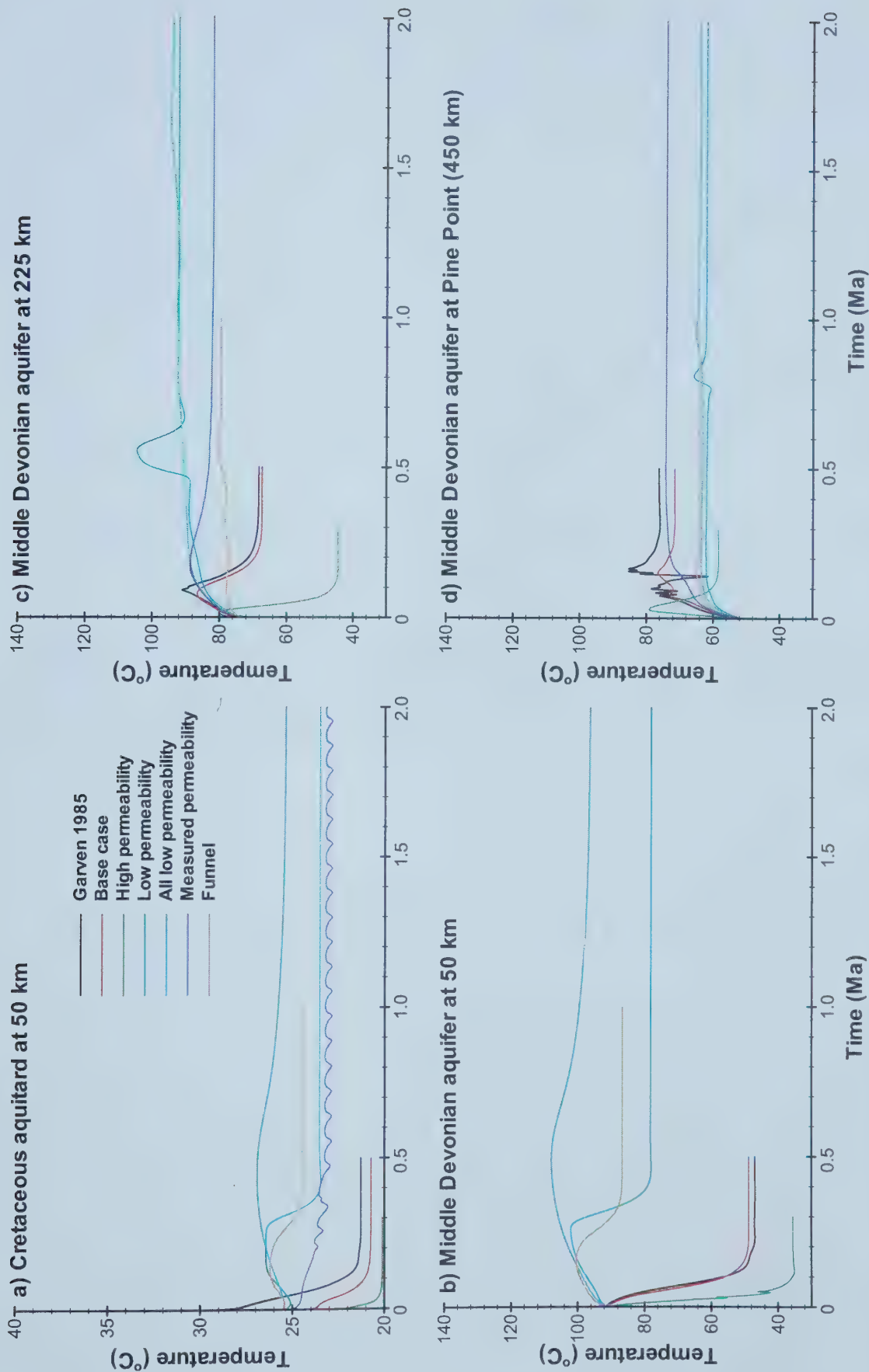


Figure 4.16: Transient variations in temperature for the base case Pine Point flow model and variations related to permeability at 4 observation points along the section. The observation points are a) situated 2500 m above the datum; and b), c), d) centred in the Middle Devonian aquifer.

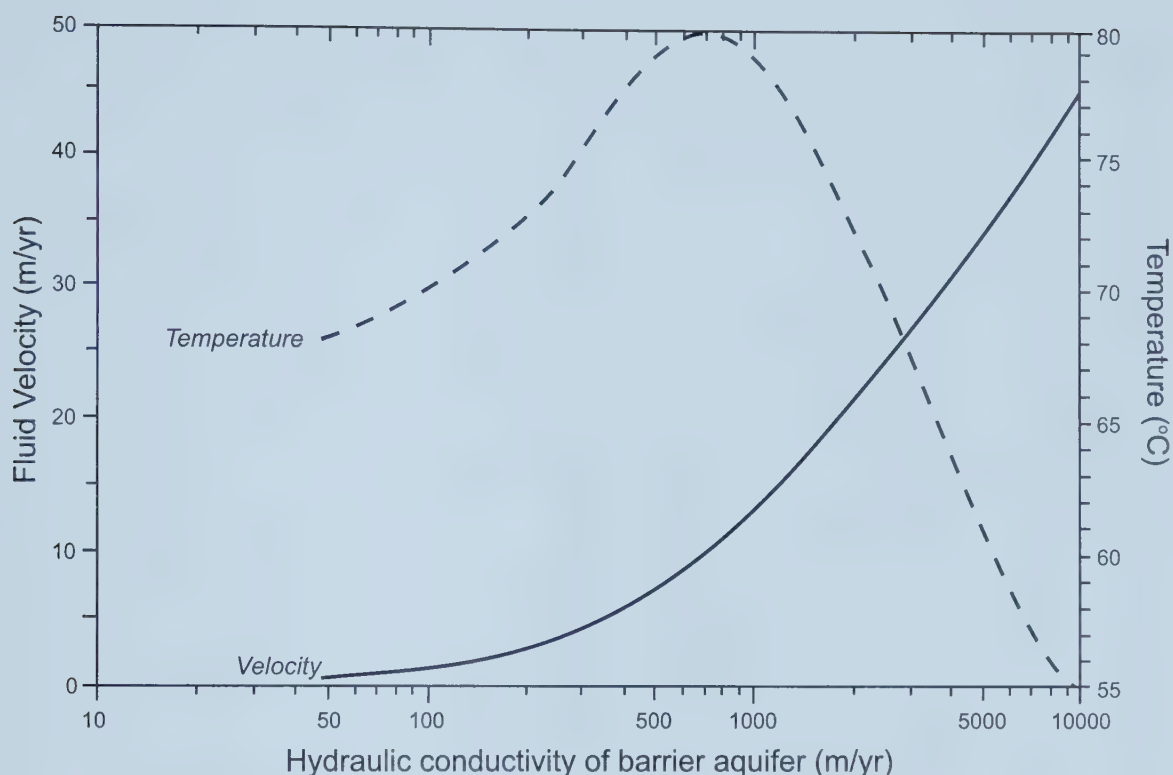


Figure 4.16e: Relationship between temperature, fluid velocity and hydraulic conductivity of the barrier aquifer at Pine Point, as defined by the original or replicated models (Taken from Garven, 1985). Note that changes in temperature parameters, permeability or density will alter the distribution shown above.

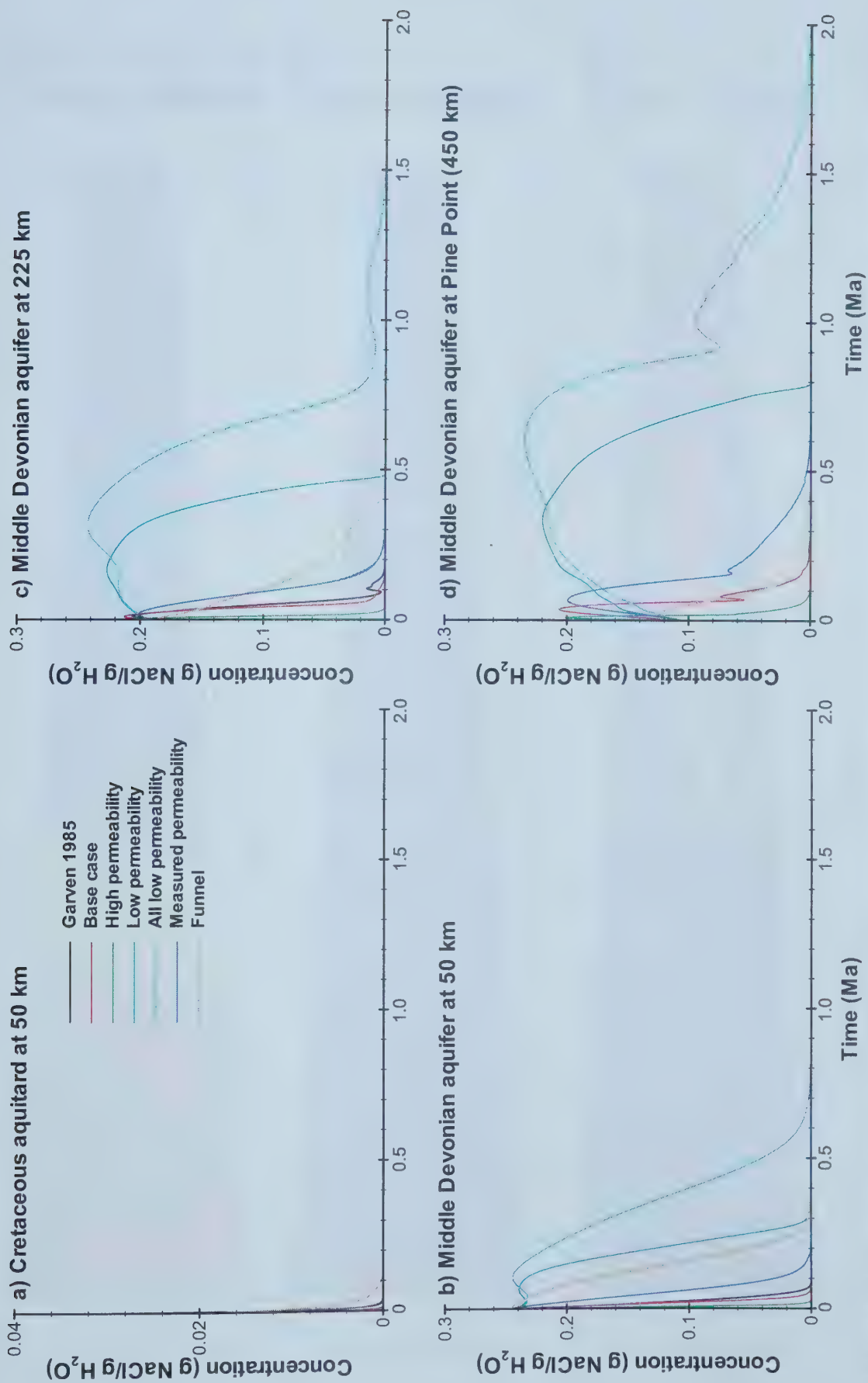


Figure 4.17: Transient variations in salinity for the base case Pine Point flow model and variations related to permeability at 4 observation points along the section. Vertically, the observation points are a) situated 2500 m above the datum; and b), c), d) centred in the Middle Devonian aquifer.

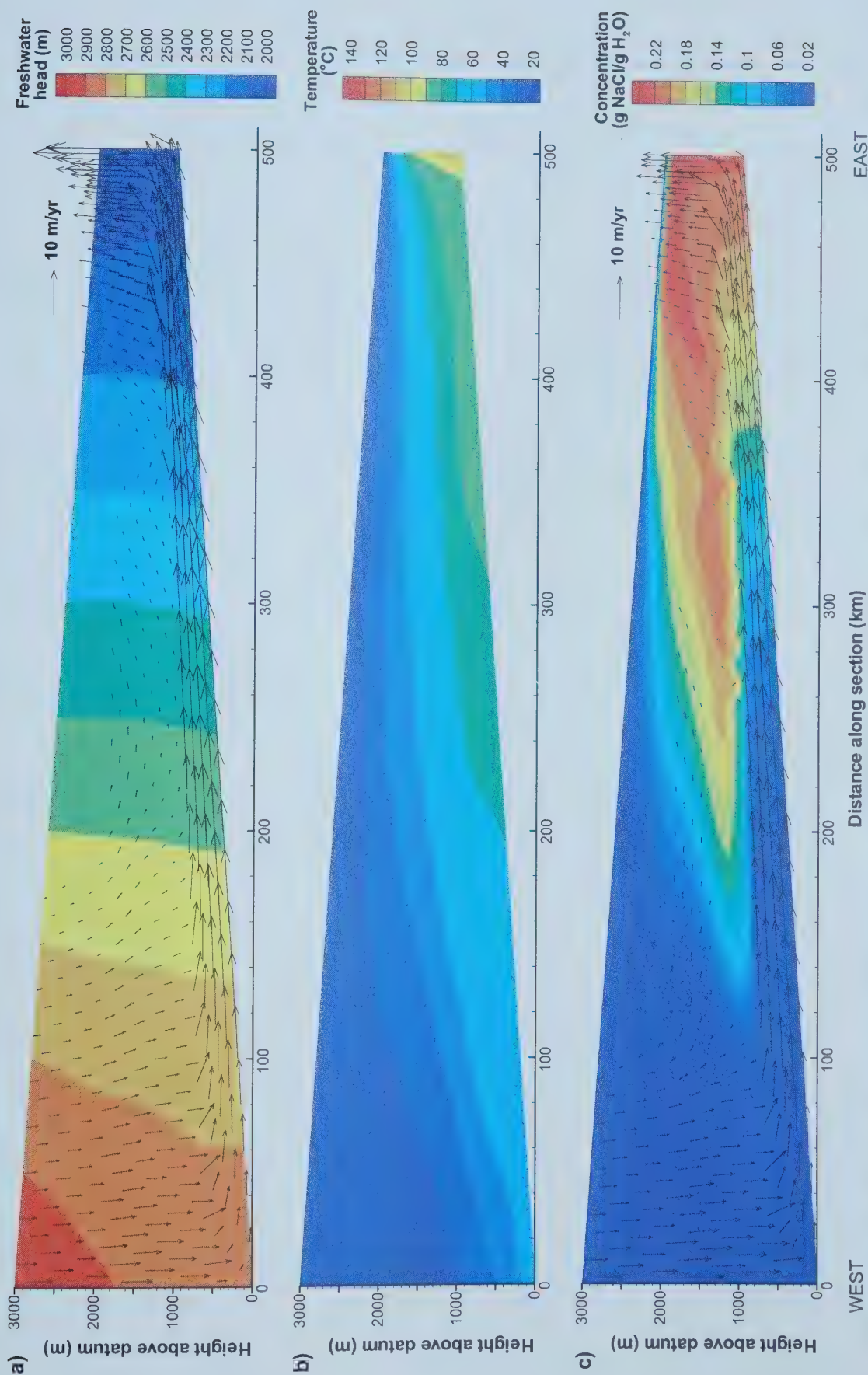


Figure 4.18: Low thermal conductivity model of Pine Point flow system, a) freshwater hydraulic heads and velocity vectors at steady state (500 000 years following instantaneous uplift); b) temperature profile at steady state; and c) salinity distribution 75 000 years after instantaneous uplift.

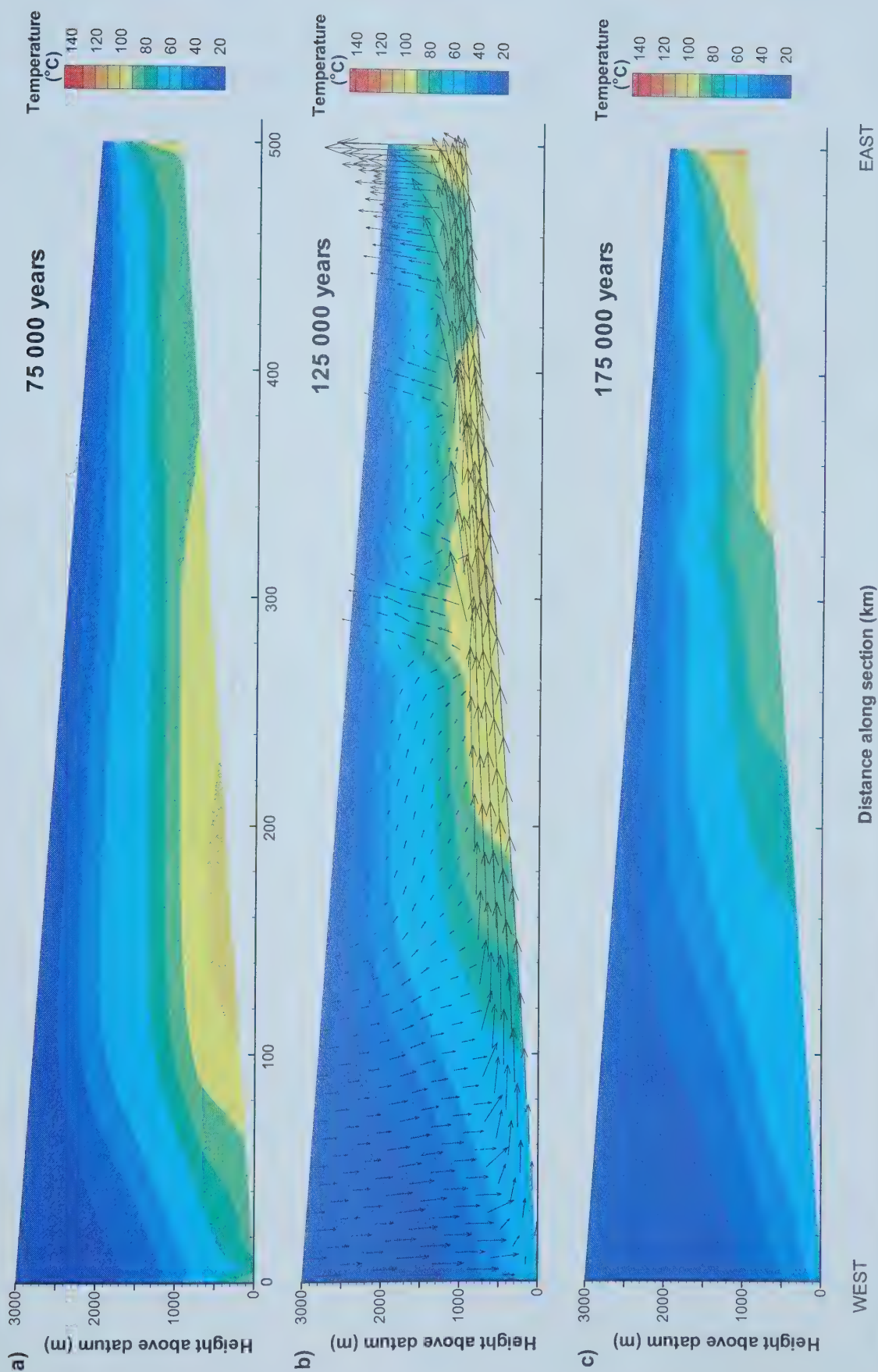


Figure 4.19: Transient simulations of temperature distributions for the low thermal conductivity model at a) 75 000 years; b) 125 000 years and velocity vectors showing distortion of the flow field by high temperature gradients; and c) 175 000 years following instantaneous uplift.

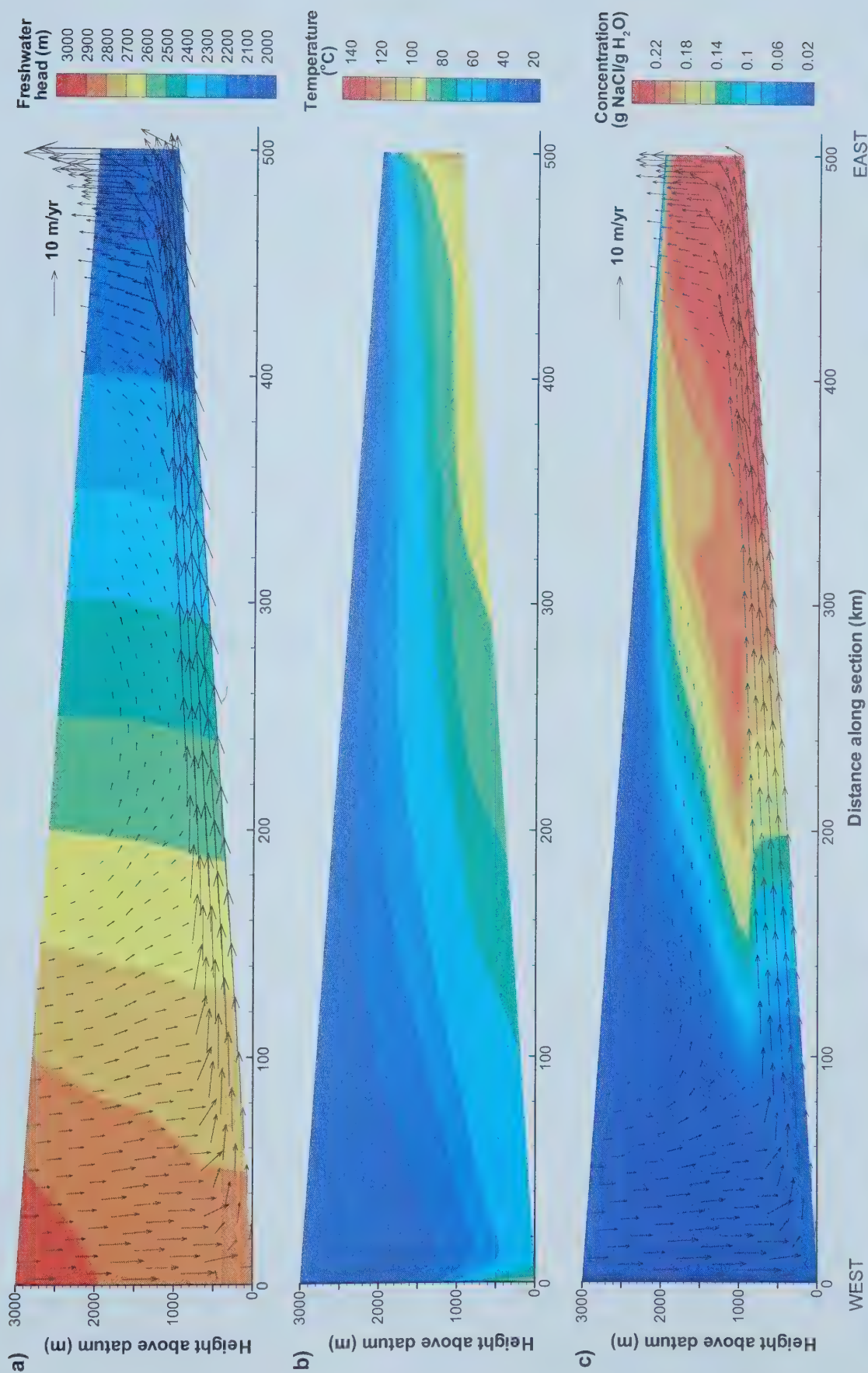


Figure 4.20: Basal heat flux of 100 mW/m² model for the Pine Point flow system, a) freshwater hydraulic heads and velocity vectors at steady state (500 000 years after instantaneous uplift); b) temperature profile at steady state; and c) salinity distribution 50 000 years after instantaneous uplift.

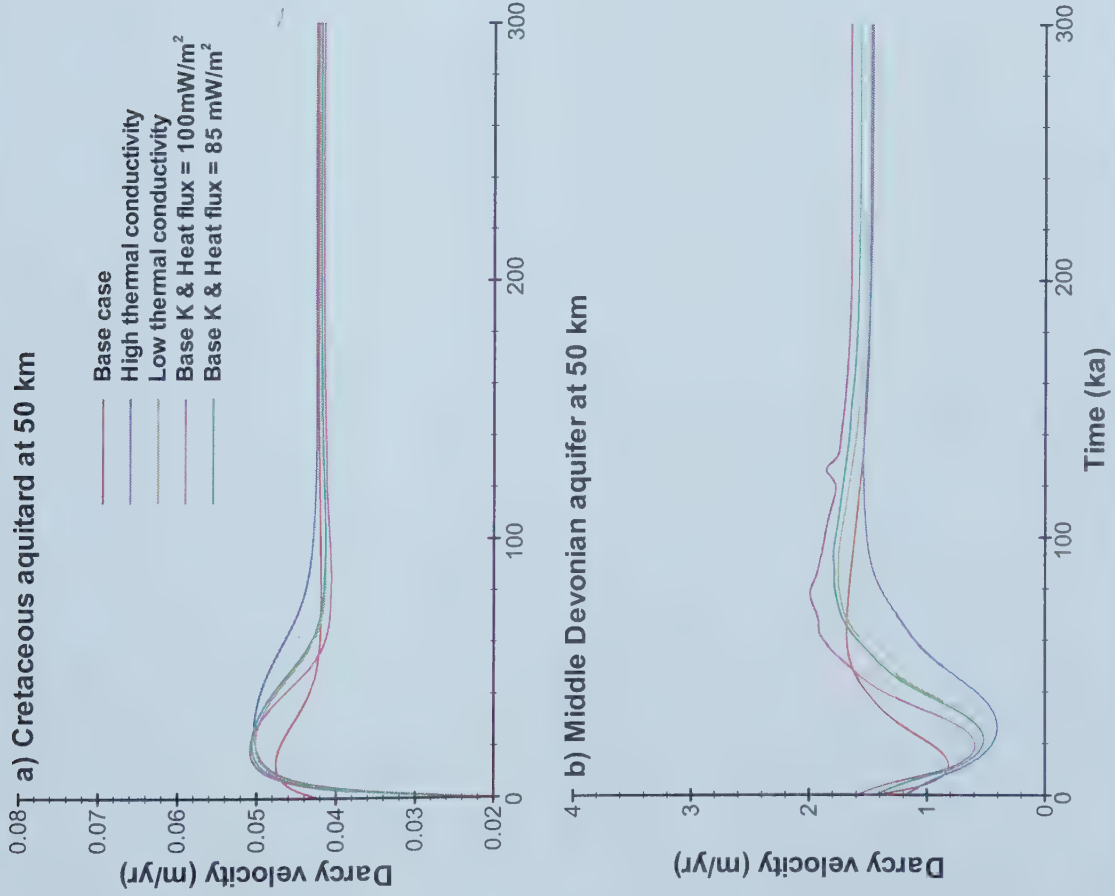


Figure 4.21: Transient variations in darcy velocity for the base case Pine Point flow model and variations related to thermal properties at 4 observation points along the section. Vertically, the points are a) situated 2500 m above the datum; and b), c), d) centred in the Middle Devonian aquifer.

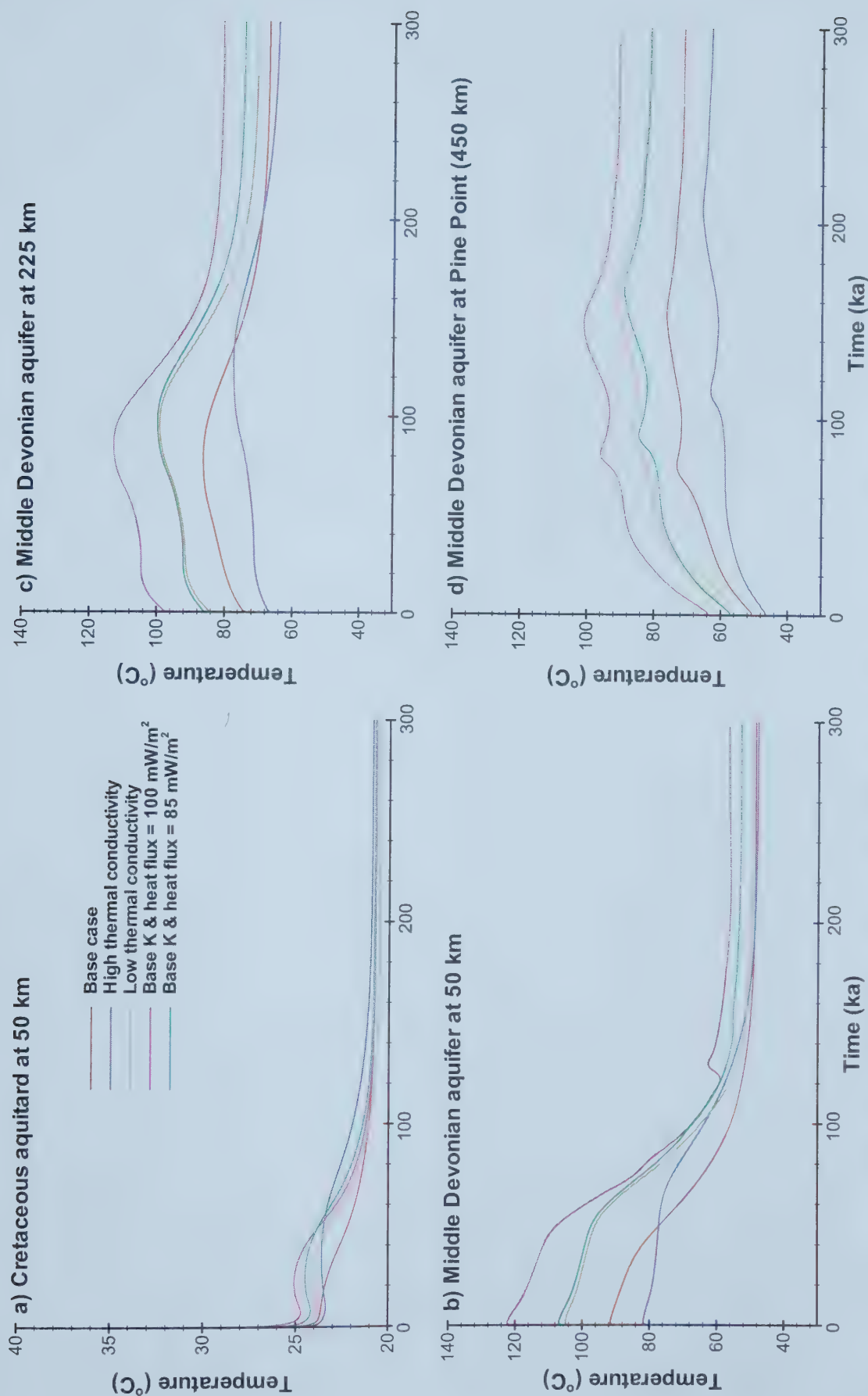


Figure 4.22: Transient variations in temperature for the base case Pine Point flow model and variations related to thermal properties at 4 observation points along the section. Vertically, the points are a) situated 2500 m above the datum; and b), c), d) centred in the Middle Devonian aquifer.

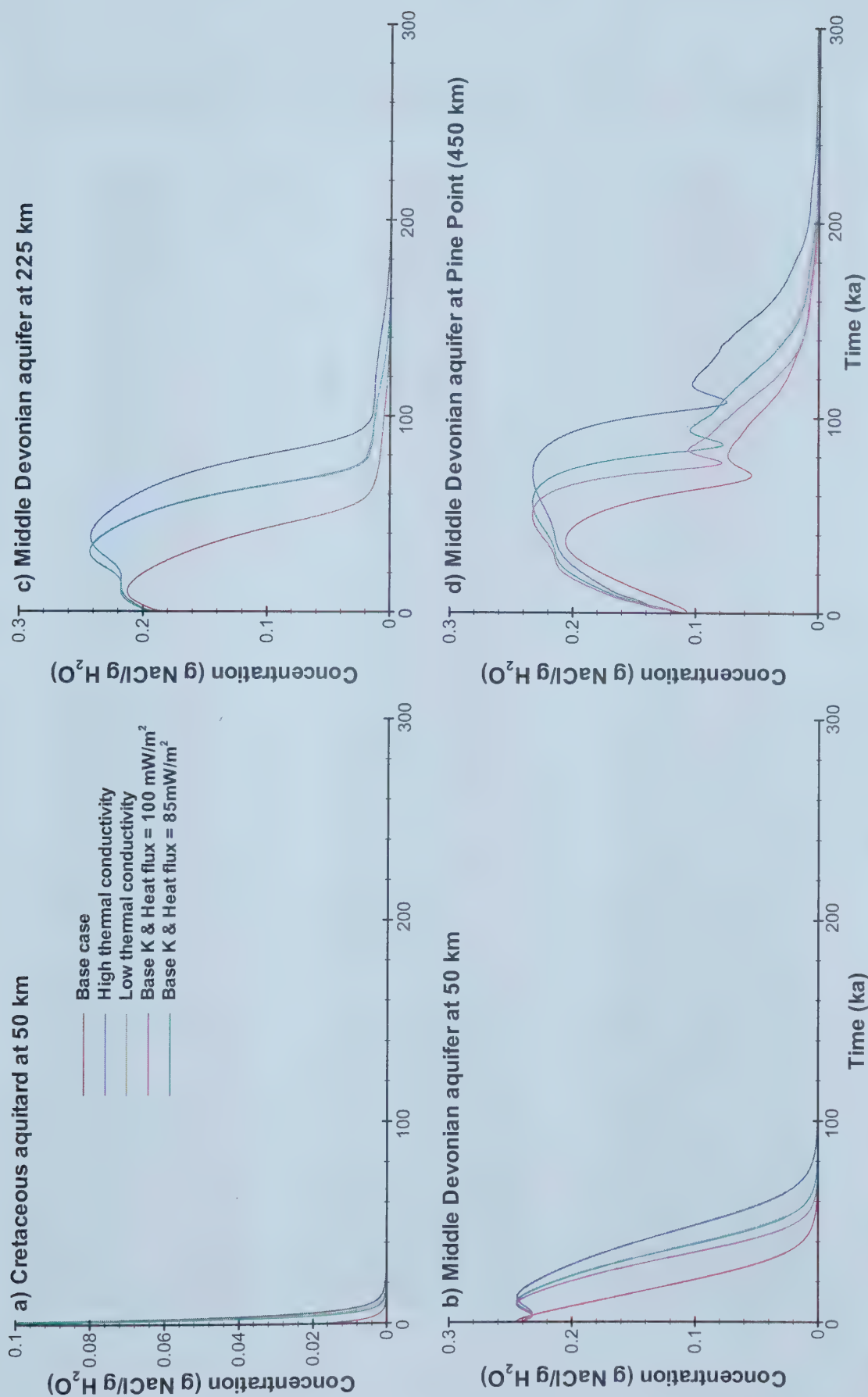


Figure 4.23: Transient variations in salinity for the base case Pine Point flow model and variations related to thermal properties at 4 observation points along the section. The observation points are a) situated 2500 m above the datum; and b), c), d) centred in the Middle Devonian aquifer.

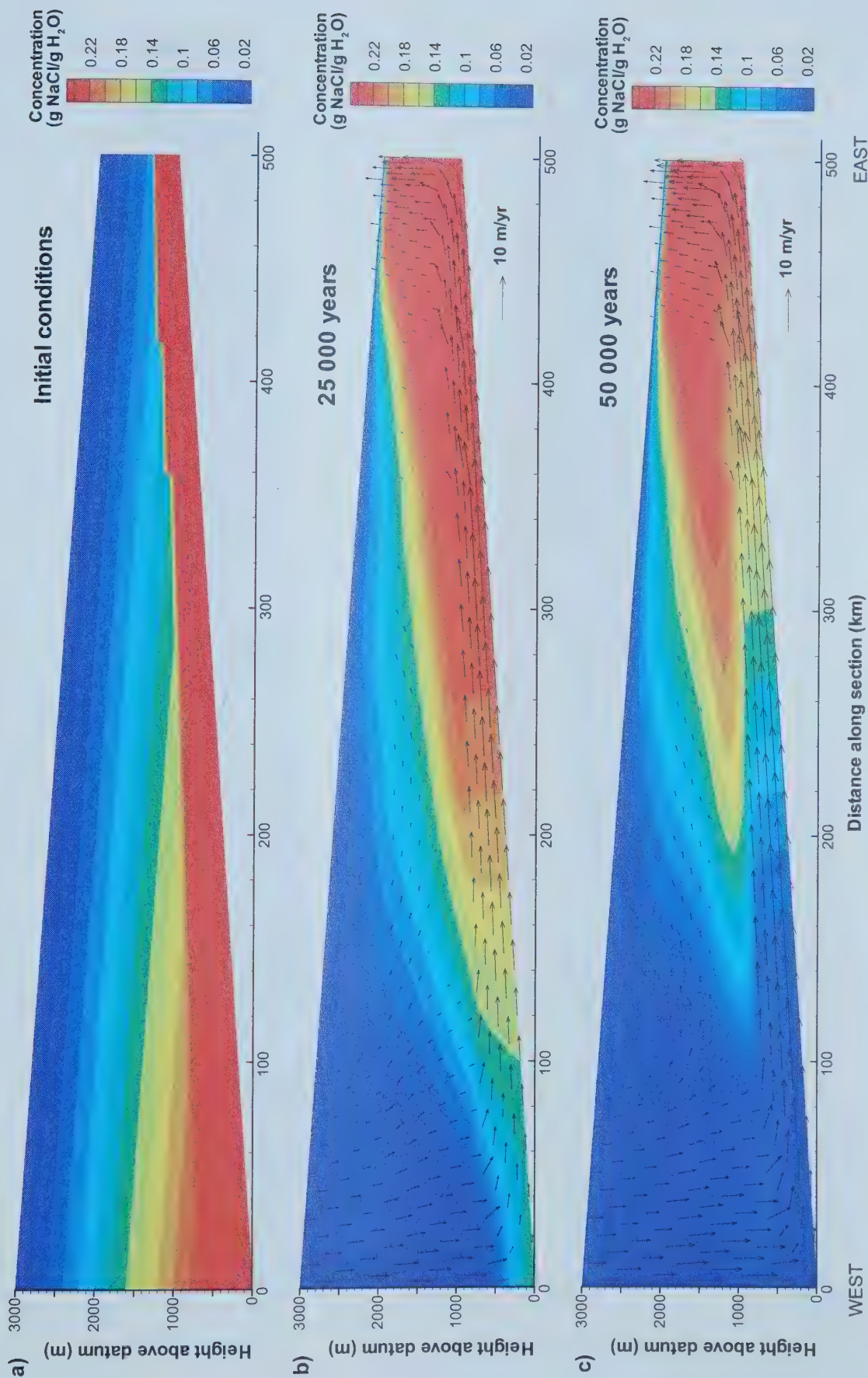


Figure 4.24: Salinity model of the Pine Point flow system, a) initial salinity profile; b) salinity distribution at 25 000 years; and c) salinity distribution, 50 000 years after instantaneous uplift.

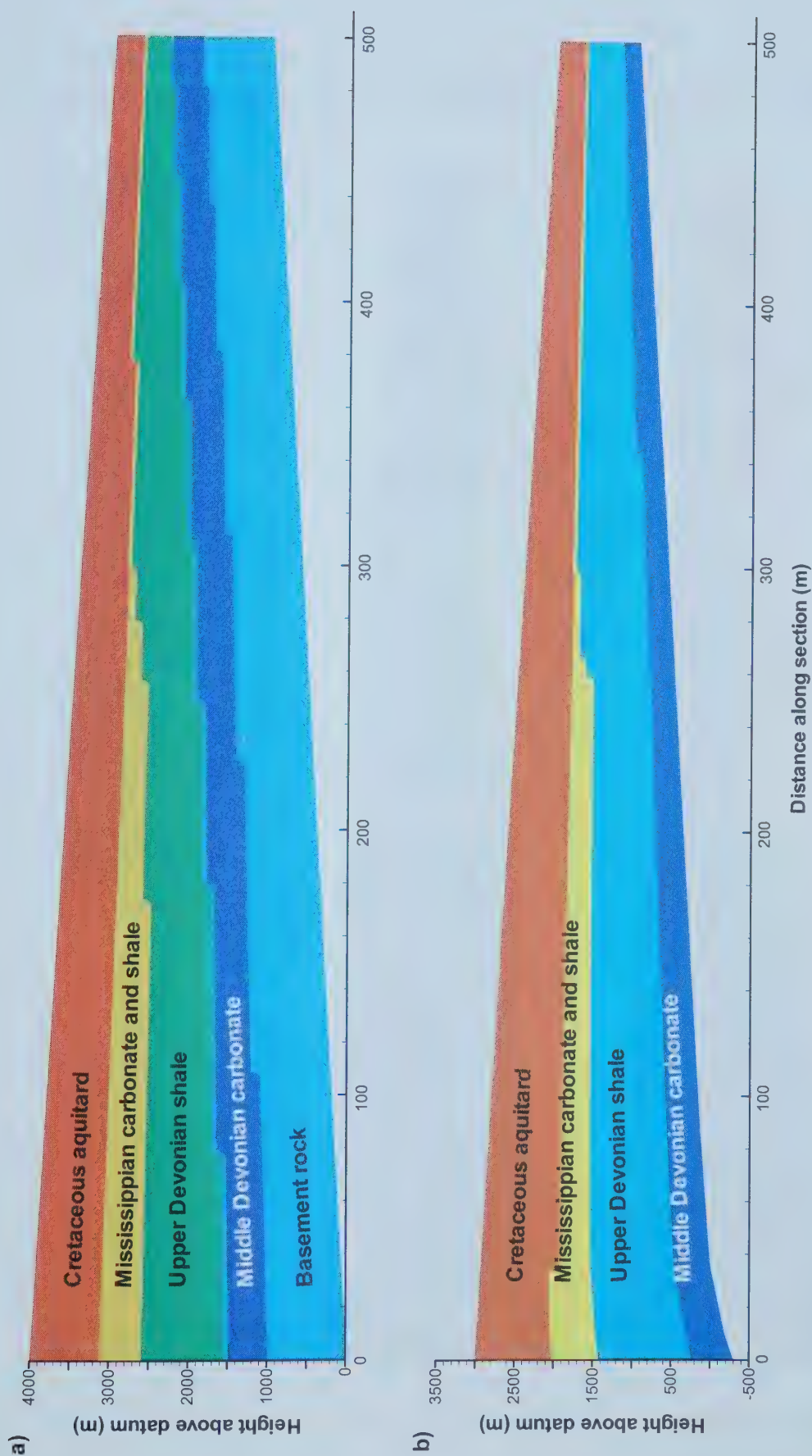


Figure 4.25: Model domains for two variations of the salinity model: a) 1 km basement rock unit added to bottom of model (basement); and b) lower boundary made 250 m deeper at western boundary (deep basin).

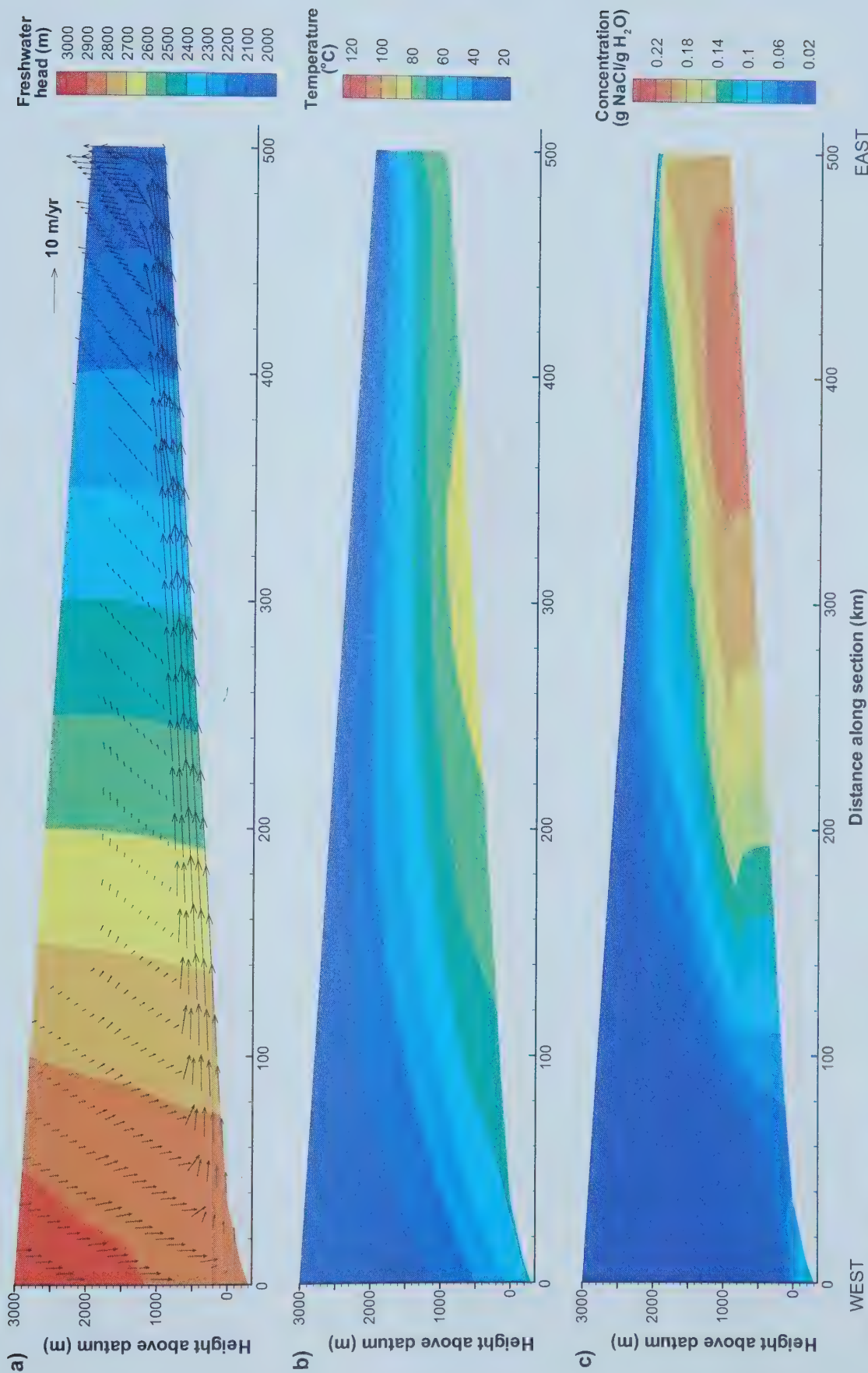


Figure 4.26: Deep basin model of Pine Point flow system, a) freshwater hydraulic heads and velocity vectors at steady state (500 000 years after instantaneous uplift); b) temperature profile at steady state; and c) salinity distribution at 50 000 years after instantaneous uplift.

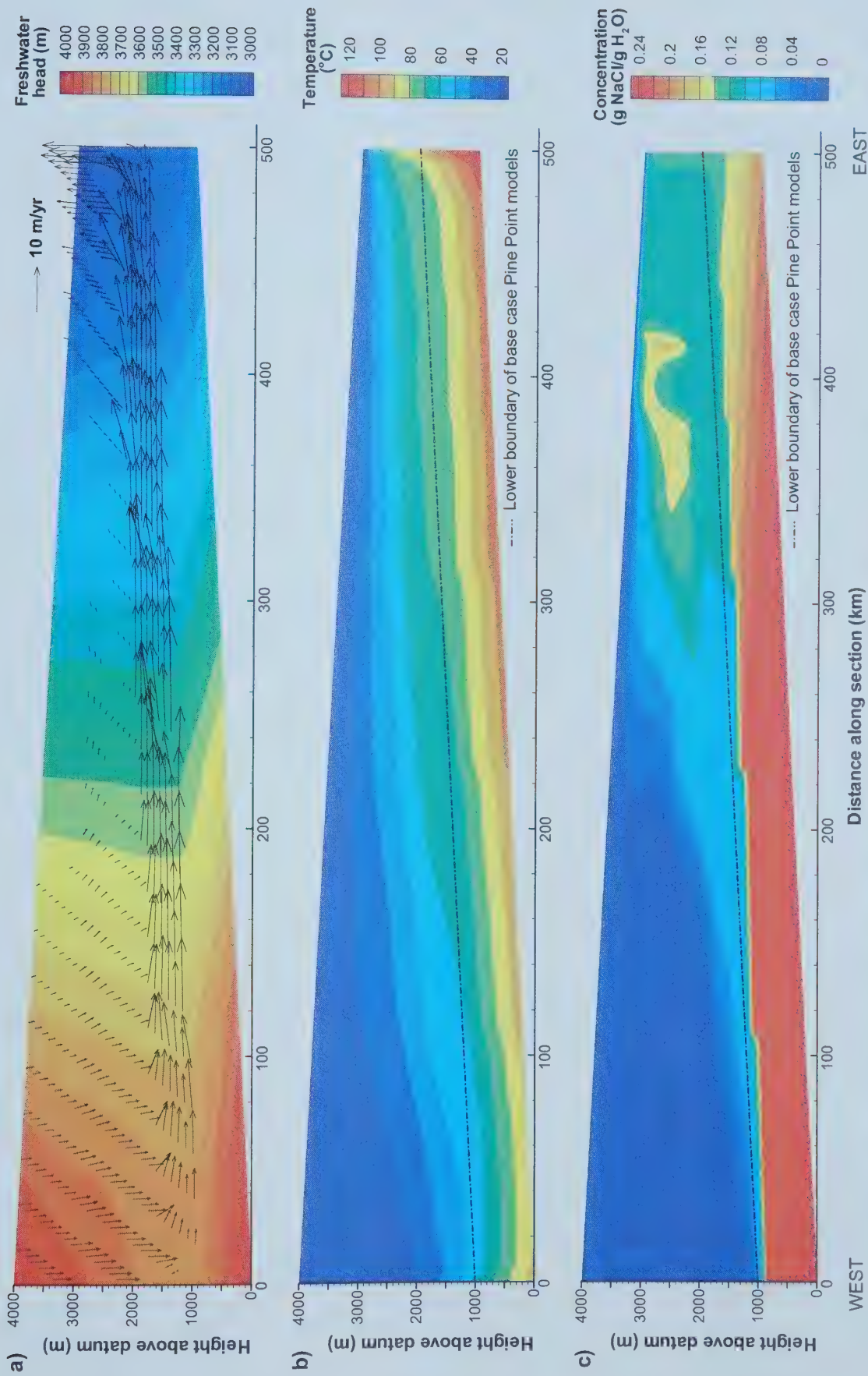


Figure 4.27: 1 km of basement rock added to base case Pine Point model, a) freshwater hydraulic heads and velocity vectors 500 000 years following instantaneous uplift; b) temperature profile at 500 000 years; and c) salinity distribution, 100 000 years after instantaneous uplift.

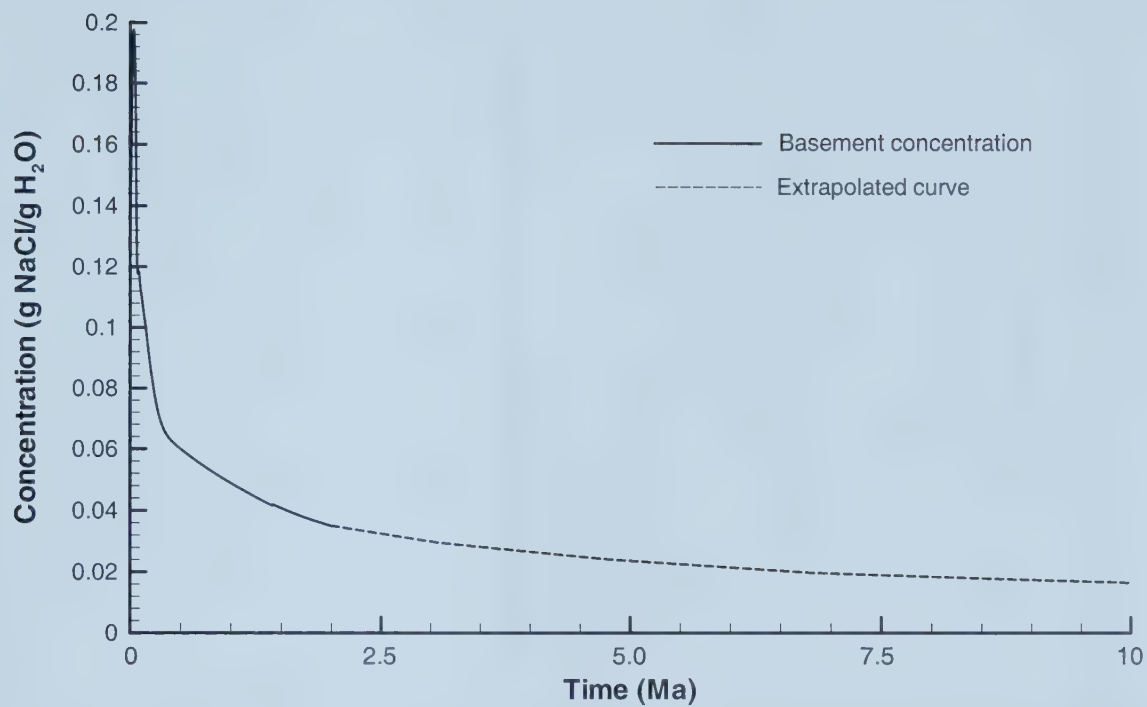


Figure 4.27d: Variation of concentration with time in the basement model. Much slower flushing is predicted with the addition of 1 km of basement rock.

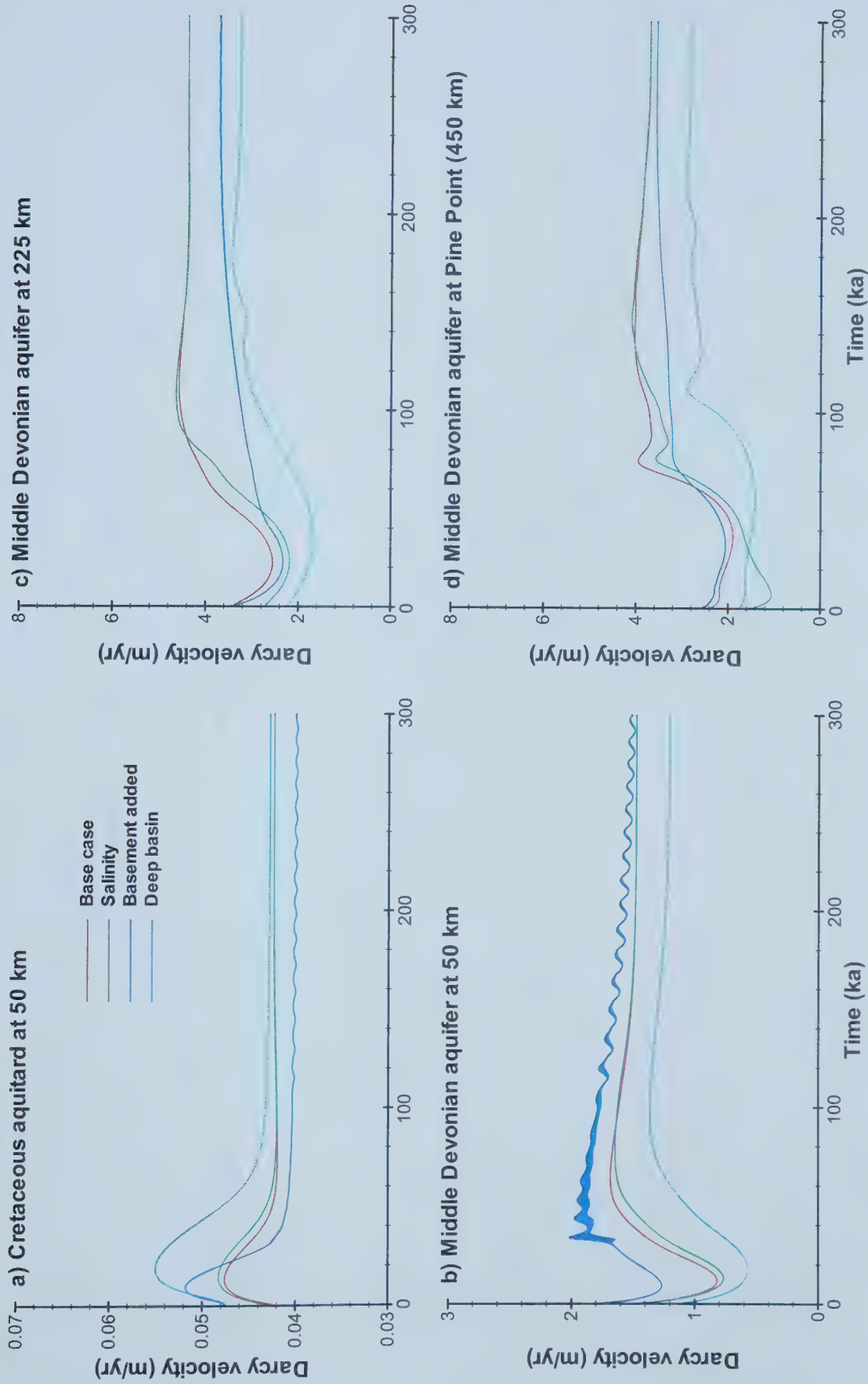


Figure 4.28: Transient variations in darcy velocity for the Pine Point model and variations of salinity conditions at 4 observation points along the section. Points are located approximately where base case points were situated previously. Thick solid blue line is made up of oscillations.

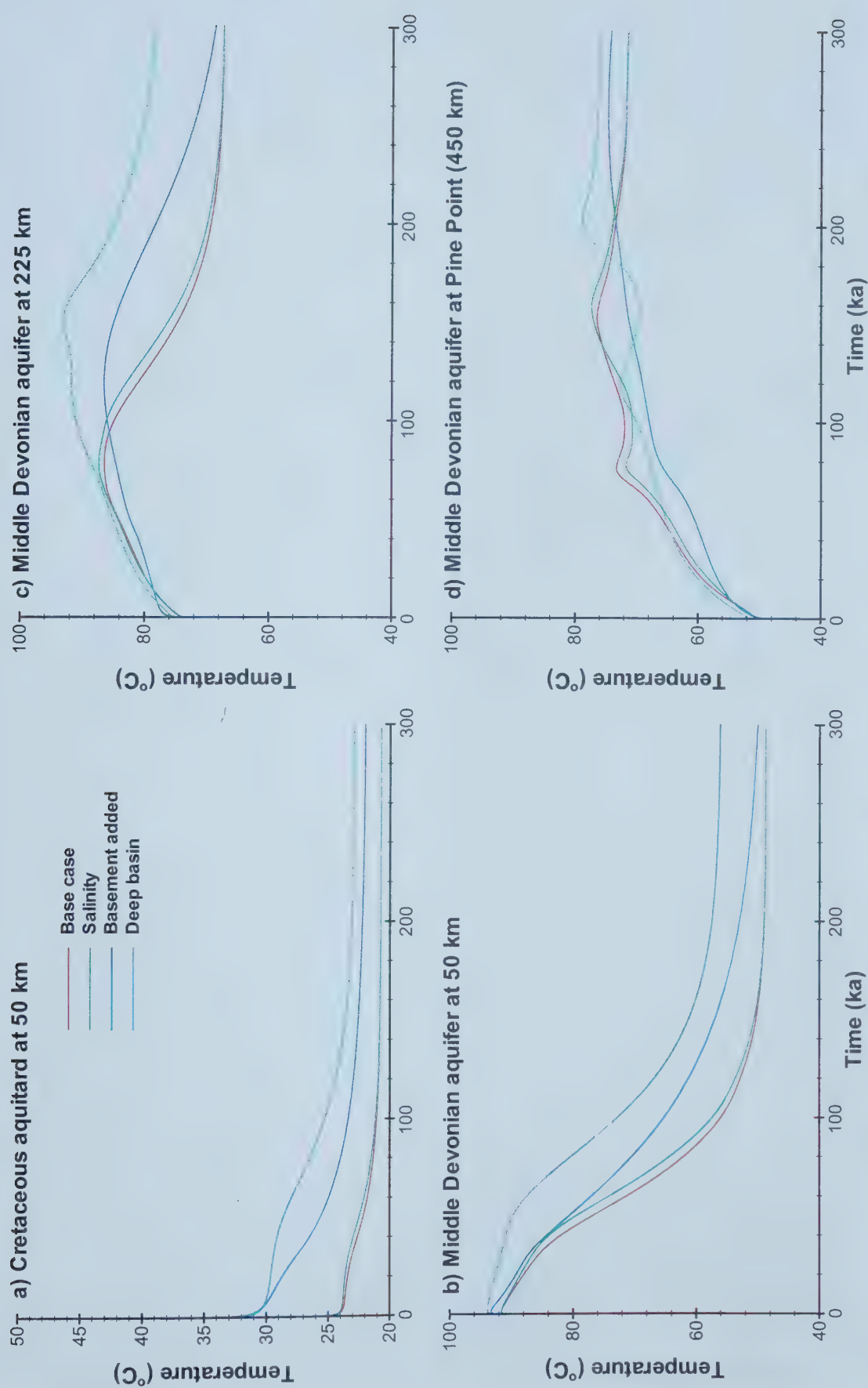


Figure 4.29: Transient variations in temperature for the base case Pine Point model and scenarios varying salinity at 4 observation points along the section. Points are located approximately where previously base case points are situated.

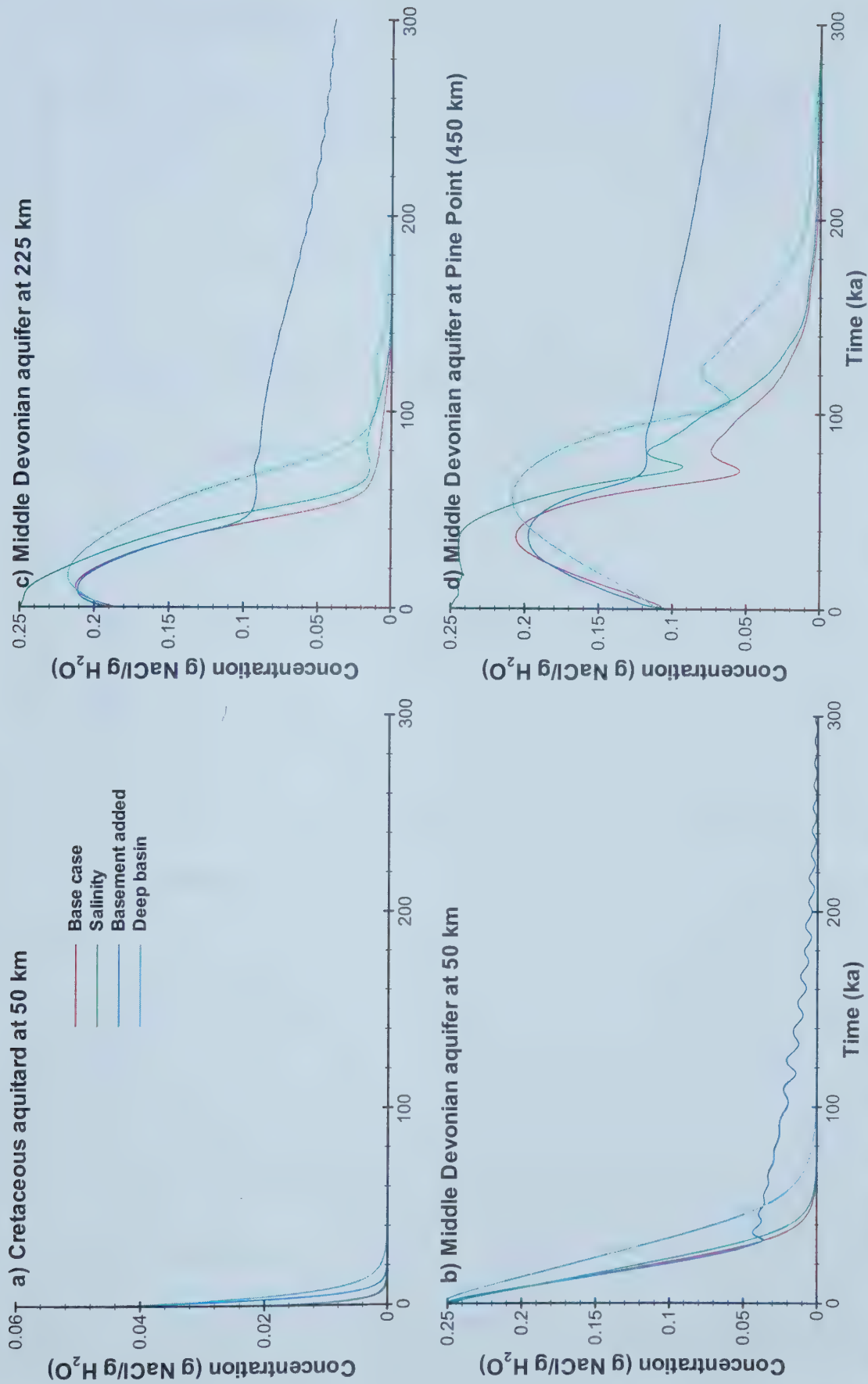


Figure 4.30: Transient variations in salinity for the base case Pine Point flow model and scenarios varying salinity at 4 observation points along the section. Points are located approximately where previous base case points are situated.

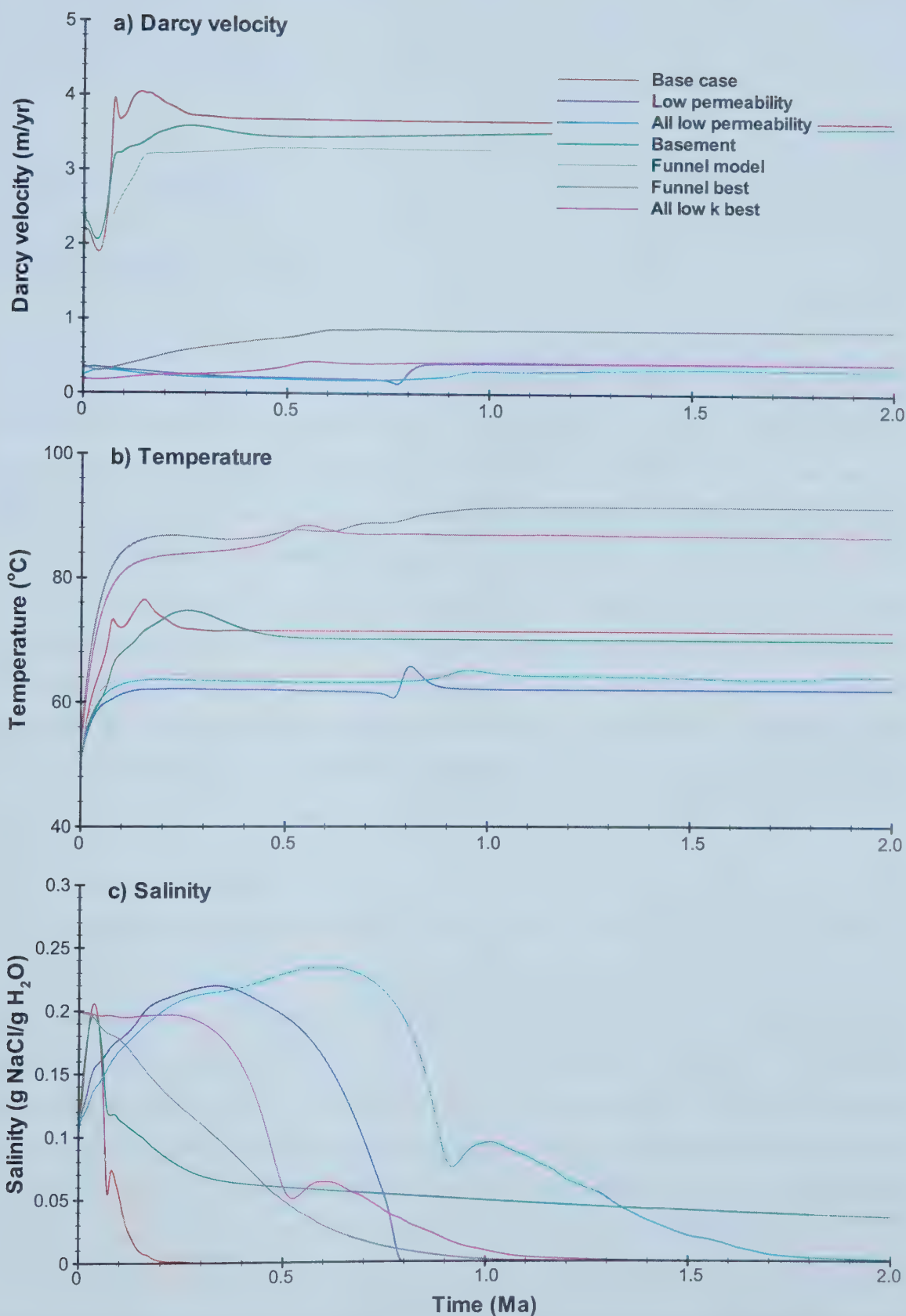


Figure 4.31: Comparison of all simulations with low permeability assigned to the Middle Devonian aquifer of the Pine Point model at the Pine Point observation point, a) darcy velocity (m/yr); b) temperature (°C); and c) salinity (g NaCl/g H₂O).

CHAPTER 5

ATHABASCA OIL SANDS

The onset of orogenesis at the margin of a sedimentary basin leads to deposition, burial and heating of sediments and organic matter. This sequence of events initiates petroleum generation and thus sedimentary basins often host large hydrocarbon accumulations. The hydrocarbons migrate out of the source rocks into permeable conduits, along which they travel until trapped. The secondary migration of petroleum through sedimentary basins is driven by buoyancy, capillary and hydrodynamic forces (England et al., 1991). The relative influence of each of these driving forces is dependent on rock and relative permeability, type of petroleum and magnitude of the driving forces. Some studies have shown that regional groundwater flow has a significant effect on the migration of petroleum (Tóth, 1980). The role of hydrodynamic forces in petroleum migration has been tested using numerical models and found to explain the accumulation of the Athabasca oil sands (Garven, 1989).

5.1 Athabasca oil sands

The Alberta basin hosts the Peace River, Cold Lake and Athabasca oil sands. The Athabasca oil sands, the largest deposit, is located at the eastern margin of the basin in Upper Devonian carbonates and Lower Cretaceous sandstones (Figure 5.1). Extensive biodegradation and water-washing has reduced parent, mature conventional oils to the present day Athabasca heavy oils (approximately 1 trillion barrels of oil). The source of the oils is hotly debated. Organic geochemistry analyses show that Athabasca oils are sourced from the Exshaw Formation (Brooks et al., 1988), whereas mass balance calculations require multiple source rocks to account for the volume of oil found in the Athabasca oil sands (Creaney and Allan, 1990). The high density and viscosity of the oils preclude further migration; however, the oils are thought to have migrated a long distance to the eastern part of the basin during latest Cretaceous time (~66-62 Ma; Ranger, 1994). Previous researchers have proposed that a

gravity-driven flow system caused the secondary migration of the petroleum found in the Athabasca oil sands (Tóth, 1978, 1980; Garven, 1989).

Numerical simulations of such a gravity-driven flow system predicted that accumulation of 80% of the Athabasca oil sands could be explained by miscible petroleum migration at rates of 2 to 10 m/yr over 10 to 50 million years (Garven, 1989). This scenario assumes dissolved hydrocarbon concentrations of 1 to 10 ppm, which are leached from source rocks overlying the Upper Devonian carbonates, the main aquifer. In the same gravity-driven flow system, immiscible petroleum migration could not account for the volume of oil in the Athabasca deposit due to slow migration rates, limited by viscosity, and an insufficient volume of oil sourced from strata underlying Upper Devonian carbonates. Capillary forces were omitted from the immiscible petroleum models (Garven, 1989).

The groundwater flow system, simulated in both the miscible and immiscible scenarios, produces high flow rates, which are a direct result of high permeabilities assigned throughout the model. These flow rates cause flushing of all basinal brine within 2 million years, implying that the basin was flushed repeatedly during accumulation of the Athabasca oil sands. The presence of large volumes of highly saline brines in the basin today (Hitchon and Friedman, 1969b; Connolly et al., 1990a) is inconsistent with Garven's (1989) simulations. Similarly, the modelled temperature profile is characterized by cool meteoric water recharging in the foothills and elevated heat flow near the basin margins, which poorly explains high formation temperatures of epigenetic minerals in the deep basin (Mountjoy et al., 1997 and others referenced).

This flow system is remodelled here, using a transient, fully-coupled (heat-solute-flow) model to more accurately simulate topography-driven flow along the Peace River transect. Such a model can now be developed using recently published measured permeabilities (Bachu and Underschultz, 1992) and calculated geothermal gradients (Bachu, 1993). A second scenario is modelled to quantify the effects of erosion following the Laramide orogeny on the Alberta basin. Erosion-induced underpressures and the longevity of the topography-driven flow system are investigated, using estimates of the thickness of eroded material removed over the past 60 million years. Both scenarios are evaluated based on their ability to predict measured salinity and temperature distributions along the section.

5.2 Numerical modelling

Garven (1989) developed a two-dimensional, finite-element model extending 724 km along the Peace River Arch from the foothills to the oil sands (Figure 5.2; Wright, 1984, cross-section C-C'). The *original* model (Figure 5.3d-f; Garven, 1989) predicts a steady-state gravity-driven flow system initiated by Laramide uplift, in which basinal brines move updip through Upper Devonian carbonates to the Lower Mannville aquifer. A basal heat flux of 70 mW/m² is assigned along the bottom boundary and a surface temperature of 20°C is imposed along the upper boundary. These conditions generate an initial geothermal gradient of approximately 30°C/km (Figure 5.4b). The simulations considered coupled fluid and heat flow, assuming a constant salinity gradient of approximately 7 eq. wt% NaCl/km depth (Figure 5.4c).

In this study, Garven's solution was reproduced (*replicated model*), using the transient RIFT2D model (Person et al., 2000; see Appendix A for description of RIFT2D). Garven's (1989) finite-element mesh was imitated, using 30 evenly-spaced rows to approximate the variably-spaced rows assigned to Garven's hydrostratigraphy. The present stratigraphic section is subdivided into nine hydrostratigraphic units, in which the Upper and Middle Devonian carbonates are the most permeable aquifers (Figure 5.2). The Lower Cretaceous sands, hosting the oil sands deposits, and Mississippian carbonates are classified as moderate aquifers. Evaporite and shale units are designated as tight aquitards and interbedded carbonate and shale or sandstone sequences are categorized as moderate aquitards. These hydrostratigraphic units are similar to those published recently (Hitchon et al., 1990; Bachu et al., 1993). Hydraulic, thermal and transport parameters were defined as in Garven (1989; Table 5.1). The *replicated* model simulates the oil sands flow system using Garven's salinity gradient only as an initial condition (see Appendix B for input file).

In the *replicated* model, steady state is reached 1.8 million years following instantaneous uplift. In the west, meteoric water recharges into the Upper Devonian aquifer, which conducts fluids to the Mannville sandstone aquifer. Calculated fluid velocities in the aquifers reach 1 to 6 m/yr, in agreement with Garven's findings. Temperatures are depressed by cool meteoric water in the foothills and elevated at shallow depths due to movement of warm basinal brines up-dip. Transient simulations of the *replicated* model show a warm pulse of saline water moving along the Upper Devonian aquifer (Figure 5.5 and 5.6b & c). The

temperature slug reaches a steady-state position between 300 and 500 km along the section, whereas the solute slug continues into the Mannville sandstone near the oil sands. A 200-km wide saline plume develops at surface, above the Upper Devonian aquifer subcrop. The Cretaceous aquitard does not seal the aquifers, but allows fluid to slowly reach the surface. Complete flushing of the basin with meteoric water occurs within 1.6 million years of instantaneous uplift, although some residual brine is trapped in both the deep basin and Prairie evaporite due to low flow rates and permeability values. Steady-state solutions match Garven's (1989) simulations; however, hydraulic heads in the deep basin differ due to the constant salinity gradient used by Garven (Figure 5.3a-f).

Table 5.1: Modelling parameters used in the Athabasca *replicated* and *revised* models. The *revised* model dispersivities are 100 times those used in the *replicated* model.

Hydrostratigraphic Unit	Porosity (%)	Replicated Horizontal Hydraulic Cond. (m/yr)*	Revised Horizontal Hydraulic Cond. (m/yr)*	Thermal Conductivity (W/m°C)**	Longitudinal Dispersivity (m)+
Lower Cretaceous Mannville sands	30	30	12	3.1	1.0
Cretaceous shale & sandstone	15	10	3×10^{-3}	2.1	0.1
Triassic-Jurassic shale & redbeds	10	1	5×10^{-2}	3.1	0.1
Mississippian-Permian carbonates	10	30	0.12	3.1	1.0
Lower Mississippian shale & carbonates (Banff/Exshaw)	10	10	6×10^{-6}	2.1	0.1
Upper Devonian carbonates	20	200	7.8	3.1	1.0
Upper Devonian shale & carbonates	10	10	1.2	2.1	0.1
Middle Devonian evaporites	5	1×10^{-3}	8×10^{-6}	4.6	0.1
Middle Devonian carbonates	20	200	3.9	3.1	0.1

* Anisotropy (k_x/k_z) was assigned as 100 for all units. Reference fluid density and viscosity are 998.2 kg/m^3 and $1.0 \times 10^{-3} \text{ Pa}\cdot\text{s}$, respectively.

** Thermal conductivity of the fluid was defined as $0.63 \text{ W/m}\cdot\text{°C}$ for all units.

+ Transverse mass and heat transport dispersivities were defined as 0.1 for all units. Apparent diffusion coefficient was assigned as $3 \times 10^{-3} \text{ m}^2/\text{yr}$ for all units.

5.3 Revised Model

The *original* model was criticized for including unrealistic permeabilities, and results in rapid flushing of the basin. New permeability data and greater computing power have allowed for the development of a more plausible model of the Peace River Arch flow system (*revised* model). The model domain was left unaltered, since Garven's topography is an average between maximum uplift and present day topographies (Willett et al., 1997). To allow for stable brine transport solutions, the finite element mesh was refined to $\Delta x = 4000 \text{ m}$, $\Delta y = 15 \text{ to } 200 \text{ m}$ and longitudinal and transverse dispersivity values were increased to 100 m and 10 m, respectively (see Appendix C). The basal heat flux was decreased to present day values along the section, which range from 40 to 60 mW/m^2 (Bachu, 1993).

New permeability and porosity data were incorporated into the *revised* model (Bachu et al., 1993; Table 5.1), and the hydrostratigraphy was adjusted accordingly. In the *original* model, the lower Mannville is classified as an aquitard in the foothills due to gas-saturation today; however, at the end of the Laramide orogeny, diluted seawater would have occupied this permeable unit (Holmden et al., 1997). In addition, the westernmost end of the aquifer is understood to be more permeable than the mid-section (Bachu and Underschultz, 1992). In the *revised* model, the Mannville aquifer extends to the foothills: up to 280 km along the section, the Mannville is assigned aquifer properties of the high permeability Middle Devonian carbonates and from 280 km to the oil sands aquifer, the Mannville unit has the same characteristics as the Upper Devonian shale and carbonates (Figure 5.8a). The rest of the hydrostratigraphy was adjusted slightly to reflect published sections (Hitchon et al., 1990; Bachu et al., 1993).

Transient fluid flow, heat flow and solute transport simulations of the Peace River Arch flow system were calculated using RIFT2D (see Appendix E for computer requirements). Instantaneous uplift was assumed to have occurred in the late Paleocene (~60 Ma). An initial salinity distribution was defined by Garven's salinity gradient, and solute transport was simulated, using over 1200 time steps of 50 000 years each. Specific storage values were assigned as zero. Thus flow system transients are only caused by temporal variations in salinity and temperature. No significant differences were observed when these solutions were compared to fully transient solutions with non-zero specific storage. The suite of Peace River Arch models simulated for this thesis is outlined in Table 5.2.

Table 5.2: Descriptions of all scenarios run along the Peace River Arch section.

Model Name	Parameter Varied
Fixed Grid Peace River Arch Models	
<i>Replicated</i> model	Copy of Garven's original model, which was run in RIFT2D with solute transport
<i>Revised</i> model	Measured heat fluxes and permeabilities are added to the <i>replicated</i> model
10^{-16} m^2	<i>Revised</i> model run with the Cretaceous aquitard permeability = 10^{-16} m^2
10^{-17} m^2 or best case	<i>Revised</i> model run with the Cretaceous aquitard permeability = 10^{-17} m^2
10^{-18} m^2	<i>Revised</i> model run with the Cretaceous aquitard permeability = 10^{-18} m^2
Salinity	Best case with 0.25 g NaCl/g H ₂ O salinity assigned to the Upper Devonian aquifer
Low permeability Mannville	Best case with low permeability Mannville section extended to disturbed belt
No Mannville	Best case with Mannville aquifer extension to disturbed belt removed
Erosion Models	
Erosion model	Best case model adapted for constant erosion of the model top surface
25% High k Mannville	Erosion model with western high k portion of Mannville shortened to 180 km
60% High k Mannville	Erosion model with western high k portion of Mannville extended along whole section

5.3.1 Best case solutions

Calibration of the *revised* model to fit present day salinity distributions was accomplished by varying the permeability of the Cretaceous aquitard (Figure 5.7; Hitchon et al., 1990; Bachu et al., 1993). The greatest uncertainty in estimates of the regional permeability is most likely in the Cretaceous strata: the majority of the Cretaceous has been eroded and the remainder is a collection of heterogeneous foreland basin sediments. In three calibration models, the Cretaceous strata were assigned a permeability of 10^{-16} , 10^{-17} , or 10^{-18} m^2 and the present day salinity distribution in the basin was compared to the observed values (Figure 5.7). In general, reducing permeability values results in flow rates more than two orders of magnitude slower than Garven's solution in the oil sands area. The 10^{-16} m^2 case predicts the highest flow rates of 20 to 28 mm/yr, whereas the 10^{-17} m^2 case produces rates of 6 to 10 mm/yr. Following 60 million years after instantaneous uplift, 10^{-16} m^2 flow rates flush the basin, whereas in the 10^{-18} m^2 case the Cretaceous aquitard caps the basin allowing little meteoric water to infiltrate. A Cretaceous aquitard permeability of 10^{-17} m^2 (*best case*) closely mimics the existing salinity profile, and predicts predominately conductive heat flow in the Alberta basin today.

The *best case* Athabasca model produces a distinctly different flow pattern from the *original* model due to the western extension of the Mannville aquifer. Recharge enters at the western end of the model, and moves along the Mannville aquifer to the oil sands (Figure 5.8b), with a small component of up-dip flow through the Upper Devonian carbonate and shale aquitard. In contrast to the *replicated* model, minor down-dip flow develops in the Upper Devonian aquifer soon after instantaneous uplift. The flow rates at the contact between the Upper Devonian aquifer and the Lower Cretaceous sands vary from 4 to 9 mm/yr, which are almost three orders of magnitude slower than the *original* model velocities. Calculation of hydraulic conductivity values in both Upper Devonian units demonstrated that convection, driven by formation water density, cannot explain the flow patterns in this area. In addition, the down-dip flow is in the opposite direction to force vector calculations for the present day flow system in the Upper Devonian carbonates (Michael and Machel, 2000). The low permeability of the Exshaw/Banff aquitard may prevent recharge into the deep basin, thereby generating underpressures in the deep basin.

The temperature distribution varies little over 60 million years and is predominately characterized by conductive heat flow (Figure 5.8c). Recharge cools the basin by approximately 10°C. The greatest deviation from a purely conductive temperature distribution is seen in the Paleozoic strata between 60 and 500 km, due to up-dip movement of brine and down-dip flow of fresher water. Slightly higher temperatures are found between 300 and 40 km along the section due to these flow patterns.

The predicted salinity distribution, 60 million years after instantaneous uplift, closely resembles the observed distribution today in the west (Figure 5.9c). The model predicts a tongue of high salinity in the mid-section of the Mannville, that is visible around 325 km. The imposed salinity gradient poorly predicts observed high salinity water in pre-Mississippian strata in the eastern portion of the model due to shallow depth (Figure 5.9c). There is some build up of saline brines at surface in the discharge zone caused by the low permeability of the Cretaceous aquitard. In the *best case* scenario, most of the saline fluids discharge east of 600 km as opposed to dispersing vertically above the Upper Devonian subcrop edge, as in the *replicated* model. The new permeabilities produce such slow flow rates that the present volume of oil sands could not have accumulated since maximum burial due to gravity-driven fluid flow alone.

5.3.2 Salinity model

To resolve the discrepancy between measured and predicted formation water salinity in the eastern end of the model, an identical scenario, the *salinity* model, to the *revised* model was simulated with an initial Upper Devonian brine concentration of 25 eqv. wt% NaCl (Figure 5.10b). This model produced slightly slower flow rates in the whole model, except in the deep basin of the Upper Devonian (Figure 5.14). This general slowing of the flow system can be attributed to an increase in fluid density associated with higher salinity across the basin (Figure 5.15). The salinity profile fits the measured salinities very closely (Figure 5.10c). In general, the Upper Devonian salinity is higher than in the *best case* model except in the deep basin where the salinity gradient becomes less steep. Applying a uniform salinity across hydrostratigraphic units may better approximate today's salinity; however, simulation constraints make this option impractical for further sensitivity analysis.

5.3.3 Western Mannville Permeability

To match observed salinity patterns in the basin today, the Mannville aquifer was extended to the west, as in the *best case*. Because this hydrostratigraphic unit has such a profound effect on the flow system, two cases were evaluated through variation of Mannville aquifer permeability (*no Mannville* and *low permeability Mannville* cases). In the *no Mannville* case, the extension of the Mannville hydrostratigraphic unit was removed to leave a permeability distribution very similar to that of the *replicated* model (Figure 5.11b). The Mannville permeability is lowered from $10^{-13.9}$ m² in the *best case* to 10^{-17} m². In the *low permeability Mannville* case, the Mannville aquifer is assigned a permeability of $10^{-14.4}$ m², which is equivalent to the permeability of the mid-section of the Mannville aquifer in the *best case* (Figure 5.11a).

Transient flow simulations show that in the *no Mannville* case, the Mississippian and Permian carbonates act as the principal conduit for water where the unit pinches out (350 km) and flow continues along the Upper Devonian aquifer (Figure 5.12c). The *low permeability Mannville* flow pattern follows the Mannville aquifer in the west and then continues through the Upper Devonian aquifer (Figure 5.12b). Flow rates monitored at four observation points show that both the *low permeability Mannville* and *no Mannville* scenarios predict slightly lower flow rates than the *best case* allowing high salinity water to remain in the western part of the model longer (Figure 5.14a and b). Compared to the *best case*, less meteoric recharge enters the basin at the uplifted area, but a second recharge zone develops between 350 and 400 km along the section (Figure 5.12b and c). The salinity distributions, predicted by these variations on the *best case*, are more concentrated in the west and more dilute in the east than the *best case* solutions due to lower flow rates (Figure 5.13 and 5.15). To better approximate the observed salinity distribution, the overlying aquitard permeability would have to be increased for both the *no Mannville* and *low permeability Mannville* cases to facilitate flow into the deep basin.

5.3.4 Fixed grid conclusions

Replicated, transient simulations of the Athabasca oil sands flow system (Garven, 1989) predicted complete flushing of the Alberta basin within 1.6 million years, in contradiction to existing water salinity along the section. The *revised* model, using published permeabilities and basal heat fluxes, simulates a gravity-driven flow system that closely replicates the

present day salinity profile, assuming uplift occurred around 60 Ma. The addition of an initial Upper Devonian brine concentration of 25 eq. wt% NaCl better reproduces high brine concentrations in the pre-Mississippian strata in the eastern portion of the basin (*salinity* model). Scenarios assuming lower permeability in the western Mannville unit do not improve the predictions of the *salinity* solution. None of the variations of the *best case* scenario alter the temperature distribution. Although the present day salinity distribution is best predicted by the *salinity* case, the estimated Alberta permeabilities produce much slower flow rates than Garven's (1989) model, and therefore formation of the Athabasca oil sands cannot be predicted assuming dissolved-phase hydrocarbon transport.

To explain the genesis of the Athabasca oil sands, other processes such as convergent flow, tectonics, structure or buoyancy/capillary forces need to be included in numerical models. The inclusion of buoyancy and capillary forces is beyond the scope of this thesis, as is a detailed analysis of structural controls. In terms of convergent flow, others have noted a correlation between the location of the Peace River, Cold Lake and Athabasca oil sands and the absence of the Lower Mannville aquifer (Figure 5.1; Creaney et al., 1994). The deposits are situated between holes or zero-isopach zones of the Lower Mannville suggesting that oil may have been funnelled along tongues of the Lower Mannville aquifer.

In terms of water flow, calibration of the *best case* suggests that the existing salinity profile is a snapshot of a basin being flushed by meteoric water. This conclusion does not fit with evidence of local- and regional-scale topography-driven flow, and erosion-induced underpressuring in the Alberta basin. However, evolution of topography during and following Laramide tectonics may provide a clearer picture of the past and present basin-wide flow systems, as well as insight into petroleum migration.

5.4 Effect of erosion

Readjustment of the stress field, following an orogeny, causes significant and relatively rapid changes in topography and consequently fluid flow systems. In response to early unloading of the crust, the foreland basin is uplifted quickly in the foredeep. When adequate relief evolves, a regional gravity-driven flow system develops. Relief and erosion rates continue to increase until the point of maximum topography (uplift rates equal maximum erosion rates). From this point, erosion dominates the system and gradually decreases the regional hydraulic

gradient across the basin. Erosion rates may exceed the diffusivity of low permeability rocks, causing disequilibrium pore pressure in response to unloading (Neuzil and Pollack, 1983).

Uplift and erosion rates control the timing of flow system development and decay. Uplift rates are approximately an order of magnitude greater than erosion rates and are controlled by unloading and isostatic rebound (Ankert, 1970). Erosion rates are primarily dependent on relief; however, climate, lithology and vegetation dictate erosion patterns and, to a minor degree, denudation rates (Pinet and Souriau, 1988). Typical erosion rates vary from 10 to 500 mm/yr and decrease as relief diminishes, i.e., away from the uplift area and through time (Ankert, 1970). Using estimates of eroded material and total relief across the Alberta basin (Issler et al., 1999), empirically-derived denudation rates (Ankert, 1970) were calculated to range from 0.3 to 0.007 mm/yr.

Engineering studies have measured the response on shales for the construction of tunnels, dams and bridges in Alberta. Similarly, many studies have shown that the high compressibility of Cretaceous shales in the Alberta basin has led to significant underpressures during erosion due to rock dilation, and low hydraulic conductivity (Tóth and Millar, 1983; Tóth and Corbett, 1986; Parks and Tóth, 1995). Analysis of hydraulic gradients in foreland clastics deposited during the Cretaceous to Tertiary, i.e., Lea Park to Paskapoo formations (Figure 3.2a), revealed convergent vertical fluid flow into the Bearpaw and lower Edmonton Group aquitards (Parks and Tóth, 1995). Such a flow field can only be explained by erosion-induced rock-pore dilation (Parks and Tóth, 1995). The degree of underpressuring is proportional to erosion rates, storage and thickness of the unit, but inversely proportional to hydraulic conductivity. Erosion, not only gradually decreases the topographic driving force, but also may generate underpressures that redirect fluid flow towards the disturbed belt. Erosion-induced underpressures short-circuit the regional topography-driven flow system when pressures are equivalent to those in the discharge zone.

5.4.1 Model design

In the Alberta basin, remnants of both a regional-scale topography-driven flow system related to uplift (Hitchon, 1969; Bachu, 1995) and erosion-induced underpressuring within Cretaceous shales near the disturbed belt have been documented (Tóth and Millar, 1983; Corbett and Bethke, 1992; Parks and Tóth, 1995). Modelling of the Athabasca flow system thus far has assumed a constant, inclined topography driving steady-state flow (Garven,

1989). Other studies in the basin have considered the transient nature of the topography; however, these solutions did not include solute transport (Bekele, 1999). Hydrogeologic modelling of the southeast Missouri Pb-Zn ore district incorporated decreasing erosion rates, but ignored rock compressibility in light of high diffusivity strata along the modelled section (Appold and Garven, 1999). Transience of the flow system was investigated by comparison of steady-state solutions at discrete moments in time following periods of erosion (Appold and Garven, 1999).

Both uplift and erosion affect the relief of a basin, and therefore the duration and timing of a topography-driven flow system. High relief conditions exist when uplift and erosion rates are close to being equal. Since maximum uplift rates are typically 10 times greater than maximum erosion rates (Ankert, 1970), typical erosion rates maintain high topography for many millions of years and may allow for long transport distances at moderate flow rates. For the following simulations, instantaneous uplift can be assumed and fluid flow is simulated from maximum uplift and to present day, i.e., 60 million years of flow, based on this analysis.

5.4.2 *Erosion case*

To test the impact of gradually decreasing the hydraulic driving force within the Alberta basin, the *best case* model was adapted to simulate erosion from maximum uplift to present day (*erosion* model). The amount of eroded material along the section was taken from estimates based on coal moisture content (Issler et al., 1999). The Cretaceous aquitard was thickened across the model to 4 km in the west and 1 km in the east, increasing the maximum basin depth to 7 km. These data suggest that erosion occurred across the whole section due to dynamic subsidence. In contrast, simulation of the Missouri flow system assumed no erosion at the discharge zone (Appold and Garven, 1999).

Morphology of the model surface controls local flow systems, and distributes the regional hydraulic gradient along the top boundary. In theory, an eroded landscape assumes an exponential shape (Ahnert, 1970), unlike the linear, inclined surface of the *best case*. With such a landscape, the regional hydraulic gradient is distributed non-uniformly across the model domain. In the Alberta basin, an exponential landscape slightly reduces the lateral driving force in the eastern portion of the model. Test simulations, which preserved

present-day geomorphologic features along the section back to the time of maximum uplift, resulted in significant distortion of the flow system. In agreement with these simulations, Tóth and Corbett (1986) reasoned that much of the morphology of today's topography is a result of erosion and glaciation during the last 5 million years. For these reasons, topography of the Alberta basin at maximum uplift was estimated using an exponential function and present day topography was incorporated later (Appendix F).

To study erosion-induced underpressuring, rock compressibility was assigned to each hydrostratigraphic unit (Table 5.3) and the finite element mesh deforms with erosion to produce truly transient solutions. Erosion rates are held constant over the duration of the simulations. This maintains maximum relief and hydraulic gradient across the section, but minimizes the effect of erosion-induced underpressures (Parks and Tóth, 1995). In the *erosion* model, the Cretaceous aquitard is eroded for 58 million years at a constant rate at each column of the mesh, e.g., at column 2 in the west, 0.0265 mm/yr is removed, whereas at column 70, near the Athabasca river, 0.0163 mm/yr is removed. These erosion rates are approximately an order of magnitude smaller than those measured today (Ahnert, 1970). Inferred erosion rates, from 63 to 54 Ma in the Black Hills of the adjacent Williston basin, are twice the simulated values (Lisenbee and Dewitt, 1993). However, it is unreasonable to adjust the thickness of eroded strata to correct rates of erosion and beyond the scope of the project to vary erosion rates in time and space. Locally, higher rates of erosion are applied after 58 million years of flow, to carve out the present day land surface (Figure 5.16c).

Table 5.3: Modelling parameters used in Athabasca *erosion* models.

Hydrostratigraphic Unit	Porosity (%)	Erosion Rock Compressibilities (10 ⁻⁹ / Pa)	Erosion Horizontal Hydraulic Cond. (m/yr)*	Thermal Conductivity (W/m°C)**	Longitudinal Dispersivity (m)#
Lower Cretaceous Mannville sands	30	2.3	12	3.1	100
Cretaceous shale & sandstone	15	7.5	3x10 ⁻³	2.1	10
Triassic-Jurassic shale & redbeds	10	6.0	5x10 ⁻²	3.1	10
Mississippian-Permian carbonates	10	6.4	0.12	3.1	100
Lower Mississippian shale & carbonates (Banff/Exshaw)	10	0.65	6x10 ⁻⁶	2.1	10
Upper Devonian carbonates	20	5.9	7.8	3.1	100
Upper Devonian shale & carbonates	10	8.0	1.2	2.1	10
Middle Devonian evaporites	5	0.65	8x10 ⁻⁶	4.6	10
Middle Devonian carbonates	20	6.4	3.9	3.1	10

* Anisotropy (k_x/k_z) was assigned as 100 for all units. Reference fluid density and viscosity are 998.2 kg/m³ and 1.0x10⁻³ Pa·s, respectively.

** Thermal conductivity of the fluid was defined as 0.63 W/m°C for all units.

Transverse mass and heat transport dispersivities were defined as 10 for all units. Apparent diffusion coefficient was assigned as 3x10⁻³ m²/yr for all units.

The *erosion* boundary conditions are generally identical to those in the *best case* model. The water table varies with the elevation of topography and all recharge is assumed to be meteoric water. The surface temperature is fixed at 10°C and the basal heat flux is varied, as in the *best case* between 40 and 60 mW/m². Addition of 900 m of Cretaceous strata at the western end of the model, necessitated a reduction in the salinity gradient from 0.07 to 0.06 g NaCl/g H₂O/km. Unloading compressibility values were assigned to each hydrostratigraphic unit based on typical values for each lithology as estimated by Neuzil (1994). The Exshaw/Banff aquitard was assigned an abnormally low compressibility because it has undergone multiple periods of burial and will not expand appreciably due to unloading.

Flow patterns

Transient simulations of the *erosion* case predict a large recharge zone and high flow rates in the Mannville aquifer due to the high topographic driving force. As in the *revised* model, flow moves along the Mannville aquifer in the west and descends into the Upper Devonian carbonates, 350 km along the section. Soon after instantaneous uplift down-dip flow begins in the Upper Devonian aquifer west of 300 km, which again is a function of the Exshaw/Banff aquitard inhibiting recharge into the deep basin. As denudation continues, the surface recharge zone shrinks and flow rates decrease. Flow rates of the *erosion* case are comparable to those in the fixed grid cases in the west, but eastern flow rates are at most a third of fixed grid values (Figure 5.21). A decrease in flow rates from west to east reflects the non-uniform distribution of topographic gradient across the model. All flow rates in the *erosion* model decrease over time in accordance with gradual erosion of relief (Figure 5.21).

The regional gravity-driven-flow system gradually decays and by 6 Ma, flow rates are generally less than 1 mm/yr except in the western Mannville aquifer. Erosional underpressuring across the whole section begins soon after instantaneous uplift (~ 58 Ma) (Figure 5.17). The surface remains normally pressured due to the boundary conditions and the shape of the pressure versus depth profile changes minimally over time. In the last 2 million years, the fluid flow in the upper 500 m of the section reverses direction and moves down-dip into the basin due to high underpressures. The rapid development of underpressures can be attributed to doubling of erosion rates in some regions to generate surface topography observed today. This response suggests that the model is highly sensitive to erosion rates, which are set to a minimum for 58 million years.

As variable topography develops, recharge at local highs and discharge at the Peace and Athabasca rivers increase significantly, dividing the regional-scale flow regime into local systems. High flow rates at the Athabasca River reflect steep topographic gradients and surface exposure of the high permeability Mannville aquifer (Figure 5.16 and 5.20). Evolution of the geomorphology is poorly understood, thus timing of river incision and localized erosion may have an appreciable effect on the duration and discharge zones of any regional-scale flow system.

Temperature distribution

During erosion, temperatures gradually cool as burial depths decrease (Figure 5.22). Over the 60 million years of erosion, temperatures drop approximately 20°C in the west and 15°C in the east. These temperature changes are equivalent to the decrease in depth of burial due to erosion, whereas Appold and Garven (1999) reported a 60°C temperature decrease during erosion. This significant decline in temperature is attributable to both decreasing advection of heat and reduction in burial depths. The present day *erosion* solution predicts maximum temperatures of approximately 130°C, equivalent to reported values (Bachu and Burwash, 1994). Simulations predict that the eastern part of the basin has lower geothermal gradients due to influx of cool water at local highs. Inclusion of the present day topography diminishes the plume of saline fluids in the discharge area, which persisted in the fixed grid cases. The dominance of conductive heat flow is most clearly demonstrated in depressed temperatures beneath river valleys along the section and by isotherms following the surface expressions of topography (Figure 5.18).

Salinity patterns

The initial solute distribution in the basin underestimates the salinity of Devonian strata at the eastern end of the model (Hitchon et al., 1990; Bachu and Underschultz, 1992). As flow moves up the Mannville aquifer, a tongue of saline fluid moves towards the oil sands and some movement of solute out of the deep basin is predicted (Figure 5.19b and c). A slug of warm brine is predicted between 300 and 450 km in the Mannville due to upward flow along the Devonian shale and carbonate unit and down-dip flow in the overlying Upper Devonian aquifer (Figure 5.18). By 21 Ma, a slightly saline plume develops near the surface between 225 and 280 km, in the vicinity of the Peace River (Figure 5.19e). This discharge zone may

be a product of the low permeability zone in the mid-section of the Mannville aquifer, which deflects flow into the Cretaceous since the Exshaw/Banff aquitard inhibits downward flow.

Differences, between the salinity distributions at present day in the *erosion* model and the *best case* include, the upwelling of brines at the Peace River, higher salinity across the whole basin, and less transport of solute out of the deep basin (Figures 5.20 and 5.9). Higher salinity values across the basin suggest that the initial salinity gradient should be decreased. Alternatively, increasing the Cretaceous aquitard permeability may increase flow rates and allow for more meteoric water infiltration, as well as transport of solute out of the deep basin. In the *erosion* case, transient salinity curves at discrete observation points represent only the initial flushing of a basin by topography-driven flow rather than moderate flushing as seen in the *best case* (Figure 5.23). Again, formation water salinity is lower in the *erosion* case than measured values at the eastern margin of the basin (Figure 5.20). Adding a uniform solute concentration along the Upper Devonian aquifer or designation of the Middle Devonian evaporites as a source of solute may ameliorate the problem. In general, the salinity pattern is similar to the observed distribution today.

5.5 Discussion

Any topography-driven flow system is controlled by the spatial distribution of permeability and the magnitude of relief or shape of the land surface. These two factors remain constant in the *best case* Athabasca model, but vary in the *erosion* case. In the *best case*, the linear shape of the ground surface provides a maximum, uniform and steady-state topographic driving force, which gradually flushes the basin of solute as dictated by permeability. In the *erosion* model, the regional topography-driven flow system decays due to gradual erosion of the land surface, which diminishes the topographic gradient and produces underpressures in high diffusivity strata. In both models, temperature patterns do not significantly affect flow patterns due to low flow rates and, therefore, dominately conductive heat flow. As demonstrated in the *salinity* model, varying salinity has only a minor impact on these regional-scale flow systems.

Both the fixed grid and erosion cases share the same spatial distribution of permeability for 30 million years following instantaneous uplift. The Lower Mannville aquifer acts as the primary conduit for fluids moving east, and the overlying, low permeability Cretaceous

aquitard inhibits discharge of these fluids until the oil sands region. Flow in the Upper Devonian aquifer moves up-dip west of the Exshaw/Banff subcrop, but underpressures develop beneath the Exshaw/Banff aquitard. This prevents fluids from infiltrating into the deep basin. The resultant down-dip flow has not been predicted by force vector calculations suggesting that either the Exshaw/Banff is not tight and/or continuous into the disturbed belt, or Upper Devonian underpressures are dissipated by fluids from the basement or disturbed belt.

Relief across a basin defines the hydraulic gradient attributable to topography, whereas the shape of the land surface or water table distributes this topographic gradient along the section. In the fixed grid cases, the uniform steady-state, but moderate, topographic gradient optimizes the driving force across the basin. This basin framework promotes lateral flow to the east and vertical flow in the recharge and discharge zones. Models predict relatively steady-state flow rates and effective flushing of solute. In contrast, the *erosion* case experiences continuous constant-rate decreases in elevation and relief along an exponential landscape. Although the regional topographic gradient in the *erosion* model is greater than the fixed grid gradient for more than 30 million years, lower flow rates are consistently simulated in the eastern portion of the *erosion* model. In explanation, the non-uniform distribution of topographic gradient generates much higher flow rates than the *best case* initially in the western portion of the *erosion* model, but an exponential decrease in gradient towards the east limits lateral driving forces. In time, constant erosion of the Cretaceous aquitard decreases the regional gradient, thereby lowering flow rates and temperatures across the basin. The combination of decreasing topographic gradient in time and space leads to high salinity conditions throughout the basin and little infiltration of meteoric water into the deep basin.

In the *erosion* model, thinning of the Cretaceous aquitard, exaggerated by the exponential landscape, results in discharge of saline fluid in the vicinity of the Peace River. This solution is supported by a discontinuous belt of solnetzic or salt-rich soil zones, approximately 150 to 200 km from the disturbed belt (Figure 5.1). These zones coincide with the Peace River along the Peace River Arch section and are located just west of the holes in the Lower Mannville aquifer. Furthermore, the presence of the Peace River oil sands may also support a discharge zone in the Peace River area as shown in the *erosion* model. The location of the

discharge zone may either be related to the extent of the high permeability section in the Mannville aquifer or indicate that the Peace River has been a drainage feature in the basin since the Tertiary. Alternatively, fluids may tend to discharge in this region due to the decrease in hydraulic gradient generated by the exponential surface.

The impact of Mannville permeability on solute discharge was tested using two scenarios, in which the length of the high permeability zone in the west was varied. Extending the high permeability section of the Mannville aquifer across the whole section (*60% High k Mannville* case) allows more solute and fluid to be conducted to the oil sands area. The flow rates increase resulting in higher salinities in the oil sands area and a surface discharge zone only at the eastern end of the model. Slightly elevated salinity waters still discharge at the Peace River, which can be attributed to either the exponential shape of topography or focused flow to the low topography due to river incision. A second scenario, in which the high permeability zone is shortened to 180 km in length, predicts highly saline discharge west of the Peace River (*25% High k Mannville* case). These models demonstrate that the extent of the high permeability zone in the Mannville aquifer directly affects the location of high salinity discharge at the surface, whereas the exponential shape of the topography plays only a minor role.

Furthermore, thickening of Cretaceous shale and higher erosion rates towards the disturbed belt lead to underpressures in the Cretaceous aquitard due to high shale compressibility, and low permeability. Previous studies could only replicate measured underpressures in the Cretaceous with low vertical permeability values of $3 \times 10^{-20} \text{ m}^2$ in shales (Corbett and Bethke, 1992). In the *erosion* model, Cretaceous permeability is an order of magnitude greater, denudation rates are lower and unloading compressibility values are essentially equivalent to Corbett and Bethke's. A comparison of *erosion* parameters with published values (Corbett and Bethke, 1992; Parks and Tóth, 1995) suggests that underpressures predicted in the *erosion* case are less than those measured in southern Alberta. Similarly, one-dimensional analyses of fluid pressures in the Cretaceous shales showed that erosion rates used in the first erosion period of the *erosion* model (0.026 mm/yr) could not produce underpressures; however, second period rates (0.2 mm/yr) could (Parks and Tóth, 1995). In Alberta, erosional underpressures may have been generated much earlier than the *erosion* case predicts, if erosion rates are controlled by relative relief, i.e., higher during high topography periods.

Garven (1989) concluded that the accumulation of the Athabasca oil sands occurred via miscible petroleum transport within a regional topography-driven flow system. Permeabilities in Garven's model were highly inflated compared to measured values, which caused solute to be completely flushed from the basin within 2 million years of instantaneous uplift. Adjustment of permeabilities within the model in both the *best case* or *erosion* case still cannot explain the accumulation of the Athabasca oil sands, because of low flow rates. However, the present day salinity distribution is closely predicted by the *best case*, suggesting that the Athabasca oil sands may have migrated due to buoyancy forces or other processes. Furthermore, a potentially younger, regional-scale topography-driven flow system may have increased water-washing and biodegradation of the Athabasca oils sands. Additional modelling would be required to determine relative roles of these parameters.



Figure 5.1: Map showing the location of oil sands in Alberta (modified after Garven, 1989). Speckled zones represent zero isopach of Lower Mannville aquifer (Taken from Creaney et al., 1994). Pale grey zones indicate areas in which solonchaks soil has been observed (Modified from Atlas of Alberta).

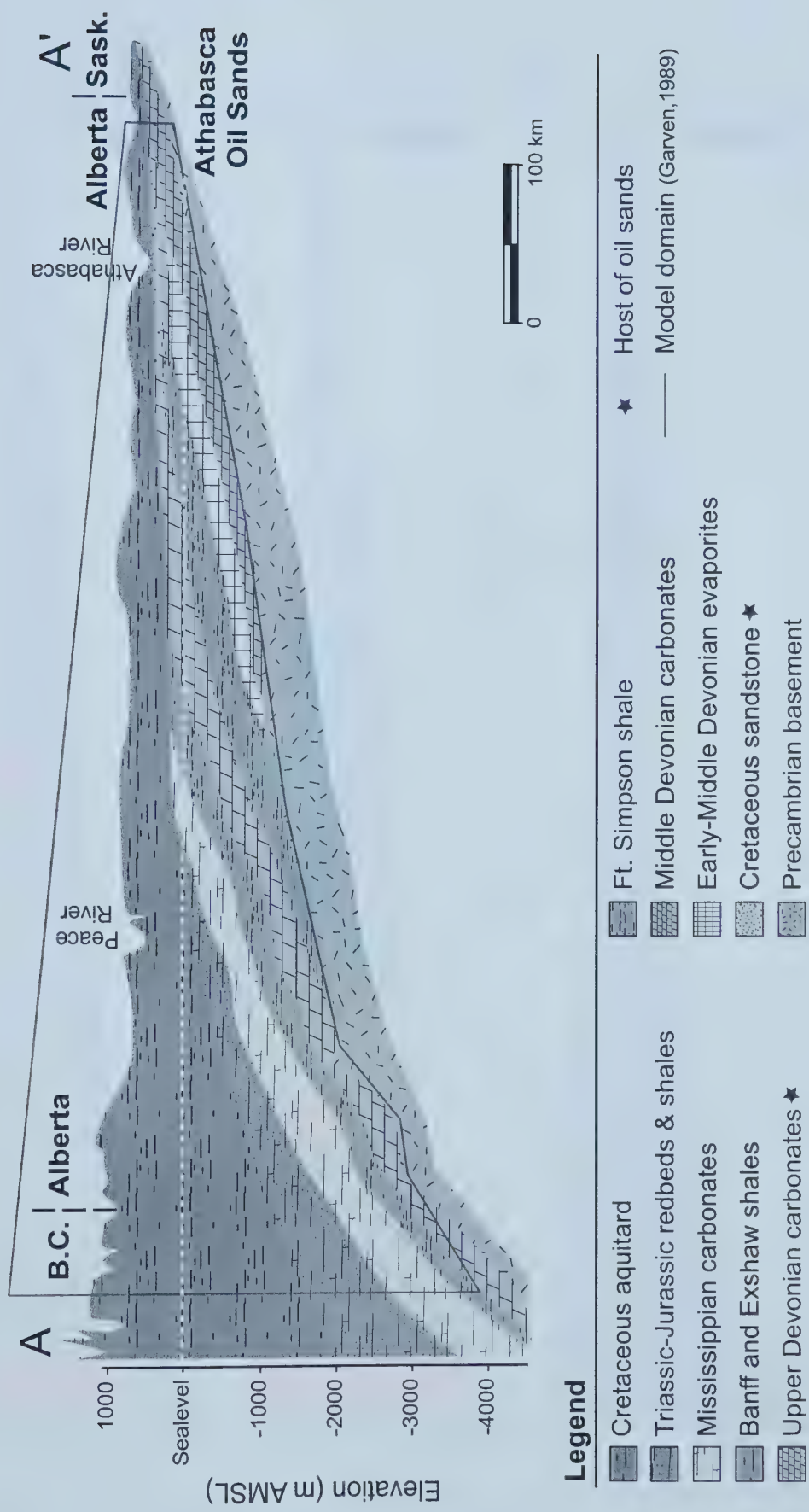


Figure 5.2: Stratigraphy along the Peace River section from the disturbed belt to the erosional edge of the WCSB. Garven's (1989) model domain is shown in a heavy grey line.

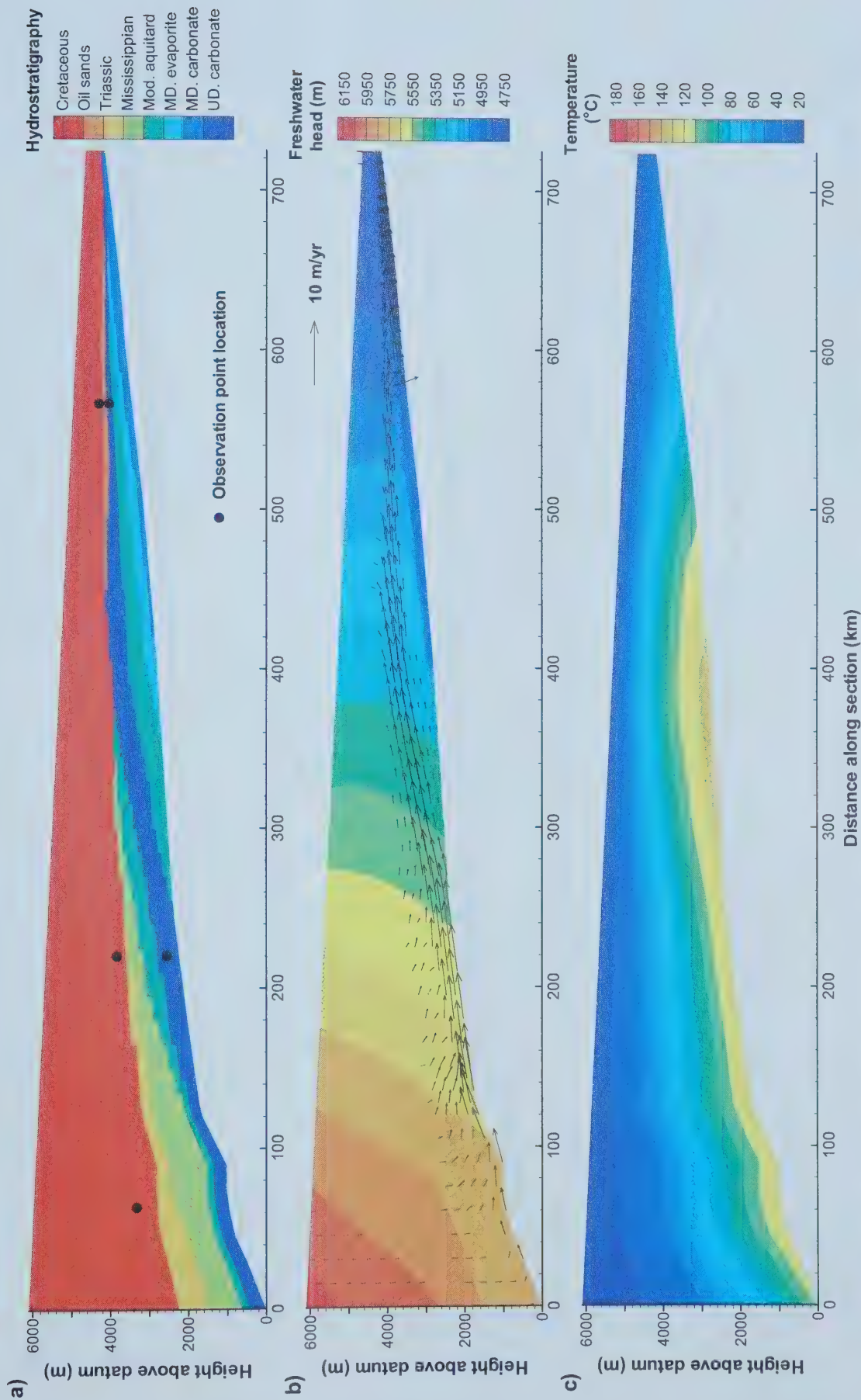


Figure 5.3: Steady-state solution for the replicated model of the Athabasca flow system (Garven, 1989), approximately 2 Ma after instantaneous uplift, a) hydrostratigraphy used in RIFT2D (Mod. aquitard includes Mississippian shale and Upper Devonian shale, MD = Middle Devonian, UD = Upper Devonian); b) freshwater hydraulic head and velocity vectors; and c) temperature.

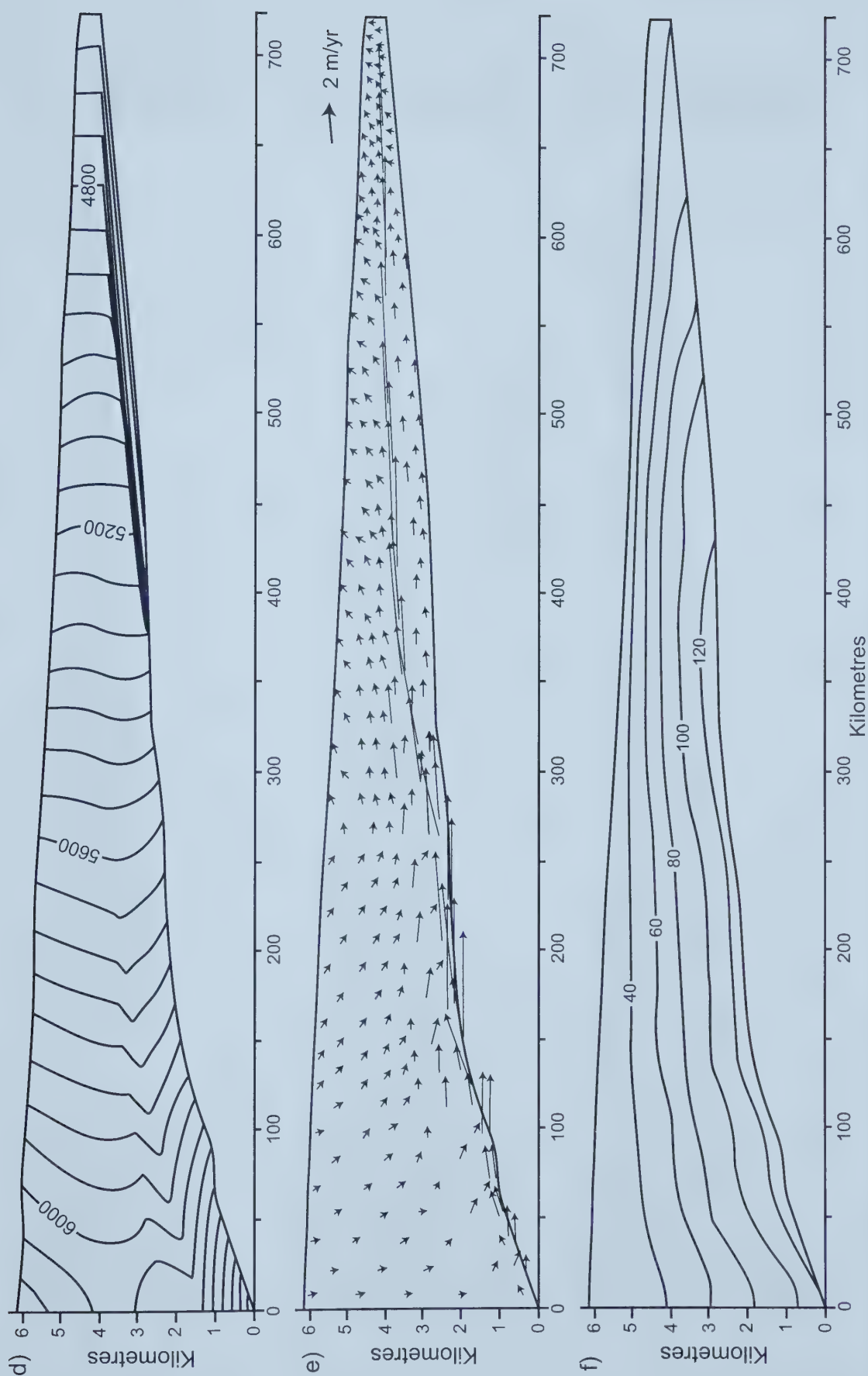


Figure 5.3: Athabasca oil sands model steady-state solution as published by Garven (1989), d) freshwater hydraulic heads displayed with a 50 m contour interval; e) darcy velocity vectors; and f) temperature distribution displayed with a 20°C contour interval.

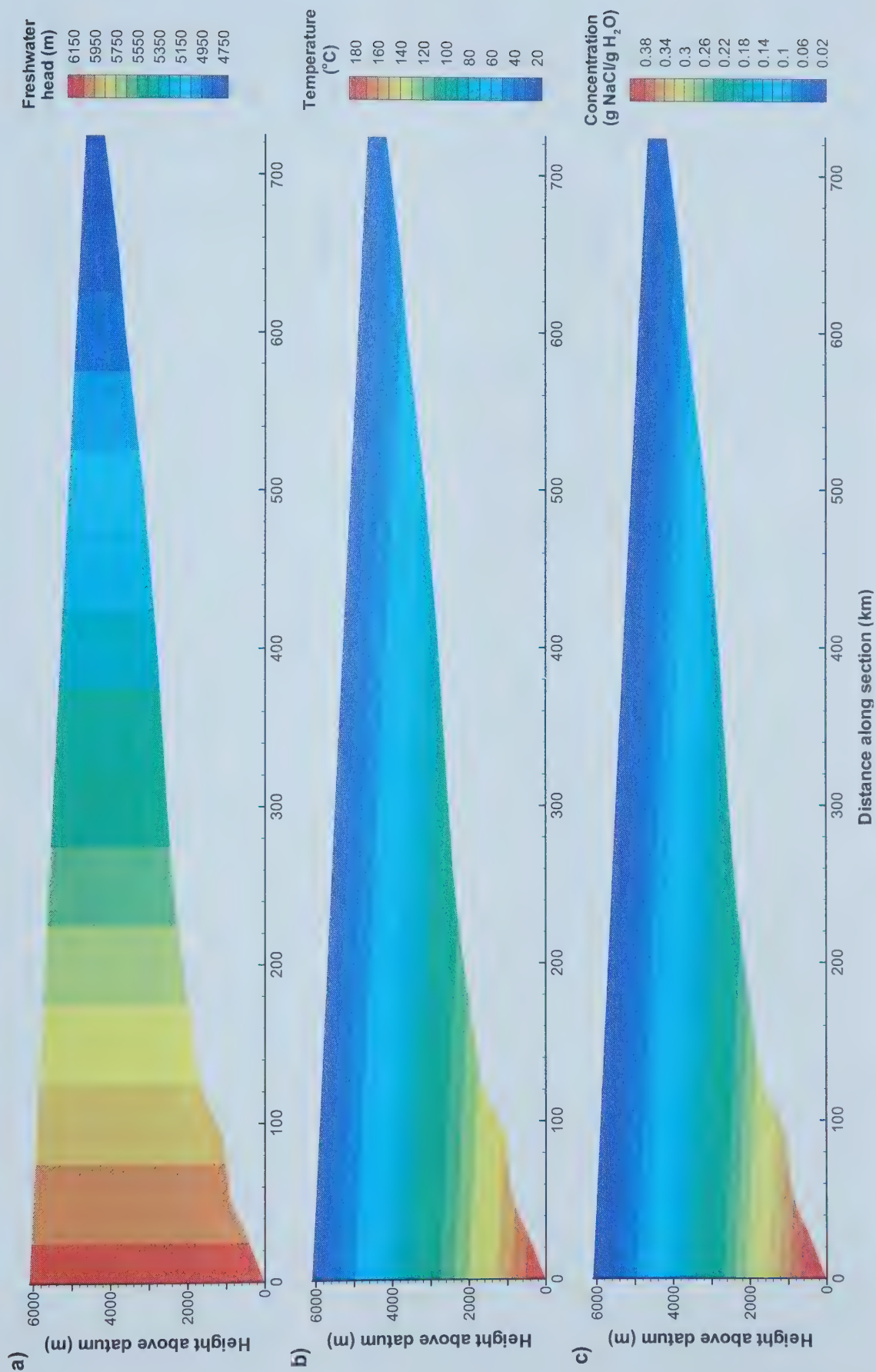


Figure 5.4: Initial a) freshwater head distribution; b) temperature profile; and c) salinity distribution applied to all fixed grid Athabasca oil sands models.

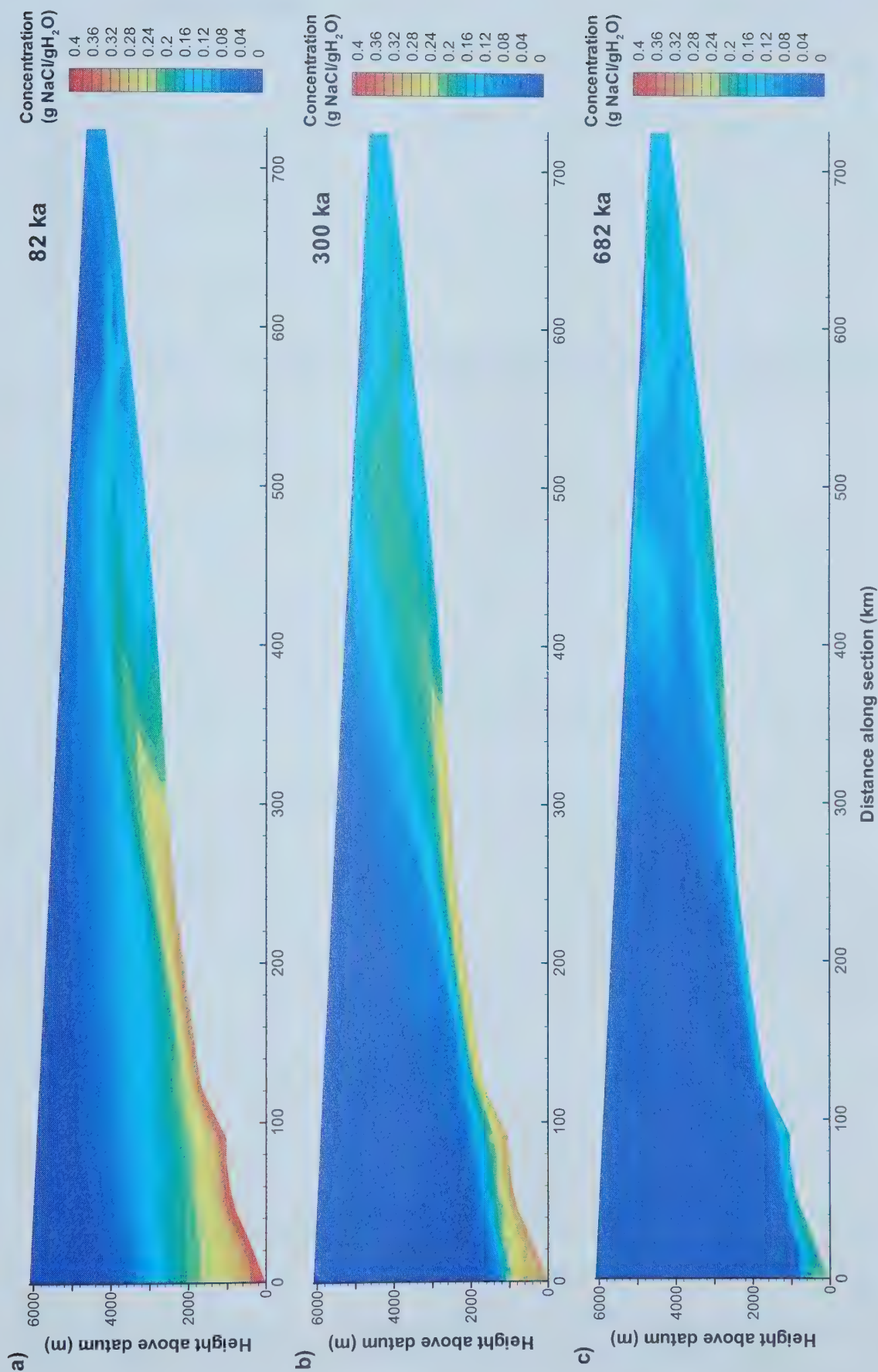


Figure 5.5: Transient solutions for salinity distributions of the Athabasca replicated model, a) 82 ka; b) 300 ka; and c) 682 ka. The whole basin is flushed with freshwater 2 Ma after instantaneous uplift.

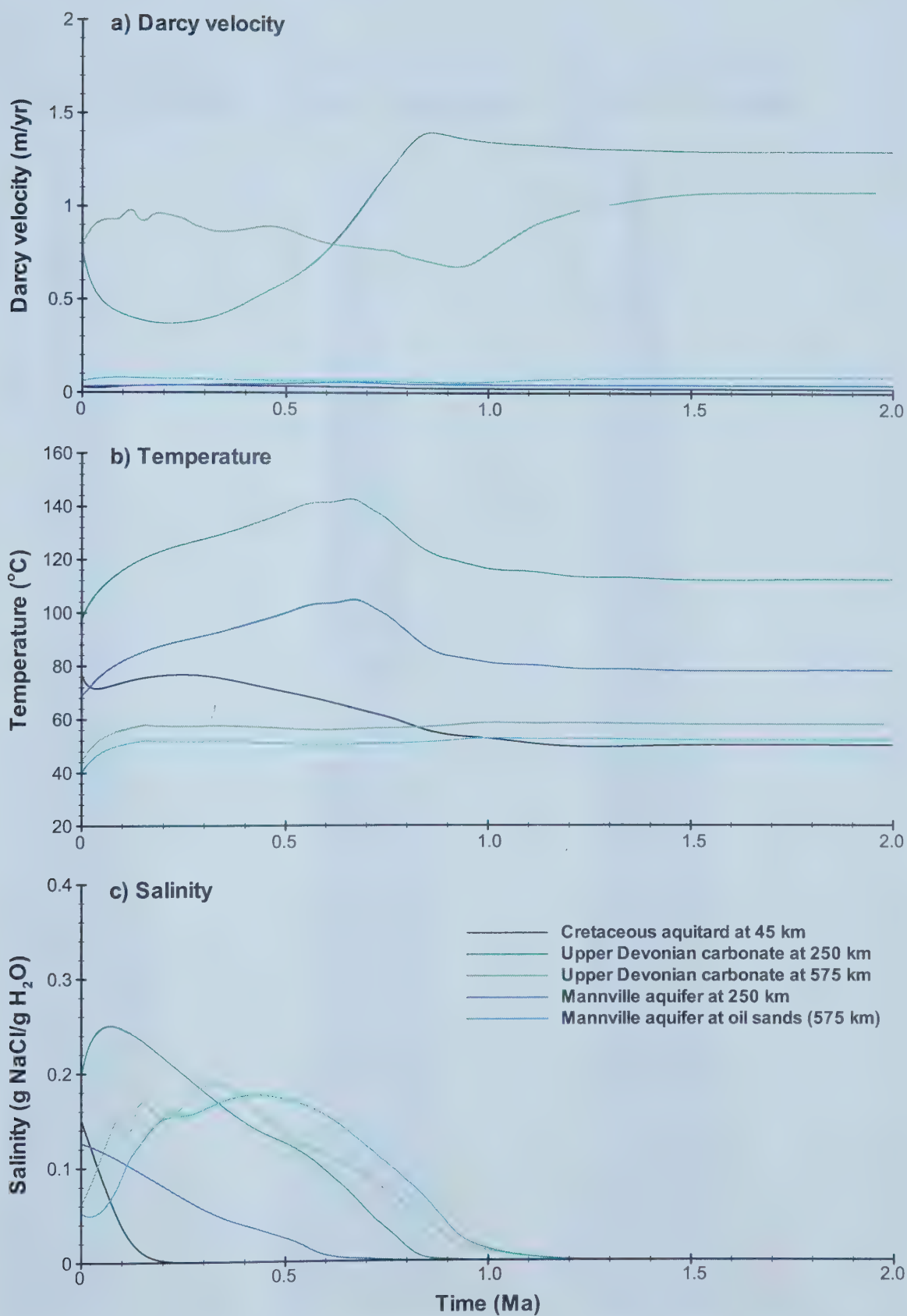


Figure 5.6: Simulation results of the replicated Athabasca model (Garven, 1989) at 5 observation points, a) darcy velocity (m/yr); b) temperature (°C); and c) salinity (g NaCl/g H₂O).

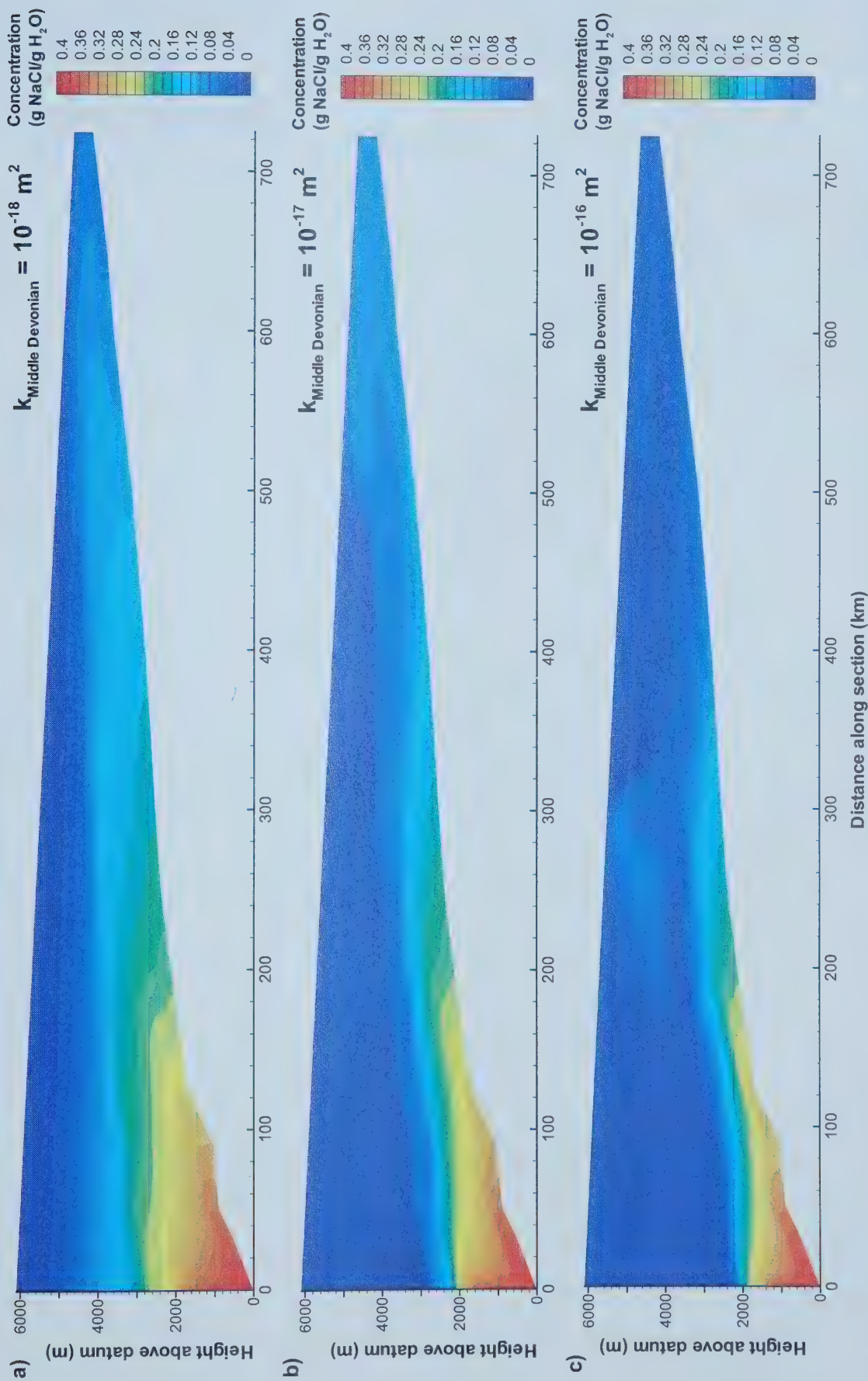


Figure 5.7: Salinity distributions at present day (60 Ma after instantaneous uplift) for models used to calibrate the best case solution for oil sands flow system. Calibration was accomplished by varying the permeability of Cretaceous aquitard, a) $k = 10^{-18} \text{ m}^2$; b) $k = 10^{-17} \text{ m}^2$; and c) $k = 10^{-16} \text{ m}^2$.

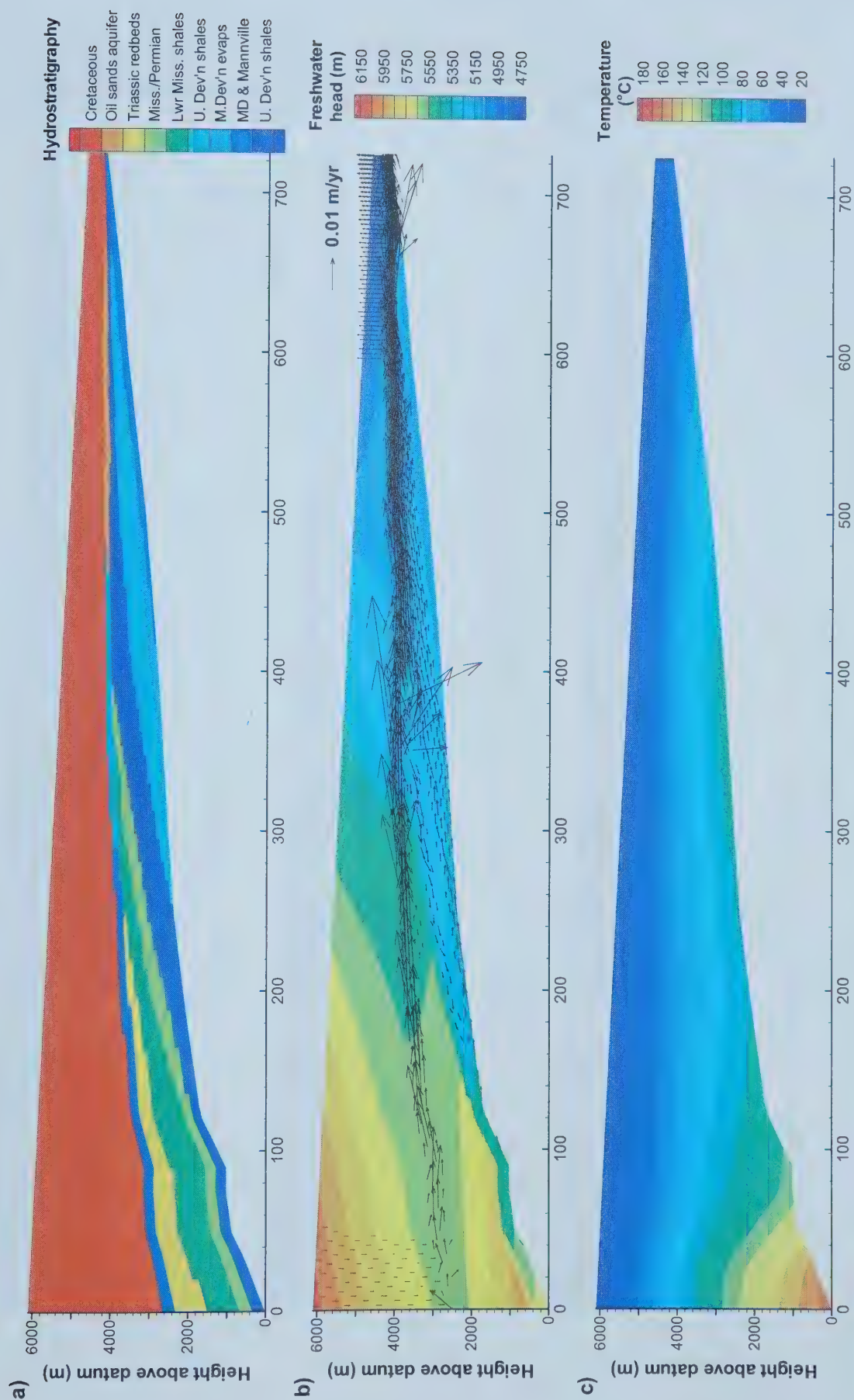


Figure 5.8: Best case Athabasca oil sands model, 60 million years following instantaneous uplift, a) hydrostratigraphy; b) freshwater hydraulic head; and c) temperature distributions.

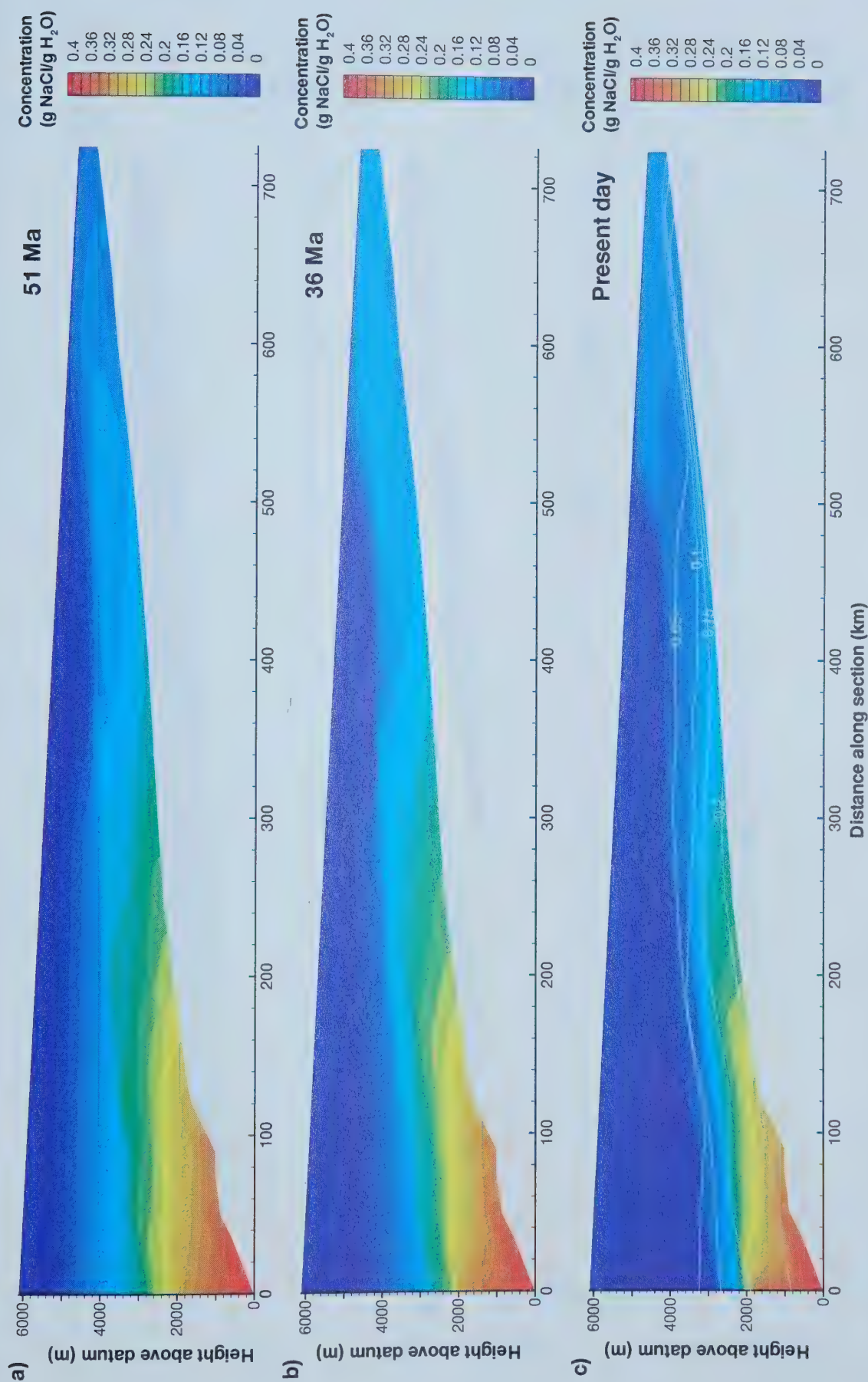


Figure 5.9: Best case scenario salinity distributions through time, a) 9 million years after instantaneous uplift (51 Ma); b) 36 million years after instantaneous uplift (24 Ma); and c) 60 million years after instantaneous uplift (0 Ma).

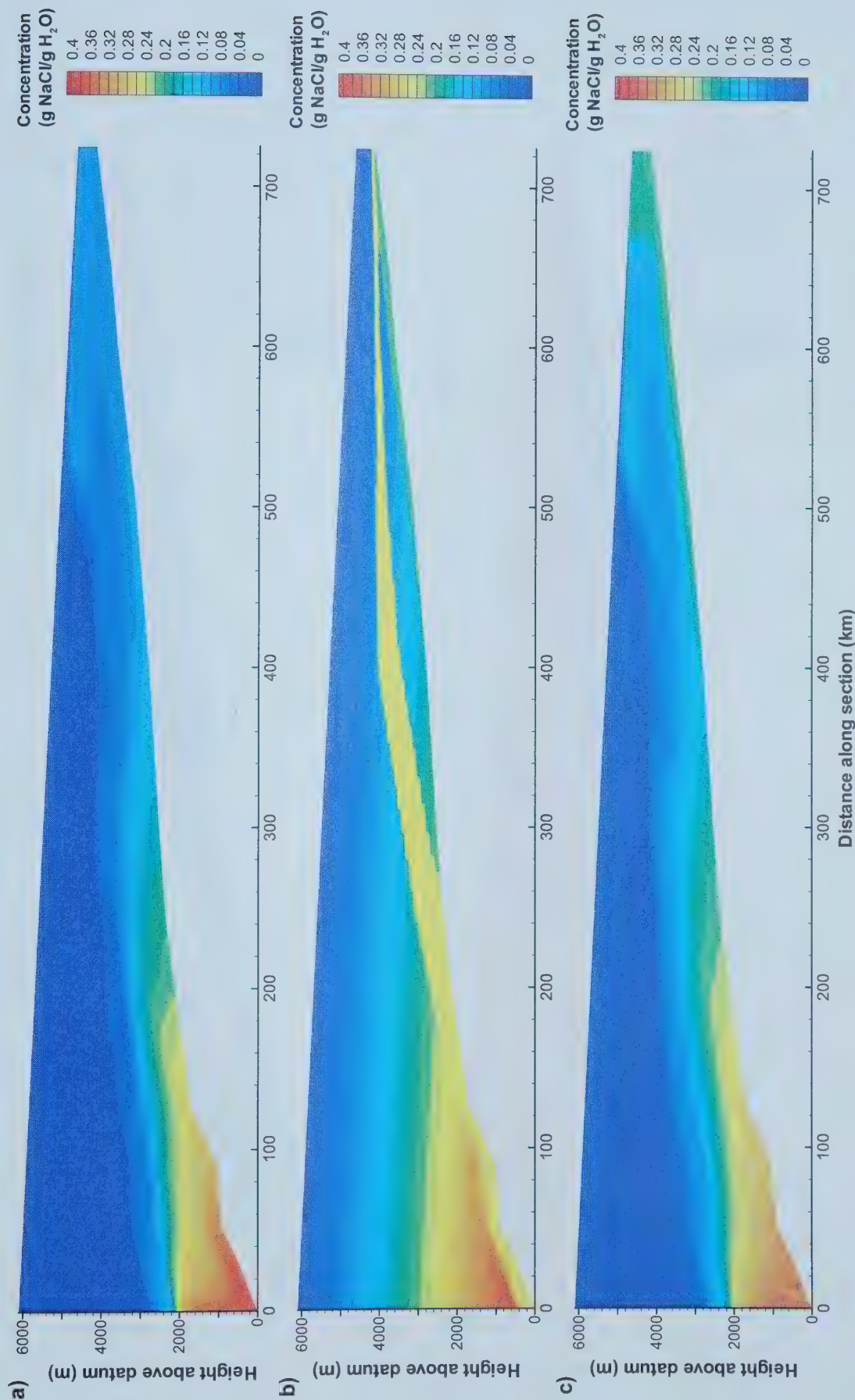


Figure 5.10: Best case scenario compared to an identical model, which is initially assigned a constant salinity in the Upper Devonian aquifer in the oil sands flow system; a) best case solution, 60 Ma after instantaneous uplift; b) initial salinity distribution with 25 eqv. wt.% NaCl salinity applied to Upper Devonian aquifer; and c) salinity distribution for the salinity case, 60 Ma after instantaneous uplift.

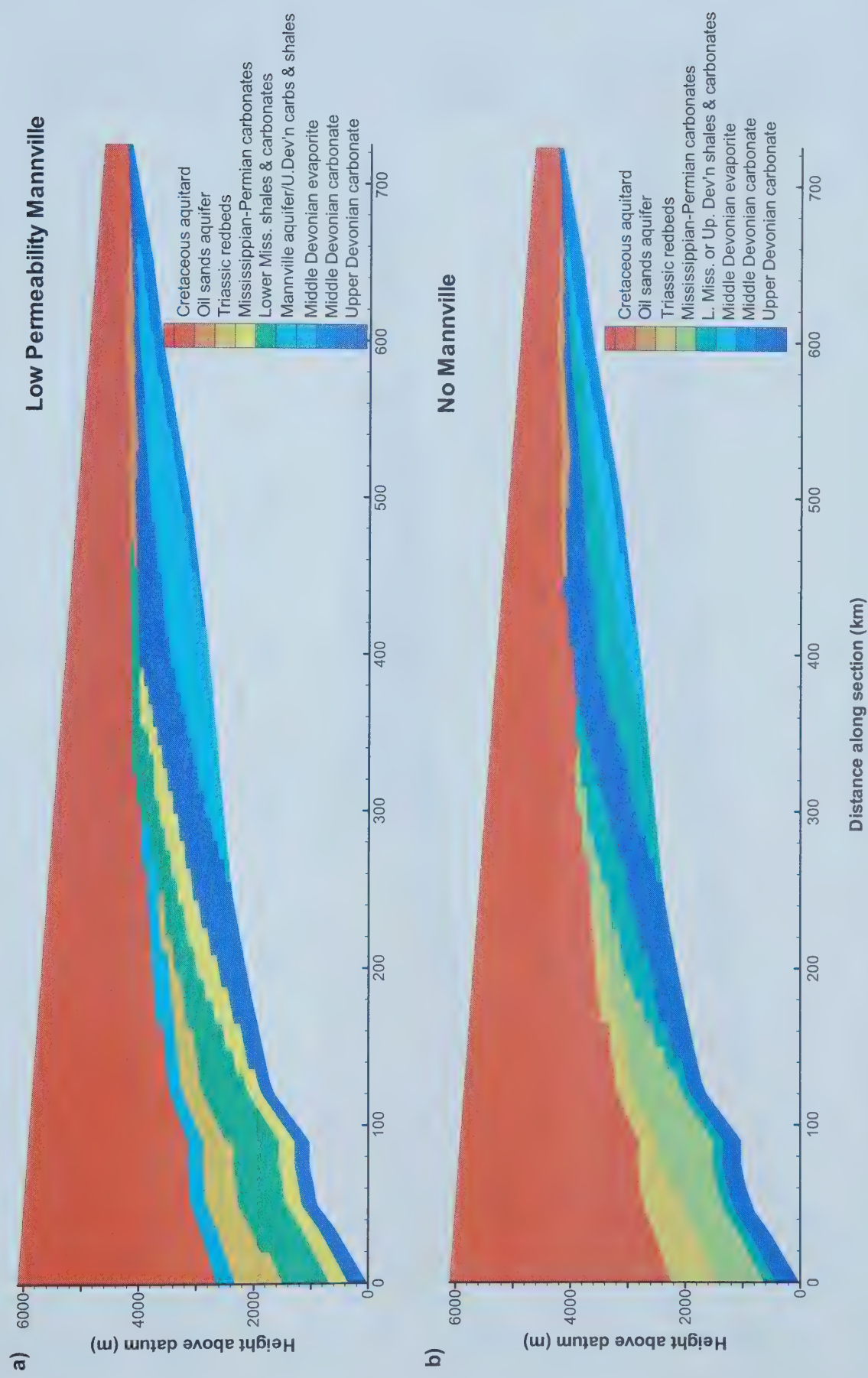


Figure 5.11: Hydrostratigraphy used in RIFT2D for low permeability Mannville and no Mannville models. The no Mannville model is most similar to Garven's original Athabasca model. The low permeability model assigns the Mannville a permeability between Garven's model and the best case.

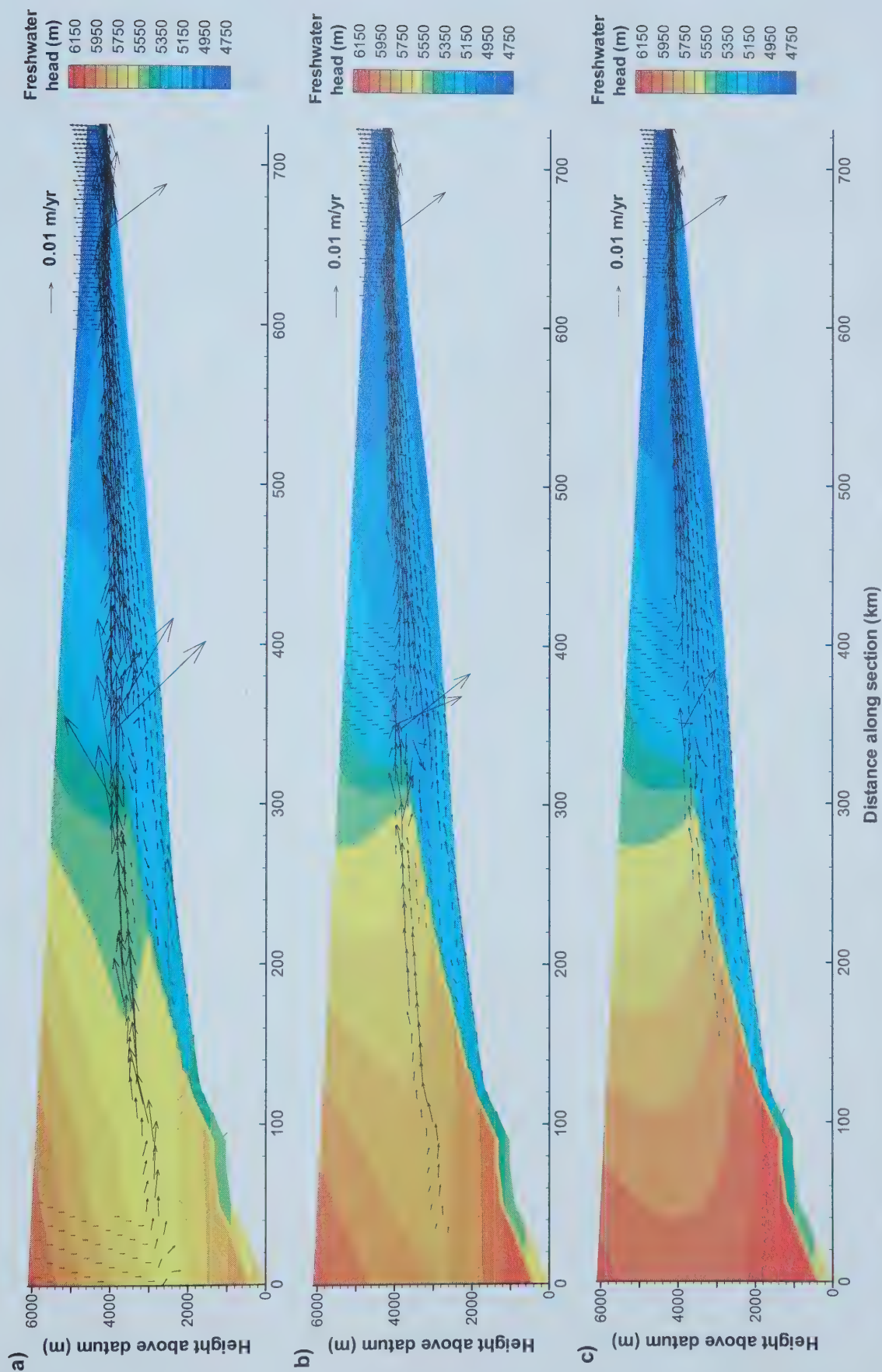


Figure 5.12: Different configurations of Mannville aquifer in the oil sands flow system, 60 million years after instantaneous uplift; a) best case solution; b) low permeability Mannville in west; and c) no permeability Mannville in west as in Garven (1989).

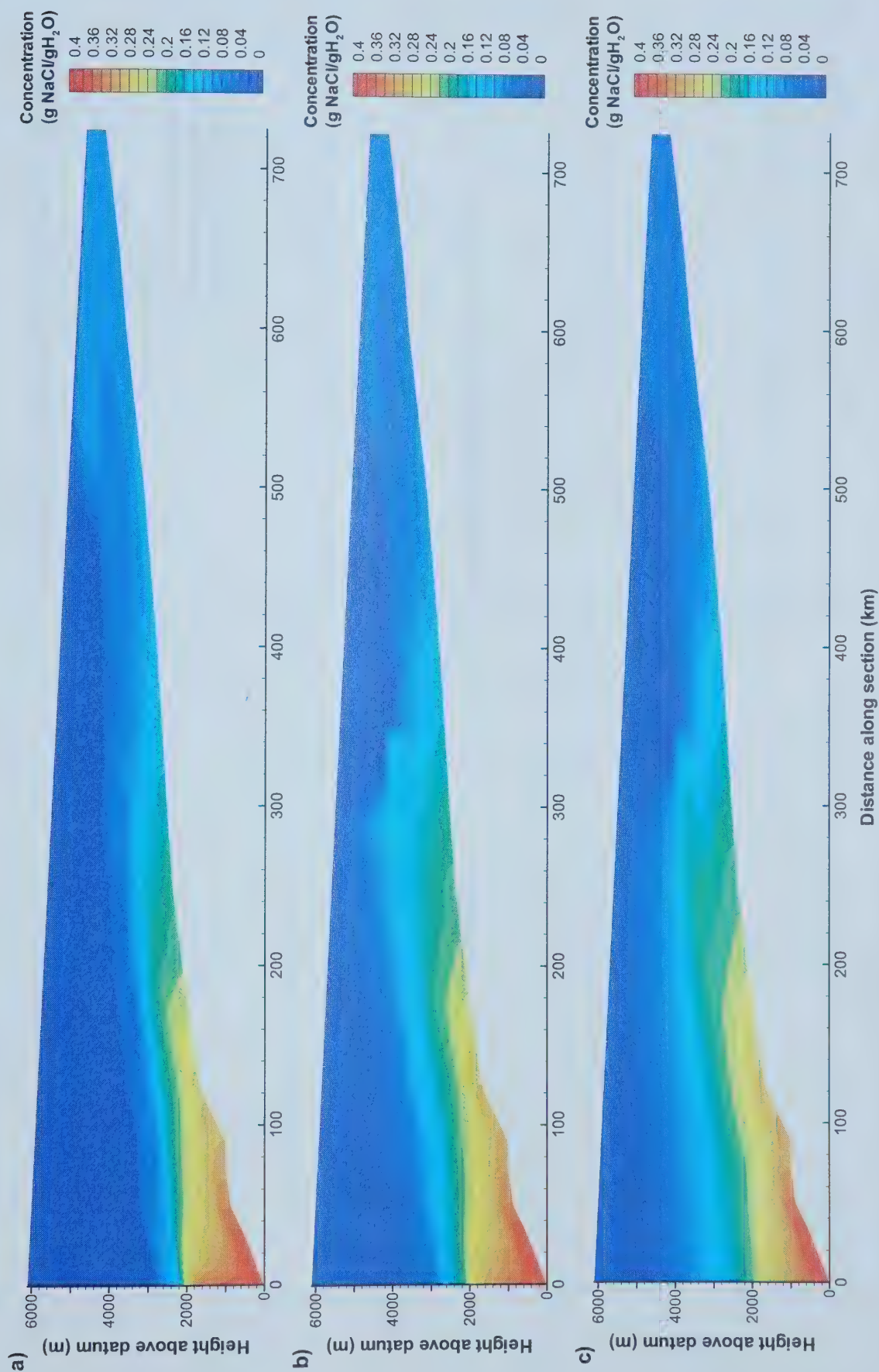


Figure 5.13: Different configurations of Mannville aquifer in the oil sands flow system 60Ma after instantaneous uplift; a) best case solution; b) low permeability Mannville in west; and c) no Mannville in west as in Garven (1989).

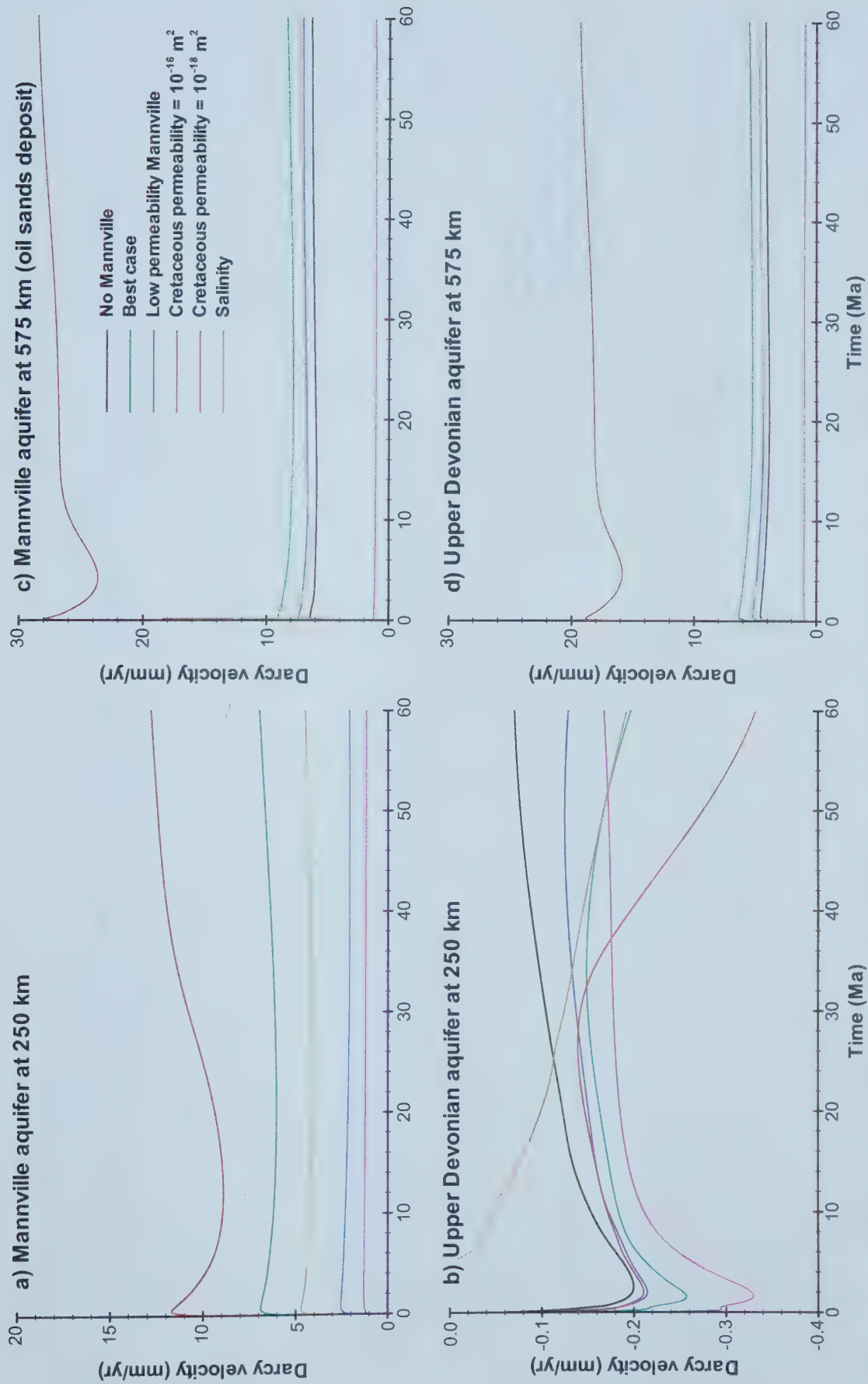


Figure 5.14: Darcy velocities for various fixed grid Athabasca flow models at 4 observation points, a) Mannville aquifer at 250 km along the section; b) Upper Devonian aquifer at 250 km; c) Mannville aquifer at the oil sands deposit (575 km); and d) Upper Devonian aquifer at 575 km.

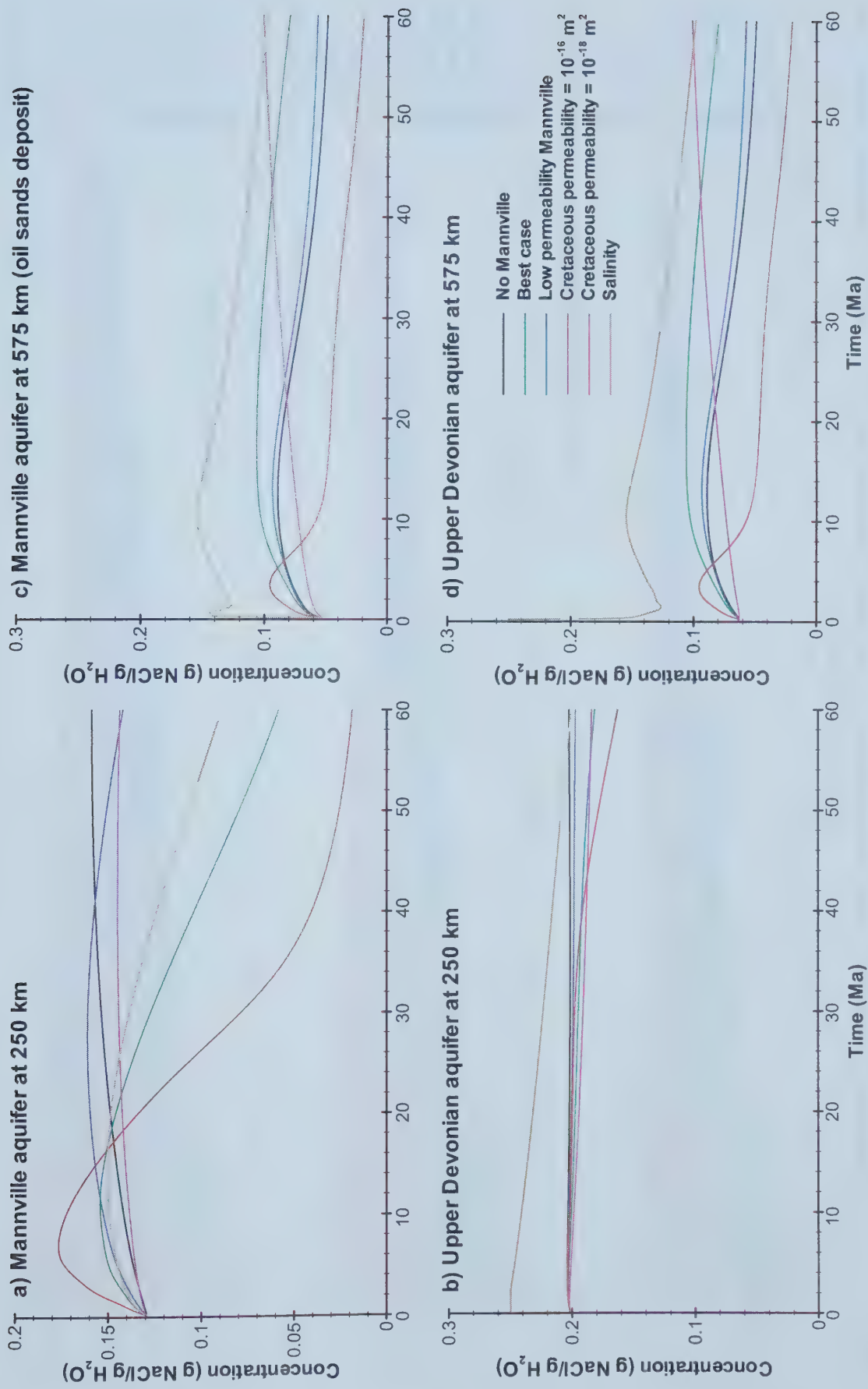


Figure 5.15: Salinity profiles for the fixed grid models of the Athabasca flow system at 4 observation points, a) Mannville aquifer at 250 km along the section; b) Upper Devonian aquifer at 250 km; c) Mannville aquifer at the oil sands deposit (575 km); and d) Upper Devonian aquifer at 575 km.

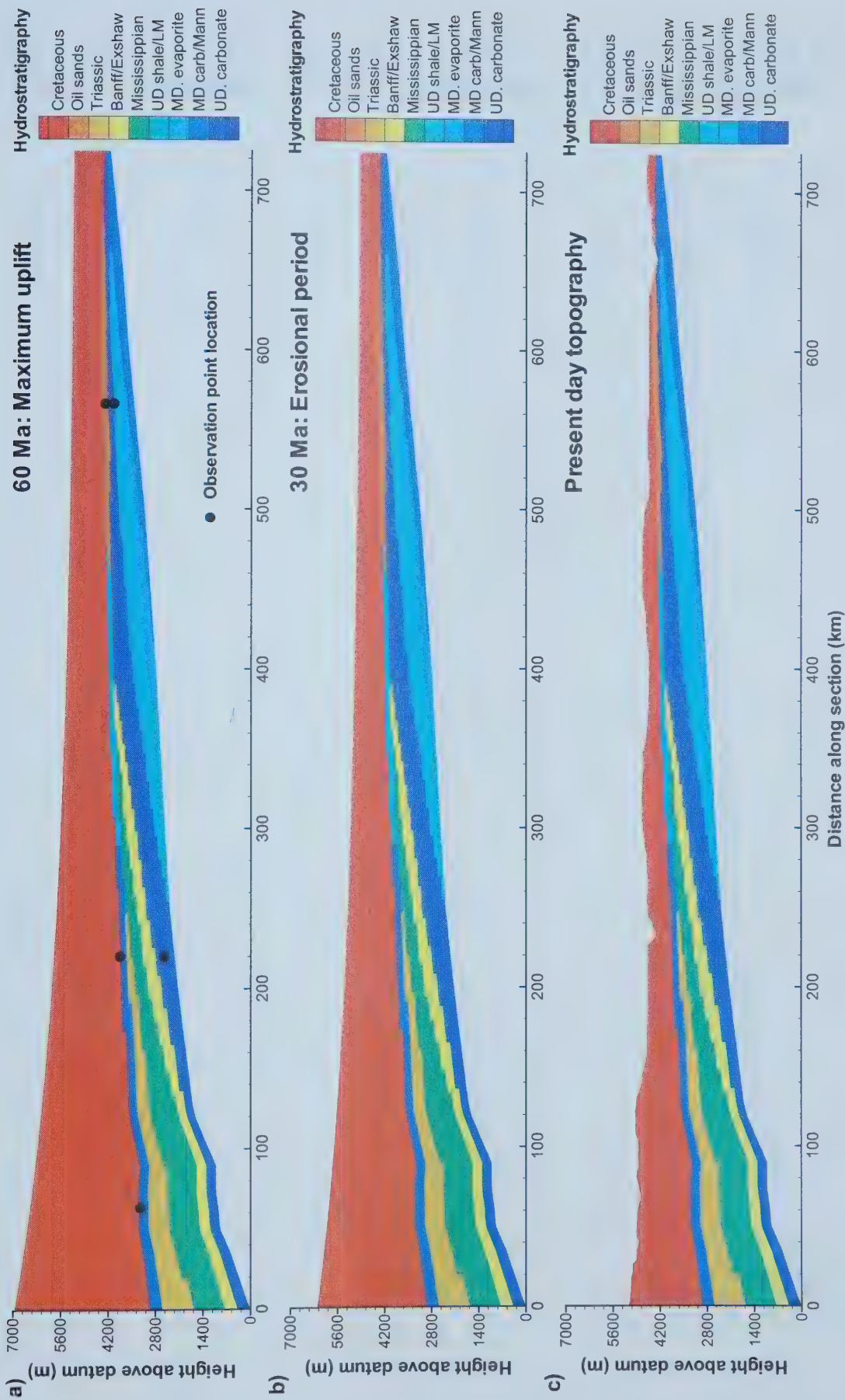


Figure 5.16: Transient evolution of the erosion model hydrostratigraphy, a) at 60 Ma or maximum uplift; b) at 30 Ma during the erosional period; and c) at present day. MD = Middle Devonian, UD = Upper Devonian, carb = carbonate, LM = low permeability Mannville, Mann = high permeability Mannville

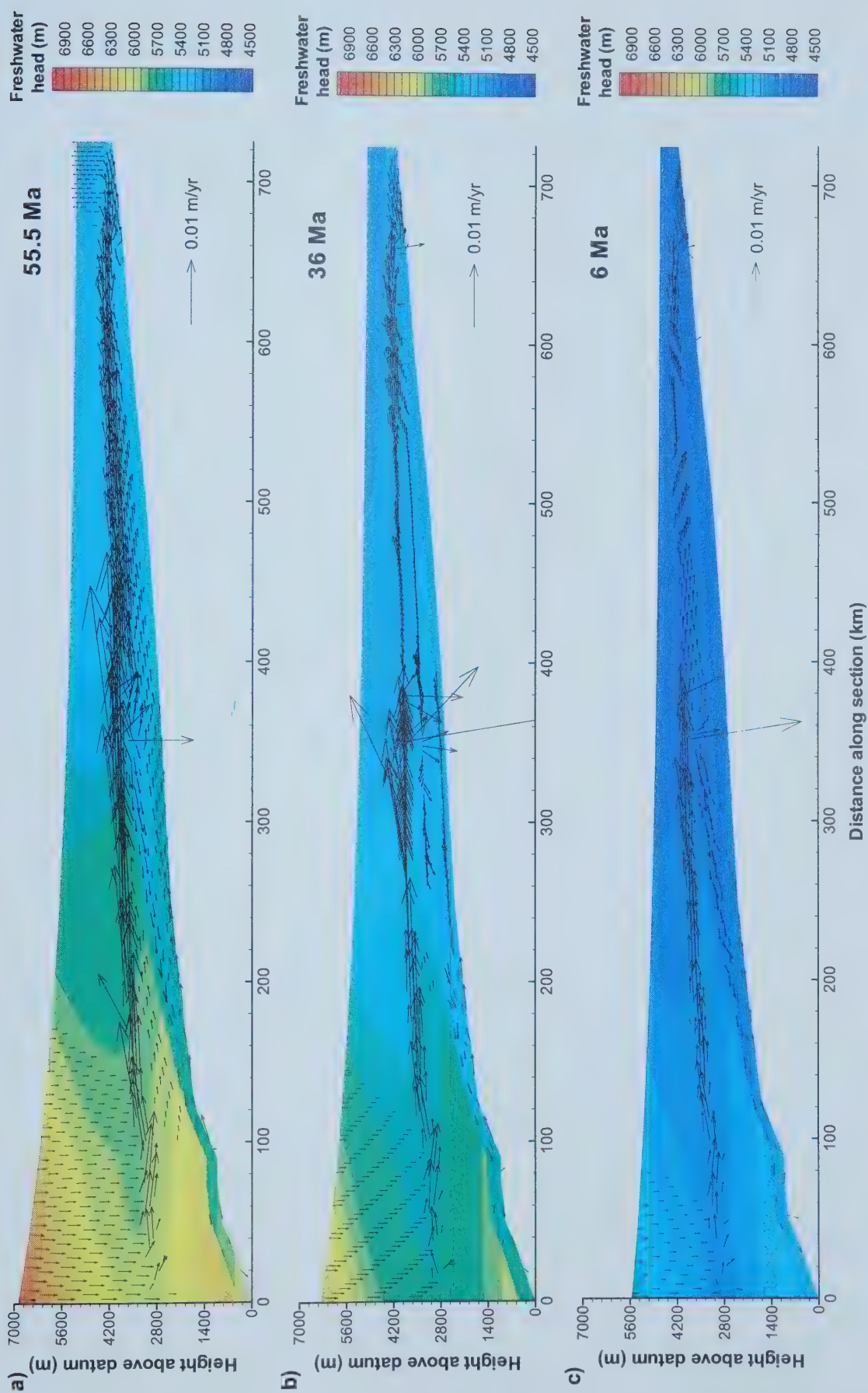


Figure 5.17: Transient evolution of freshwater hydraulic heads and darcy velocities in the erosion model, a) 55.5 Ma; b) 36 Ma; and c) 6 Ma.

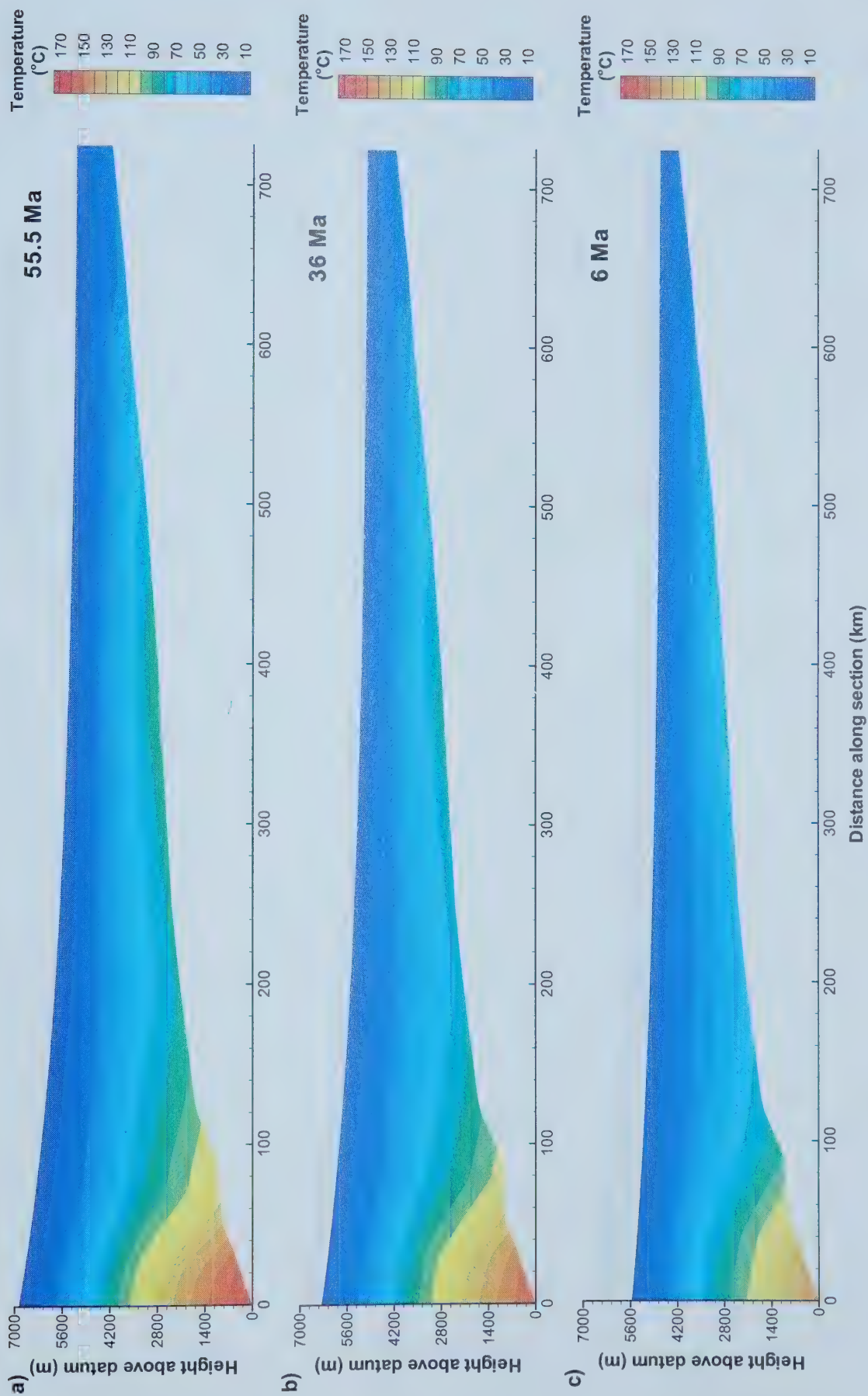


Figure 5.18: Transient evolution of temperature in the erosion model, a) 55.5 Ma; b) 36 Ma; and c) 6 Ma.

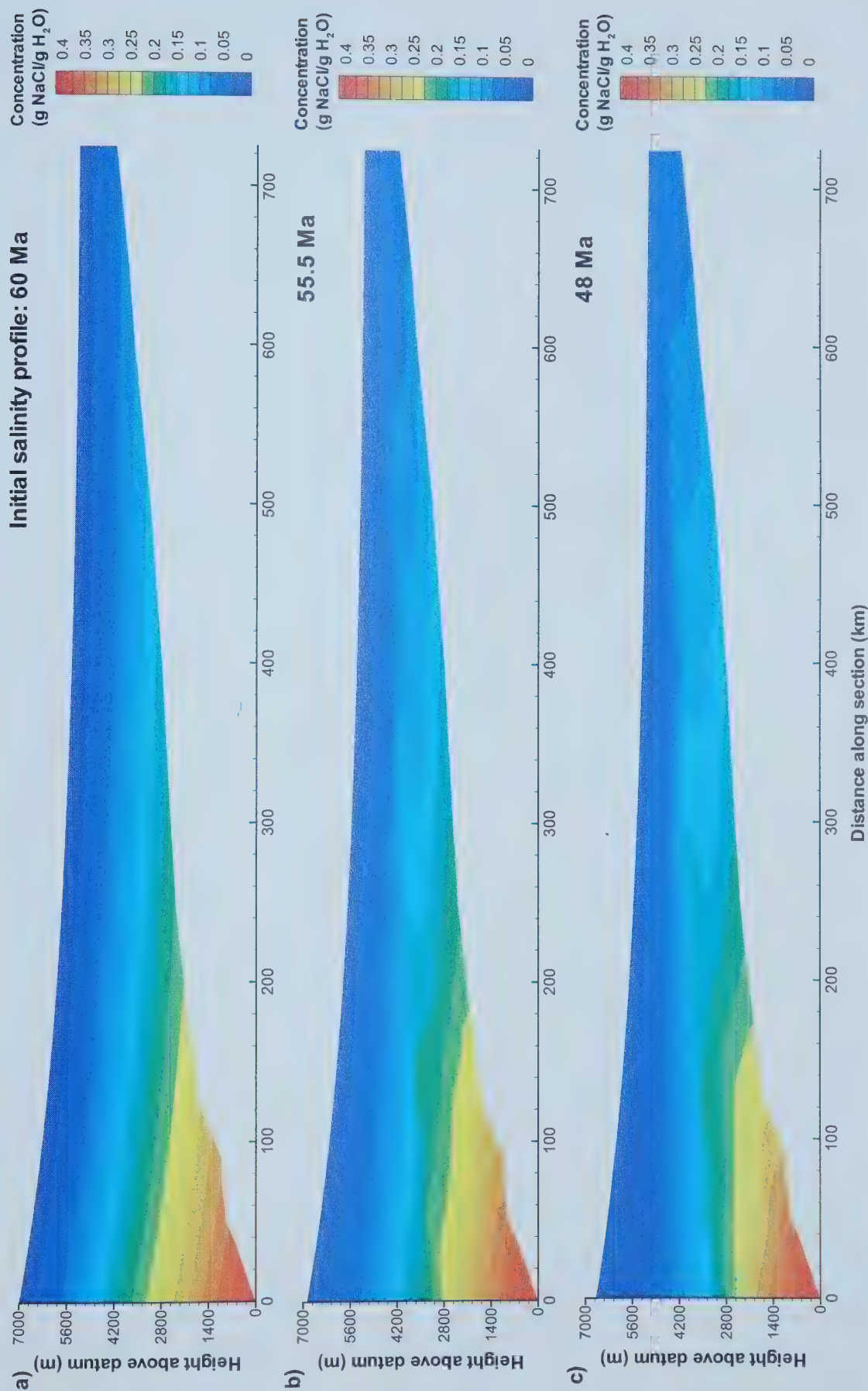


Figure 5.19: Transient salinity solutions in erosion model, a) initial salinity profile applied at instantaneous uplift; b) 55.5 Ma; and c) 48 Ma. In Area B, Upper Devonian water moves downdip cooling the area, while updip flow in the carbonate/shale unit advects heat towards the discharge zone.

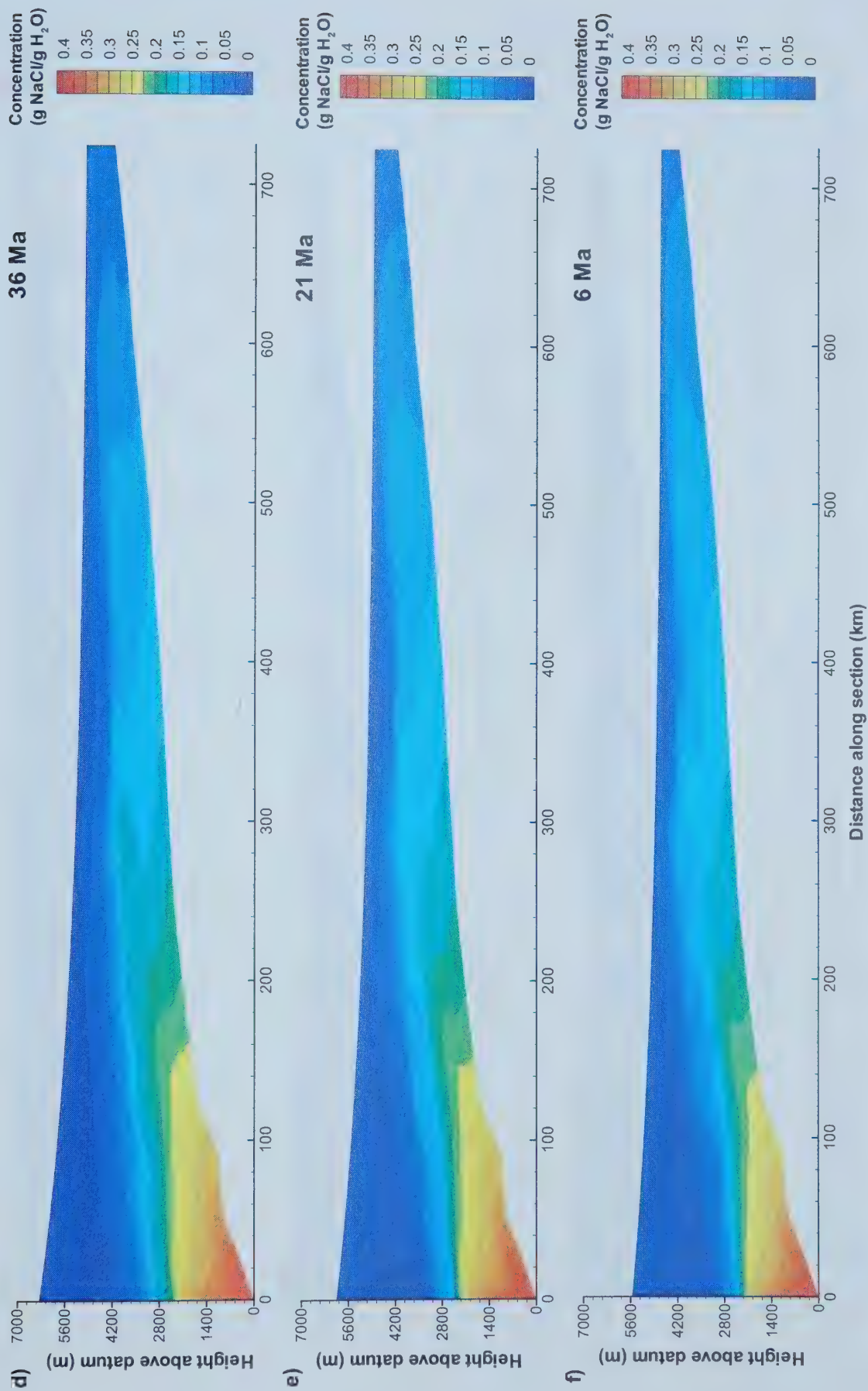


Figure 5.19: Transient evolution of salinity in erosion model, d) 36 Ma; e) 21 Ma; and f) 6 Ma profiles.

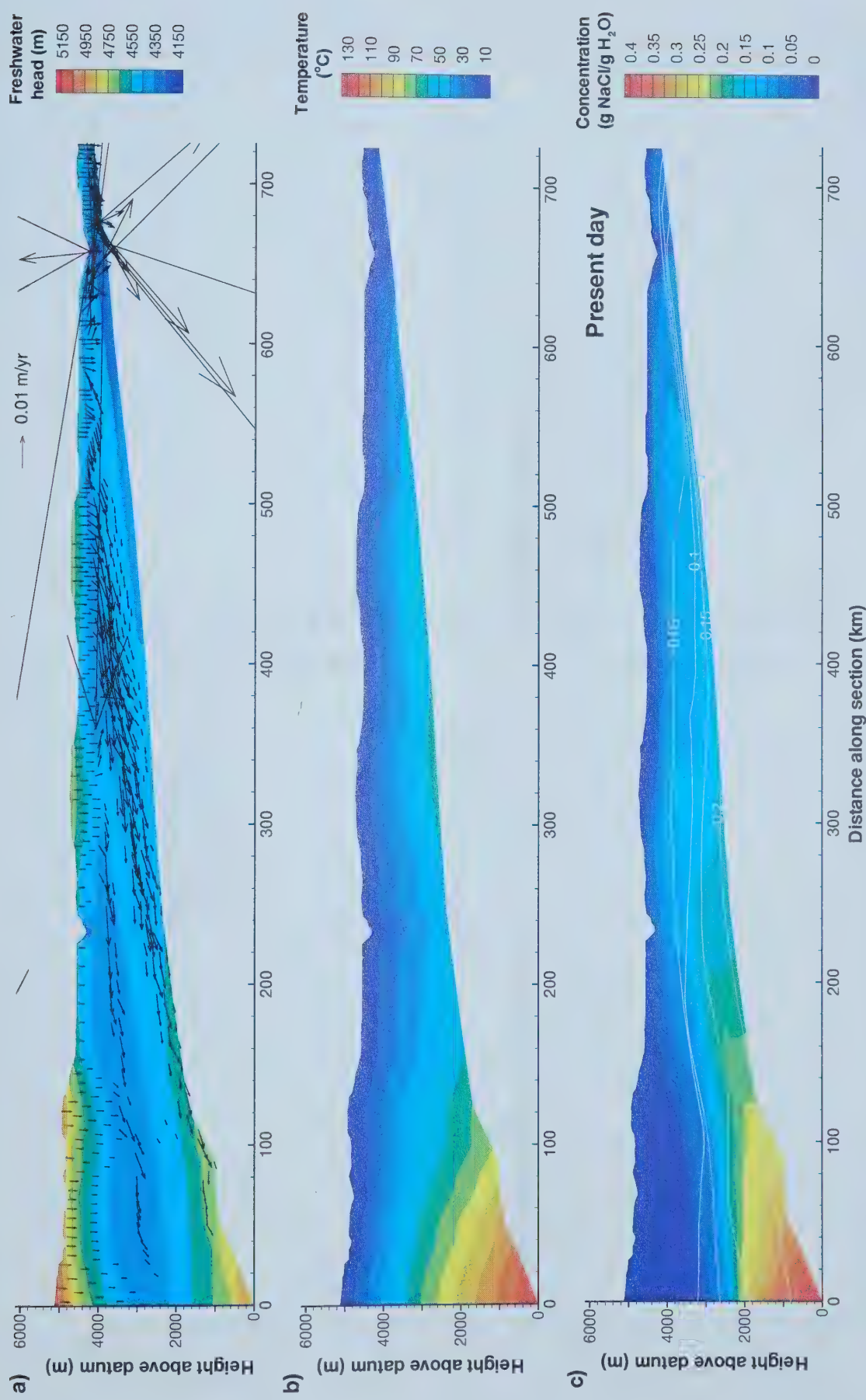


Figure 5.20: Solution for present day (60 Ma after instantaneous uplift) for the erosion model, a) freshwater hydraulic head and darcy velocity vectors; b) temperature distribution; and c) salinity distribution.

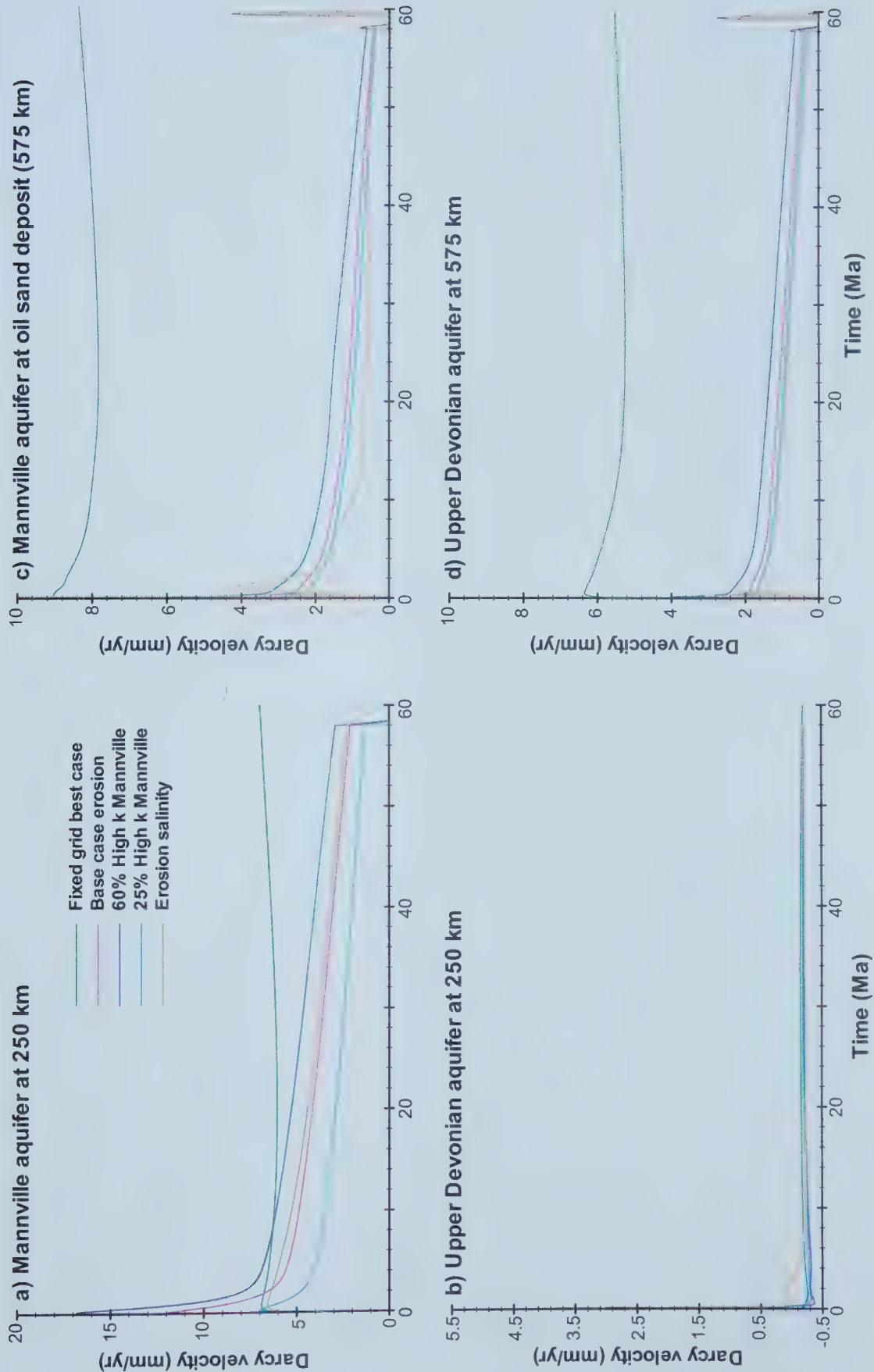


Figure 5.21: Transient variations in darcy velocity at 4 observation points in the various erosion scenarios.

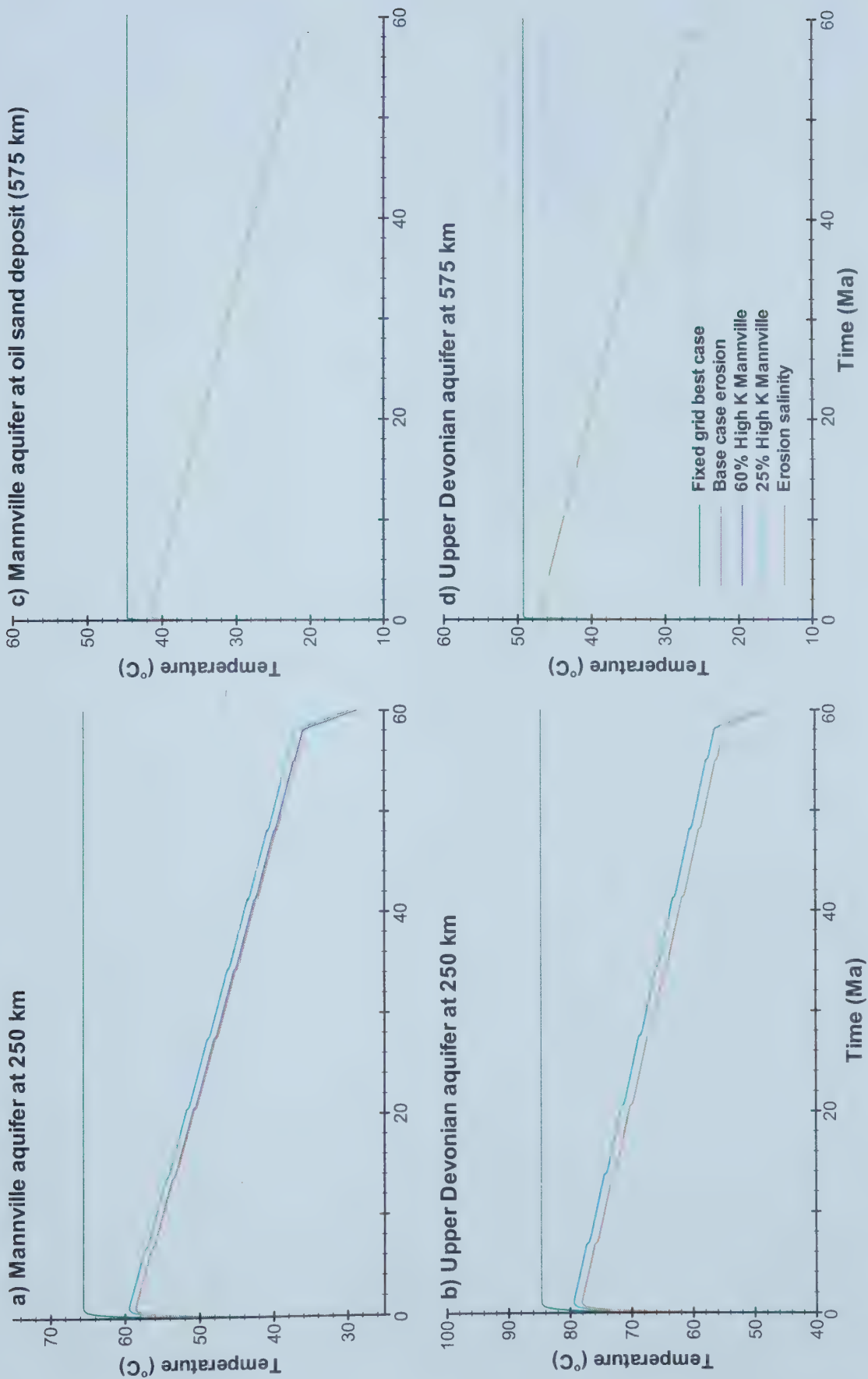


Figure 5.22: Transient variations in temperature at 4 observation points in the various erosion scenarios.

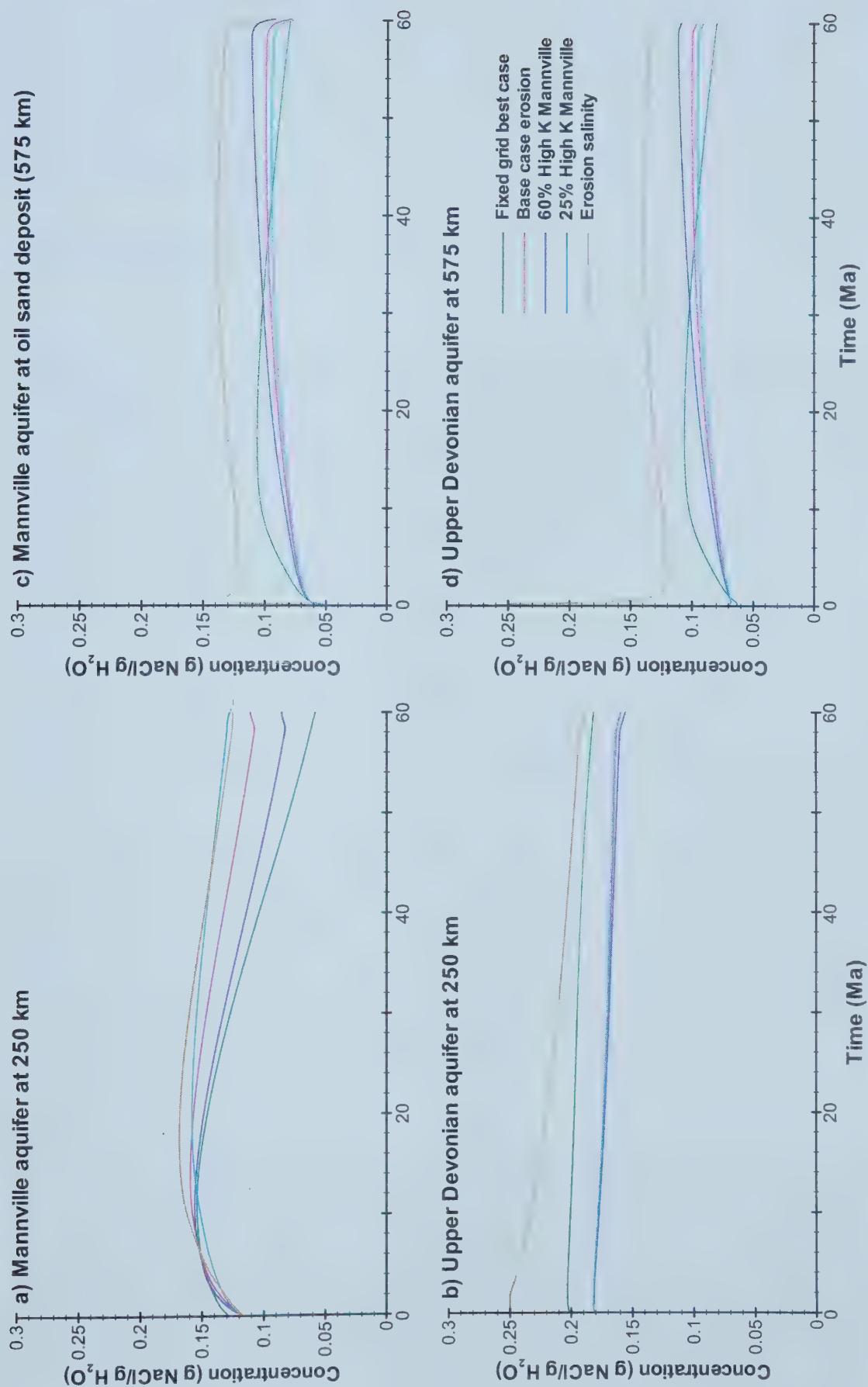


Figure 5.23: Transient variations in salinity at 4 observation points in the various eroion scenarios.

CHAPTER 6

CONCLUSIONS

Giant economic resources, such as the Athabasca oil sands and Pine Point ore district, have been interpreted as products of regional-scale fluid flow associated with the Laramide orogeny (Beales and Jackson, 1968; Garven, 1985; 1989). Previous numerical modelling has simulated flow systems that transport the required volume of fluids through these deposits during ore mineralization (Garven, 1985; 1989). However, these simulations cannot account for the observed salinity and temperature distributions present today across the basin and therefore need revision (Adams et al., 2000a). In Alberta, fluid pressures, formation water salinity and basinal temperatures have been mapped in detail throughout the sedimentary succession (Connolly et al., 1990a and b; Bachu, 1993; Bachu, 1999; and others referenced). Measurement of permeabilities in the basin and estimation of eroded overburden thickness facilitate transient numerical modelling of the most recent flow systems following the Laramide orogeny. Fluid pressures, in parts of the basin, document relicts of a regional topography-driven flow system (Hitchon, 1969; Bachu, 1995), and low salinity formation waters record infiltration of meteoric water near the disturbed belt (Connolly et al., 1990a; Bachu, 1997). Other studies in low permeability Colorado shales report erosion-induced underpressures related to Tertiary erosion (Tóth and Millar, 1983; Tóth and Corbett, 1986; Corbett and Bethke, 1992; Parks and Tóth, 1995).

Pine Point

Mineralization of 80 million tonnes of ore at Pine Point required approximately 3000 km³ of metal-bearing brine to pass through the host rock over a period of 1 million years. However, in Garven's (1985) topography-driven flow model, metal-complexing Cl is completely flushed from the basin within 500 000 years of instantaneous uplift, curtailing Pb-Zn mineralization. Thus, either the conceptual flow model is incorrect or another source

of saline fluids or solute is required to explain ore formation at Pine Point. Solute chemistry of ore fluid inclusions refutes significant dissolution of halite (Telser, 1999); however, evidence does exist for mixing of two fluids during mineralization (Adams et al., 2000b). In this study, the necessity for a different flow system to predict mineralization at Pine Point was tested by modifying the basin shape, permeability, salinity and temperature parameters in Garven's model. None of these modifications could predict ore-forming conditions for an adequate period of time to account for the observed ore tonnage at Pine Point.

Sensitivity analysis of the Pine Point model identified some basin features that improve the potential for MVT mineralization within the Alberta basin. For instance, the basin shape was altered to mimic present day characteristics by adding 1 km of basement rock. This buffered temperatures and acted as a source of salinity for tens of millions of years. To match present day basement relief, the lower boundary of the model was deepened near the disturbed belt, which increased maximum temperatures and salinity in the ore district. An increase in basal heat flux, to 85 mW/m², or reduction in thermal conductivity, in accordance with measured and estimated values near Pine Point, greatly increased the volume of ore-forming fluids, temperatures and duration of flow through Pine Point. However, lowering of the barrier permeability to measured values predicted slower flow rates and lower, time-independent temperatures due to dominantly conductive heat flow. Adjustment of all permeabilities to maximum measured values curtailed ore-forming conditions quickly because the Fort Simpson shale inhibits recharge into the underlying Middle Devonian aquifer. Finally, the impact of lateral narrowing of the Presqu'ile barrier on the flow system was difficult to assess without refinement of the hydrostratigraphy and addition of a correction for additional saline water funnelled along the barrier. Nonetheless, the basin is still flushed within a few million years. Thus Pine Point ore tonnage cannot be predicted by any of these new models, although the addition of basin characteristics along the Pine Point section often lengthened the duration of ore-forming conditions.

A different or more elaborate flow system is required to predict the formation of the Pine Point ore district. Further modelling should incorporate the dynamics of both topography-driven and erosion-induced flow along a section following the Presqu'ile barrier. Furthermore, the modelled section should be extended to the Rockies, to increase relief and include all the relevant topographic driving forces. More detailed hydrostratigraphy and

basin morphology would elucidate the role of funnelling and aquitard permeability during mineralization. Use of measured permeabilities in the basin inhibits advective heat transfer, which suggests that the short duration of MVT mineralization is related to either the availability of metals, Cl and reduced sulphur, or transient driving forces. Simulation of the secular variations in relief and heat flow along the Pine Point section would clarify the importance and longevity of various ore-forming processes and features.

Athabasca Oil Sands

Numerical simulations of the Athabasca oil sands flow system (as defined by Garven, 1989) predict complete flushing of the Alberta basin within 1.6 million years, and accumulation of the oil sands over 10 to 50 million years of fluid flow. Existing salinity patterns in the basin refute such rapid and repeated flushing. Published permeabilities, basal heat fluxes and hydrostratigraphy were incorporated into Garven's (1989) model. Assuming maximum uplift around 60 Ma and a permeability of 10^{-17} m² in the Cretaceous aquitard, simulations of this scenario predict a regional gravity-driven flow system and closely replicate the present day salinity profile.

In comparison to Garven's original model, extension of the Mannville aquifer to the disturbed belt significantly alters the basin-wide flow pattern: fluids recharge at the uplift and move along the Mannville aquifer for 300 km, then through the Upper Devonian carbonates to the Athabasca oil sands area. The measured permeabilities produce very slow flow rates in the aquifers (4 to 9 mm/yr), which are at least two orders of magnitude lower than those predicted by Garven (1989). These slow flow rates dictate that heat transport occurs primarily by conduction. The simulated temperature distribution is equivalent to today's if corrected for depth of burial. After 60 million years of fluid flow, the Alberta basin salinity distribution is representative of a basin that is being flushed by slow topography-driven fluid flow. However, the Exshaw/Banff aquitard acts as a barrier to fluid migration and inhibits recharge into the deep basin, causing erroneous down-dip flow in the western portion of the Upper Devonian aquifer. Thus, if the Exshaw/Banff aquitard is continuous and tight into the disturbed belt, some component of flow into the Upper Devonian aquifer must have been derived from basement or Devonian strata in the disturbed belt.

In summary, incorporation of measured permeabilities into a two-dimensional section adequately predicts temperature and salinity distributions in the basin, but poorly reproduces flow patterns in the deep basin. These new simulations cannot explain the formation of the Athabasca oil sands following the Laramide orogeny due to low flow rates. Other processes such as convergent flow, tectonics, higher hydrocarbon concentrations, structure or other mechanisms must have been active during the accumulation of the oil sands.

Erosion Scenario

In the Alberta basin, the effect of erosion on fluid driving forces needs to be considered for simulation of topography-driven flow following the Laramide orogeny. Application of constant erosion rates to the Peace River Arch model results in development of a robust topography-driven flow system, which decays due to erosion and underpressures. Erosion of the Peace River Arch model does not affect flow patterns, but flow rates, temperatures and freshwater hydraulic heads uniformly decrease during 60 million years of erosion. The exponential shape of the landscape and gradually decreasing topographic gradient dampen flow rates considerably. After 30 million years of erosion, underpressures develop in the Cretaceous aquitard, which cause further decay of the regional flow system. These simulations assume a minimum erosion rate and therefore predicted underpressures can be considered a minimum. Near present day, simulated erosion rates increase 5 fold to replicate the development of present topographic features. These higher erosion rates generate greater underpressures, which stimulate a flow reversal, i.e., fluids move down-dip into the basin. Simultaneously, local-scale flow systems develop in the upper 500 m of the basin, thereby curtailing regional topography-driven fluid flow. These results suggest that episodic erosion and development of local relief may have significantly altered regional flow systems.

In an erosional environment, low flow rates (~ 1 mm/yr) limit the transport of heat and solute in the basin. Simulated temperature distributions are a product of mostly conductive heat flow, which produce simulated present day temperatures matching estimated values (Bachu and Burwash, 1994). In contrast, decreasing relief and an exponential land surface configuration lead to decreased flow rates, such that high salinity is predicted across the basin at present day. To address this discrepancy, the Cretaceous aquitard permeability could be increased to facilitate meteoric recharge. Another solution might be the inclusion of fluid flow during uplift, which would add a few million years of fluid flow prior to

underpressuring. Lastly, the assumption of a linear salinity gradient with depth may be unreasonable or result in salinities that are too high.

The exponential shape of the land surface results in thinning of the Cretaceous aquitard and preferential upward flow where the topographic gradient flattens. Brines begin discharging at surface around 21 Ma at the eastern margin of the basin and in the vicinity of the Peace River. Sensitivity analyses showed that the upwelling of solute, 200 km from the disturbed belt, is a result of low permeability in the Exshaw/Banff aquitard and the mid-section of the Mannville aquifer. The presence of salt-rich soils and the Peace River oil sands in the upwelling area support this conclusion. Finally, breaches in the Lower Mannville aquifer are located to the north and south of the Peace River Arch section (Figure 5.1). These discontinuities may necessitate a three-dimensional analysis of Laramide flow systems to explain the Athabasca oil sands.

Calibration of the Athabasca models relies on salinity as a tracer. The present day salinity distribution is closely predicted by a constant topography scenario, whereas in the erosion scenario, the simulated solute distribution is too saline. To accurately calibrate a fluid flow model associated with uplift and erosion, an understanding of the proportion of Cretaceous/Tertiary meteoric water in the Devonian sequence is required. In the Alberta basin, formation water δD values are a good indication of the amount of meteoric water introduced into certain areas. To date, only a small number of samples have been analysed for deuterium (Connolly et al., 1990b) and three-dimensional variations in permeability make basin-wide extrapolation of these data invalid.

Summary

Modifications to Garven's (1985, 1989) models allowed for predictions of the current salinity and temperature distributions along the Peace River section and prolonged the duration of mineralization at Pine Point. However, neither of the revised models was able to account for either the accumulation of the Athabasca oil sands or the ore tonnage at Pine Point. The inability of these two-dimensional cross-sections, under a number of different conditions, to predict the formation of giant resources at discrete locations within the basin suggests that these features may be products of three-dimensional, convergent fluid flow. Both the oil sands and Pine Point are located in laterally discontinuous aquifers at regional discharge

zones. Alternatively, transient topographic driving forces or other flow mechanisms may be responsible for accumulation of these giant deposits. Uplift and erosion may account for both the short duration, and high fluid flux of MVT mineralization. Episodic erosion may accelerate underpressuring and decay of a regional topography-driven flow system. At the surface, the development of local topography and river valleys also undermines large-scale flow systems discharging to the margins of the basin, but locally focuses fluid discharge. A comprehensive flow model in the Alberta basin must consider the transience of driving forces and three-dimensional spatial distribution of permeability, to accurately integrate the accumulation of economic resources and present day conditions in the basin over many millions of years.

REFERENCES

- Adams, J. J., B. J. Rostron, and C. A. Mendoza, 2000a, Regional fluid flow and the Athabasca oil sands: numerical simulations using a fully-coupled heat, solute and groundwater flow model. Proceedings of GeoCanada 2000, Calgary, May 31 to June 4, Paper 476.
- Adams, J.J., B.J. Rostron, and C.A. Mendoza, 2000b, Evidence for two fluid mixing at Pine Point, NWT. *Journal of Geochemical Exploration*, v. 69-70, p. 103-108.
- Aitken, J.D., 1993, Interior Platform, Western basins, and Eastern Cordillera; Tectonic framework, *in* D.F. Stott and J.D. Aitken, *Geology of Canada*, v. 5, p. 45-54.
- Anderson, G. M., and R. W. Macqueen, 1982, Ore deposit models - 6. Mississippi Valley-Type lead-zinc deposits: *Geoscience Canada*, v. 9, p. 108-117.
- Anhert, F., 1970, Functional relationship between denudation, relief and uplift in large mid-latitude drainage basins: *American Journal of Science*, v. 268, p. 243-263.
- Appold, M. S., and G. Garven, 1999, The hydrology of ore formation in the Southeast Missouri district: Numerical models of topography-driven fluid flow during the Ouachita Orogeny: *Economic Geology*, v. 94, p. 913-935.
- Arne, D. C., 1991, Regional thermal history of the Pine Point area, Northwest Territories, Canada, from apatite fission-track analysis: *Economic Geology*, v. 86, p. 428-435.
- Arnold, B. W., J. M. Bahr, and R. Fantucci, 1996, Paleohydrogeology of the Upper Mississippi Valley zinc-lead district, *in* D. F. Sangster, ed., *Carbonate-Hosted Lead-Zinc Deposits*, Littleton, CO, Society of Economic Geologists, p. 378-389.
- Aulstead, K. L., R. J. Spencer, and H. R. Krouse, 1988, Fluid inclusion and isotopic evidence on dolomitization, Devonian of Western Canada: *Geochimica et Cosmochimica Acta*, v. 52, p. 1027-1035.
- Bachu, S., B. Hitchon and P. Mortensen, 1986, Hydrogeology of sedimentary basins: application to exploration and exploitation, *in* Proceedings of the Third Canadian/American Conference on Hydrogeology: Banff, Canada, National Water Well Association, p. 118-126.
- Bachu, S., 1993, Basement heat flow in the Western Canada Sedimentary Basin: *Tectonophysics*, v. 222, p. 119-133.
- Bachu, S., 1995, Synthesis and model of formation-water flow, Alberta Basin, Canada: *AAPG Bulletin*, v. 79, p. 1159-1178.
- Bachu, S., 1997, Flow of formation waters, aquifer characteristics and their relation to hydrocarbon accumulations, northern Alberta Basin: *AAPG Bulletin*, v. 81, p. 712-733.
- Bachu, S., 1999, Flow systems in the Alberta Basin: Patterns, types and driving mechanisms: *Bulletin of Canadian Petroleum Geology*, v. 47, p. 455-474.
- Bachu, S. and R.A. Burwash, 1994, Geothermal regime in the Western Canada Sedimentary Basin, *in* Mossop, G., and I. E. Shetsen, eds., *Geological Atlas of the Western Canada Sedimentary Basin*, Canadian Society of Petroleum Geologists and Alberta Research Council, p. 447-454.

- Bachu, S., and J. R. Undershultz, 1992, Regional-scale porosity and permeability variations, Peace River Arch area, Alberta, Canada: AAPG Bulletin, v. 76, p. 547-562.
- Bachu, S., J. R. Undershultz, B. Hitchon and D. Cotterhill, 1993, Regional-scale subsurface hydrogeology in northeast Alberta: Alberta Research Council Bulletin, No. 61, 44 p.
- Barrett, T. J., and G. M. Anderson, 1982, The solubility of sphalerite and galena in NaCl brines: Economic Geology, v. 77, p. 1923-1933.
- Barson, D., S. Bachu and P. Esslinger, in press, Flow systems in the Mannville Group in the east-central Athabasca area and implications for steam-assisted gravity drainage (SAGD) operations for in-situ bitumen production: Bulletin of Canadian Petroleum Geology.
- Beales, F. W., and S. A. Jackson, 1967, Precipitation of lead-zinc ores in carbonate reservoirs as illustrated by Pine Point ore field, Canada: Transactions of the Institution of Mining and Metallurgy, Section B, p. B278-B285.
- Beaumont, C., G. M. Quinlan, and G. S. Stockmal, 1993, The evolution of the Western Interior Basin: causes, consequences and unsolved problems, *in* W. G. E. Caldwell, and E. G. Kauffman, eds., Evolution of the Western Interior Basin, Geological Association of Canada, p. 97-117.
- Bekele, E., 1999, Hydrogeologic controls on petroleum distribution within the Alberta Basin, Canada. Ph.D. Thesis, University of Minnesota, 190 p.
- Bethke, C. M., 1985, A numerical model of compaction-driven groundwater flow and heat transfer and its application to the paleohydrology of intracratonic sedimentary basins: Journal of Geophysical Research, v. 90, p. 6817-6828.
- Bethke, C. M., 1986, Hydrologic constraints on the genesis of the Upper Mississippi Valley mineral district from Illinois Basin brines: Economic Geology, v. 81, p. 233-249.
- Bethke, C. M. and T.F. Corbet, 1989, Linear and nonlinear solutions for one-dimensional compaction flow in sedimentary basins: Water Resources Research, v. 24, p. 461-467.
- Bethke, C. M., and S. Marshak, 1990, Brine migrations across North America - The plate tectonics of groundwater: Annual Reviews of Earth and Planetary Science, v. 18, p. 287-315.
- Blackwell, D.D. and J.L. Steele, 1989, Thermal conductivity of sedimentary rocks: measurement of significance *in* N.D. Naeser, T.H. McCulloh, eds., Thermal History of Sedimentary Basins: Methods and Case Histories, Springer-Verlag, New York, p. 13-36.
- Brannon, J. C., F. A. Podosek, and R. K. McLimans, 1992, A Permian Rb-Sr age for sphalerite from the Upper Mississippi Valley zinc-lead district, Wisconsin: Nature, v. 356, p. 509-511.
- Bredehoft, J.D., and D.F. Norton, 1990, Mass and energy transport in a deforming Earth's crust. *in* The Role of Fluids in Crustal Processes, National Academy, Washington, D.C., p. 27-41.
- Brooks, P. W., M. G. Fowler, and R. W. MacQueen, 1988, Biological marker and conventional organic geochemistry of oil sands/heavy oils, Western Canada Basin: Organic Geochemistry, v. 12, p. 519-538.
- Campbell, N., 1966, The lead-zinc deposits of Pine Point: Canadian Institute of Mining and Metallurgy Bulletin, v. 59, p. 953-960.

- Campbell, N., 1967, Tectonics, reefs and stratiform lead-zinc deposits of the Pine Point area, Canada: *Economic Geology*, Monograph 3, p. 59-70.
- Carpenter, A. B., 1978, Origin and chemical evolution of brines in sedimentary basins: *Oklahoma Geological Survey Circular*, v. 79, p. 60-77.
- Cathles, L. M., and A. T. Smith, 1983, Thermal constraints on the formation of Mississippi Valley-type lead-zinc deposits and their implications for episodic basin dewatering and deposit genesis: *Economic Geology*, v. 78, p. 983-1002.
- Catuneanu O., A.R. Sweet and A.D. Miall, 1999, Concept and styles of reciprocal stratigraphies: Western Canada foreland system: *Terra Nova*, v. 11, p. 1-8.
- Catuneanu O., C. Beaumont and P. Waschbursh, 1997. Interplay of static loads and subduction dynamics in foreland basins: reciprocal stratigraphies 'missing' peripheral bulge: *Geology*, v. 25, p. 1087-1090.
- Christensen, J. N., A. N. Halliday, J. R. Vearncombe, and S. E. Kesler, 1995, Testing models of large-scale crustal fluid flow using direct dating of sulfides: Rb-Sr evidence for early dewatering and formation of Mississippi Valley-Type deposits, Canning Basin, Australia: *Economic Geology*, v. 90, p. 877-884.
- Connolly, C. A., L. M. Walter, H. Baadsgaard, and F. J. Longstaffe, 1990a, Origin and evolution of formation waters, Alberta Basin, Western Canada Sedimentary Basin. I. Chemistry: *Applied Geochemistry*, v. 5, p. 375-395.
- Connolly, C. A., L. M. Walter, H. Baadsgaard, and F. J. Longstaffe, 1990b, Origin and evolution of formation waters, Alberta Basin, Western Canada Sedimentary Basin. II. Isotope systematics and water mixing: *Applied Geochemistry*, v. 5, p. 397-413.
- Corbet, T. F., and C. M. Bethke, 1992, Disequilibrium fluid pressures and groundwater flow in the Western Canada Sedimentary Basin: *Journal of Geophysical Research*, v. 97, p. 7203-7217.
- Creaney, S., and J. Allan, 1990, Petroleum Generation and migration in the Western Canada Sedimentary Basin, *in* J. Brooks, ed., *Classic Petroleum Provinces*, Geological Society Special Publication, p. 189-202.
- Creaney, S., J. Allan, S. Colek, M.G. Fowler, P.W. Brooks, K.G. Osadetz, R.W. Macqueen, L.R. Snowdon, and C.L. Riediger, 1994, Hydrocarbon generation and migration in the Western Canada Sedimentary Basin, *in* Mossop, G., and I. E. Shetsen, eds., *Geological Atlas of the Western Canada Sedimentary Basin*, Canadian Society of Petroleum Geologists and Alberta Research Council, p.455-468.
- Cumming, G. L., J. R. Kyle, and D. F. Sangster, 1990, Pine Point: A case history of lead isotope homogeneity in a Mississippi Valley-Type district: *Economic Geology*, v. 85, p. 133-144.
- Daus, A.D., E.O. Frind, and E.A. Sudicky, 1985, Comparative error analysis in finite element formulations of the advection-dispersion equation: *Advances in Water Resources*, v. 8, p. 86-95.
- Deming, D., 1994, Fluid flow and heat transport in the upper continental crust, *in* J. Parnell, ed., *Geofluids: Origin, Migration and Evolution of Fluids in Sedimentary Basins*, Geological Society Special Publication, p. 27-42.

- Deming, D., and J. A. Nunn, 1991, Numerical simulations of brine migration by topographically driven recharge: *Journal of Geophysical Research*, v. 96, p. 2485-2499.
- Domenico, P.A. and V.V. Palciauskas, 1979, Thermal expansion of fluids and fracture initiation in compacting sediments: *Geological Society of America Bulletin*, Part II, v. 90, p. 953-979.
- Downey, J. S., 1986, Geohydrology of bedrock aquifers in the northern Great Plains in parts of Montana, North Dakota, South Dakota, and Wyoming: U.S. Geological Survey Professional Paper, v. 1402-E, U.S. Geological Survey, 87 p.
- Dullien, F.A.L., 1992, Porous Media: fluid transport and pore structure. Academic Press, Inc.: New York, 594 p.
- England, W.A., A.L. Mann and D. M. Mann, 1991, Migration from source to trap, *in* R.K. Merrill, ed., Source and Migration Processes and Evaluation Techniques, American Association of Petroleum Geologists, p. 23-46.
- Evans, D. and J. Nunn, 1993, Free thermohaline convection in sediments surrounding a salt column: *Journal of Geophysical Research*, v. 98, p. 413-422.
- Fermor, P.R. and I.W. Moffat, 1992, Tectonics and structure of the Western Canada foreland basin, *in* R.W. Macqueen, D.A. Leckie, eds., Foreland Basins and Fold Belts, AAPG Memoir 55, American Association of Petroleum Geologists, p. 81-105.
- Fishman, H. S., 1997, Basin-wide fluid movement in a cambrian paleoaquifer: Evidence from the Mt. Simon Sandstone, Illinois and Indiana, *in* E. Montanez, J. Gregg and K. Shelton, eds., Basin-Wide Diagenetic Patterns: Integrated Petrologic, Geochemical and Hydrologic Considerations, p. 221-234.
- Fowler, A. D., 1986, The role of regional fluid flow in the genesis of the pine point deposit, Western Canada Sedimentary Basin - A Discussion: *Economic Geology*, v. 81, p. 1014-1015.
- Fritz, P., and S. A. Jackson, 1972, Geochemical and isotopic characteristics of Middle Devonian dolomites from Pine Point, Northern Canada: 24th International Geol. Congress, p. 230-243.
- Garven, G., 1985, The role of regional fluid flow in the genesis of the pine point deposit, Western Canada Sedimentary Basin: *Economic Geology*, v. 80, p. 307-324.
- Garven, G., 1989, A hydrogeologic model for the formation of the giant oil sands deposits of the Western Canada Sedimentary Basin: *American Journal of Science*, v. 289, p. 105-166.
- Garven, G., and R. A. Freeze, 1984a, Theoretical analysis of the role of groundwater flow in the genesis of stratabound ore deposits. 1. Mathematical and numerical model: *American Journal of Science*, v. 284, p. 1085-1124.
- Garven, G., and R. A. Freeze, 1984b, Theoretical analysis of the role of groundwater flow in the genesis of stratabound ore deposits. 2. Quantitative results: *American Journal of Science*, v. 284, p. 1125-1174.
- Garven, G., S. Ge, M. A. Person, and D. A. Sverjensky, 1993, Genesis of stratabound ore deposits in the midcontinent basins of North America. 1. The role of regional groundwater flow: *American Journal of Science*, v. 293, p. 497-568.

- Garven, G., M. S. Appold, V. I. Toptygina, and T. J. Hazlett, 1999, Hydrogeologic modeling of the genesis of carbonate-hosted lead-zinc ores: *Hydrogeology Journal*, v. 7, p. 108-126.
- Ge, S., and G. Garven, 1994, A theoretical model for thrust-induced deep groundwater expulsion with application to the Canadian Rocky Mountains: *Journal of Geophysical Research*, v. 99, p. 13,851-13868.
- Garven, G., 1995, Continental-scale groundwater flow and geological processes: *Annual Reviews Earth and Planetary Science*, v. 23, p. 89-117.
- Giordano, T. H., and Y. K. Kharaka, 1994, Organic ligand distribution and speciation in sedimentary basin brines, diagenetic fluids and related ore solutions: *Geofluids: Origin, Migration and Evolution of Fluids in Sedimentary Basins*, v. 78, p. 175-202.
- Hanmer, S., 1988, Great Slave Shear Zone, Canadian Shield: reconstructed vertical profile of a crustal-scale fault zone: *Tectonophysics*, v. 149, p. 245-264.
- Hanor, J. S., 1994, Physical and chemical controls on the composition of waters in sedimentary basins: *Marine and Petroleum Geology*, v. 11, p. 31-45.
- Hanor, J. S., 1996, Controls on the solubilization of lead and zinc in basinal brines, *in* D. F. Sangster, ed., *Carbonate Pb-Zn Deposits*, SEPM Special Publication No. 4, Society of Economic Geologists, p. 483-500.
- Haynes, F. M., and S. E. Kesler, 1987, Chemical evolution of brines during Mississippi Valley-type mineralization: Evidence from East Tennessee and Pine Point: *Economic Geol.*, v. 82, p. 53-71.
- Hitchon, B., 1993, Geochemistry of formation water, northern Alberta, Canada: their relation to the Pine Point ore deposit, Edmonton, Alberta Geological Survey, Open File Report 1993-14, p. 99.
- Hitchon, B., S. Bachu, and J. R. Undershultz, 1990, Regional subsurface hydrogeology, Peace River Arch area, Alberta and British Columbia. *Bulletin of Canadian Petroleum Geology*, v. 38A, p. 196-217
- Hitchon, B., and I. Friedman, 1969, Geochemistry and origin of formation waters in the Western Canada Sedimentary Basin - I. Stable isotopes of hydrogen and oxygen: *Geochimica et Cosmochimica Acta*, v. 33, p. 1321-1349.
- Hitchon, B., 1969, Fluid flow in the Western Canada Sedimentary Basin 1. Effect of topography: *Water Resources Research*, v. 5, p. 186-195.
- Hitchon, B., G. K. Billings, and J. E. Klován, 1971, Geochemistry and origin of formation waters in the Western Canada Sedimentary Basin - III. Factors controlling chemical composition: *Geochimica et Cosmochimica Acta*, v. 35, p. 567-598.
- Holmden, C., K. Muehlenbachs, and R. A. Creaser, 1997, Depositional environment of the early Cretaceous ostracod zone: Paleohydrologic constraints from oxygen, carbon and strontium isotopes: *Canadian Society of Petroleum Geologists, Memoir 18*, p. 77-92.
- Hubbert, M.K., 1953, Entrapment of petroleum under hydrodynamic conditions, *AAPG Bulletin*, v. 37, p. 1954-2026.
- Ingebritsen, S.E. and W.E. Sanford, 1998, *Groundwater in geologic processes*, University Press, Cambridge , 341 p.

- Issler, D. R., S. D. Willett, C. Beaumont, R. A. Donelick, and A. M. Grist, 1999, Paleotemperature history of two transects across the Western Canada Sedimentary Basin: Constraints from apatite fission track analysis: *Bulletin of Canadian Petroleum Geology*, v. 47, p. 475-486.
- Jackson, S. A., and F. W. Beales, 1967, An aspect of sedimentary basin evolution: The concentration of Mississippi Valley-type ores during late stages of diagenesis: *Bulletin of Canadian Petroleum Geology*, v. 15, p. 383-433.
- Jones, G., University of Bristol, personal communication, 1999.
- Krebs, W., and R. Macqueen, 1984, Sequence of diagenetic and mineralization events, Pine Point lead-zinc property, Northwest Territories, Canada: *Bulletin of Canadian Petroleum Geology*, v. 32, p. 434-464.
- Kutz, K. B., and P. G. Spry, 1989, The genetic relationship between Upper Mississippi Valley district lead-zinc mineralization and minor base metal mineralization in Iowa, Wisconsin and Illinois: *Economic Geology*, v. 84, p. 2139-2154.
- Kyle, J. R., 1981, Geology of the Pine Point lead-zinc district, *in* K. H. Wold, ed., *Handbook of Strata-Bound and Stratiform Ore Deposits*, New York, Elsevier Scientific Publishing Co., p. 643-741.
- Leach, D., 1999, Mississippi Valley-Type lead-zinc deposits through geologic time: Implications for the exploration of undiscovered deposits, Notes from Prospectors and Developers Association Conference Short Course, Toronto, p. 211-237.
- Lewis, T., and R. Hyndman, 1999, High heat flow along the SNORCLE transect: Slave-Northern Cordillera Lithospheric Evolution (SNORCLE) Transect and Cordilleran Tectonics Workshop Meeting, p. 83-84.
- Lisenbee, A.L. and E. DeWitt, 1993, Laramide evolution of the Black Hills uplift, *in* A.W. Snoke, J.R. Steidtmann, and S.M. Roberts, eds., *Geology of Wyoming: Geological Survey of Wyoming Memoir No.5*, p. 374-412.
- Machel, H. G., and P. A. Cavell, 1999, Low-flux, tectonically-induced squeegee fluid flow ("hot flash") into the Rocky Mountain Foreland Basin: *Bulletin of Canadian Petroleum Geology*, v. 47, p. 510-533.
- Michael, K. and H.G. Machel, 2000, Flow of variable-density brines in deep Devonian aquifers west-central Alberta. *Proceedings of GeoCanada 2000*, Calgary, May 31 to June 4, Paper 339.
- Morrow, D. W., 1998, Regional subsurface dolomitization; models and constraints: *Geoscience Canada*, v. 25, p. 57-70.
- Mossop, G., and I. E. Shetsen, 1994, Geological atlas of the Western Canada Sedimentary Basin, Calgary, Canadian Society of Petroleum Geologists and Alberta Research Council, 510 p.
- Mountjoy, E., S. Whittaker, A. Williams-Jones, H. Qing, E. Drivet, and X. Marquez, 1997, Variable fluid and heat flow regimes in three Devonian dolomite conduit systems, Western Canada Sedimentary Basin: isotopic and fluid inclusion evidence/constraints, Basin-Wide Diagenetic Patterns: Integrated Petrologic, Geochemical and Hydrologic Considerations, *Society of Sedimentary Geology*, p. 119-137.

- Nakai, S., A. N. Halliday, S. E. Kesler, H. D. Jones, J. R. Kule, and T. E. Lane, 1993, Rb-Sr dating of sphalerites from Mississippi Valley-type (MVT) ore deposits: *Geochemica et Cosmochimica Acta*, v. 57, p. 417-427.
- Nesbitt, B. E., and K. Muehlenbachs, 1994a, Paleohydrogeology of the Canadian Rockies and origins of brines, Pb-Zn deposits and dolomitization in the Western Canada Sedimentary Basin: *Geology*, v. 22, p. 243-246.
- Nesbitt, B. E., and K. Muehlenbachs, 1994b, Paleohydrogeology of the Canadian Rockies and origins of brines, Pb-Zn deposits and dolomitization in the Western Canada Sedimentary Basin: Comment and Reply: *Geology*, v. 22, p. 1149-1151.
- Neuzil, C. E., 1994, How permeable are clays and shales?: *Water Resources Research*, v. 30, p. 145-150.
- Neuzil, C. E., and D. W. Pollock, 1983, Erosional unloading and fluid pressures in hydraulically "tight" rocks: *Journal of Geology*, v. 91, p. 179-193.
- Oliver, J., 1986, Fluids expelled tectonically from orogenic belts: Their role in hydrocarbon migration and other geologic phenomena: *Geology*, v. 14, p. 99-102.
- Parks, K. P., and J. Tóth, 1995, Field evidence for erosion-induced underpressuring in Upper Cretaceous and Tertiary strata, west central Alberta, Canada: *Bulletin of Canadian Petroleum Geology*, v. 43, p. 281-292.
- Parrish, R.R., 1995, Thermal evolution of the southeastern Canadian Cordillera: *Canadian Journal of Earth Sciences*, v. 32, n. 10, p. 1618-1642.
- Person, M., C. Neuzil, P. Hsieh, B. Mailloux, E. Bekele, J. Swenson and P. Eadington, 2000, RIFT2D: A Finite element model for simulating two-dimensional ground water flow, heat, solute mass transport and petroleum generation within evolving sedimentary basins, University of Minnesota, in preparation.
- Person, M., and G. Garven, 1994, A sensitivity study of the driving forces on fluid flow during continental-rift basin evolution: *Geological Society of America Bulletin*, v. 106, p. 461-475.
- Pinet, P. and M. Souriau, 1988, Continental erosion and large-scale relief: *Tectonics*, v. 7, p. 563-582.
- Porter, J. W., R. A. Price, and R. G. McCrossan, 1982, The Western Canada Sedimentary Basin: *Philosophical Trans. Royal Society of London*, v. A 305, p. 169-192.
- Qing, H., 1998a, Geochemical constraints on the origin and timing of palaeofluid flow in the Presqu'île Barrier reef, Western Canada Sedimentary Basin, *in* J. Parnell, ed., *Dating and Duration of Fluid Flow and Fluid-Rock Interaction*, London, Geological Society, p. 173-187.
- Qing, H., 1998b, Petrography and geochemistry of early-stage, fine- and medium-crystalline dolomites in the Middle Devonian Presqu'île at Pine Point, Canada: *Sedimentology*, v. 45, p. 433-446.
- Qing, H., and E. Mountjoy, W., 1994a, Origin of dissolution vugs, caverns and breccias in the Middle Devonian Presqu'île Barrier, host of Pine Point Mississippi Valley-type deposits: *Economic Geology*, v. 89, p. 858-876.

- Qing, H., and E. W. Mountjoy, 1994b, Formation of coarsely crystalline, hydrothermal dolomite reservoirs in the Presqu'ile Barrier, Western Canada Sedimentary Basin: AAPG Bulletin, v. 78, p. 55-77.
- Qing, H., and E. W. Mountjoy, 1994c, Rare earth element geochemistry of dolomite in the Middle Devonian Presqu'ile barrier, Western Canada Sedimentary Basin: Implications for fluid-rock ratios during dolomitization: Sedimentology, v. 41, p. 787-804
- Qing, H., and E. W. Mountjoy, 1992, Large-scale fluid flow in the Middle Devonian Presqu'ile barrier, Western Canada Sedimentary Basin: Geology, v. 20, p. 903-906.
- Raffensperger, J. P., and G. Garven, 1995, The formation of unconformity-type uranium ore deposits 1. coupled groundwater flow and heat transport modeling: American Journal of Science, v. 295, p. 581-636.
- Ravenhurst, C. E., S. D. Willet, R. A. Donelick, and C. Beaumont, 1994, Apatite fission track thermochronometry from central Alberta: Implications for the thermal history of the Western Canada Sedimentary Basin: Journal of Geophysical Research, v. 99, p. 20023-20041.
- Ranger M.J., 1994, A basin study of the southern Athabasca oil sands deposit, University of Alberta, Department of Geology Ph.D. Thesis, 290 p.
- Rayer, R., G. Garven and D. Rickard, 1998, Fluid migration and coal-rank development in foreland basins: Geology, v. 26, p. 679-682.
- Rhodes, D., E. A. Lantos, J. A. Lantos, R. J. Webb, and D. C. Owens, 1984, Pine Point Ore bodies and Their Relationship to the Stratigraphy, Structure, Dolomitization and Karstification of the Middle Devonian Barrier Complex: Economic Geology, v. 79, p. 991-1055.
- Ricketts, B.D. (ed.), 1989, Western Canadian Sedimentary Basin - A case history. Calgary Canadian Society of Petroleum Geologists, 320 p.
- Ringrose, P.S. and P.W.M. Corbett, 1994, Controls of two-phase fluid flow in heterogeneous sandstones, *in* J. Parnell, ed., Geofluids: Origin, Migration and Evolution of Fluids in Sedimentary Basins, Geological Society Special Publications, v. 78, p. 141-150.
- Roedder, E., 1968, Temperature, salinity and origin of the ore-forming fluids at Pine Point, Northwest Territories, Canada, from fluid inclusion studies: Economic Geology, v. 63.
- Rostron, B. J., J. Tóth, and H. G. Machel, 1997, Fluid flow, hydrochemistry, and petroleum entrapment in Devonian reef complexes, south-central Alberta, Canada, *in* I. P. Montanez, J. M. Gregg, and K. L. Shelton, eds., Basin-Wide Diagenetic Patterns: Integrated Petrologic, Geochemical, and Hydrologic Considerations, Tulsa, Oklahoma, SEPM, p. 139-155.
- Sangster, D. F., G. S. Nowlan, and A. D. McCracken, 1994, Thermal comparison of Mississippi Valley-Type lead-zinc deposits and their host rocks using fluid inclusion and conodont color alteration index data: Economic Geology, v. 89, p. 493-514.
- Sangster, D. F., 1988, Breccia-hosted lead-zinc deposits in carbonate rocks, *in* N. P. James, and P. W. Choquette, eds., Paleokarst, New York, Springer Verlag, p. 102-116.
- Skall, H., 1975, The paleoenvironment of the Pine Point lead-zinc district: Economic Geology, v. 70, p. 22-47.

- Spirakis, C. S., and A. V. Heyl, 1994, Precipitation of Mississippi Valley-Type ores: the importance of organic matter and thiosulphate, *in* Fontbote, and Boni, eds., *Sediment-Hosted Zn-Pb Ores*, Berlin, Springer Verlag, p. 27-41.
- Stott, D. F., 1982, Lower Cretaceous Fort St. John Group and Upper Cretaceous Dunvegan Formation of the foothills and plains of Alberta, British Columbia, District of Mackenzie and Yukon Territory: Geological Survey of Canada, Bulletin 328, 124 p.
- Stueber, A.M. and L.M. Walter, 1994, Glacial recharge and paleohydrologic flow systems in the Illinois basin: Evidence from chemistry of Ordovician carbonate (Galena) formation waters: Geological Society of America Bulletin, v. 106, p. 1430-1439.
- Symons, D. T. A., H. Pan, D. F. Sangster, and E. C. Jowett, 1993, Paleo-magnetism of the Pine Point Zn-Pb deposits: Canadian Journal of Earth Sciences, v. 30, p. 1028-1036.
- Telser, H., 1999, Significance of inclusion fluid chemistry for the origin of the Pine Point mineralization, NWT: M.Sc. thesis, University of Leoben, Leoben, Austria, 99 p.
- Tóth, J., 1962, A theory of groundwater motion in small drainage basins in central Alberta, Canada: Journal of Geophysical Research, v. 67, p. 4375-4387.
- Tóth, J., 1963, A theoretical analysis of groundwater flow in small drainage basins: Journal of Geophysical Research, v. 68, p. 4795-4812.
- Tóth, J., 1978, Gravity-induced cross-formational flow of formation fluids, Red Earth region, Alberta, Canada: Analysis, patterns, evolution: Water Resources Research, v. 14, p. 805-843.
- Tóth, J., 1980, Cross-formational gravity-flow of groundwater: A mechanism of the transport and accumulation of petroleum (The generalized hydraulic theory of petroleum migration), *in* W. H. Roberts III, and R. J. Cordell, eds., *Problems of Petroleum Migration*, Tulsa, American Association of Petroleum Geologists, p. 121-167.
- Tóth, J., 1984, The role of gravity flow in the chemical and thermal evolution of ground water: First Canadian/American Conference on Hydrogeology; Practical Applications of Groundwater Geochemistry, p. 3-39.
- Tóth, J., and T. F. Corbet, 1986, Post-Paleocene evolution of regional groundwater flow-systems and their relation to petroleum accumulations, Taber area, southern Alberta, Canada: Bulletin of Canadian Petroleum Geology, v. 34, p. 339-363.
- Tóth, J., and R. F. Millar, 1983, Possible effects of erosional changes of the topographic relief on pore pressures at depth: Water Resources Research, v. 19, p. 1585-1597.
- Welte, D.H., R.G. Schaefer, W. Stoessinger, and M. Radke, 1984, Gas generation and migration in the deep basin of Western Canada: AAPG Memoir 38, p. 35-47.
- Willett, S. D., D. R. Issler, C. Beaumont, R. A. Donelick, and A. M. Girst, 1997, Inverse modeling of annealing of fission tracks in apatite 2: Application to the thermal history of the Peace River Arch region, Western Canada Sedimentary Basin: American Journal of Science, p. 970-1011.
- Wright, G.N., ed. 1984. The Western Canada Sedimentary basin - A series of geological sections illustrating basin stratigraphy and structure. Calgary, Canadian Society of Petroleum Geologists & Geological Association of Canada.

APPENDIX A: DESCRIPTION OF THE RIFT2D NUMERICAL MODEL

Rift2D (Person et al., 2000) is a two-dimensional, finite-element numerical model, which is designed to simulate flow systems in sedimentary basins. Density-dependent fluid flow, heat flow, solute transport and petroleum generation can be coupled in transient simulations. The processes of sedimentation, subsidence, compaction, erosion and uplift are simulated using a deformable mesh. In addition, rifting can be simulated by either block- or domino-style faulting; however, the code cannot accommodate compressional tectonics.

The porous media in the mesh are assumed to be elastic; however, rock-compressibility can vary through time, allowing for pseudo non-elastic behaviour. An Athy's Law type porosity-depth expression is used to determine porosity (ϕ), effective stress (σ_e) and the deformation modulus ($1/K'$).

$$\phi = \phi_o \exp(-\beta [\sigma_e/g \cdot (\rho_s - \rho_f)] + \phi_{ir}) \quad (\text{for loading}) \quad (1)$$

$$\phi = \phi_o \exp(-\beta_{ul}[(\sigma_e - \sigma_{max})/g \cdot (\rho_s - \rho_f)] + \phi_{ir}) \quad (\text{for unloading}) \quad (2)$$

where ϕ_o is the porosity at the watertable, ϕ_{ir} is the irreducible porosity, σ_e is the effective stress (Pa), and β or β_{ul} are the loading and unloading rock compressibility (Pa^{-1}), respectively. All porosity loss is assumed to be the result of effective stress variations rather than diagenetic dissolution or precipitation reactions in the subsurface.

Deformation of the mesh is calculated based on vertical loading or unloading of the rock matrix or changes in effective stress due to variations in fluid pressure. Following adjustment of the finite element mesh, changes in porosity and compressibility are returned to the flow equation.

The continuum approach was used to develop the transport equations in Rift2D. Conservation of fluid mass, solute mass and thermal energy is maintained using Darcy's Law, Fick's law and Fourier's Law respectively.

The flow equation in Rift2D is formulated to account for vertical compaction and decompaction, water density, watertable topographic gradients and petroleum volume variations during generation. The resulting partial differential equation for flow is:

$$\begin{aligned} \nabla_x[\mathbf{K}\mu_r\rho_f\nabla_x(h + \rho_r)] = S_s\rho_o(\partial h/\partial t) - \rho_f/K'\rho_s g(\partial\sigma_v/\partial t) \\ - \phi\rho_f\Lambda(\partial T/\partial t) + (\rho_k - \rho_{oil})(\partial T_r/\partial t) \end{aligned} \quad (3)$$

where ∇_x is the divergence/gradient operator, \mathbf{K} is the hydraulic conductivity tensor, h is hydraulic head, T is temperature, Λ is the thermal response coefficient, T_r is the kerogen transformation ratio, ρ_{oil} is oil density, ρ_k is the density of kerogen, σ_v is the vertical total stress, K' is the one-dimensional deformation modulus of the medium, μ_r is the viscosity of water, ρ_o is the density of water at 10°C and atmospheric pressure, ρ_s is the sediment density, ρ_r is the relative density ($\rho_r = \{\rho_f - \rho_o\}/\rho_o$), μ_r is the relative viscosity of water ($\mu_r = \mu_f/\mu_o$), S_s is specific storage, ρ_f is the density of groundwater and ϕ is porosity.

Rift2D can simulate conductive and advective-dispersive heat transfer, using the equation from Bethke (1985). This formulation requires that the solid and fluid phases be in thermal equilibrium.

Solute transport is calculated using the following expression, which accounts for diffusion and dispersion:

$$\partial C/\partial t + C(\phi)^{-1} \cdot \partial \phi/\partial t = \nabla_x[\mathbf{D}\nabla_x C] - \mathbf{v}\nabla_x C \quad (4)$$

where \mathbf{D} is the hydrodynamic dispersion-diffusion tensor, \mathbf{v} is the groundwater velocity and C is the solute concentration.

First-order rate kinetic equations are used to calculate the onset of petroleum generation; however, this capability was not used in the simulations discussed in this thesis.

The limitations of Rift2D include:

- 1) Only single-phase water flow systems can be simulated, i.e., petroleum generating zones are treated only as fluid sources.
- 2) The effects of capillary forces are neglected.
- 3) Solute transport is limited to mixtures of soluble salts. Rift2D does not track the fate of individual constituents or account for geochemical reactions common during diagenesis, fluid mixing or rock-water interaction.

- 4) Lateral tectonic compression cannot be incorporated into simulations, whereas extensional environments can be accommodated by faulting.

No fluid flow, heat flow and solute transport boundary conditions are explicitly defined along the vertical limits of any Rift2D model domain. These boundaries are assumed to be zero gradient boundaries for the respective quantities.

The top surface of a model can be assigned surface temperature values that can change in time and space, but must be greater than 0°C. Specified hydraulic head values can be defined along the upper surface of model. They can vary in time and space. Alternatively, Rift2D can assume that the watertable is defined by the elevation of the top boundary of the model at all times. Solute sources can be defined in the subsurface or at surface. In addition, a constant salinity gradient, defined by depth, can be applied as an initial condition.

Along the lower boundary, only a basal heat flux can be defined. These values can vary in space along the boundary or can linearly increase or decrease with time, but they may not shift to a new base value partway through a simulation. Head and concentration gradients are assumed to be zero along the base, representing impermeable conditions.

Aquifer parameters are assigned to the finite element mesh using ‘material tags’, which define a set of aquifer parameters. Thus, each element is assigned a material tag, which defines the permeability, anisotropy, initial porosity, thermal conductivity, heat capacity, rock compressibility, and dispersivity values, as well as, the molecular diffusion coefficient and density of the rock matrix. Permeability values can be either explicitly defined or permeability models can be used such as the Carmen Kozeny or $\log(k_{\max}) = k_1 + k_2 \cdot \phi$. Water density and viscosity values are calculated based on the temperature, pressure and salinity of the water in a given element.

The type (e.g., uplift or subsidence) and amount of movement of the mesh over one year is defined for each grid column. Rift2D can simulate a series of ‘tectonic periods’, which are periods of simulation during which the boundary conditions remain the same. The mesh movement, distribution of material tags, hydraulic heads, and solute source boundary conditions can be changed for each tectonic period. Individual elements can be monitored over the simulation or full columns can be monitored to study pressure variations.

APPENDIX B: RIFT2D INPUT FILES AND SIMULATIONS

Input files for the Pine Point base case, Athabasca best case and erosion models are available from the author (jadams@darcy.eas.ualberta.ca) or Drs B. Rostron (ben.rostron@ualberta.ca) and C. Mendoza (carl.mendoza@ualberta.ca). Descriptions of each variable are available in Person et al. (2000).

APPENDIX C: PECLET NUMBERS

In both of Garven's original models (1985; 1989), solute transport was not simulated; however, water density values remained constant and increased with depth. For this study, the finite element mesh for the Pine Point and Athabasca models had to be adjusted adequately to simulate transient solute transport. The reason being that numerical error, such as smearing of concentrations or oscillations in the solution, can develop when simulating solute transport. To minimize these errors, maximum grid spacing and time step values can be constrained.

The Peclet number is a measure of the relative strength of advection to dispersion and is defined as:

$$P_e = v\Delta x/D$$

where v is the average water velocity, Δx is the distance between horizontal nodes and D is the dispersion coefficient. The Peclet criterion ($P_e \leq 2$) limits the optimal grid spacing (Daus et al., 1985). If molecular diffusion is negligible compared to dispersion, $D \approx \alpha_x v$, where α_x is longitudinal dispersivity in m. Thus, $\Delta x \leq 2\alpha_x$ results from strict adherence to this criterion. In practise, the Peclet number can be as great as 10 (Anderson and Woessner, 1992) without causing undue errors. The vertical grid spacing can be chosen from the aspect ratio, as follows: $(\Delta y)^2/\alpha_y \approx (\Delta x)^2/\alpha_x$. The aspect ratio should ideally be 1 within the principal area of interest; however, values of 10 to 100 are reasonable in many cases.

The Courant number is:

$$C_r = v\Delta t/\Delta x$$

where Δt is the time step size. This number provides a measure of the advective distance a particle moves relative to the grid spacing. The Courant criterion, $C_r \leq P_e/2$, constrains the time step length, such that particles do not move more than one element per time step. Thus, to satisfy the Courant criterion, $\Delta t \leq \Delta x/v$. In all simulations, the Courant number was set to 0.5. Within the RIFT2D code, this means that two or three solute transport steps are simulated for each fluid flow calculation.

For the *base case* Pine Point and *best case* Athabasca models, different meshes were used to evaluate the impact of the Peclet number on the solution. Table C.1 shows that Garven's meshes have very high Peclet numbers and grid aspect ratios. For the *base case* Pine Point and *best case* Athabasca models, the finite element meshes were refined significantly to minimize aspect ratio and Peclet criteria violations. The dispersion coefficients were increased by two orders of magnitude, to values approximating the scale of heterogeneity within each hydrostratigraphic unit. In all the Pine Point simulations, the barrier aquifer was assigned a longitudinal dispersivity of 240 m to account for the interconnected karst networks, parallel to the Great Slave Lake shear zone.

Table C.1: Parameters describing the finite element meshes for both the Pine Point models and Athabasca models.

Model Name	Columns	Rows	Δx min	Δx max	Δy min	Δy max	α_x	α_y	Peclet min	Peclet max	Aspect ratio max	Aspect ratio min
Pine Point models												
Garven Pine Point	42	10	7200	19000	100	300	1	0.1	7200	19000	518	401
Base Case	200	20	2500	2500	50	160	240	10	10	10	104	10
400 columns	400	20	1250	1250	50	160	240	10	5	5	26	3
Athabasca models												
Garven Athabasca	60	30	12067	12067	16	203	1	0.1	12067	12067	55710	352
Best Case	250	37	2896	2896	13	165	100	10	29	29	4881	31
700 columns	700	37	1034	1034	13	165	100	10	10	10	623	4

In the Pine Point *base case*, two meshes were simulated (Figure C.1); however, neither mesh had a Peclet number less than 2 (Table C.1). The *400 columns* model takes 8 times more computer time, but has a lower Peclet number and aspect ratios than the *base case* model. The salinity distributions of both models were compared and the *400 columns* model shows more detail in the salinity patterns and eliminates numerical oscillations; however, the *base case* and *400 columns* models generate very similar solutions. The lengthier computer time required to solve the *400 columns* model (Appendix E) meant that the *base case* mesh was used for the sensitivity analysis.

The Athabasca models require much larger meshes than the Pine Point models to account for the greater number of hydrostratigraphic units and longer model domain. For this reason, the Peclet number of the *700 columns* model could only be reduced to 10 (Table C.1). The salinity distributions of both models were compared (Figure C.2) and the *700 columns*

model produces better definition of salinity plumes in the Mannville. Again, the *best case* and *700 columns* models generate regionally identical solutions. Due to lengthier computer time required for the *700 columns* model (Appendix E), the *best case* mesh was used for the sensitivity analysis.

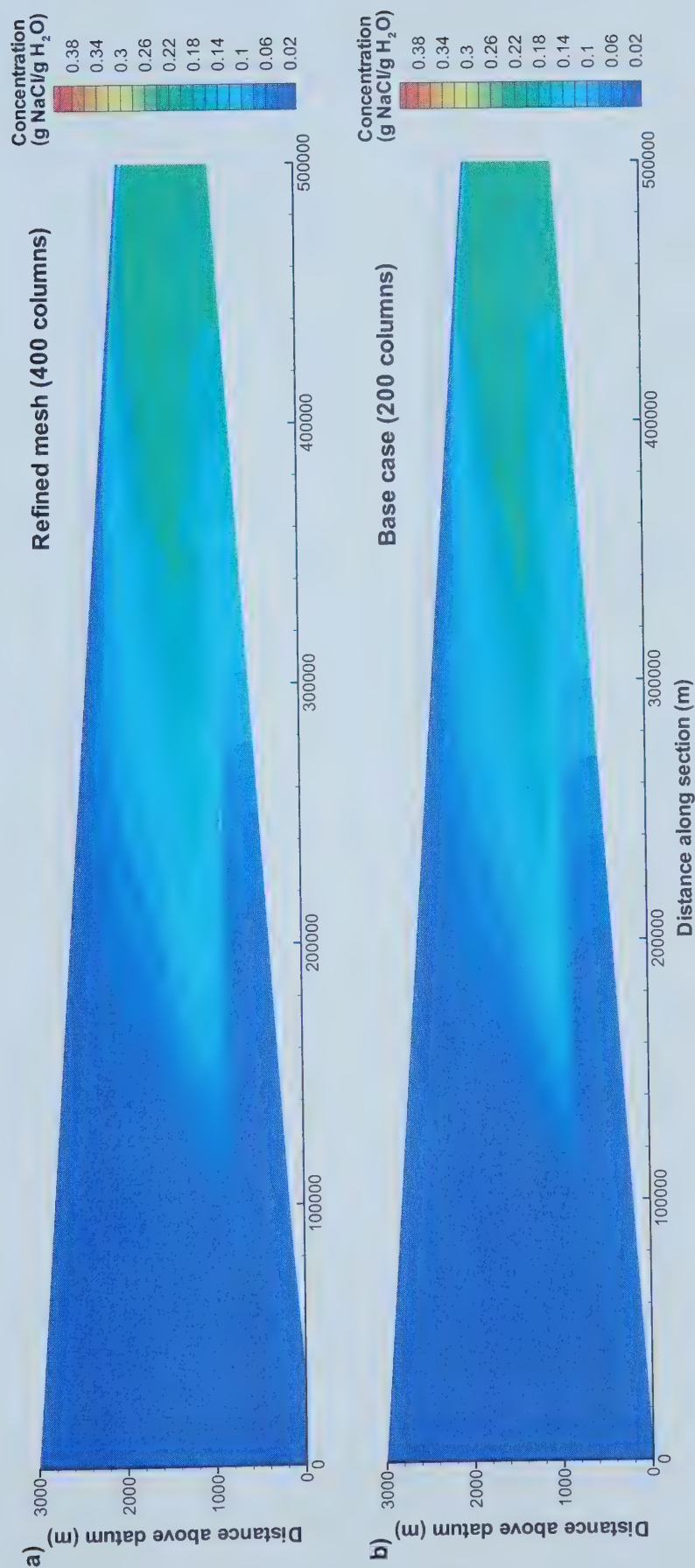


Figure C.1: Comparison of salinity distributions of the a) 400 column base case model and b) Pine Point base case model 100 000 years after instantaneous uplift.

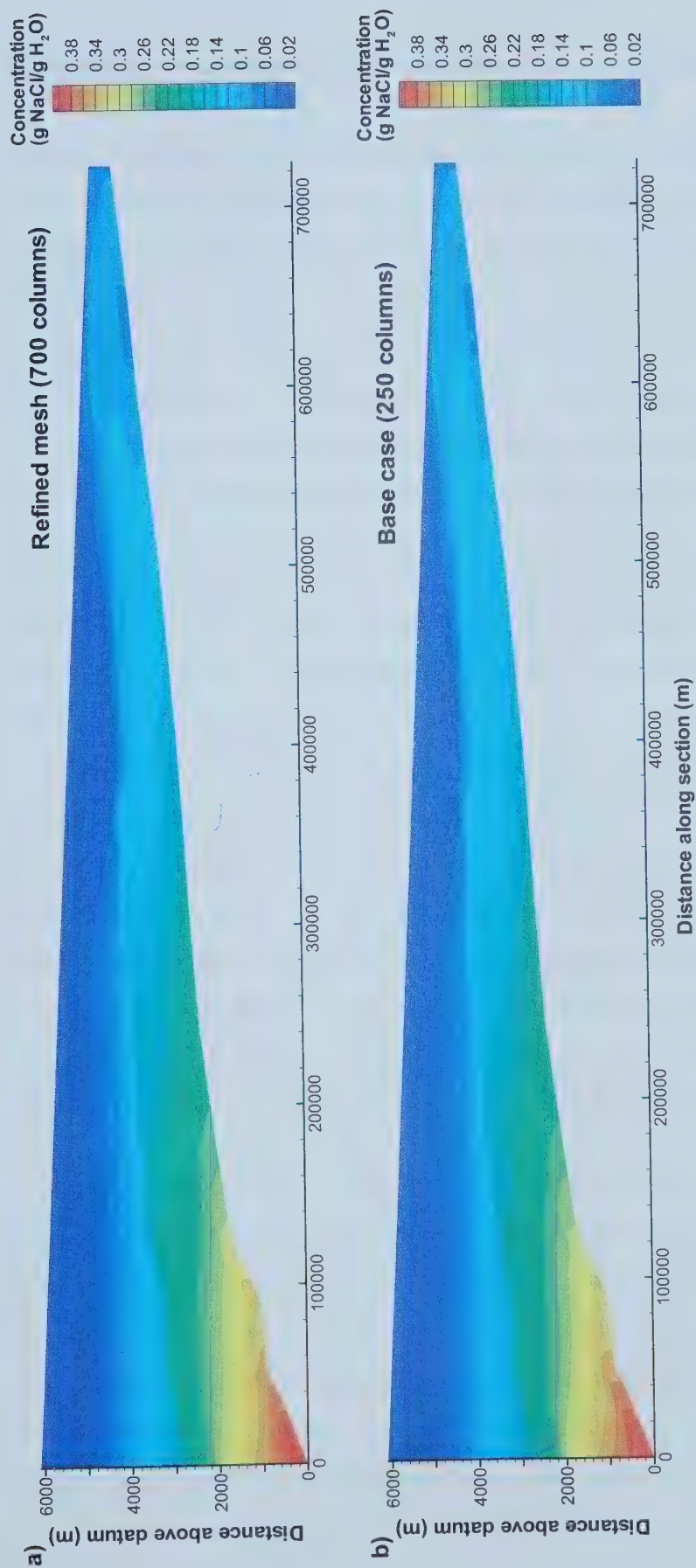


Figure C.2: Comparison of salinity distributions of the a) 700 column best case model and b) Athabasca best case model 12 million years after instantaneous uplift.

APPENDIX D: PINCHOUT MODEL ALONG PINE POINT SECTION

Boundary conditions of a numerical model define the framework that constrains a flow system. Within sedimentary basins, flow system boundary conditions vary through time due to tectonics and erosion, therefore the model domain should be designed to fit the basin configuration at the time of the flow system. Garven (1985) used present groundwater divides to define the Pine Point model domain; however, maximum topography-driven flow occurred at maximum uplift soon after 60 Ma. Thus, boundary conditions of the *base case* model should be re-evaluated in context of the basin configuration during mineralization to ensure that the *base case* model properly describes the flow system.

The top and bottom limits of the *base case* model domain impose the following assumptions on the flow model. The upper boundary provides a maximum uniform driving force across the section. However, natural erosional topographies are best approximated by exponential shapes (Anhert, 1970; Appold and Garven, 1999). This facet of the system is difficult to incorporate since no erosional data exists for this area, and therefore the transience of topography cannot be accurately simulated. The lower, no-flow boundary was assigned at the base of the Middle Devonian carbonate to optimize mesh size and computer time. In some basins, a portion of the underlying basement rock does participate in the basinal flow system (Fishman et al., 1997). Recently, large packages of basement rock have been added onto the lower boundary of basin models. This scenario is evaluated as a variation of the *base case* (Chapter 4, *basement* model) rather than part of a sensitivity analysis due to poor constraint on basement permeability and thickness active in the flow system.

Garven chose lateral limits of the modelled section based on present day groundwater divides located near Fort Nelson and 50 km east of Pine Point. The western boundary of the model defines the depth or maximum salinity and temperature in the section. Extension of the model domain west to the disturbed belt would increase the volume of hot brine that passed through Pine Point; however, flow rates and temperatures would remain the same as the hydraulic gradient remains unchanged. His eastern no flow boundary forces fluid to discharge near Pine Point. However, at maximum uplift, the basin extended much farther east. Mineralization is thought to have taken place at 500 to 1000 m of depth, suggesting

that the Middle Devonian aquifer may have extended much farther east (Sangster et al., 1994).

As discussed only the eastern boundary needs to be tested for the purposes of this study. To evaluate the importance of the eastern boundary, the *base case* model domain was extended 220 km to the east using the same topographic and basement gradients (*pinchout* model; Figure D.1). This extension results in a thickness of the *pinchout* model domain at its eastern limit of 50 m. The hydrostratigraphy was extended into the new region maintaining the same proportions as in the *base case*. Simulations of the *pinchout* flow system are similar to the *base case* solution, however the discharge zone has shifted 60 km east and is much wider. Transient solutions predict local vertical flow in the vicinity of the temperature slug, which passes through Pine Point before steady state is reached (Area A, Figure D.1). The eastward shift of the discharge zone increases lateral flow rates at Pine Point due to a decrease in the component of vertical flow. Cooler temperatures exist at Pine Point as a result of higher flow rates. The temperature and brine slugs move up the barrier at more or less the same time as the *base case*, however the longer section promotes lateral flow, dampening the effects of the slugs. Brine flushing is similar to the base case, but there is less congestion at the discharge zone (Figure D.2).

The *pinchout* model behaves in a more natural way than the cropped *base case* model. Fluids discharge freely as strata pinch out rather than being forced upward by a no-flow boundary. The highest temperature zone in the Middle Devonian aquifer ends at 470 km. By 580 km, the temperature drops below 50°C in the barrier aquifer. In the *pinchout* model, vertical flow is focused in a 10-km wide zone (460 to 470 km), which is approximately the length and at the location of Pine Point. Here we assume that the location of mineralization is controlled by localized vertical flow through the ore district, where high temperatures and discharge are coincident rather than a chemical trap, which cannot be simulated using Rift2D. Therefore the eastern boundary in the *base case* model does not adversely distort the flow system or alter the placement of the ore district. The *pinchout* model solution would be preferred as a base case; however, uncertainties in geology and computer time makes use of this model impractical. Thus, the *base case* model has been used to investigate controls on flow rates, temperature, and salinity at Pine Point over time.

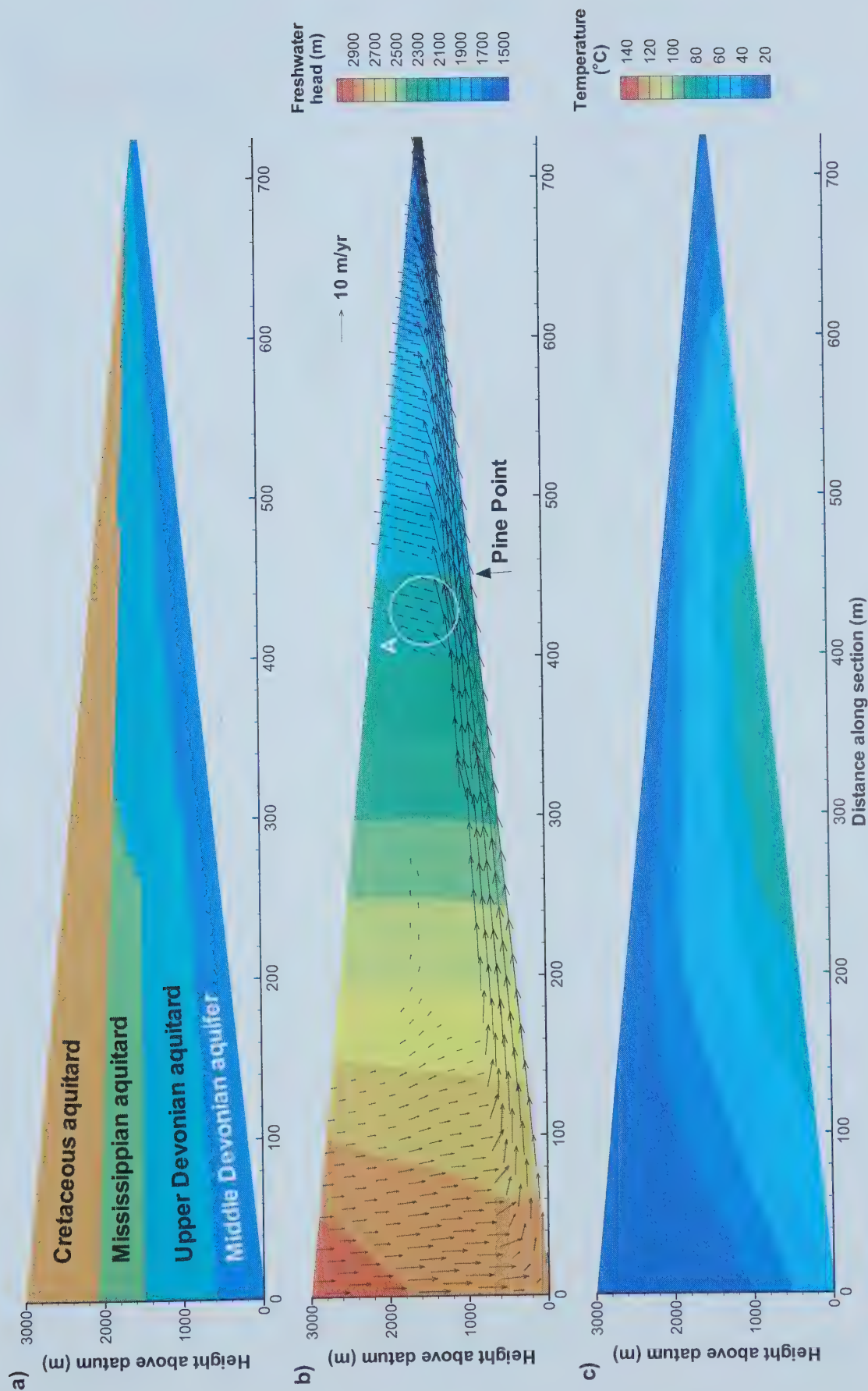


Figure D.1: Pinch out simulation 500 000 years after instantaneous uplift, a) hydrostratigraphic units; b) freshwater hydraulic heads and velocity vectors; and c) temperature distribution. White circle labelled A outlines area of transient flow.

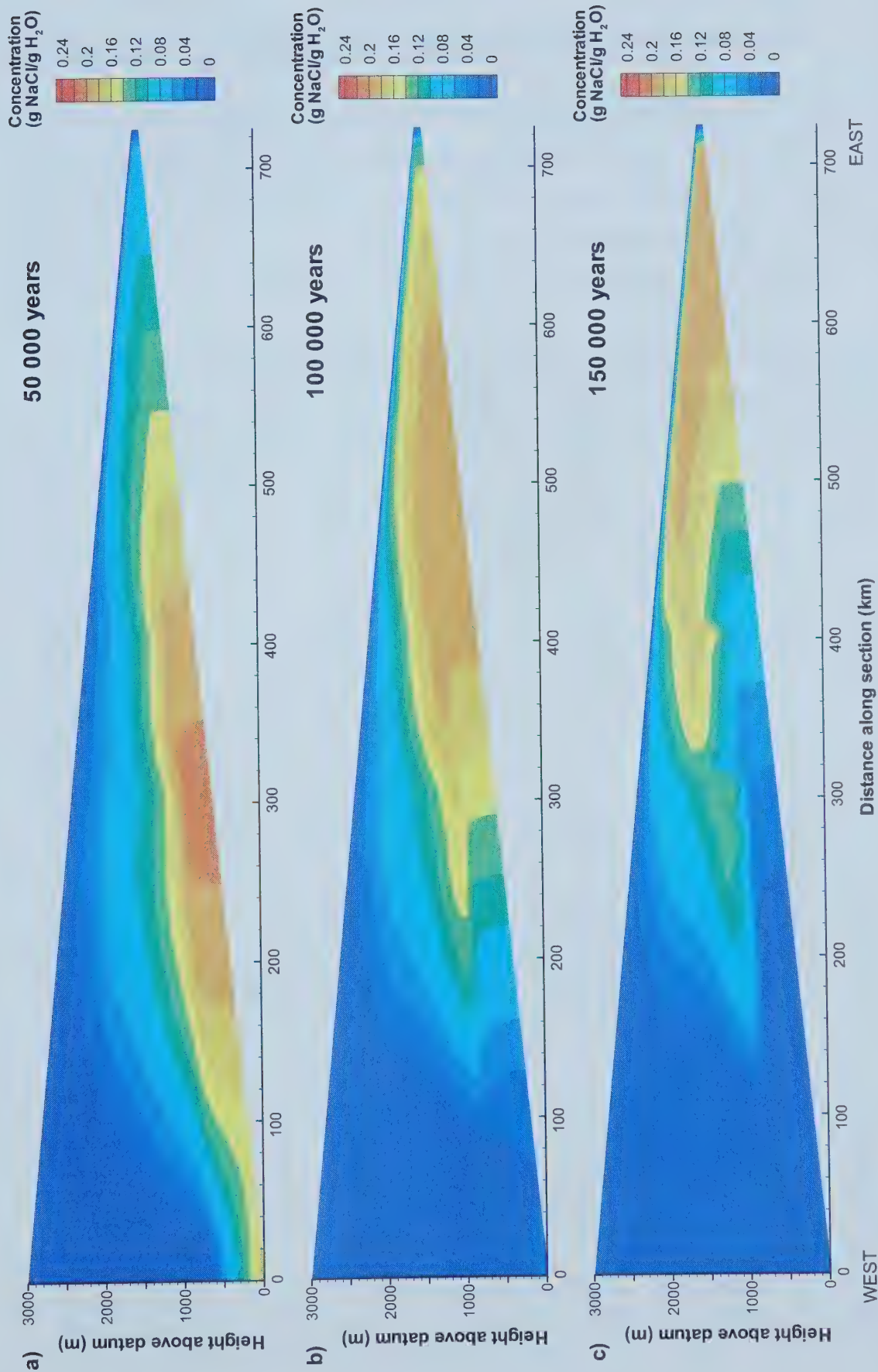


Figure D.2: Transient simulations of salinity for the pinchout model a) 50 000 years; b) 100 000 years; and c) 150 000 years following instantaneous uplift.

APPENDIX E: COMPUTER SIMULATION REQUIREMENTS

All of the models presented in this thesis were run on an IBM RS/6000 43P model 260 workstation, which contains two Power 630, 200 MHz processors and 2 GB of memory. The workstation runs the AIX version 4.3 operating system. The code was compiled using the XLF version 5.1.1 Fortran compiler with the O3 option. Table E.1 shows the approximate CPU time required to run each model, as well as the time step length.

Table E.1: Comparison of computer simulation time and time steps for each model discussed.

Model Name	Δx (km)	Time step length	Simulated time	CPU run time	Normalized* CPU run time
<i>Original Pine Point model</i>	7.2 to 19.0	250 yr	500 ka	2m23s	2m23s
<i>Base case Pine Point model</i>	2.5	200 yr	500 ka	1h58m	1h58m
<i>400 columns model</i>	1.25	125 yr	100 ka	2h49m	14h05m
<i>Pinchout model</i>	2.5	20 yr	200 ka	17h17m	43h13m
<hr/>					
Permeability variations:					
<i>High permeability</i>	2.5	50 yr	300 ka	4h41m	7h48m
<i>Low permeability</i>	2.5	500 yr	2000 ka	3h10m	0h48m
<i>All low permeability</i>	2.5	1000 yr	4000 ka	3h12m	0h24m
<i>Measured permeability</i>	2.5	200 yr	2000 ka	8h04m	2h01m
<i>Funnel</i>	2.5	200 yr	1000 ka	4h05m	2h03m
<hr/>					
Temperature variations:					
<i>High thermal conductivity</i>	2.5	200 yr	500 ka	1h57m	1h57m
<i>Low thermal conductivity</i>	2.5	200 yr	500 ka	2h07m	2h07m
<i>Medium heat flux: 85 mW/m²</i>	2.5	125 yr	500 ka	3h15m	3h15m
<i>High heat flux: 100 mW/m²</i>	2.5	125 yr	500 ka	3h10m	3h10m
<hr/>					
Salinity variations:					
<i>Salinity</i>	2.5	200 yr	500 ka	2h08m	2h08m
<i>Deep basin</i>	2.5	200 yr	500 ka	2h14m	2h14m
<i>Basement</i>	2.5	200 yr	2000 ka	16h27m	4h07m
<hr/>					
<i>Replicated Athabasca model</i>	7.7 to 15	625 yr	2000 ka	42m52s	N/A
<i>Best case Athabasca model</i>	2.896	50 000 yr	60 Ma	4h32m	4h32m
<i>700 columns model</i>	1.034	30 000 yr	60 Ma	~26h	~26h
<hr/>					
Fixed grid variations:					
<i>Calibration 10⁻¹⁶ m²</i>	2.896	15 000 yr	60 Ma	14h51m	14h51m
<i>Calibration 10⁻¹⁸ m²</i>	2.896	50 000 yr	60 Ma	4h23m	4h23m
<i>Salinity</i>	2.896	50 000 yr	60 Ma	4h49m	4h49m
<i>Low permeability Mannville</i>	2.896	50 000 yr	60 Ma	4h10m	4h10m
<i>No Mannville</i>	2.896	50 000 yr	60 Ma	4h32m	4h32m
<hr/>					
Erosion variations:					
<i>Erosion model</i>	2.896	50 000 yr	60 Ma	8h35m	8h35m
<i>25% High k Mannville</i>	2.896	30 000 yr	60 Ma	13h52m	13h52m
<i>60% High k Mannville</i>	2.896	30 000 yr	60 Ma	13h46m	13h46m

* Run times calculated for 500 ka and 60 Ma for the Pine Point and Athabasca models respectively.

APPENDIX F: EROSION MODEL PARAMETERS

Along the Peace River Arch section, constant erosion rates at each column of the *erosion* model are applied in two consecutive tectonic periods: 60 to 2 Ma and 2 Ma to present day. Maximum relief was estimated from eroded thickness values derived from coal moisture (Issler et al., 1999). An exponential curve was fit to these estimates along the section (Figure F.1). Erosion rates were calculated by dividing the eroded thickness by the duration of the tectonic period, in which it was eroded. Simulations that used only the maximum uplift surface and present day topography produced a distorted topography-driven flow system that did not fit today's observations. For this reason, a second erosional surface was determined, such that it skims the top of the present day topography. This surface is considered to be the topography at 2 Ma. For the last 2 million years of simulation, the model topography is eroded at constant rates to the morphology known today.

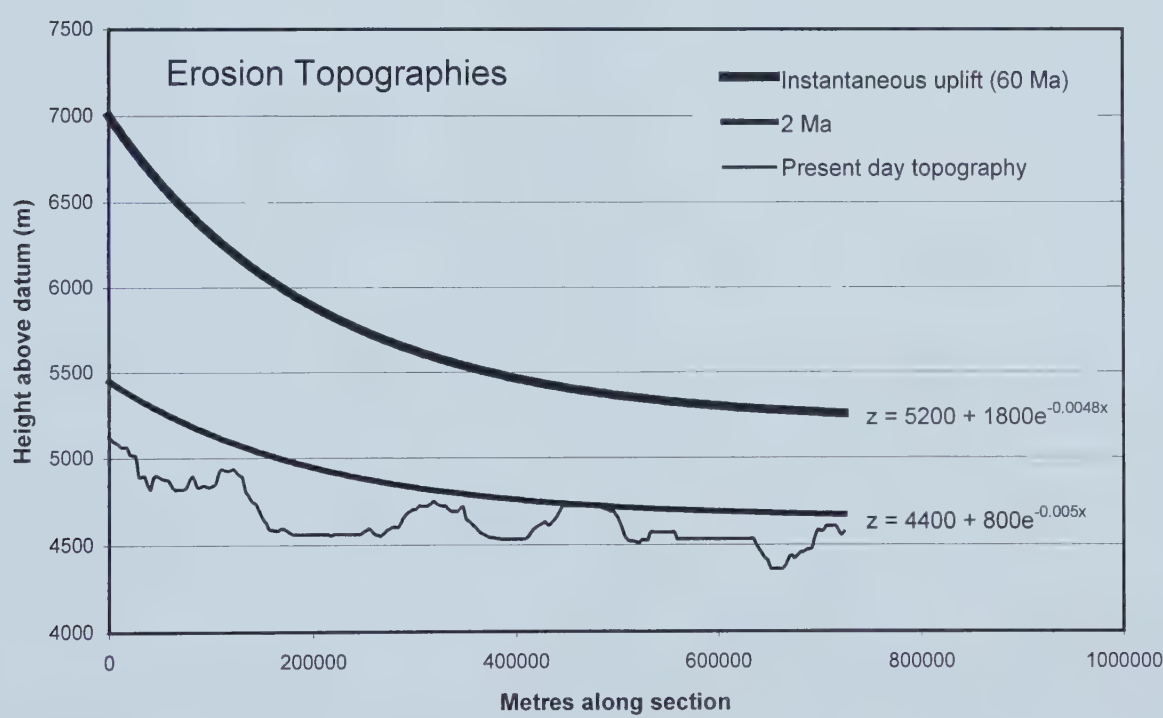


Figure F.1: Estimated topography curves at instantaneous uplift and at 2 Ma, compared to present day topography. Exponential functions describing each estimated topography are shown adjacent to the curve, where z is equivalent to the height above the datum in metres and x is the distance along the section in kilometres. The present day topography is derived from Wright et al. (1984). Note the Peace River valley is not included because it distorted the flow system significantly and is thought to have formed very recently.

University of Alberta Library



0 1620 1492 0613

B45436